NASA Tech Briefs

National
Aeronautics and
Space
Administration

Improved techniques for fabricating wood-composite structures, such as the wind-turbine blade shown here, have emerged from work by a NASA contractor. The fabrication methods are also being applied to boatbuilding, resulting in stronger, lighter weight masts that require no rigging. *[See the bottom of page A1.]*

Vol. 7, No. 1

Fall 1982

About the NASA Technology Utilization Program

The National Aeronautics and Space Act of 1958, which established NASA and the United States civilian space program, requires that "The Administration shall provide for the widest practicable and appropriate dissemination of information concerning its activities and the results thereof."

To help carry out this objective, NASA's Technology Utilization (TU) Program was established in 1962. Now, as an element of NASA's Technology Utilization and Industry Affairs Division, this program offers a variety of valuable services to help transfer aerospace technology to nonaerospace applications, thus assuring American taxpayers maximum return on their investment in space research; thousands of spinoffs of NASA research have already occurred in virtually every area of our economy.

The TU program has worked for engineers, scientists, technicians, and businessmen; and it can work for you.

NASA Tech Briefs

Tech Briefs is published quarterly and is free to engineers in U.S. industry and to other domestic technology transfer agents. It is both a current-awareness medium and a problem-solving tool. Potential products . . . industrial processes . .. basic and applied research . . . shop and lab techniques . . . computer software . . . new sources of technical data . . . concepts . . . can be found here. The short section on New Product Ideas highlights a few of the potential new products contained in this issue. The remainder of the volume is organized by technical category to help you quickly review new developments in your areas of interest. Finally, a subject index makes each issue a convenient reference file.

Further Information on Innovations

Although some new technology announcements are complete in themselves, most are backed up by Technical Support Packages (TSP's). TSP's are available without charge and may be ordered by simply completing a TSP Request Card found at the back of this volume. Further information on some innovations is available for a nominal fee from other sources, as indicated. In addition, Technology Utilization Officers at NASA Field Centers will often be able to lend necessary guidance and assistance.

Patent Licenses

Patents have been issued to NASA on some of the inventions described, and patent applications have been submitted on others. Each announcement indicates patent status and availability of patent licenses if applicable.

Other Technology Utilization Services

To assist engineers, industrial researchers, business executives, Government officials, and other potential users in applying space technology to their problems, NASA sponsors Industrial Applications Centers. Their services are described on page A7. In addition, an extensive library of computer programs is available through COSMIC, the Technology Utilization Program's outlet for NASA-developed software.

Applications Program

NASA conducts applications engineering projects to help solve public-sector problems in such areas as safety, health, transportation, and environmental protection. Two applications teams, staffed by professionals from a variety of disciplines, assist in this effort by working with Federal agencies and health organizations to identify critical problems amenable to solution by the application of existing NASA technology.

Reader Feedback

We hope you find the information in *NASA Tech Briefs* useful. A reader-feedback card has been included because we want your comments and suggestions on how we can further help you apply NASA innovations and technology to your needs. Please use it; or if you need more space, write to the Manager, Technology Transfer Division, P.O. Box 8757, Baltimore/ Washington International Airport, Maryland 21240.

NASA Tech Briefs

National Aeronautics and Space Administration

Fall 1982
Volume 7, Number 1

COVERS: The photographs on the front and back covers illustrate developments by NASA and its contractors that have resulted in commercial and nonaerospace spinoffs. You can use the TSP Request Card at the back of this issue to learn more about the Wood Composite Structures [Circle 90] and Sewer-Monitoring System [Circle 91].

About This NASA Publication

NASA Tech Briefs, a quarterly publication, is distributed free to qualified U.S. citizens to encourage commercial application of U.S. space technology. For information on publications and services available through the NASA Technology Utilization Program, write to the Manager, Technology Transfer Division, P.O. Box 8757, Baltimore/Washington International Airport, Maryland 21240.

"The Administrator of National Aeronautics and Space Administration has determined that the publication of this periodical is necessary in the transaction of the public business required by law of this Agency. Use of funds for printing this periodical has been approved by the Director of the Office of Management and Budget."

Change of Address

If you wish to have NASA Tech Briefs forwarded to your new address, use the Subscription Card enclosed at the back of this volume of NASA Tech Briefs. Be sure to check the appropriate box indicating change of address, and also fill in your identification number (T number) in the space indicated.

Communications Concerning Editorial Matter

For editorial comments or general communications about NASA Tech Briefs, you may use the Feedback card in the back of NASA Tech Briefs, or write to: The Publications Manager, Technology Utilization Office (LGT-1), NASA Headquarters, Washington, DC 20546. Technical questions concerning specific articles should be directed to the Technology Utilization Officer of the sponsoring NASA Center (addresses listed on page A4).

Acknowledgements

NASA Tech Briefs is published quarterly by the National Aeronautics and Space Administration, Technology Transfer Division, Washington, DC: Administrator: **James E. Beggs;** Director, Technology Utilization and Industry Affairs Division: **Ronald J. Philips;** Publications Manager: **Leonard A. Ault.** Prepared for the National Aeronautics and Space Administration by **Logical Technical Services Corp.:** Editor-in-Chief: **Jay Kirschenbaum;** Art Director: **Ernest Gillespie;** Managing Editor: **Jerome Rosen;** Chief Copy Editor: **Oden Browne;** Staff Editors: **Donald Blattner, Larry Grunberger, Ted Selinsky, George Watson;** Graphics: **Luis Martinez, Janet McCrie, Huburn Profitt;** Editorial & Production: **Richard Johnson, Frank Ponce, Elizabeth Texeira, Vincent Susinno, Ernestine Walker.**

NASA TU SERVICES

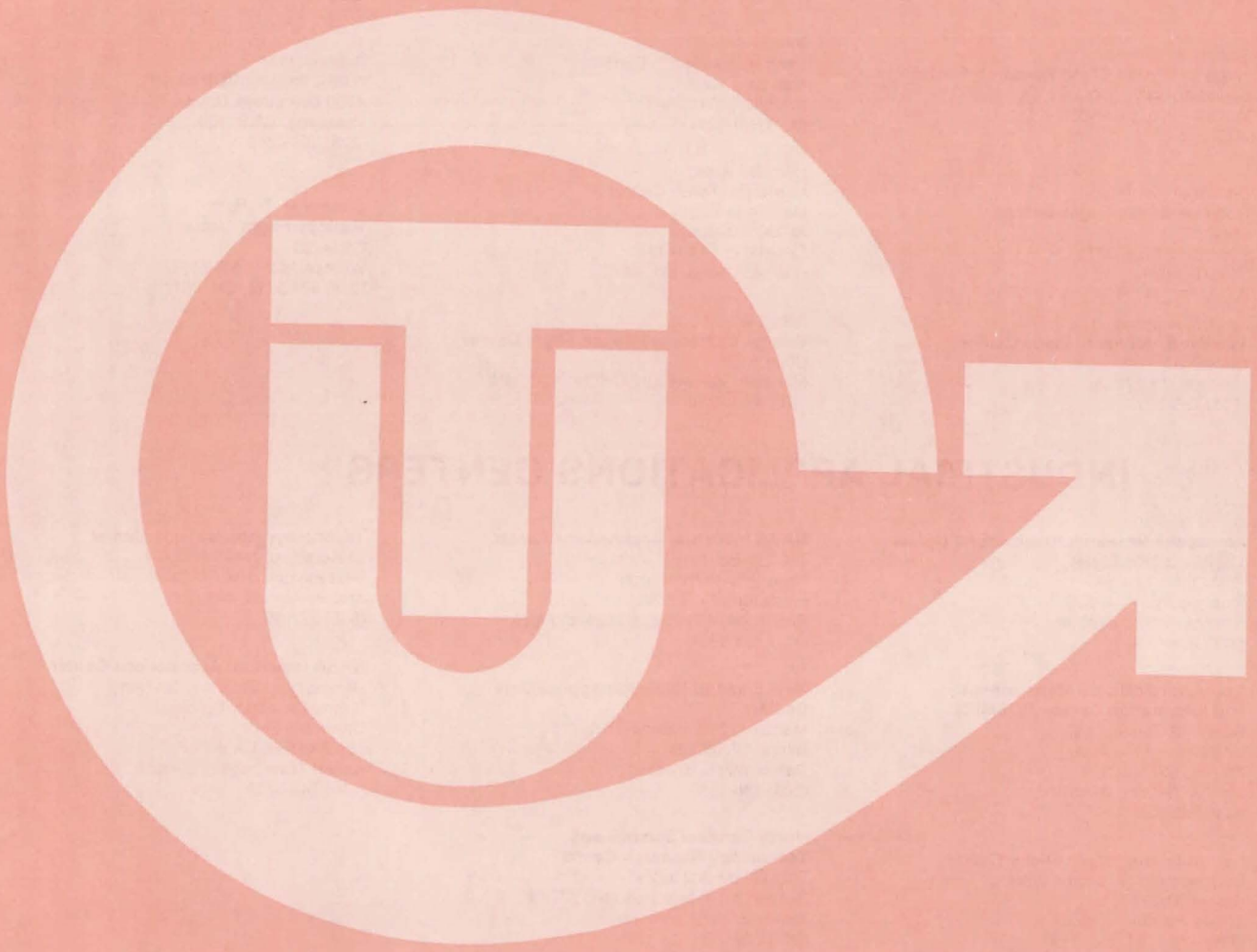

NASA TECHNOLOGY UTILIZATION NETWORK

★ TECHNOLOGY UTILIZATION OFFICERS

Stanley A. Miller
Ames Research Center
Code 240-10
Moffett Field, CA 94035
(415) 965-6471

Stanley A. Miller
Hugh L. Dryden Flight Research Center
Code 240-10
Moffett Field, CA 94035
(415) 965-6471

Donald S. Friedman
Goddard Space Flight Center
Code 702.1
Greenbelt, MD 20771
(301) 344-6242

John T. Wheeler
Lyndon B. Johnson Space Center
Code AT-3
Houston, TX 77058
(713) 483-3809

U. Reed Barnett
John F. Kennedy Space Center
Code PT-SPD
Kennedy Space Center, FL 32899
(305) 867-3017

John Samos
Langley Research Center
Mail Stop 139A
Hampton, VA 23665
(804) 827-3281

Harrison Allen, Jr.
Lewis Research Center
Mail Code 7-3
21000 Brookpark Road
Cleveland, OH 44135
(216) 433-4000, Ext. 6422

Ismail Akbay
George C. Marshall Space Flight Center
Code AT01
Marshall Space Flight Center, AL 35812
(205) 453-2224

Leonard A. Ault
NASA Headquarters
Code ETD-6
Washington, DC 20546
(202) 755-2244

Aubrey Smith
NASA Resident Office-JPL
4800 Oak Grove Drive
Pasadena, CA 91103
(213) 354-4849

Gilmore H. Trafford
Wallops Flight Center
Code OD
Wallops Island, VA 23337
(804) 824-3411, Ext. 201

● INDUSTRIAL APPLICATIONS CENTERS

Aerospace Research Applications Center
1201 East 38th Street
Post Office Box 647
Indianapolis, IN 46223
John M. Ulrich, director
(317) 264-4644

Computer Software Management and Information Center (COSMIC)
Suite 112, Barrow Hall
University of Georgia
Athens, GA 30602
John A. Gibson, director
(404) 542-3265

Kerr Industrial Applications Center
Southeastern Oklahoma State University
Durant, OK 74701
James Harmon, director
(405) 924-0121, Ext. 413

NASA Industrial Applications Center
710 LIS Building
University of Pittsburgh
Pittsburgh, PA 15260
Paul A. McWilliams, executive director
(412) 624-5211

New England Research Applications Center
Mansfield Professional Park
Storrs, CT 06268
Daniel Wilde, director
(203) 486-4533

North Carolina Science and Technology Research Center
Post Office Box 12235
Research Triangle Park, NC 27709
James E. Vann, director
(919) 549-0671

Technology Applications Center
University of New Mexico
Albuquerque, NM 87131
Stanley Morain, director
(505) 277-3622

NASA Industrial Applications Center
University of Southern California
Denny Research Building
University Park
Los Angeles, CA 90007
Robert Mixer, acting director
(213) 743-6132

■ STATE TECHNOLOGY APPLICATIONS CENTERS

NASA/University of Florida
State Technology Applications Center
500 Weil Hall
University of Florida
Gainesville, FL 32611
J. Ronald Thornton, director

Gainesville:	(904) 392-6760
Boca Raton:	(305) 395-5100, Ext. 2292
Fort Lauderdale:	(305) 776-6645
Jacksonville:	(904) 646-2478
Orlando:	(305) 275-2706
Pensacola:	(904) 476-9500, Ext. 426
Tampa:	(813) 974-2499

NASA/University of Kentucky
State Technology Applications Program
109 Kinkead Hall
University of Kentucky
Lexington, KY 40508
William R. Strong, manager
(606) 258-4632

◆ PATENT COUNSELS

Robert F. Kempf
Asst. Gen. Counsel for patent matters
NASA Headquarters
Code GP-4
400 Maryland Avenue, SW.
Washington, DC 20546
(202) 755-3954

Darrell G. Brekke
Ames Research Center
Mail Code: 200-11A
Moffett Field, CA 94035
(415) 965-5104

Darrell G. Brekke
Hugh L. Dryden Flight Research Center
Mail Code: 200-11A
Moffett Field,.CA 94035
(415) 965-5104

John O. Tresansky
Goddard Space Flight Center
Mail Code: 204
Greenbelt, MD 20771
(301) 344-7351

Marvin F. Matthews
Lyndon B. Johnson Space Center
Mail Code: AL-3
Houston, TX 77058
(713) 483-4871

James O. Harrell
John F. Kennedy Space Center
Mail Code: SA-PAT
Kennedy Space Center, FL 32899
(305) 867-2544

Howard J. Osborn
Langley Research Center
Mail Code: 279
Hampton, VA 23665
(804) 827-3725

Norman T. Musial
Lewis Research Center
Mail Code: 500-311
21000 Brookpark Road
Cleveland, OH 44135
(216) 433-4000, Ext. 346

Leon D. Wofford, Jr.
George C. Marshall Space Flight Center
Mail Code: CC01
Marshall Space Flight Center, AL 35812
(205) 453-0020

Paul F. McCaul
NASA Resident Office-JPL
Mail Code: 180-601
4800 Oak Grove Drive
Pasadena, CA 91103
(213) 354-2700

▲ APPLICATION TEAMS

Doris Rouse, director
Research Triangle Institute
Post Office Box 12194
Research Triangle Park, NC 27709
(919) 541-6980

James P. Wilhelm, director
SRI International
333 Ravenswood Avenue
Menlo Park, CA 94026
(415) 326-6200, Ext. 3520

TECHNOLOGY UTILIZATION OFFICERS

Technology transfer experts can help you apply the innovations in NASA Tech Briefs.

The Technology Utilization Officer at each NASA Field Center is an applications engineer who can help you make use of new technology developed at his center. He brings you NASA Tech Briefs and other special publications, sponsors conferences, and arranges for expert assistance in solving technical problems.

Technical assistance, in the form of further information about NASA innovations and technology, is one of the services available from the TUO. Together with NASA scientists and engineers, he can often help you find and implement NASA technology to meet your specific needs.

Technical Support Packages (TSP's) are prepared by the center TUO's. They provide further technical details for articles in NASA Tech Briefs. This additional material can help you evaluate and use NASA technology. You may receive most TSP's free of charge by using the TSP Request Card found at the back of this issue.

Technical questions about articles *in NASA Tech Briefs are answered in the TSP's. When no TSP is available, or you have further questions, contact the Technology Utilization Officer at the center that sponsored the research* [see page A4].

NASA INVENTIONS AVAILABLE FOR LICENSING

Over 3,500 NASA inventions are available for licensing in the United States — both exclusive and nonexclusive.

Nonexclusive licenses for commercial use of NASA inventions are encouraged to promote competition and to achieve the widest use of inventions. They must be used by a netotiated target date.

Exclusive licenses may be granted to encourage early commercial development of NASA inventions, especially when considerable private investment is required. These are generally for 5 to 10 years and usually require royalties based on sales or use.

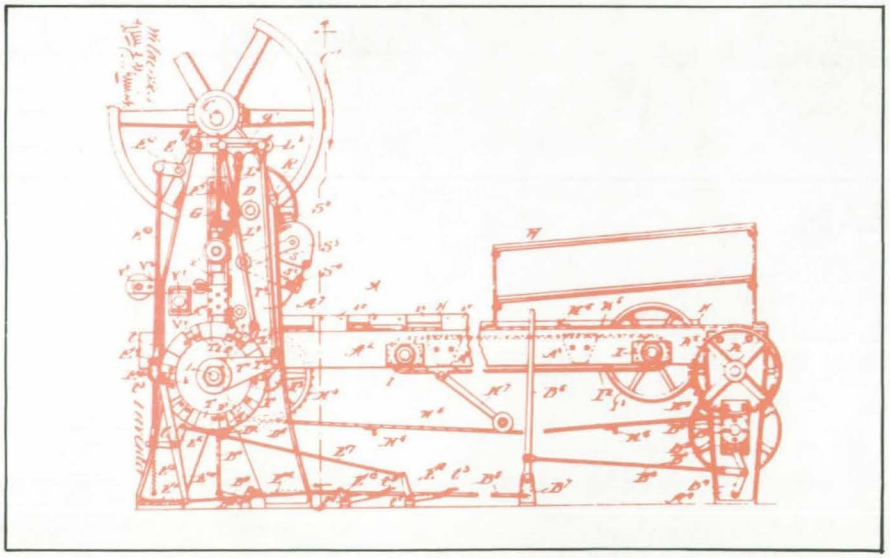

Additional licenses available include those of NASA-owned foreign patents. In addition to inventions described in NASA Tech Briefs, *"NASA Patent Abstract Bibliography"* (PAB), containing abstracts of all NASA inventions, can be purchased from National Technical Information Service, Springfield, VA 22161. The PAB is updated semiannually.

Patent licenses for Tech Briefs *are frequently available. Many of the inventions reported in NASA Tech Briefs are patented or are under consideration for a patent at the time they are published. The current patent status is described at the end of the article; otherwise, there is no statement about patents. If you want to know more about the patent program or are interested in licensing a particular invention, contact the Patent Counsel at the NASA Field Center that sponsored the research* [see page A5]. *Be sure to refer to the NASA reference number at the end of the Tech Brief.*

APPLICATION TEAMS

Technology-matching and problem-solving assistance to public-sector organizations

Application engineering projects are conducted by NASA to help solve public-sector problems in such areas as safety, health, transportation, and environmental protection. Some application teams specialize in biomedical disciplines; others, in engineering and scientific problems. Staffed by professionals from various disciplines, these teams work with other Federal agencies and health organizations to identify critical problems amenable to solution by the application of existing NASA technology.

Public-sector organization *representatives can learn more about application teams by contacting a nearby NASA Field Center Technology Utilization Office* [*see page A4*].

INDUSTRIAL APPLICATIONS CENTERS

Computerized access to over 10 million documents worldwide

Computerized information retrieval from one of the world's largest banks of technical data is available from NASA's network of industrial Applications Centers (IAC's). The IAC's give you access to 1,800,000 technical reports in the NASA data base and to more than 10 times that many reports and articles found in nearly 200 other computerized data bases.

The major sources include:

- *750,000 NASA Technical Reports*
- *Selected Water Resources Abstracts*
- *NASA Scientific and Technical Aerospace Reports*
- *Air Pollution Technical Information Center*
- *NASA International Aerospace Abstracts*
- *Chem Abstracts Condensates*
- *Engineering Index*
- *Energy Research Abstracts*
- *NASA Tech Briefs*
- *Government Reports Announcements*

and many other specialized files on food technology, textile technology, metallurgy, medicine, business, economics, social sciences, and physical science.

The IAC services range from tailored literature searches through expert technical assistance:

- *Retrospective Searches:* Published or unpublished literature is screened, and documents are identified according to your interest profile. IAC engineers tailor results to your specific needs and furnish abstracts considered the most pertinent. Complete reports are available upon request.
- *Current-Awareness Searches:* IAC engineers will help design a program to suit your needs. You will receive selected monthly or quarterly abstracts on new developments in your area of interest.
- *Technical Assistance:* IAC engineers will help you evaluate the results of your literature searches. They can help find answers to your technical problems and put you in touch with scientists and engineers at appropriate NASA Field Centers.

Prospective clients *can obtain more information about these services by contacting the nearest IAC* [*see page A4*]. *User fees are charged for IAC information services.*

STATE TECHNOLOGY APPLICATIONS CENTERS

Technical information services for industry and state and local government agencies

Government and private industry in Florida and Kentucky can utilize the services of NASA's State Technology Applications Centers (STAC's). The STAC's differ from the Industrial Applications Centers described on page A7, primarily in that they are integrated into existing state technical assistance programs and serve only the host state, whereas the IAC's serve multistate regions.

Many data bases, including the NASA base and several commercial bases, are available for automatic data retrieval through the STAC's. Other services such as document retrieval and special searches are also provided. (Like the IAC's, the STAC's normally charge a fee for their services.)

To obtain information *about the services offered, write or call the STAC in your state* [*see page A4*].

COSMIC®

An economical source of computer programs developed by NASA and other government agencies

A vast software library is maintained by COSMIC — the Computer Software Management and Information Center. COSMIC gives you access to approximately 1,600 computer programs developed for NASA and the Department of Defense and selected programs for other government agencies. Programs and documentation are available at reasonable cost.

Available programs range from management (PERT scheduling) to information science (retrieval systems) and computer operations (hardware and software). Hundreds of engineering programs perform such tasks as structural analysis, electronic circuit design, chemical analysis, and the design of fluid systems. Others determine building energy requirements and optimize mineral exploration.

COSMIC services go beyond the collection and storage of software packages. Programs are checked for completeness; special announcements and an indexed software catalog are prepared; and programs are reproduced for distribution. Customers are helped to identify their software needs; and COSMIC follows up to determine the successes and problems and to provide updates and error corrections. In some cases, NASA engineers can offer guidance to users in installing or running a program.

Information about programs *described in NASA Tech Briefs articles can be obtained by completing the COSMIC Request Card at the back of this issue. Just circle the letters that correspond to the programs in which you are interested.*

NEW PRODUCT IDEAS

NEW PRODUCT IDEAS are just a few of the many innovations described in this issue of NASA Tech Briefs and having promising commercial applications. Each is discussed further on the referenced page in the appropriate section in this issue. If you are interested in developing a product from these or other NASA innovations, you can receive further technical information by requesting the TSP referenced at the end of the full-length article or by writing the Technology Utilization Office of the sponsoring NASA center (see page A4). NASA's patent-licensing program to encourage commercial development is described on page A6.

"Dropproof" Handtools

A mechanism originally developed for space applications makes two-part handtools "dropproof." Tools that include the new device can be used without risk on scaffolds, underwater, and in other hazardous work areas. In an explosive atmosphere, for example, tools

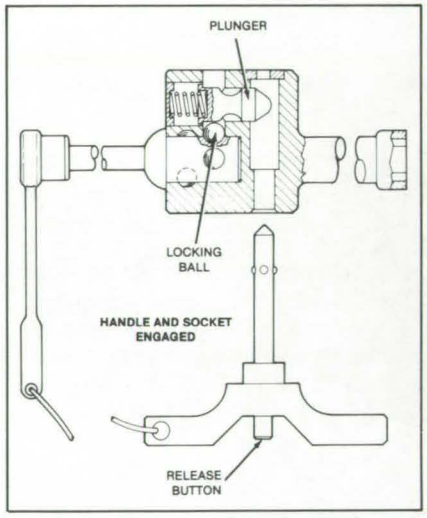

are less likely to be dropped and generate sparks that could ignite an explosion. A tethered retaining pin must be inserted into the tool before it can be separated into its two parts — a wrench handle and a wrench socket, for example. The tether on the pin secures one part of the tool after the separation, and a tether on the other part secures the other part. In use, the tool is not encumbered by two tethers, so there is little interference with the use of the tool by the operator.
(See page 69.)

Fire-Retardant Epoxy Adhesives

A new phosphorus-containing epoxy is fire-retardant and translucent. Intended as an adhesive for laminated plastic sheets, the new material bonds well to titanium dioxide-filled plastic film, which ordinarily shows little surface interaction with adhesives. Both the epoxy resin and

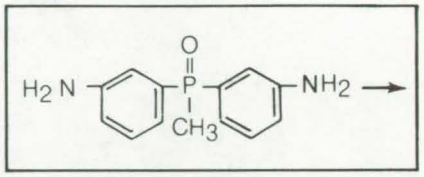

its diamine curing agent include covalently bonded phosphorus in their molecular structures. Since the curing agent contains phosphorus, it does not dilute it in the epoxy resin. As a result, the phosphorus content of the adhesive can be kept above 7 percent, a condition necessary to ensure fire retardancy in air. When a phenolic/glass laminate was bonded to a titanium dioxide-pigmented film with the new adhesive, the bond strength exceeded the tear strength of the film.
(See page 41.)

Implantable Drug Dispenser

A new implantable, programable liquid dispenser has wide application for around-the-clock, measured drug administration to humans as well as animals. Liquids and drugs, such as insulin, saline solution, sugar solution, and blood plasma, can be injected directly into the patient's bloodstream at a predetermined, controlled rate. Smaller than previous similar devices, the implantable dispenser contains a programable microprocessor. Drug administration is controlled by differential vapor pressure, in

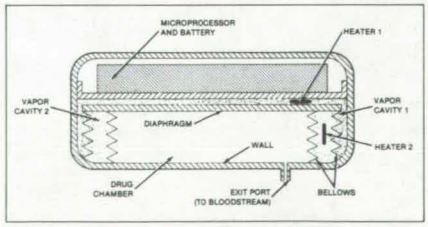

turn controlled by an integrated heating system. A 30-day drug supply can be applied at the rate of 1 cm^3 per day. The vapor can be a fluorocarbon or other volatile material sensitive to temperature changes.
(See page 48.)

Compact, Rugged Temperature Recorder

A self-contained temperature recorder originally developed for use in space experiments can store 2,048 temperature readings taken over a period of almost a year (or much less) and then

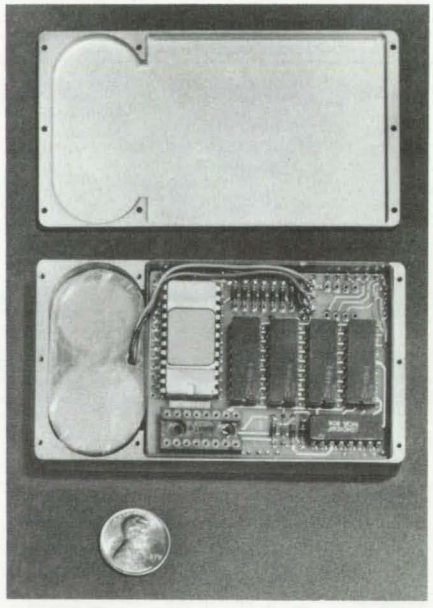

read them out when a special readout unit is plugged into it. The temperatures may be anywhere in the range from −0° to +50° and are recorded at intervals selectable by factors of 2 from 1.875 up to 240 minutes. The data are retained in the battery-operated recorder for at least 4 months before readout, if desired.
(See page 19.)

Magnetic Bearings Increase Pump Efficiency

Magnetic bearings compensate for rotor displacements and for asynchronous rotation of a counterrotating helical-screw gas compressor, making the two-element pump efficient enough for many applications. In the new design, each screw shaft is supported at

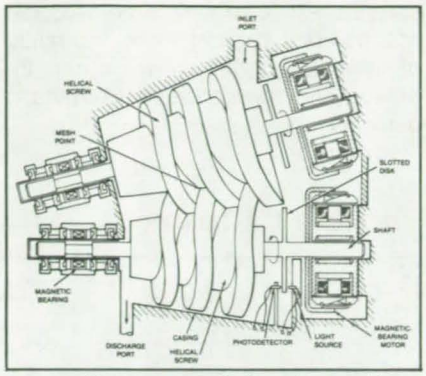

one end by a magnetic bearing and by a drive motor at the other end. The magnetic bearings balance the axial and radial forces that displace the screws from equilibrium. As a result, frictional losses are lowered, and a tight seal is maintained between the moving parts. The two-element pump could be used to compress gases in a mechanical refrigerator and in other counterrotating machinery; for example, in a pulverizer with a pair of counterrotating mills.
(See page 76.)

Miniature Two-Axis Joystick Controller

A movable-button-actuated self-centering controller uses optoelectronics to produce X and Y signals for aircraft control. In addition to being extremely small, the device is relatively immune to electrical noise. The combination of a new saddle-shaped button and positive centering gives a feel and

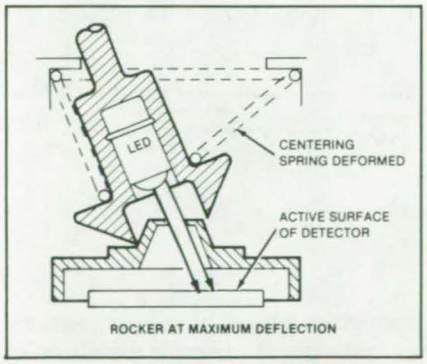

breakout that have met with pilot approval. In the miniature controller, the motion of a spring-centered rocker varies the position of a lensed light-emitting diode (LED). These changes in the position are sensed by a two-axis photodetector. Other suitable applications for the joystick controller would include radar trackers/cursors, aircraft moving-map display controls, weapon pointing, and the like.
(See page 78.)

Composite Tubular Connector

Joining composite tubular structural members with new connectors of the same composite materials can eliminate stress and weight problems encountered with metal connectors. Joint strengths can be optimized with proper choice of fiber orientation and fabric. Only two basic shapes are needed to

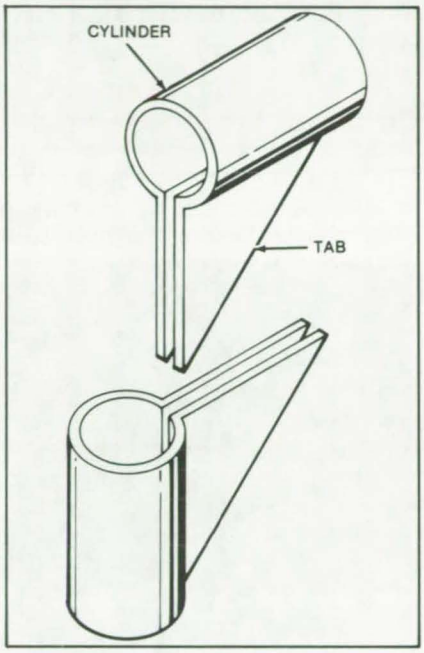

make a 90° joint and a T-joint. The basic shapes can be modified to join tubular members having different diameters.
(See page 53.)

Stable Polyurethane Coatings for Electronic Circuits

Polyurethane coatings and encapsulation compounds based on alkanes instead of ethers have superior chemical, electrical, and mechanical properties. High temperature and humidity have little effect on the alkane-based polyurethanes, and water-vapor transmission rates through polyurethane film prepared from alkanes are low in comparison with those for ether-based materials. The alkane-based polyurethanes have major uses as connector potting materials and as conformal coatings for printed-circuit boards. In the alkane-based materials, a double bond is removed from the polymer chain by the hydrogenation of polyol. This process eliminates the point of attack for

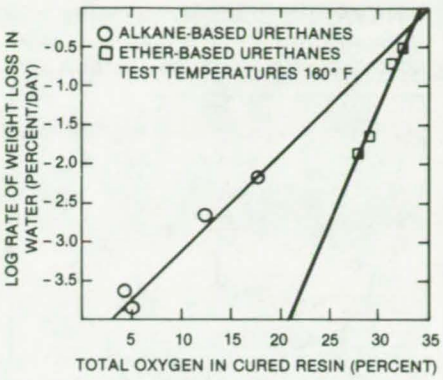

ozone, which is known to affect the double bond and to sever the polymer chain in the butadiene structure of polybutadiene-based polymers.
(See page 103.)

Spine Immobilizer for Accident Victims

A conformal bladder, made of resilient plastics and filled with microballons, immobilizes the spine of an accident victim, permitting the victim to be safely removed from the scene of the accident. The bladder, which is strapped to the victim and to a rescue chair, includes a socket for connecting a vacuum pump. When the air is withdrawn, the tightly compressed microballoons become firm and rigidly support the victim's spine. Included in the connection tubing is an adjustment valve that controls the

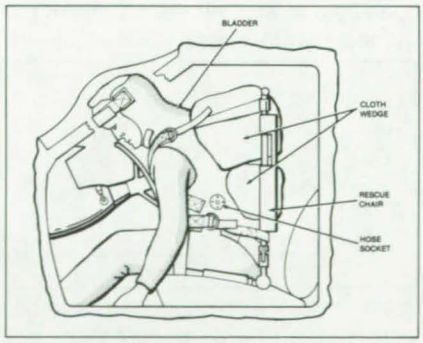

air evacuation rate. In this way, a conformal blanket, formed by the bladder, can be reversibly softened and hardened so as best to fit the victim.
(See page 47.)

Dipole-Excited Ring Antenna

A dipole radiator drives a ring radiator in a new compact antenna. The antenna, which has been breadboarded and

tested, can be mounted flush with a surface. Compared with a horn or a parabolic dish with the same aperture, the

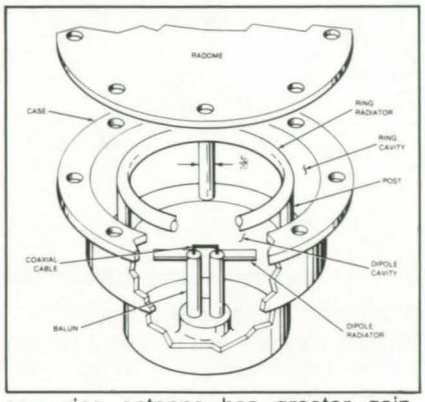

new ring antenna has greater gain, lower side lobes, and narrower beamwidth. It can be used on vehicles requiring flush-mounted antennas with very-directive signals. For example, it could be used as a radar altimeter antenna for an aircraft. The new antenna exhibits a 2.5-dB improvement in gain over that of a waveguide horn antenna with the same aperture.
(See page 12.)

Mobile Air Sampler

A container mounted on a moving vehicle gathers air samples along highways and in tunnels. The air sampler consists of a hollow cylinder with spring-activated sealing caps at both ends held open by a thread. Air flows through the cylinder, which closes when a hot-wire

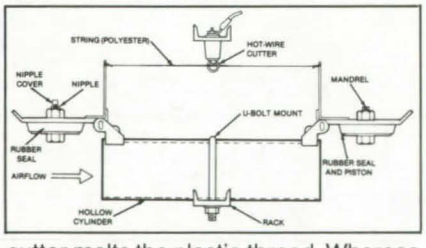

cutter melts the plastic thread. Whereas conventional fixed air-collection systems usually require official approval, the mobile air samples can be used without government validation.
(See page 55.)

Clear Film Protects Against Ultraviolet Radiation

An acrylic film contains a screening agent that filters ultraviolet radiation up to 380 nanometers in wavelength but passes other components of Sunlight. The new film, which contains about 0.5 weight percent of an agent with a molecular weight of 60,000, absorbs substantially more ultraviolet radiation than commercial materials with similar properties. It can protect rubber and plastics that are degraded by ultraviolet light, solar cells, and outdoor sheets or pipes made of polyethylene or polypropylene. The film is applied to surfaces by solvent casting, coextrusion, or laminating. It may also be applied as a latex.
(See page 33.)

Cutter for Woven Material

A guillotine cutting tool makes it easy to produce accurate, square cuts in strips of woven or felted materials, such

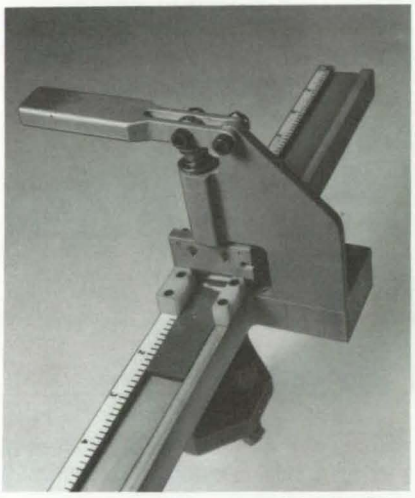

as high-temperature aramid fabric. The guillotine cutter can improve and increase production: It can cut faster than a scissors, papercutter, or knife with roller; and it gives the operator better control of the cut, resulting in sharper, better defined edges.
(See page 79.)

Spectrometer Analyzes Pollutants

A "real-time" mass spectrometer monitors and analyzes aerosol pollutant particles as small as 2 microns. The system can analyze changes in chemical composition to yield pollutant source information, which is particularly useful in coal-fired powerplants. Analytic capabilities include sulfur oxidation to sulfates, sodium sulfate and sodium sulfite ratios, lithium nitrate, and adipic and glutaric acids. By comparing each analysis with a reference aerosol, the spectrometer can determine the ratios of individual particles, which can indicate the presence of pollutant particles.
(See page 54.)

Portable I/V Tester

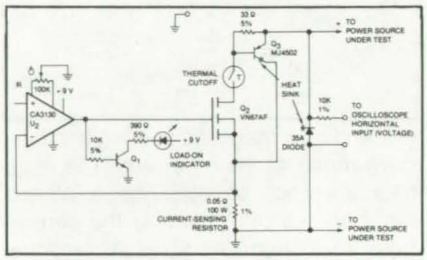

A portable, battery-operated unit tests the current/voltage characteristics of dc power supplies and sources, such as photovoltaic cells. The I/V characteristic curve is displayed on an oscilloscope. The curve tester functions as a 60 Hz sawtooth signal generator and variable load for the dc power supply under test, and it also supplies drive signals to the horizontal (voltage) and vertical (current) inputs of the oscilloscope. A 9-volt transistor battery operates the tester.
(See page 9.)

Carbon Cloth Supports Catalytic Electrodes

New carbon-cloth-supported electrodes, originally developed for a sulfur-cycle hydrogen process, are more efficient, more stable, and require less

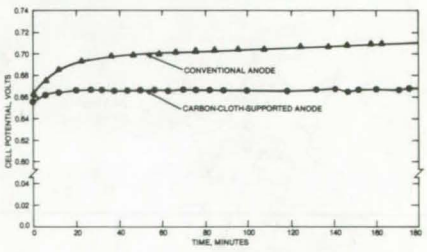

catalyst. In the sulfur-cycle process, the carbon-cloth electrode is the anode or "electrolyzer." A comparison of a cell containing the new flexible anode and a conventional anode made of pressed carbon powder, catalyst, and binder demonstrated the better stability and efficiency of the carbon-cloth design. After 2-½ hours in sulfuric acid at a constant-current density, the cell voltage using the carbon-cloth electrode was 40 mV less than that of the conventional cell.
(See page 95.)

Electronic Components and Circuits

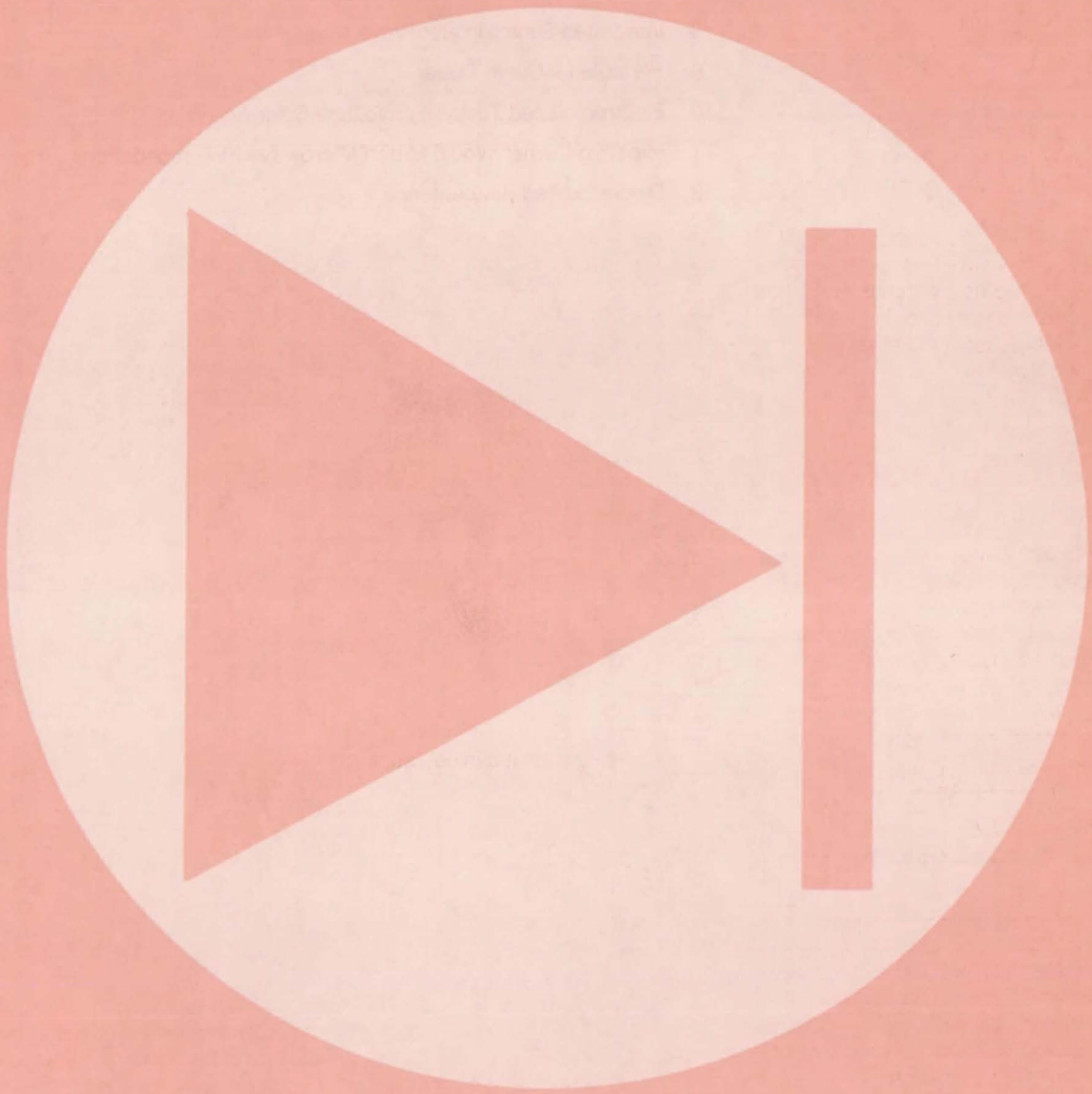

Hardware, Techniques, and Processes

Power-Factor Controller Avoids False Turnoff

A phase-difference signal is utilized to ensure triggering each half cycle.

Marshall Space Flight Center, Alabama

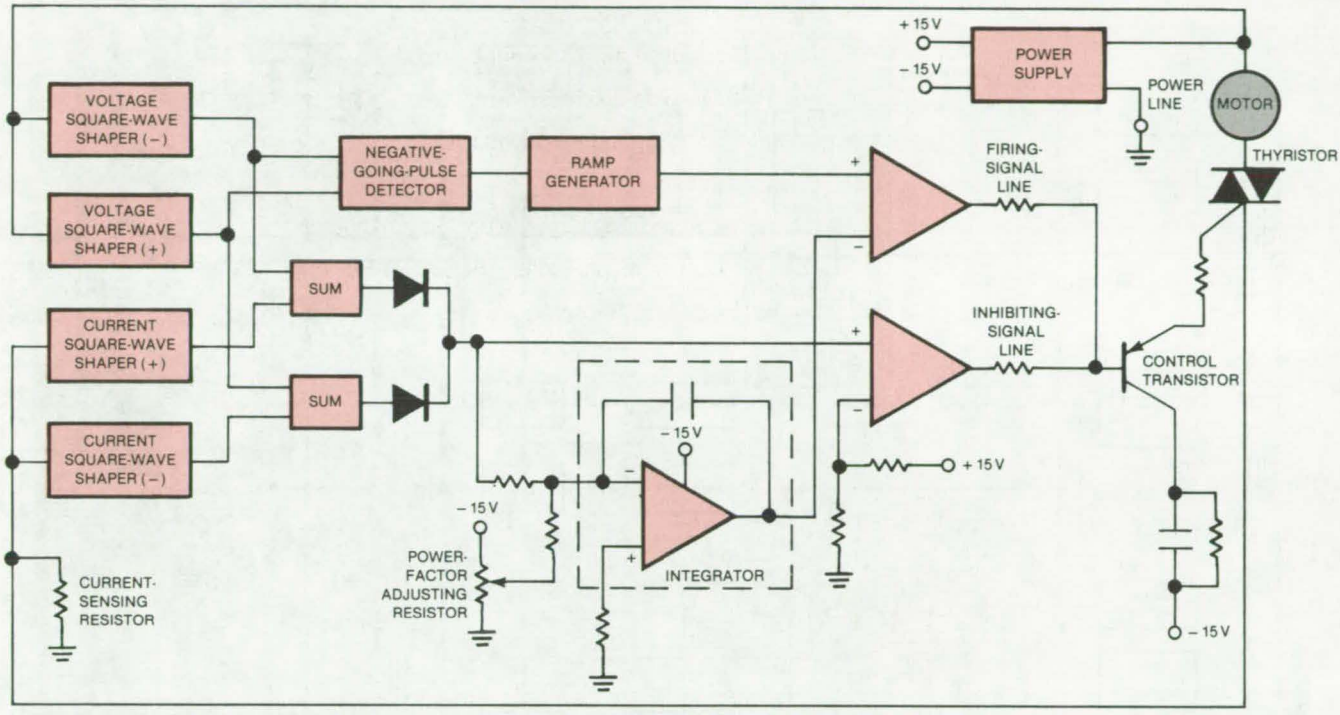

A Single-Phase Power-Factor Controller includes a special inhibiting circuit to avoid false turnoff. If the thyristor trigger signal occurs during the flow of current from the preceding half cycle, the inhibiting signal delays the application of the trigger pulse until the beginning of the next current half cycle.

An improved triggering circuit for power-factor motor controllers insures effective triggering at all current/voltage phase angles. The new circuit triggers the thyristor in the normal manner unless current from the preceding half cycle is flowing, but a signal already present in the power-factor controller is used to inhibit the transmission of the firing pulse to the thyristor gate until the current returns to zero.

A power-factor controller, used with inductive loads such as induction motors, samples line voltage and load current. A controller contains one or more thyristors that feed power to the load during a portion of the voltage cycle that depends on the phase difference between the sampled voltage and current.

In normal operation, the thyristor switches on when a trigger current pulse of a few microseconds is applied to the gate electrode and remains on until the anode current goes to zero. However, if the current phase lag is such that the trigger pulse occurs when current from the preceding half cycle is flowing, the thyristor will already be on. When the current goes to zero, the thyristor will go off and remain off during the following half cycle. The trigger pulse thus has no effect.

The new inhibiting circuit (see figure) establishes a reference time (namely, the moment the current goes to zero) for firing the thyristor based on the phase-difference signal and prevents generation of the firing pulse in advance of this reference time. An inhibiting pulse is generated if current is flowing from the preceding half cycle.

The base of the control transistor for the thyristor is connected to receive the signal from the inhibiting circuit and the signal from the thyristor firing-control circuit. The thyristor is connected so as to fire only when both signals are negative. If the firing signal occurs after the end of the inhibiting signal, it controls the transistor firing time; if it precedes the reference time, the transistor will not fire until the inhibiting signal is turned off. Thus, the trigger signal is delayed at least until the start of the next positive current half cycle and triggering of the thyristor is assured.

This work was done by Frank J. Nola of **Marshall Space Flight Center.** *For further information, Circle 1 on the TSP Request Card.*

Inquiries concerning rights for the commercial use of this invention should be addressed to the Patent Counsel, Marshall Space Flight Center [see page A5]. *Refer to MFS-25616.*

Soft-Starting Power-Factor Motor Controller

Starting current surges and motor vibrations are suppressed.

Marshall Space Flight Center, Alabama

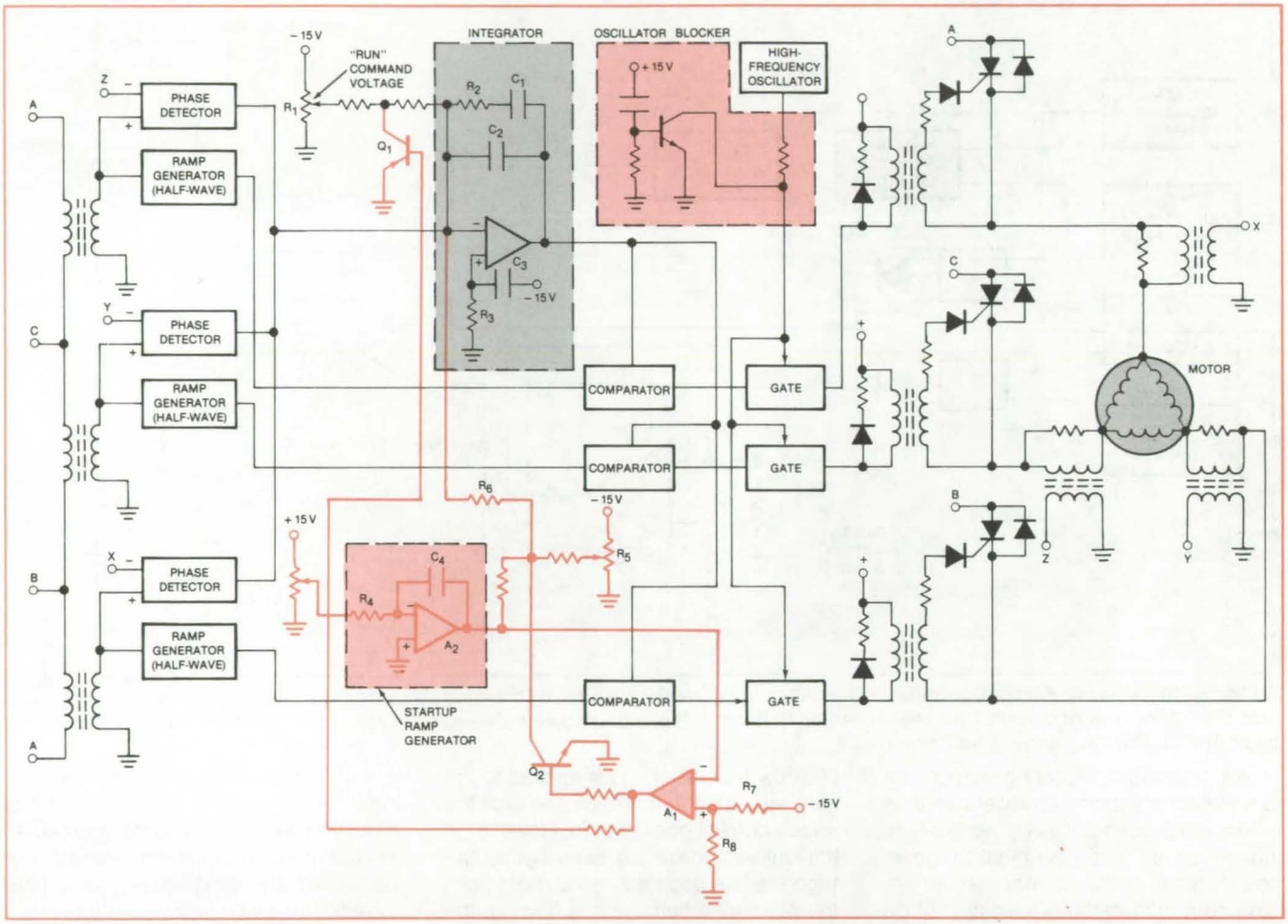

The **Three-Phase Power-Factor Controller With Soft Start** is based on an earlier version that does not control starting transients. The additional components (color) serve to turn off the "run" command signal and to substitute a gradual startup command signal during a preset startup interval.

An improved three-phase power-factor controller reduces the large current surge that usually accompanies starting. Unlike circuits that apply power in discrete increments, the improved controller applies power smoothly, without causing motor vibrations.

The operation of the controller, after the decay of the starting transients, is described in "Three-Phase Power-Factor Controller," page 3, *NASA Tech Briefs*, Vol. 6, No. 1 (Spring 1981). In that version, a constant power-factor command voltage is applied at all times, with no provision for gradual turn-on.

In the improved version (see figure), the constant command voltage is disconnected during a startup interval of 5 to 30 seconds. During that interval, the constant command voltage is replaced by a ramp signal that is summed with the operating power-factor signal from the phase detectors to produce a starting control signal.

The combination of R_3 and C_3 applies a disabling voltage to the integrator during the first 100 or so milliseconds, to insure that no control signals are processed by the integrator until the substitute control signals are established. Similarly, the oscillator blocker grounds the oscillator output for the first 10 milliseconds until the integrator is fully disabled.

Transistor Q_1 is turned on during the entire startup time, so as to short the "run" command voltage from the R_1 cursor to ground. Transistor Q_2 is held in the "off" state during this period and is turned on at the end to short the startup command signal to ground, thus preventing the startup signal from being processed in the integrator with the other control signals during steady running.

The startup ramp signal is generated by the integrating circuit of R_4, C_4, and A_2. A negative-going ramp is produced, with a time constant determined by R_4 and C_4 selected so that the motor turns on at the desired rate. A positive bias

from potentiometer R_5 is added to the ramp voltage, and this combined startup command signal is applied through R_6 to the integrator. The startup ramp is also applied to the inverting input of operational amplifier A_1. Acting as a comparator, A_1 switches Q_1 off and Q_2 on when the ramp voltage starts to go below the non-inverting-input bias voltage set by R_7 and R_8. This transition marks the end of the startup interval.

In all other respects, the circuit functions like the earlier version. The startup or "run" command signal is summed with the phase-detector outputs, and the resulting combined control signal is processed through the integrator and the remainder of the circuit. The modification extends the capability of the controller to reduce power consumption during starting as well as during full-speed operation and to provide a single control circuit for all stages of operation.

This work was done by Frank J. Nola of **Marshall Space Flight Center.** *For further information, Circle 2 on the TSP Request Card.*

This invention is owned by NASA, and a patent application has been filed. Inquiries concerning nonexclusive or exclusive license for its commercial development should be addressed to the Patent Counsel, Marshall Space Flight Center [see page A5]. Refer to MFS-25586.

Implementing Exclusive-OR Logic

A basic four-input XOR is assembled from one decoder and one NAND gate.

Lyndon B. Johnson Space Center, Houston, Texas

A BCD-to-decimal decoder and one four-input NAND gate can be wired as a four-input exclusive-OR (XOR) gate. Combining several of the basic two-IC arrangements allows XOR of any number of inputs.

The four-input version is shown in Figure 1. When the BCD input for 1, 2, 4, or 8 is applied, the corresponding decimal pin goes low; all other decimal pins stay high. Only the 1, 2, 4, and 8 decimal pins are connected to the NAND, and none of them would go low if two or more inputs went high or if no inputs went high. Thus the output from the NAND can go high only if just one of the four inputs is high.

Any number of inputs can be treated by expanding this basic concept. For example, a 16-input circuit is shown in Figure 2; the same function using standard logic elements would require more than 50 logic gates.

Not all complementary-symmetry metal-oxide-semiconductor (CMOS) decoders can be used for this application; some produce outputs with invalid inputs (BCD inputs above N = 9) and therefore are not acceptable. Many transistor-transistor-logic (TTL) BCD-to-decimal decoders are satisfactory.

This work was done by Monty E. Hough of Rockwell International Corp. for **Johnson Space Center.** *No further documentation is available.*
MSC-18458

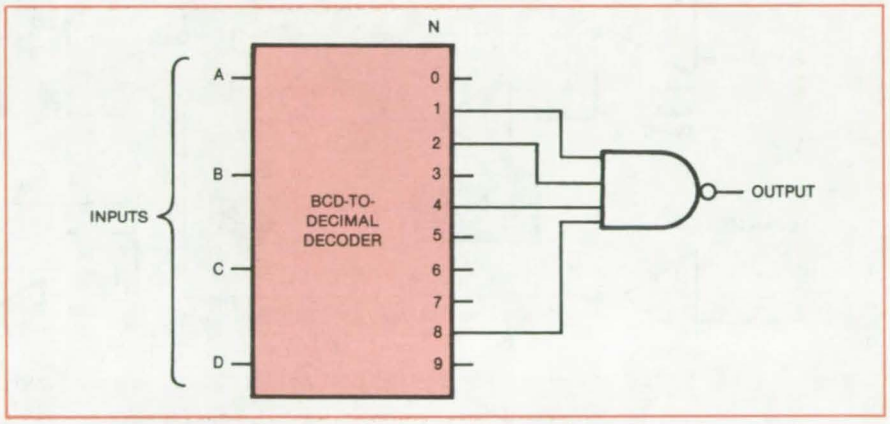

Figure 1. **Two Integrated Circuits,** a BCD-to-decimal decoder and a four-input NAND gate, form the basic four-input XOR circuit. Multiple-input exclusive-OR logic is implemented by combining several of the basic elements as shown in Figure 2.

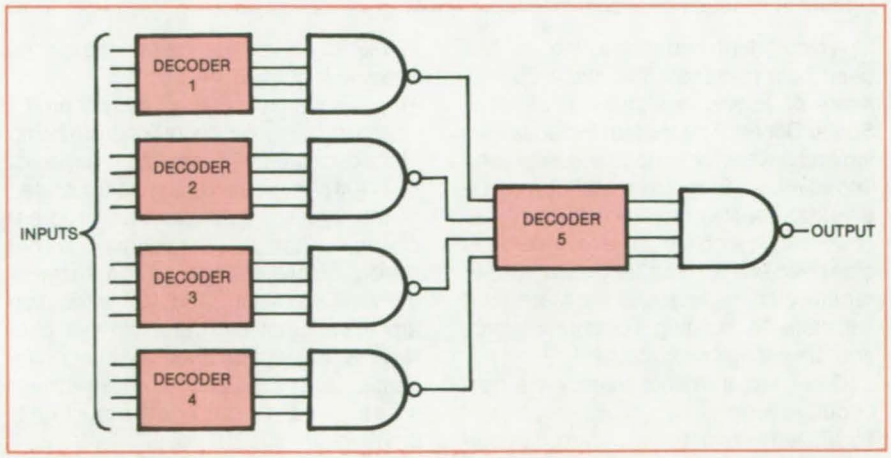

Figure 2. A **16-Input XOR Gate** is assembled from five NAND gates and five decoders. The same principle can be extended to handle more inputs.

Audio Distribution and Monitoring Circuit

A versatile circuit accepts and distributes TV audio signals.

Lyndon B. Johnson Space Center, Houston, Texas

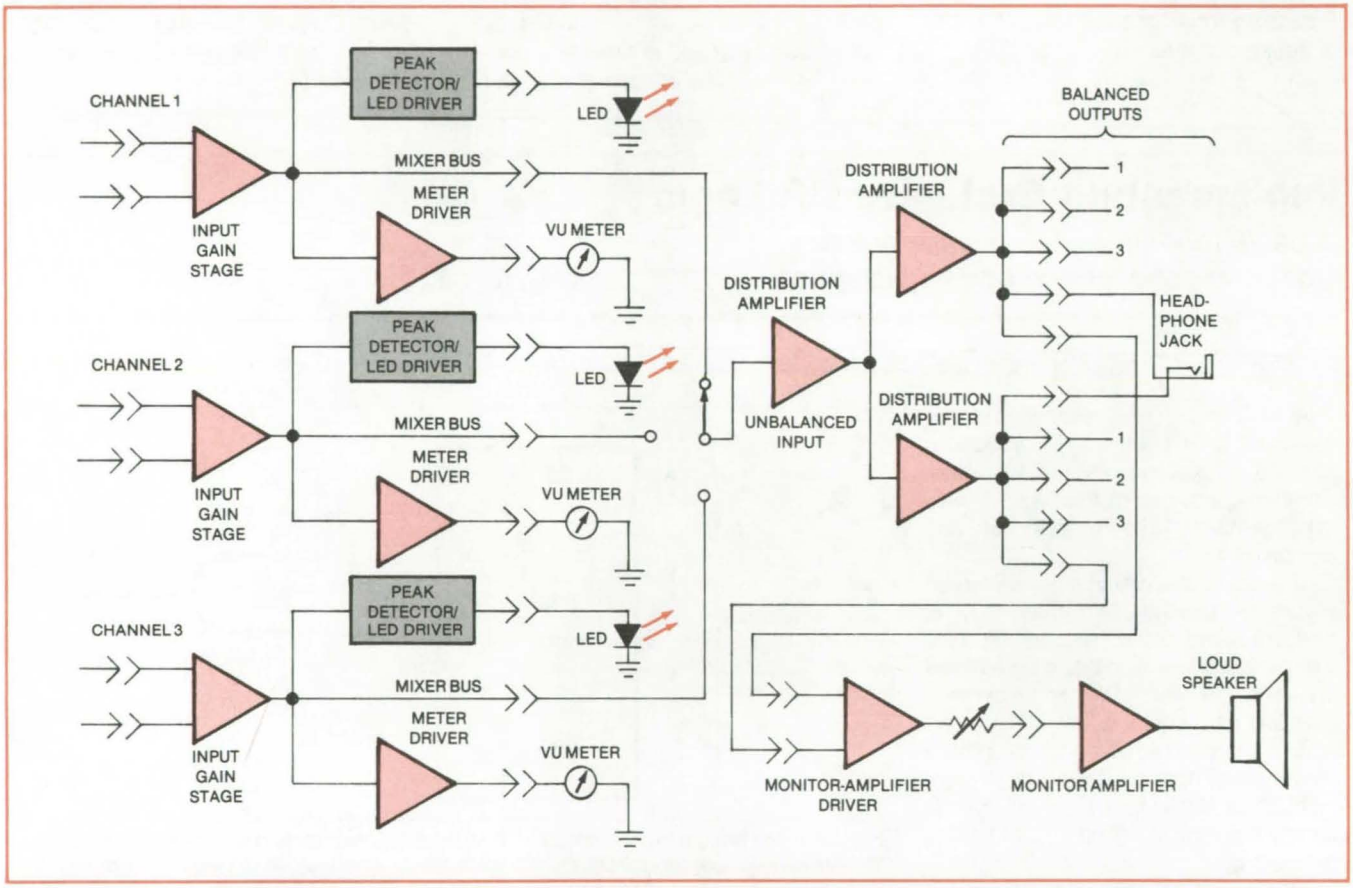

The **Three-Meter Audio Distribution and Monitoring Circuit** provides flexibility in monitoring, mixing, and distributing audio inputs and outputs at various signal and impedance levels.

A distribution and monitoring unit has been built to handle the audio components of television signals at Johnson Space Center. The system includes mixing and drivers for various line levels and impedances. Program material may be simultaneously monitored on three channels. A single-channel version has also been built to monitor transmitted or received signal levels, drive a speaker, interface to building communications, and drive long-line circuits.

Other requirements met by the new circuit include:

- Sufficient drive for standard volume-unit (VU) indicators,
- Flexibility of VU reference levels so that meter indications reflect operating levels relative to those required for local or long-line circuits,
- One output stage to drive a monitor amplifier and/or a long line,
- Flexibility of impedance matching of inputs and outputs, and
- Input isolation to prevent more than 0.1 percent harmonic distortion from being introduced onto lines being monitored.

The three-meter version is illustrated in the figure. There are four program channels (the fourth channel is not used), a driver stage for an external monitor amplifier, and a distribution amplifier. Each program channel contains a balanced, bridging input gain stage, an unbalanced meter-driver stage, and a peak detector/light-emitting-diode (LED) driver.

The input stage provides input isolation and level correction for matching to any source and provides drive for a mixer bus if required. The meter driver isolates the meter from the mixer bus and allows independent calibration of each meter. The peak detector/LED driver gives a visual indication of peaks above a predetermined level that may be too fast to be indicated on a VU meter. The three inputs are normally terminated in the broadcast-standard 600 ohms, but can be left open for special applications.

Tests of the three-meter prototype yielded low noise (−80 dBm unweighted), low harmonic distortion (0.015 percent unweighted), excellent frequency response (−0.3 dB at 10 Hz, 1,000 Hz reference, −0.5 dB at 50 kHz), and low intermodulation distortion (0.007 percent).

This work was done by James M. Kirkland of Taft Broadcasting Corp. for **Johnson Space Center.** *For further information, Circle 3 on the TSP Request Card.*
MSC-20073

500-Watt, 10-GHz Solid-State Amplifier

X-band system amplifies
low-duty-cycle pulses.

NASA's Jet Propulsion Laboratory, Pasadena, California

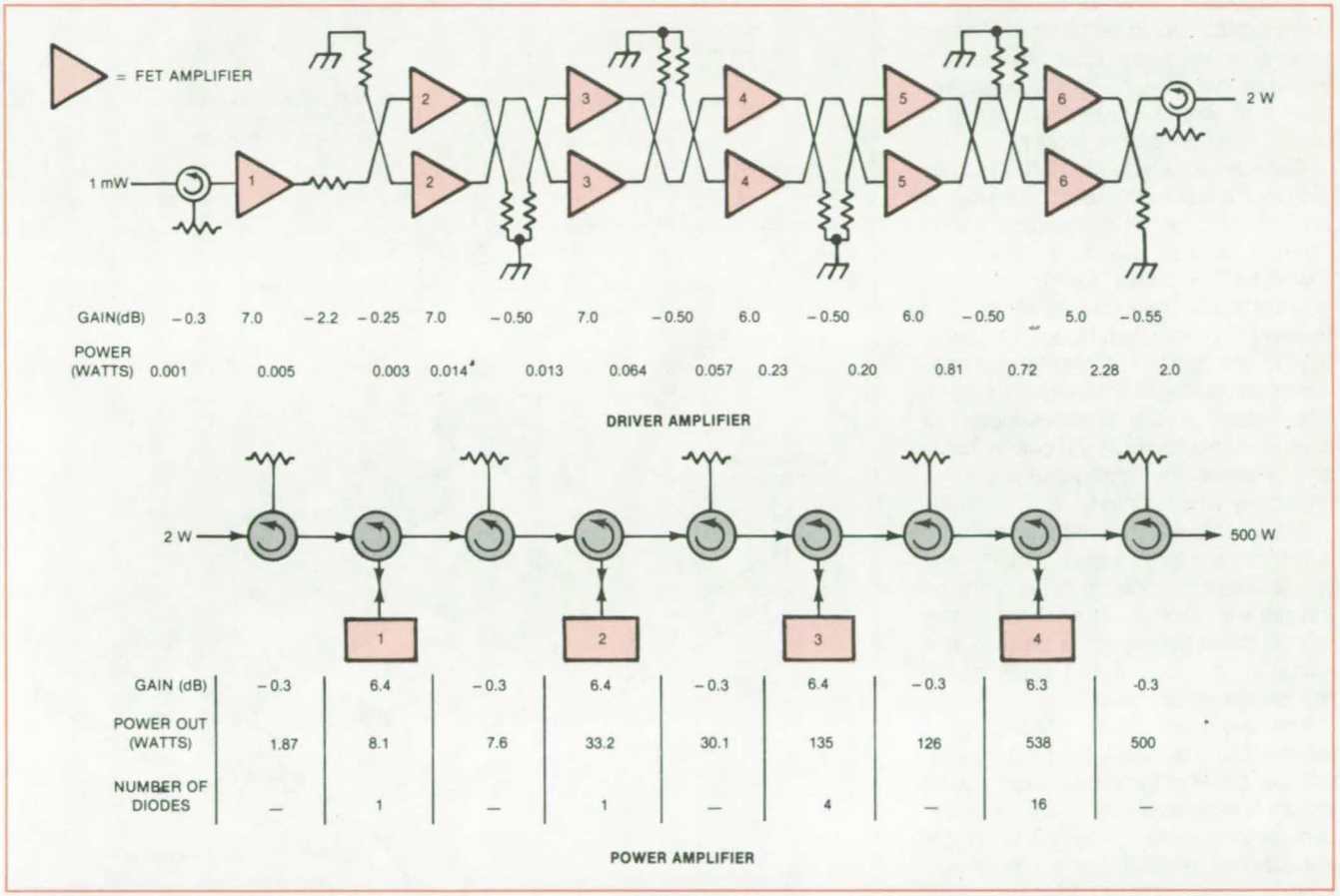

This Amplifier Chain consists of a driver-amplifier section (top), using GaAs FET's with hybrid couplers, and a power-amplifier section (bottom), using IMPATT diodes with circulators for input/output coupling and for isolation between stages.

A new, all-solid-state amplifier chain delivers a pulsed 10-GHz signal with peak power of 500 watts. The chain consists of two sections: A six-stage driver amplifier using gallium arsenide field-effect transistors (FET's) to boost milliwatt input pulses to 2 watts, and a four-stage power amplifier using impact-avalanche-and-transit-time (IMPATT) diodes to raise the 2-watt pulses to 500 watts. The duty cycle of the 10-GHz pulses is sometimes too low (duration 4 μs, repetition period 4 ms) to keep the IMPATT diodes at the temperature for proper operating impedance, so preheat bias pulses are applied to them by a bias-pulse modulator before RF output is to be produced. Likewise, for efficient, class A operation of the FET's, their biases are turned on before each RF pulse and turned off afterward.

As can be seen in the figure, the first stage of the driver is a single FET, and the next five stages use 3-dB quadrature hybrid power splitters/combiners to combine pairs of FET's in a balanced configuration. The balanced-pair power combining is essential for the 2-watt output from the sixth stage. In addition, the hybrids isolate the successive stages to improve the stability and phase linearity of the amplification. The driver has a certain inherent reliability in that it will continue to produce one-fourth of its normal output power if either device in a balanced pair should fail.

In the power-amplifier portion of the circuit, where two-terminal devices (i.e., diodes) are used for amplification, three-port circulators are used for input/output and for isolation between stages. The first two IMPATT stages are single-diode coaxial reflection amplifiers. The final two stages are cylindrical-resonant-cavity power combiners with 4 and 16 diodes, respectively.

The new solid-state X-band amplifier package constitutes a reliable, lightweight, compact, RF source. It can be used for many applications involving low- and variable-duty-cycle operation as well as fixed- and high-duty-cycle operation.

This work was done by Kenneth J. Russell and Octavius Pitzalis, Jr., of Hughes Aircraft Co. for **NASA's Jet Propulsion Laboratory.** *For further information, Circle 4 on the TSP Request Card.*
NPO-15022

Integrated Submillimeter-Wave Mixer

Planar construction would improve reliability and reduce noise.

NASA's Jet Propulsion Laboratory, Pasadena, California

A proposed mixer for submillimeter-wave signals would be fabricated as an integrated semiconductor structure. It would be made by molecular-beam epitaxy and would contain an array of planar Schottky-barrier diodes.

Gallium arsenide Schottky-barrier diodes are commonly used as mixers at wavelengths longer than about 1 mm. These devices have a fine wire ("whisker") contact for the low-frequency signal produced by mixing and for coupling the high-frequency radiation to the diode. At shorter submillimeter wavelengths, however, the parasitic losses in the semiconductor increase. The whisker is difficult to install and makes an unreliable contact, especially when cooled.

The losses would be reduced by using a semiconductor of higher mobility and by placing both contacts of the diode on the same surface. Integrating the diodes with a thin-metal antenna pattern in a planar technology would yield stable, repeatable structures.

The proposed mixer consists of a substrate of near-intrinsic gallium antimonide on which are deposited doped indium arsenide regions and a metalization pattern (see figure). Parts of the metalization pattern act as a phase-array antenna. With a dielectric superstrate on top of the pattern, it efficiently couples incident radiation from a signal source and from a local oscillator to the diodes. The undoped GaSb substrate is an insulator at submillimeter-wave frequencies. The InAs regions contain a highly-doped n+ part and a smaller moderately-doped n part. The n layer and the metal contact atop it form the active Schottky-barrier diode. The n+ layer provides a low-resistance path between the diode and the opposing metal contact.

The n layer must be precisely controlled in terms of doping (in the 10^{14}-to-10^{16}-cm^{-3} range) and thickness (0.2-to-2.0-μm range) to match the depletion-layer width of the Schottky barrier at the operating bias, otherwise parasitic resistance will be excessive.

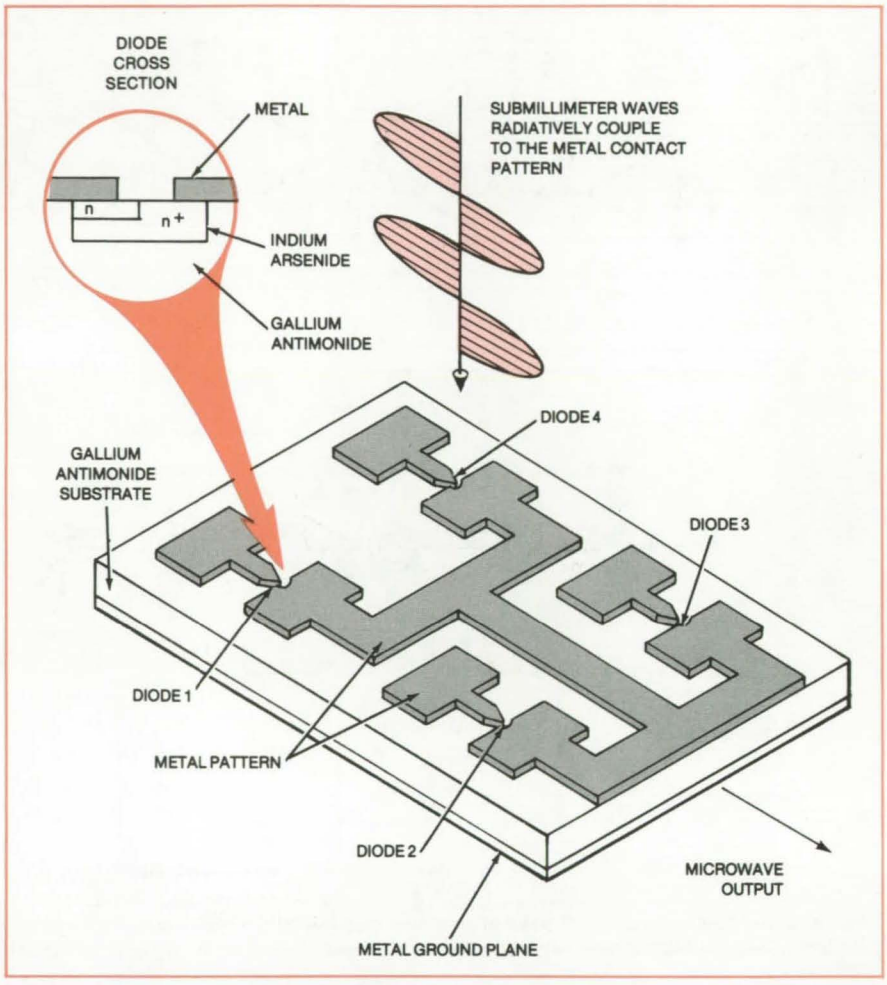

Indium Arsenide Schottky-Barrier Diodes in a gallium antimonide substrate mix submillimeter waves, producing a much lower frequency output. The integrated diode array has a relatively-high signal-to-noise ratio and wide frequency band. It operates at moderate cryogenic temperatures (100 K).

Furthermore, because of charge accumulation at an abrupt InAs/GaSb interface, a transition layer has to be implemented that avoids a short circuit along the edge of the lightly-doped InAs region. The nessary control over composition and doping on an atomic scale has recently become possible with molecular-beam epitaxy.

InAs was selected as the diode material in preference to indium antimonide because its lattice matches that of GaSb, which functions as a dielectric over a wider range of submillimeter wavelengths. InSb, in contrast, though giving slightly lower losses in the diode than InAs, would be useful as dielectric substrate only at the shortest wavelength of interest (0.15 mm).

This work was done by Joseph Maserjian, Udo Lieneweg, and Marvin Litrak of Caltech for **NASA's Jet Propulsion Laboratory.** *For further information, Circle 5 on the TSP Request Card.*

NPO-15238

Portable I/V-Curve Tester

Battery-operated electronic load displays current/voltage characteristic on a portable oscilloscope.

NASA's Jet Propulsion Laboratory, Pasadena, California

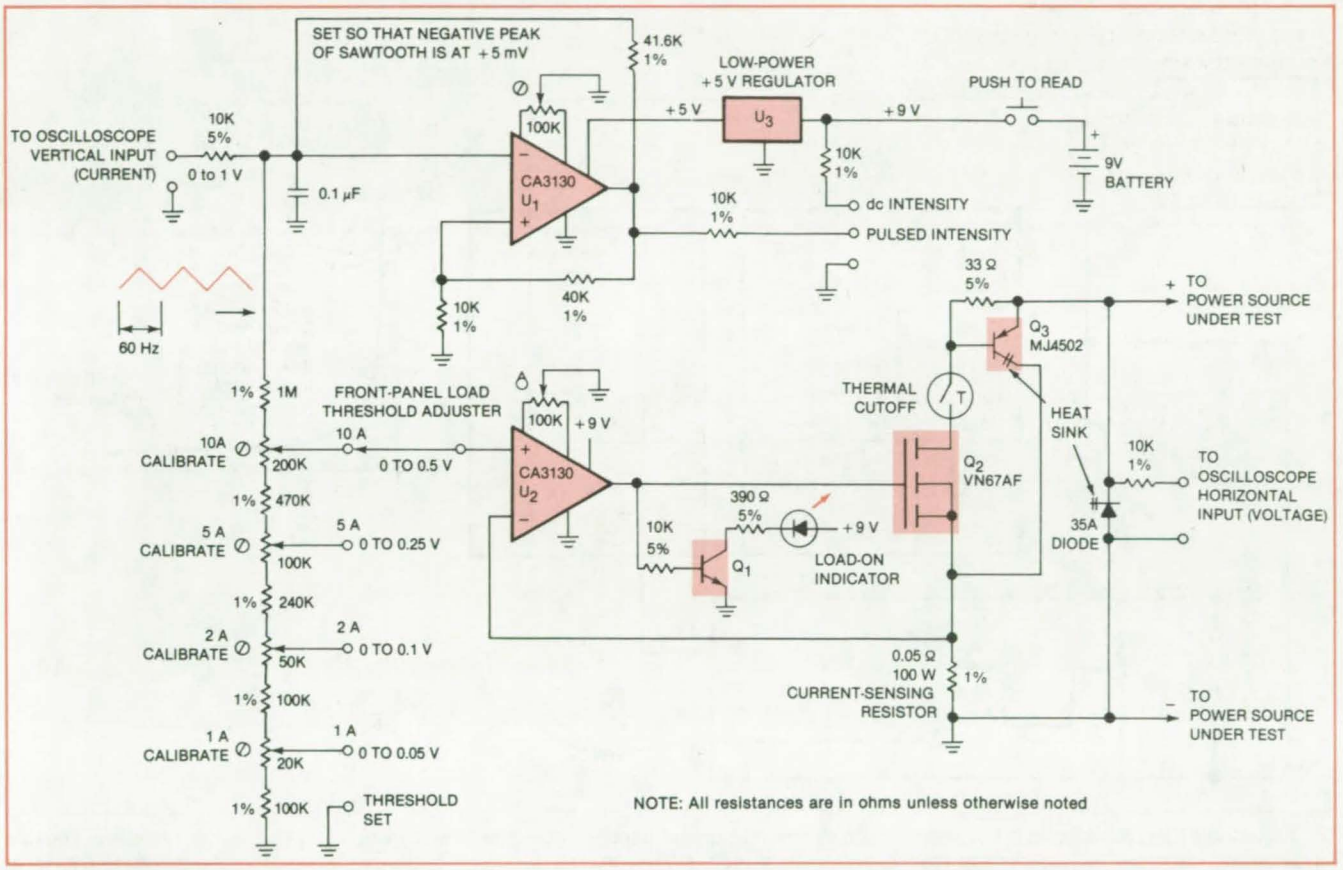

An **Electronic Load Circuit** for displaying current/voltage characteristic curves of power sources uses low-cost low-power CMOS operational amplifiers to control load current flowing through power MOSFET Q_2 and main load transistor Q_3. A thermal cutoff device turns off transistor Q_3 in case of overload. To maximize battery life, the battery is connected via a "push-to-read" momentary-contact pushbutton switch.

A load-simulator circuit measures the current/voltage characteristics of photovoltaic solar-cell arrays. Since low-power complementary-metal-oxide-semiconductor integrated circuits are used, a 9-volt transistor-radio battery could power the circuit for field use.

The circuit is shown in the figure. Operational amplifier U_1 produces a 1-volt peak-to-peak sawtooth waveform. The sawtooth signal is proportional to, and is used to control, the current drawn from the power source being tested.

The sawtooth signal is also connected to the oscilloscope vertical input (current axis). The horizontal axis (voltage axis) is across the power source through a 10-kΩ resistor. The sawtooth energizes a voltage divider to provide a control signal for the servo loop controlling the main load transistor Q_3. A switch selects the tap corresponding to the desired current range, and a calibration adjustment potentiometer is provided for each tap.

Operational amplifier U_2 compares the sawtooth voltage to the voltage drop across the 0.05-Ω load-current sensing resistor. U_2 drives the gate of transistor Q_2, which in turn drives the base of the main load transistor Q_3. If the load current is lower than it should be at any moment, the voltage across the sensing resistor will be lower than the sawtooth voltage. This will cause the output of U_2 to go further positive, increasing the currents through Q_2 and Q_3 until the error is corrected.

An extra position on the range switch is used when adjusting the load threshold control so that the load current goes to zero when the sawtooth voltage goes to zero. The control is adjusted until the light-emitting diode "load-on" indicator goes out.

The circuit could be adapted for use with a slower display device, such as an X/Y recorder by increasing the value of the 0.1-μF integrating capacitor connected to the inverting input of U_1. The CA3130 operational amplifiers chosen for this circuit have good power-supply rejection so that they are well suited to portable battery operation. A regulator keeps the sawtooth amplitude constant.

This work was done by Steven W. Cole of Caltech for **NASA's Jet Propulsion Laboratory.** *For further information, Circle 6 on the TSP Request Card.*
NPO-15266

Electronic Load Tests High-Voltage Solar Arrays

An adjustable load is provided by a combination of transistors and resistors.

NASA's Jet Propulsion Laboratory, Pasadena, California

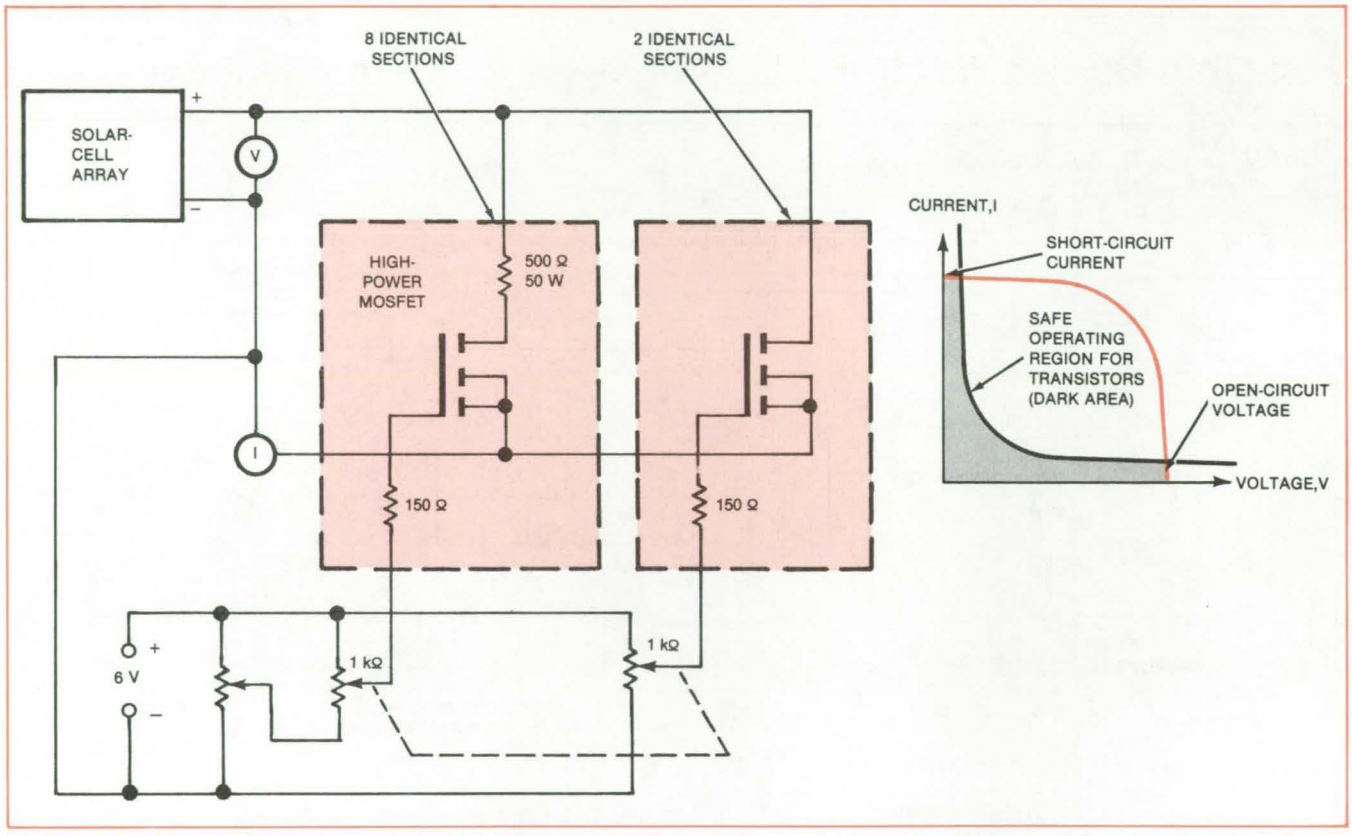

The **Adjustable Electronic Load** in the solar-cell-array test instrument uses ten power MOSFET's and eight 50-Ω series resistors. The two gate-control voltages that adjust the load are derived from a single, manually-operated, ganged potentiometer control. The third adjustable resistor adjusts the relative turn-on points of the two groups of transistors. A typical current/voltage curve for the solar array is shown at the right.

An electronic load instrument for field and laboratory measurement of photovoltaic power systems has digital displays of solar-cell-array output current and voltage. It also supplies analog signals for driving an x-y plotter. The instrument has been used to measure current/voltage characteristics of solar-cell arrays with open-circuit voltage of 350 volts and short-circuit current of 2.5 amperes.

Fixed resistors and high-voltage, high-power metal-oxide-semiconductor field-effect transistors (MOSFET's) are used in the circuit (see figure). A single control continuously adjusts the load from open circuit to short circuit. Unlike the bipolar power transistors used in conventional circuits, MOSFET's are immune to second breakdown (thermal runaway) and are thus easy to operate in parallel. The transistors are turned on at different points over the control range in a manner that operates each transistor within its power dissipation limit.

To avoid exceeding the power dissipation limit of the transistors, it is necessary to use current-limiting resistors in series with the transistors, except at lower voltages. In the circuit shown in the figure, a group of eight transistors is operated in this manner. (Alternatively, a larger number of transistors could have been used without the resistors.)

As the eight transistors are gradually turned on, the current/voltage curve of the solar-cell array is traced out from the open-circuit voltage point, past the knee of the curve where the power output is greatest, into the lower-voltage, constant-current region. Because of the series resistors, however, that part of the circuit cannot load the solar-cell array sufficiently to reach the short-circuit, zero-voltage point.

A second group of two transistors without series resistors gradually takes over the load from the first group in the low-voltage region to continue the current/voltage curve down to zero volts.

This type of electronic load is also suitable for testing other types of high-

voltage power supplies. Since it is controlled by the voltage signals applied to the gates of the transistors, it could be controlled by electrical signals from other devices to present any sort of time-varying load that might be required. It can thus also be remotely controlled.

This work was done by Emmett L. Miller of Caltech for **NASA's Jet Propulsion Laboratory.** *For further information, Circle 7 on the TSP Request Card.*

Inquiries concerning rights for the commercial use of this invention should be addressed to the Patent Counsel, NASA Resident Office-JPL [see page A5]. Refer to NPO-15358.

Flip-Chip Carrier Would Match Microwave FET Impedances

Impedance transformers are part of the mounting and contact strips.

Goddard Space Flight Center, Greenbelt, Maryland

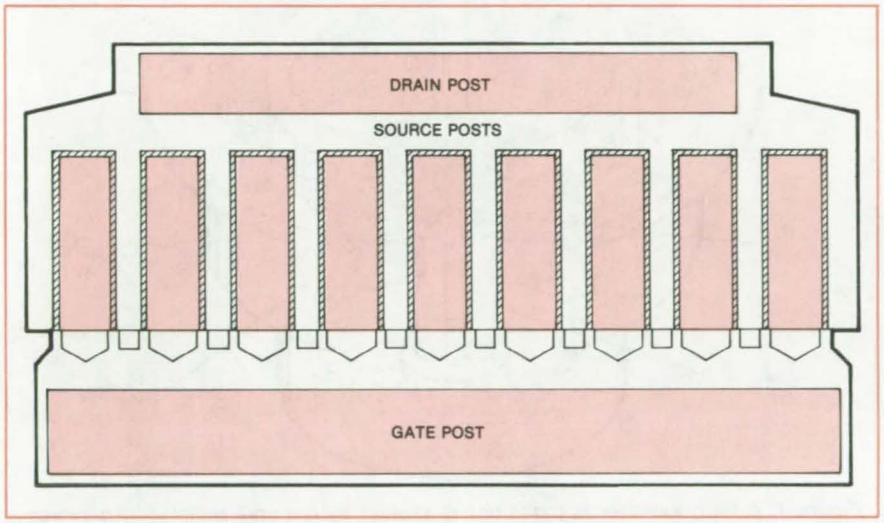

Figure 1. The **Proposed Field-Effect Transistor** would consist of three cells, such as the one shown here.

A proposed field-effect transistor (FET), roughly 2.5 mm long and 0.6 mm wide, would put out 3.5 watts at frequencies from 12 to 16 GHz. Posts plated onto the source, gate, and drain pads would allow flip-chip mounting to a special carrier. The gate and drain pads would be bonded directly to the carrier at metalized areas that are the proper width and length to serve as impedance-transformer sections of transmission line. Unwanted parasitic impedances are thus eliminated, and the bandwidth of the FET amplifier is greatly improved because the matching starts right at the terminal of the active channel.

Figure 1 shows a unit cell of the FET: Three such cells make up one complete FET pellet. A schematic of the three-cell FET, flip-chip mounted onto the carrier, is shown in Figure 2.

The gate pad width is 650 microns, which corresponds to a line impedance of about 15 ohms. The drain pad width is 500 microns, corresponding to a line impedance of 20 ohms. The input (gate) lines are paralleled after an electrical length of 40° at band center (14 GHz), and the output (drain) lines are paralleled after about 50°. These stub lengths and impedances for matching each cell were found by computer-aided design.

This work was done by Ho Chung Huang of RCA Corp. for **Goddard Space Flight Center.** *For further information, Circle 8 on the TSP Request Card.*

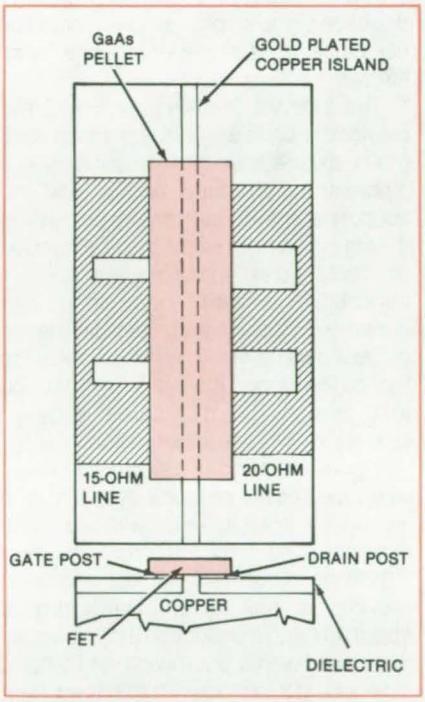

Figure 2. The **Pellet is Flip-Chip Mounted** on a carrier, with the source grounded and the gate and drain posts connected directly to impedance-matching transmission-line segments.

This invention is owned by NASA, and a patent application has been filed. Inquiries concerning nonexclusive or exclusive license for its commercial development should be addressed to the Patent Counsel, Goddard Space Flight Center [see page A5]. Refer to GSC-12442.

Dipole-Excited Ring Antenna

Two-cavity antenna radiates low-side-lobe patterns.

Lyndon B. Johnson Space Center, Houston, Texas

A dipole radiator drives a ring radiator in a new compact C-band antenna. The antenna, which has been breadboarded and tested, can be mounted flush with a surface. Compared with a horn or a parabolic dish with the same aperture, the new ring antenna has greater gain, lower side lobes, and narrower beamwidth. It can be used on vehicles requiring flush-mounted antennas with very directive signals; for example, it could be used as a radar altimeter antenna for an aircraft.

The antenna (see Figure 1) has two cylindrical cavities, with the same symmetry axis: a lower cavity containing a dipole primary radiator and its feed and support and an upper cavity containing the ring. The ring, which can be circular or rectangular in cross section, is parasitically excited by the dipole. It is supported by posts that rise from the top of the dipole cavity. A radome covers the top of the upper cavity. A variation on this design might include crossed dipoles for circular polarization.

Figure 2 shows the gain improvement of the two-cavity antenna over that of a waveguide horn antenna with the same aperture. The new antenna exhibits a 2.5-dB improvement in gain. It also radiates a half-power beamwidth of about 40° and side lobes 18 dB down, as compared with a beamwidth of 60° and side lobe 13 dB down for a feed horn antenna. For comparison, the depth of the new antenna is about half a wavelength and the horn antenna more than a wavelength.

This work was done by Haynes Ellis, Jr., of Rockwell International Corp. for **Johnson Space Center.** *No further documentation is available.*
MSC-20201

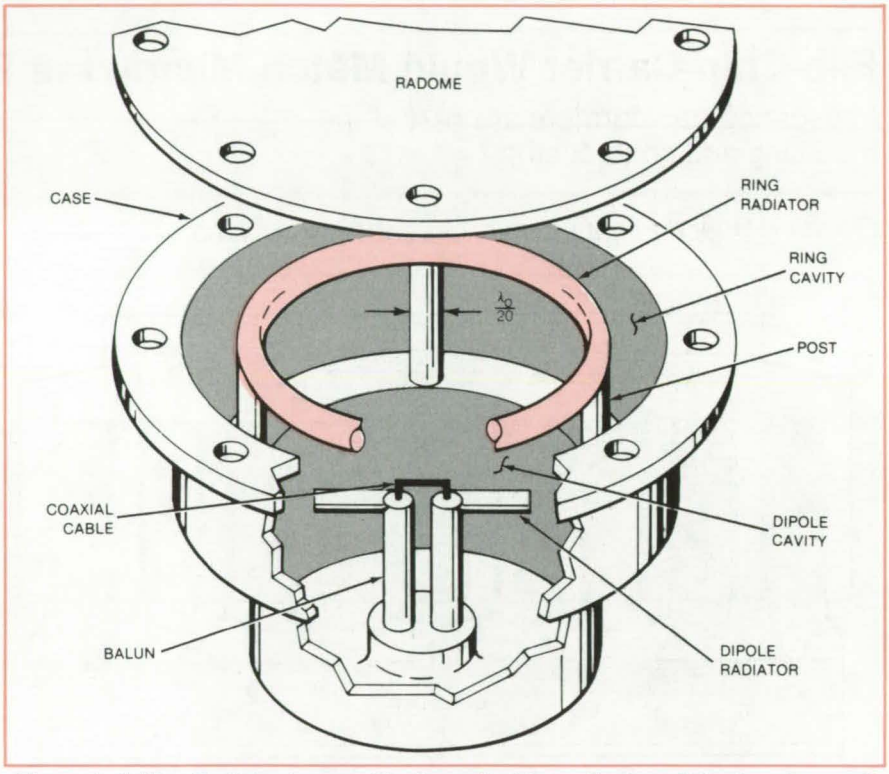

Figure 1. A **Ring Radiator** is parasitically excited by a dipole radiator in a two-cavity antenna. The lower cavity diameter is four thirds the wavelength of the center frequency (λ_0) and is $\lambda_0/4$ deep; the upper cavity is about $5\lambda_0/3$ in diameter and is also $\lambda_0/4$ deep.

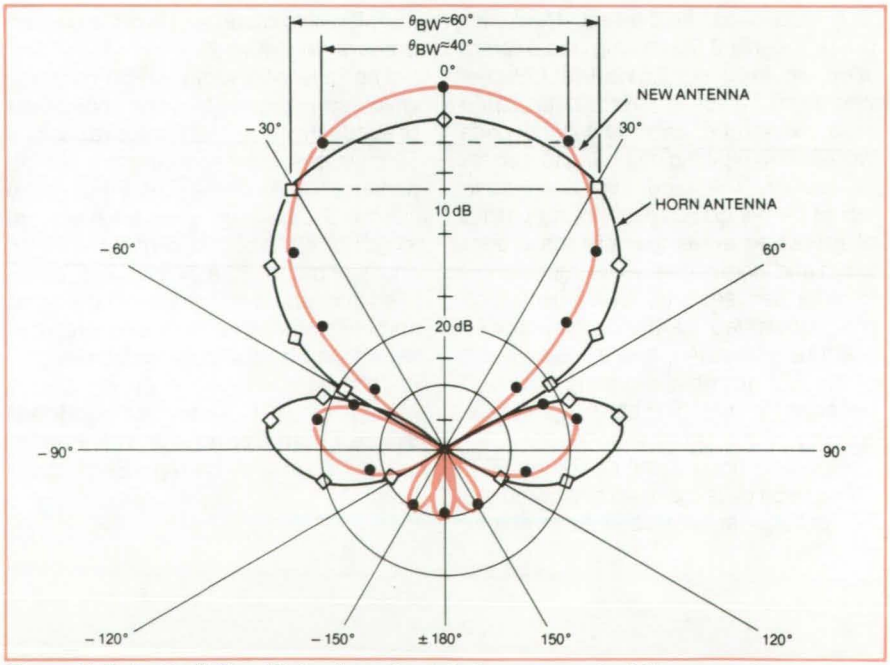

Figure 2. **Polar-Radiation Plots** show the gain improvement of the new antenna over a horn antenna.

Electronic Systems

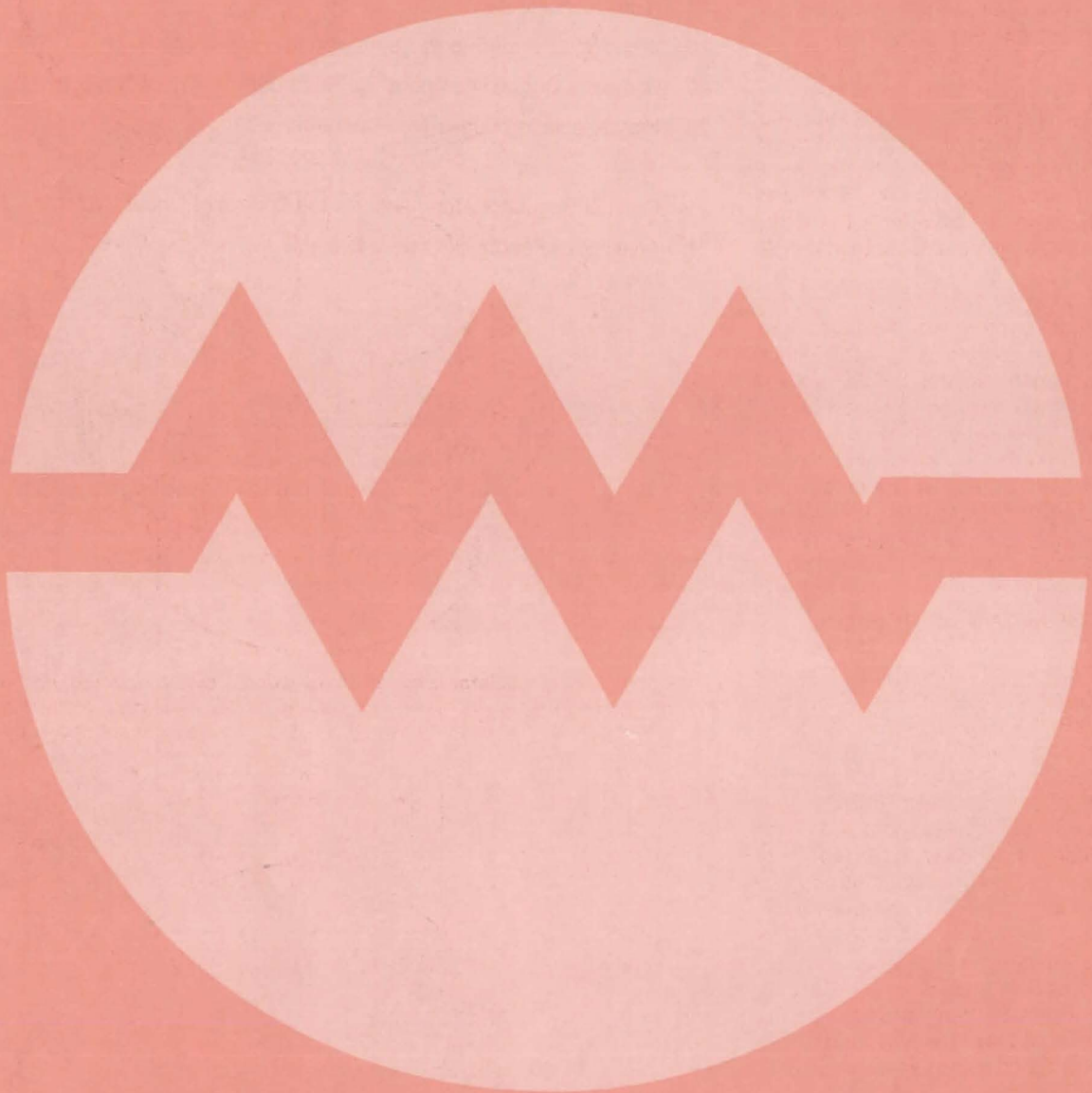

Hardware, Techniques, and Processes

Computer Programs

Pulsed Phase Shifter Improves Doppler Radar

Periodic phase inversion puts Doppler signal on a carrier for easy amplification and processing.

Lyndon B. Johnson Space Center, Houston, Texas

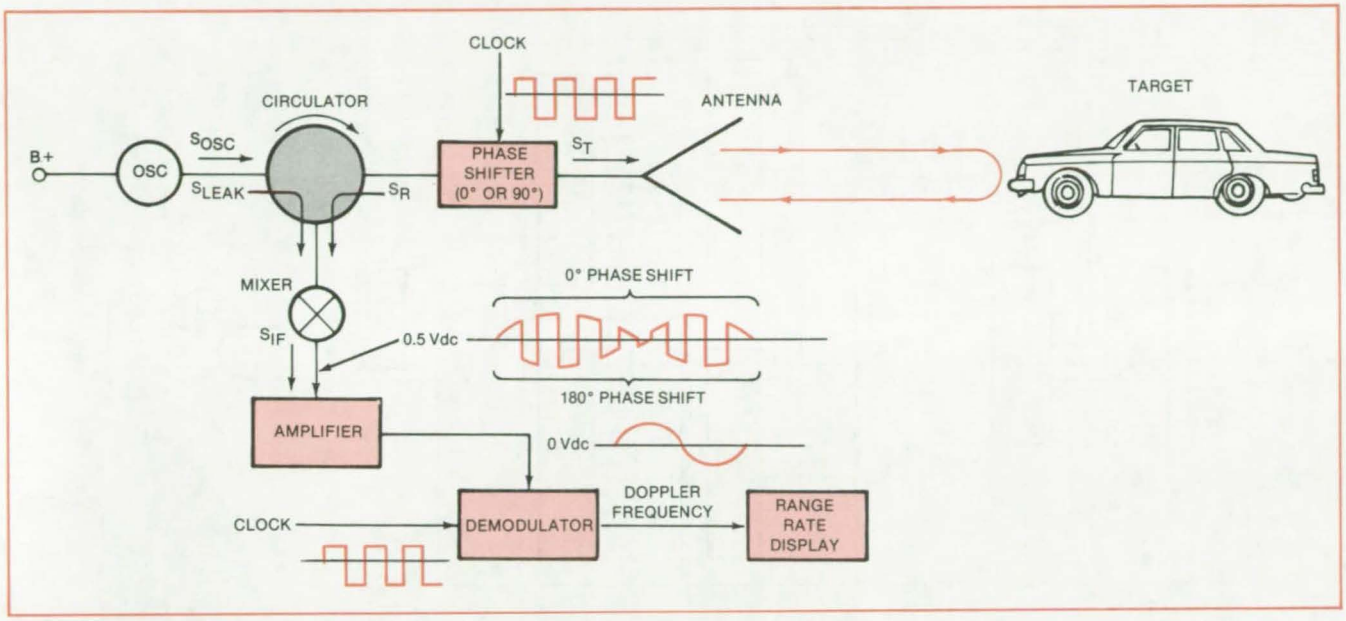

Periodic 90° Phase Shifting of both the transmitted and received radar signals occurs at a rate that is slow compared to the travel times to and from the moving target but fast compared to the Doppler waveform. The effect is a 180° phase reversal in the detected signal. The reversal rate is fast compared to the Doppler frequency, however, and therefore serves as a carrier for the Doppler signal after mixing. The Doppler signal can therefore be amplified and processed more conveniently than if it were at baseband.

The ability of a microwave Doppler radar to measure the velocity of a slow-moving nearby target is enhanced by a pulsed 90° phase shifter in the radar transmission line between the circulator and the antenna. Because of the phase shifting, the Doppler frequency is detected as modulation on a carrier instead of as a baseband signal. The carrier can be amplified and filtered before demodulation, resulting in a strong, clean demodulated Doppler for measurement and display.

The system is shown schematically in the figure. The oscillator is a Gunn diode, driven by a low-voltage dc source and generating a continuous-wave output at approximately 10 GHz. This microwave signal goes to a circulator, where some leaks to the detection port; most of it emerges from the transmit/receive port, however, and passes through the pulsed phase shifter to the antenna. The phase shifter is driven by a clock signal that periodically delays the phase of the microwave signal by $\pi/2$. The phase-modulated microwaves are then transmitted from the antenna. If they are reflected from a moving target (such as an automobile), the frequency of the reflected signal differs from the transmitted frequency by the Doppler frequency.

The reflected signal received by the antenna is carried back through the phase shifter again, where it undergoes another 90° delay (if the clock signal is still in that phase of its cycle). Thus the reflected wave that finally reaches the circulator has a phase modulation of 180°; the modulation frequency is the clock frequency.

The phase-delayed reflected signal emerges from the detector port of the circulator along with the leakage signal of the (unmodulated) oscillator frequency, and the two are heterodyned in a mixer. The resultant waveform is a carrier at the clock frequency, amplitude-modulated with the Doppler frequency. This signal can be amplified and filtered to reduce the noise component much more easily than a baseband signal of the sort produced by prior Doppler radars, so that the Doppler signal can even be displayed for velocity values as low as zero. Furthermore, the dc signal formed in the mixer is filtered out and therefore does not affect the velocity information.

This work was done by Herbert S. Kobayashi, Paul W. Shores, and Patrick Rozas of **Johnson Space Center.** *For further information, Circle 9 on the TSP Request Card.*

This invention is owned by NASA, and a patent application has been filed. Inquiries concerning nonexclusive or exclusive license for its commercial development should be addressed to the Patent Counsel, Johnson Space Center [see page A5]. *Refer to MSC-18675.*

Converting Time Signals From BCD to IRIG-B

Nine IC's convert parallel binary-coded-decimal time signals to serial IRIG standard time format B.

Lyndon B. Johnson Space Center, Houston, Texas

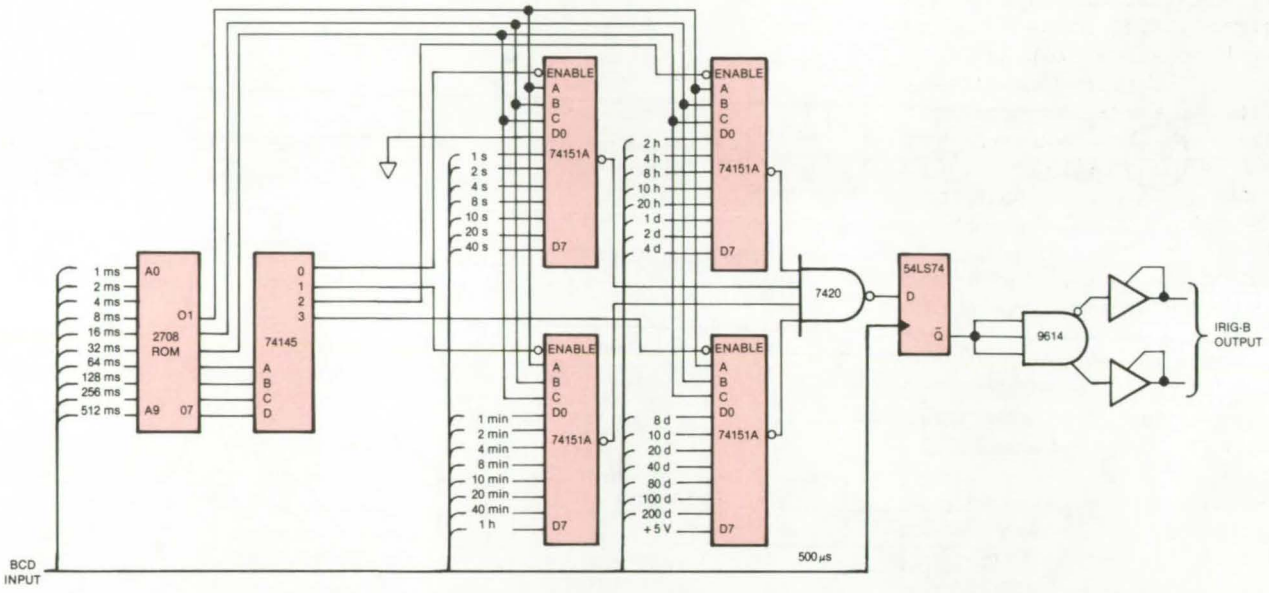

This **Time-Code Converter** converts time signals from BCD representation to IRIG-B representation so that it can be read on a standard time-code reader.

The coded representation of time signals — day, hour, minute, second — can be changed from the binary-coded decimal (BCD) to the IRIG standard time-code format B by a circuit that uses nine integrated circuits. The input to the code-converter circuit is parallel BCD pulses on a bus; the output is the serial pulses of IRIG-B on a single line.

As can be seen from the diagram of the code converter, the BCD representations of milliseconds, seconds, minutes, hours, and days are put to different uses. The milliseconds signals are used to address sequentially a read-only memory (ROM) that is loaded with a pattern corresponding to addresses in four multiplexers. The seconds, minutes, hours, and days BCD signals go directly to the multiplexers.

The contents of the 2708 ROM operate the four 74151A multiplexers, which in turn generate the IRIG-B signal. Thus the converter operates as a lookup table. The outputs from the four multiplexers are combined in the 7420 NAND gate to produce one signal, which is then filtered through a 7474 multivibrator and fed out through a 9614 line driver.

This circuit was developed to drive a display in a simulated cockpit. The IRIG-B generator is synchronized with the master timing-unit emulator.

This work was done by John B. Houston of Rockwell International Corp. for **Johnson Space Center.** *For further information, Circle 10 on the TSP Request Card.*
MSC-18963

Sled Control and Safety System

Microprocessor control keeps the velocity and acceleration within safe limits.

Lyndon B. Johnson Space Center, Houston, Texas

A computerized system for controlling the motion of a linear-track accelerator could be applied to other automated equipment, such as numerically-controlled machine tools and robot manipulators on assembly lines. The system supervises the motion and automatically shuts down if a safety hazard develops.

The original application was in generating drive signals for a "sled" used in tests with human subjects. The sled and subject move along a linear track in a sinusoidal motion of up to 1.5 meters amplitude. The frequency and amplitude are both variables in the tests. To insure the safety of the subject, the system shuts off automatically if the sled acceleration becomes too high, if there is a failure of the computer or other component, or if brake pressure falls.

The control paths between the major system components are shown in the figure. Test parameters, such as the frequency and amplitude of the sled motion, are entered from a control panel and fed to the central processing unit (CPU) through the parallel interface.

The CPU generates the required sine wave digitally; a digital-to-analog converter in the data acquisition and control subsystem (DACS) converts it to the analog form required by the motor controller. The CPU also monitors acceleration, velocity, and position signals from the motor controller; these are digitized in the DACS. In addition, the CPU monitors position-sensing switches located near the ends of the track.

The motor control amplifier maintains a motor speed proportional to the sine-wave signal from the CPU. The amplifier output is the drive current of the motor. The amplifier compares the commanded speed to the actual motor speed and adjusts the current as necessary to speed up or slow down the motor. Inhibiting inputs on the amplifier are used to prevent the amplifier from driving the sled on beyond limit switches near the ends of the track. In normal operation the sled does not quite reach these switches.

The fail-safe system checks for the various runaway and safety-hazard conditions and sends out the interruption and inhibition signals when trouble occurs. Automatic shutdown is accomplished by inhibiting the motor drive current and simultaneously applying the brake. In addition, the test operator may force an emergency shutdown via a single switch located on the control panel.

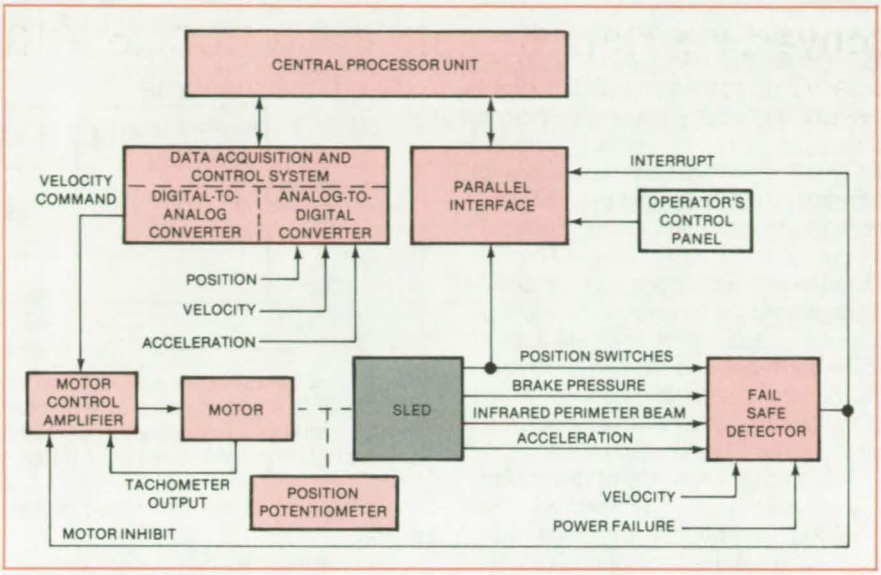

The Control and Safety System controls the motions of the sled with a sine-wave signal created digitally by the microprocessor. Dynamic parameters of the sled motion are monitored so that the sled may be stopped safely if a malfunction occurs. The sled is capable of sinusoidal accelerations up to 0.5 g with a 125-kg load.

This work was done by Larry J. Forrest of Technology, Inc., for **Johnson Space Center.** *Further information, may be found in NASA CR-167425 [N82-10061/NSP], "Operations and Maintenance Manual for the Linear Accelerator (Sled)" [$9.00]. A copy may be purchased [prepayment required] from the National Technical Information Service, Springfield, Virginia 22161.*
MSC-20082

Ride-Quality Meter

Noise and vibration components are summed to produce an index of passenger discomfort.

Langley Research Center, Hampton, Virginia

A portable "ride-quality" meter measures passenger discomfort and the acceptability of vehicle interior noise and vibration. The meter is especially suited for determining vehicle comfort and design tradeoffs and for comparing the ride quality of vehicles.

The ride-meter output is in terms of "discomfort units," which directly relate to passenger subjective acceptance of the measured environment. It is derived from software implementation of psychophysical laws governing human response to combined noise and vibration. Complete recording, analysis, and transformation of measured data into subjective units are done on board the vehicle and in real time. The effects of multiple frequencies and multiple axes of vibration are automatically accounted for, as are the combined effects of noise and vibration (see figure).

Experimental studies utilizing approximately 2,200 test subjects have led to the development of an empirical model for predicting passenger discomfort. The ranges of noise and vibration amplitudes and frequencies used to derive the model include those known to influence passenger comfort most.

The ride-quality meter consists of the following components: sensing elements to measure vibration in five axes (vertical, lateral, longitudinal, roll, and pitch) and interior noise; analysis elements to weight and average the signals generated by the sensing elements; software elements to process the spectral data generated by the analysis elements in accordance with the specialized and detailed psychophysical relationships that define human response to noise and vibration; and readout elements that display all or selected components of subjective discomfort produced by the noise and vibration environment.

The electrical signal corresponding to the acoustical pressure fluctuations is applied to the input of an octave-band analyzer and filter, the output of which is applied as input to a noise-discomfort module that computes the subjective discomfort, D_N, due to the interior-noise environment. The electrical signals corresponding to each of the five vibration

(continued on next page)

acceleration levels are applied to the input of a set of frequency weighting filters that reflect the effect of vibration frequency on human discomfort. The outputs of the filters are then applied to rms detection circuits, which provide weighted rms levels for each axis of vibration. These weighted rms accelerations are then applied to the "comfort" modules, which transform the physical vibration characteristics into subjective discomfort units for each axis. The individual-axis discomfort units are applied to the combined-axis module and then to the duration-correction module, which outputs the total duration-corrected discomfort due to vibration, D_{vib}.

The noise component of discomfort, D_N, is algebraically summed with the vibration component of discomfort, D_{vib}, to generate the total subjective discomfort, D_{total}, attributable to the measured noise and vibration environment. The D_{total} signal is then applied to the visual-display module, which can also display selected values of discomfort produced at earlier stages of the process.

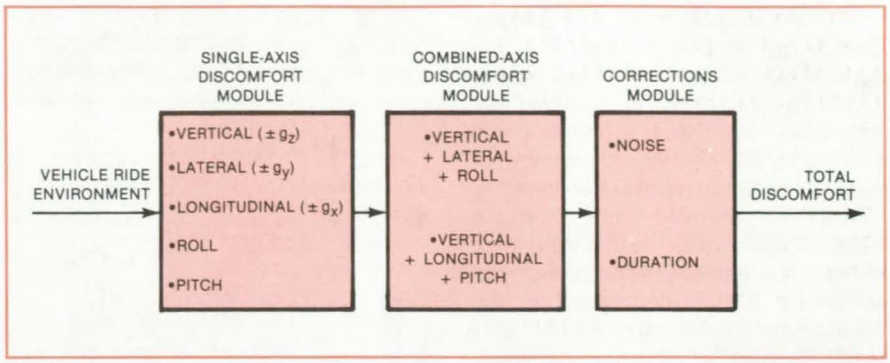

Single- and Combined-Axis Discomfort Are Corrected by the effects of noise and vibration to yield a measure of the total discomfort experienced by a rider. The three modules shown transform mathematically-weighted rms accelerations, which represent the physical vibration characteristics, into subjective discomfort units.

This work was done by Jack D. Leatherwood, Thomas K. Dempsey, Sherman A. Clevenson, and David G. Stephens of **Langley Research Center.** *For further information, Circle 11 on the TSP Request Card.*

This invention is owned by NASA, and a patent application has been filed. Inquiries concerning nonexclusive or exclusive license for its commercial development should be addressed to the Patent Counsel, Langley Research Center [see page A5]. Refer to LAR-12882.

Improving Power-Supply Regulation for Pulsed Loads

A bypass circuit speeds up regulator response to turn-on transients.

Lyndon B. Johnson Space Center, Houston, Texas

A new power-supply voltage-regulator circuit speeds up the response to sudden load changes. As soon as the load increases, an additional feedback path is enabled. This path bypasses, and provides faster loop response than, the normal feedback path. Steady-state instability due to the faster loop response is avoided by progressively disabling the bypass loop and allowing the normal feedback path to take over.

A regulated power supply is supposed to maintain a constant voltage despite changes in the load current. If the current increases quickly, however, as in pulsed applications, the voltage may drop and then recover slowly.

To reduce these voltage changes, pulsed devices such as radar transmitter tubes use power supplies that have a fast-response feedback loop: Any drop in output voltage is sensed and fed to a correcting amplifier, which increases the supply voltage. High-voltage regulators with fast response, however, tend to be unstable under steady-state conditions.

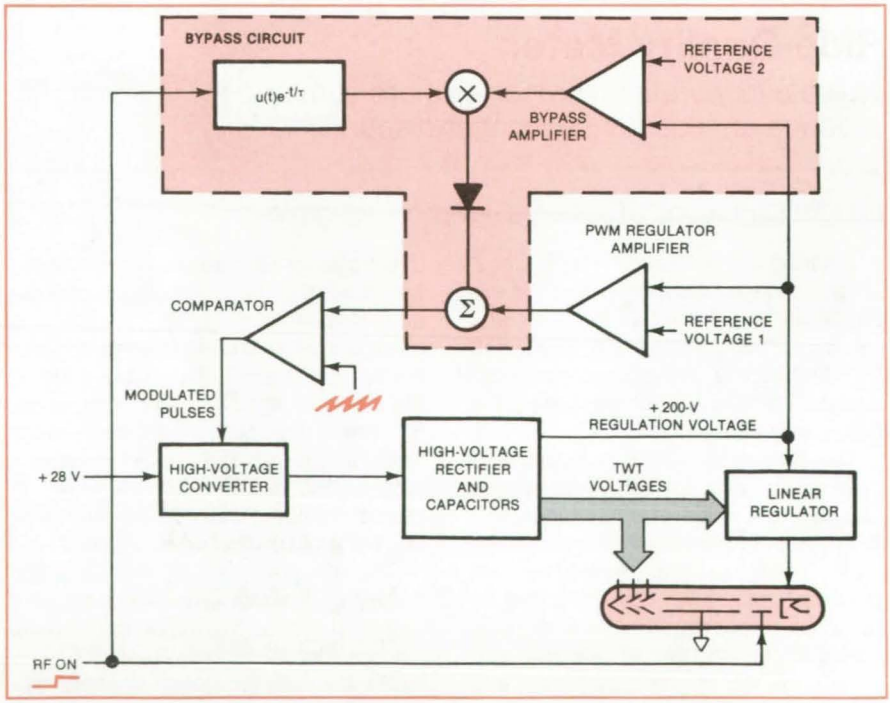

Fast-Response Regulation in this TWT power supply is enabled when the RF ON pulse suddenly increases the power load. The bypass circuit is activated to meet the sudden demand and then is progressively disabled.

The new bypass circuit was devised for a converter power supply that applies voltage to the collector in a pulsed traveling-wave tube (TWT). To minimize power-supply size and weight, the electron-beam collector in the TWT is operated at the lowest possible voltage. Any excessive decay of the collector voltage causes high TWT helix current, which can damage the fragile helix structure.

The power supply with bypass circuit is shown in the figure. During normal operation the bypass amplifier is disabled, and the pulse-width-modulated (PWM) regulator amplifier provides the feedback necessary to maintain the 200-volt regulation voltage on the TWT collector. When the application of a radio-frequency (RF) pulse to the input end of the TWT increases the load from 15 to 150 watts, the 200-V regulation voltage drops significantly, because of the slow response of the PWM regulator amplifier.

The fast-response bypass amplifier is enabled when the RF pulse is turned on. Reference voltage 2 is chosen so that the bypass amplifier will try to regulate the 200-V voltage at a predetermined fraction of its normal value. However, the output of the bypass amplifier is rectified so that it can raise, but not lower, the 200-V regulation voltage. This rectification and the fact that the bypass amplifier output is multiplied by the exponentially-decaying RF ON signal dampens potential oscillations.

The bypass signal is added to the output of the PWM regulator amplifier. Approximately 100 ms after TWT turn-on, the PWM regulator amplifier output is near its steady-state value, the rectifier becomes reverse-biased, and the bypass circuit no longer affects power-suppy operation.

This work was done by Charles R. Gulick and Ronnie B. Chan of Hughes Aircraft Co. for **Johnson Space Center.** *No further documentation is available.*
MSC-20016

Compact, Rugged Temperature Recorder

Unattended solid-state unit stores 2,048 readings taken at intervals of 1.875 to 240 minutes.

Ames Research Center, Moffett Field, California

A small, light, self-contained temperature recorder that was originally developed for use in space experiments can store 2,048 temperature readings taken over a period of almost a year (or much less) and then read them out when a special readout unit is plugged into it. The temperatures may be anywhere in the range from −10° to +50° C and are recorded at intervals selectable by factors of 2 from 1.875 up to 240 minutes. The data can be retained in the recorder for at least 4 months before readout, if desired.

The battery-operated recorder has no moving parts — it is completely solid-state electronic (see figure). The temperature sensor is a linear integrated circuit that produces a current proportional to absolute temperature. Its output signals are converted to 8-bit digital data and stored in read/write memories. After the 2,048 readings have been taken at the predetermined intervals, the recorder switches to an ultra-low-power data-retention mode.

When the data are to be extracted, the recorder is connected to a unit that has analog, digital, and visual light-emitting-diode outputs. The unit also stores the data in semipermanent memories.

The basic recorder can be simplified to accommodate a variety of applications by such changes as the addition of extra memory to store more data, by

(continued on next page)

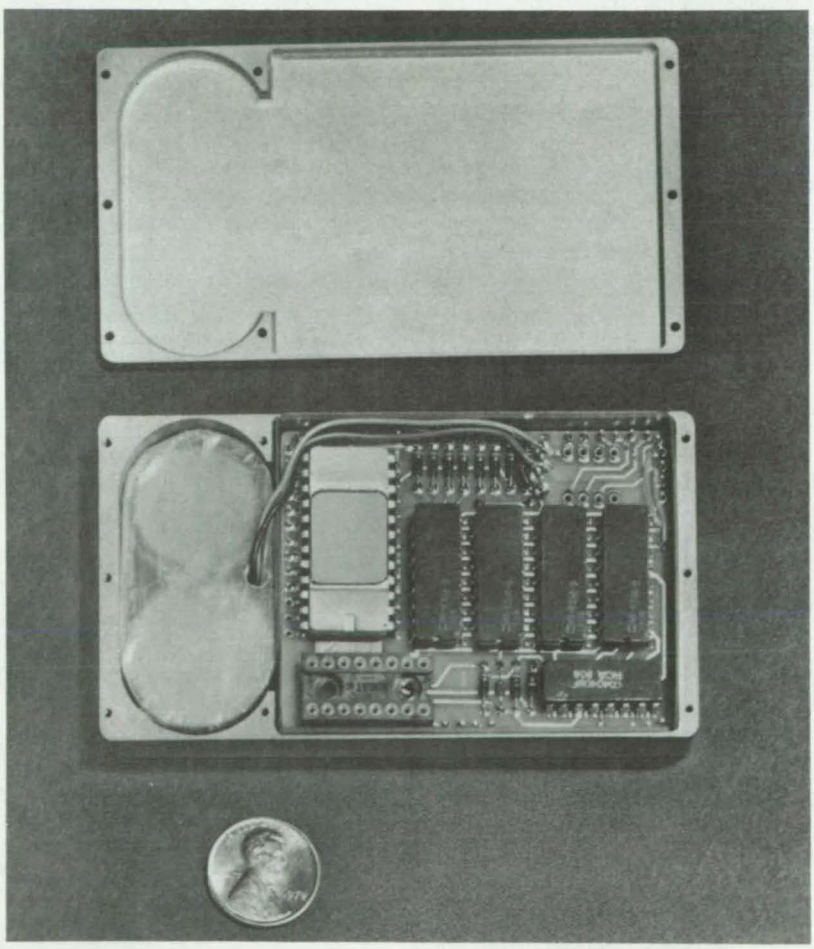

This **Solid-State Temperature Recorder,** shown here in its entirety with the cover removed, is compact, lightweight, and rugged. It can record 2,048 temperature readings over a period of up to nearly a year and retain them for at least another 4 months using just the batteries shown.

changing the front end to permit measurements other than temperature to be made, or by using different batteries to obtain different operating periods.

This work was done by Richard M. Westbrook, Lawrence D. Bennett, Robert A. Steinhauer, and Gordon J. Deboo of **Ames Research Center.** *Further information may be found in NASA TM-81267 [N81-23434/NSP], "A Solid-State Digital Temperature Recorder for Space Use" [$9]. A copy may be purchased [prepayment required] from the National Technical Information Service, Springfield, Virginia 22161.*
ARC-11304

High-Resolution Subsurface-Interface Radar

Mathematical technique yields more accurate information about depth of soil layers.

John F. Kennedy Space Center, Florida

Homomorphic deconvolution signal processing can enhance the information obtained in high-resolution soil-depth measurements by radar. The proposed technique is expected to increase the accuracy with which soil-layer depths are gaged.

The homomorphic deconvolution process involves the use of the inverse forward Fourier transform and complex forward and inverse natural logarithms (see Figure 1). The logarithmic processing forms a time-domain function, or cepstrum.

The intended use is with subsurface-interface radar sounding, in which the subsurface features of soils are mapped. An antenna placed near the ground is shock-excited by a capacitor discharge. The signal penetrates the soil, is reflected by subsurface discontinuities, and is received by the antenna. However, the return signal also contains unwanted multiple reflections created by the soil surface itself and by the mismatch in impedance of the antenna and the soil.

Homomorphic deconvolution aids in separating the unwanted returns. Slowly varying components of the return signal (which represent the transmitted signal) are discarded. Rapidly varying components, which yield information about the separation between soil layers, are preserved (Figure 2). Although homomorphic deconvolution demands considerable data processing beyond that ordinarily required for radar returns, it yields sharper resolution.

This work was done by William J. Steinway of the Georgia Institute of Technology for **Kennedy Space Center.** *For further information, Circle 12 on the TSP Request Card.*
KSC-11212

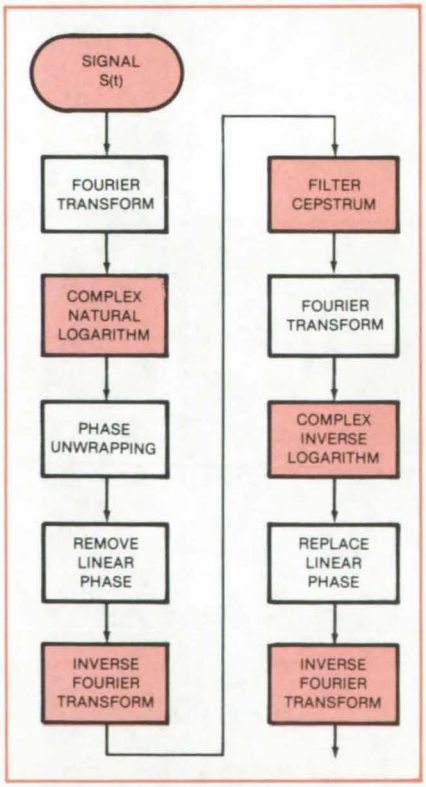

Figure 1. **Homomorphic Deconvolution** processes a time-varying signal S(t) and includes forward and inverse Fourier transform and complex logarithmic operations.

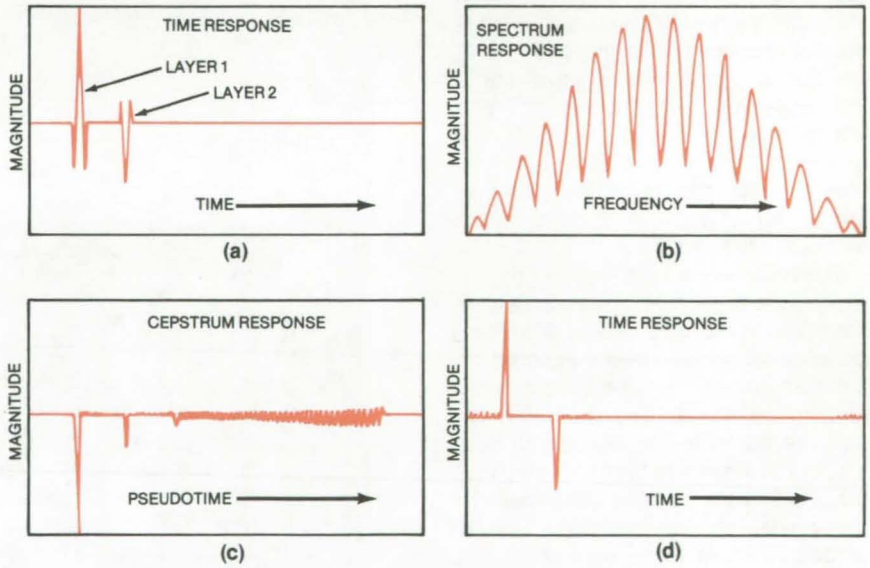

Figure 2. **Signal Processing Is Shown** for unequal signal returns from soil layers at two depths. The reflected pulses appear in (a). The spectrum of the composite returns appears in (b). The period of the rapidly varying component of the spectrum is inversely proportional to the separation of the layers. The high-pass portion of the cepstrum appears in (c). The deconvoluted return appears in (d). The time spread of each of the two returns is smaller in (d) than in (a), so that the resolution of the layer-depth measurement has been increased.

Computer Programs

These programs may be obtained at very reasonable cost from COSMIC, a facility sponsored by NASA to make new programs available to the public. For information on program price, size, and availability, circle the reference letter on the COSMIC Request Card in this issue.

Optimal Regulator Algorithms for the Control of Linear Systems

A rigorous tool for designing multi-input/multi-output control systems

A control-theory design package, called Optimal Regulator Algorithms for the Control of Linear Systems (ORACLS), aids in the design of controllers and optimal filters for systems that can be modeled by linear, time-invariant differential and difference equations. ORACLS is particularly attractive because it is a rigorous tool for dealing with multi-input and multi-output dynamic systems in both continuous and discrete forms.

Optimal linear quadratic regulator theory, currently referred to as the linear-quadratic-Gaussian (LQG) problem, has become the most widely accepted method of determining optimal control policy. Within this theory, the infinite-duration time-invariant problems, which lead to constant-gain feedback control laws and constant Kalman-Bucy filter gains for reconstruction of the system state, are highly tractable and potentially easy to implement. Various new and efficient methods in the field of numerical linear algebra have been combined in ORACLS, which solves time-invariant continuous or discrete LQG problems.

ORACLS is a collection of subroutines that can be used to formulate, manipulate, and solve various LQG design problems. By providing primary operations, an analysis of linear time-invariant systems, and control synthesis based on LQG methodology, ORACLS maintains considerable flexibility at each operational state. The input/output routines handle the reading and writing of numerical matrices, printing heading information, and accumulating output information. The basic vector-matrix operations include addition, subtraction, multiplication, equation, norm construction, tracing, transposition, scaling, juxtaposition, and the construction of null and identity matrices. The analysis routines provide for the following computations: the eigenvalues and eigenvectors of real matrices; the relative stability of a given matrix, matrix factorization; the solution of linear constant-coefficient vector-matrix algebraic equations; the controllability properties of a linear time-invariant system; the steady-state covariance matrix of an open-loop stable system forced by white noise; and the transient response of continuous linear time-invariant systems.

The control law design routines of ORACLS implement some of the more common techniques of time-invariant LQG methodology. For the finite-duration optimal linear regulator problem with noise-free measurements, continuous dynamics, and integral performance index, a routine is provided that implements the negative exponential method for finding both the transient and steady-state solutions to the matrix Riccati equation. For the discrete version of this problem, the method of backward differencing is applied to find the solutions to the discrete Riccati equation. A routine is also included to solve the steady-state Riccati equation by the Newton algorithms described by Klein for continuous problems and by Hewer for discrete problems.

Another routine calculates the prefilter gain to eliminate control-state cross-product terms in the quadratic performance index and the weighting matrices for the sampled-data optimal linear regulator problem. For cases with measurement noise, duality theory and optimal regulator algorithms are used to calculate solutions to the continuous and discrete Kalman-Bucy filter problems. Finally, routines are included to implement the continuous and discrete forms of the explicit (model-in-the-system) and implicit (model-in-the-performance-index) model following theory. These routines generate linear control laws that cause the output of a dynamic time-invariant system to track the output of a prescribed model.

In order to apply ORACLS, the user is required to write an executive (driver) program that inputs the problem coefficients, formulates and selects the routines to be used to solve the problem, and specifies the desired output. The ORACLS routines are written in FORTRAN IV for batch execution. Both CDC and IBM versions of the code are available. The CDC version has been implemented on a CDC 6000-series computer with a central memory requirement of approximately 13K (octal) of 60-bit words. The IBM version has been implemented on an IBM 370-series computer with a central memory requirement of approximately 300K of 8-bit bytes. The CDC version was developed in 1978, and the IBM version was generated in 1981.

This program was written by Ernest S. Armstrong of **Langley Research Center** *(CDC version) and by the Mechanical Engineering Department of Howard University (IBM version). For further information, Circle A on the COSMIC Request Card.*
LAR-12313 and LAR-12953

Analysis of Feedback-Control Systems

Reduced-order feedback-control equations are obtained for use in time- and frequency-domain analysis.

BLOCK IT implements an algorithm that obtains reduced-order feedback-control equations for use in both time- and frequency-domain analysis. In a more general context, BLOCK IT computes a real nonsingular similarity-transformation matrix that reduces a real nonsymmetric matrix to block-diagonal form, each block of which is a real quasi-upper triangular matrix.

The algorithm works with both defective and derogatory matrices. If the program should fail, the algorithm generates data output that can be used as a guide for reformulation of the mathematical equations that lead to the ill-conditioned matrix that could not be block-diagonalized.

(continued on next page)

Frequency response methods are of fundamental importance in the design and performance evaluation of feedback-control systems. Nearly all of the frequency response methods require that the user obtain transfer functions. For multivariable systems, a matrix of transfer functions must be obtained. BLOCK IT offers an automated procedure for obtaining transfer functions expressible as a partial fraction expansion that may be truncated via engineering judgment. Truncation decisions may be based upon gain coefficients that are real numbers formed by a direct multiplication of a modal observability coefficient and a modal controllability coefficient, along with system frequencies.

BLOCK IT utilizes an algorithm for computing reducing subspaces for block diagonalization. The program is tailored to meet the needs of the analyst requiring reduced-order dynamic models for feedback-control analysis. The algorithm is basically a continuation of the procedure used to compute eigenvalues. A sequence of similarity transformations is computed that keeps reducing the partially reduced matrix to successively simpler forms. This sequential procedure ends when the reduced form of the matrix is block-diagonal. The resultant similarity transformation is the accumulated product of the entire sequence of similarity transformations used in the reduction process.

BLOCK IT is written in FORTRAN IV for batch execution and has been implemented on an IBM 370-series computer with a central memory requirement of approximately 500K of 8-bit bytes. The program was developed in 1981.

This program was written by Harold P. Frisch of **Goddard Space Flight Center.** *For further information, Circle B on the COSMIC Request Card.*
GSC-12723

Physical Sciences

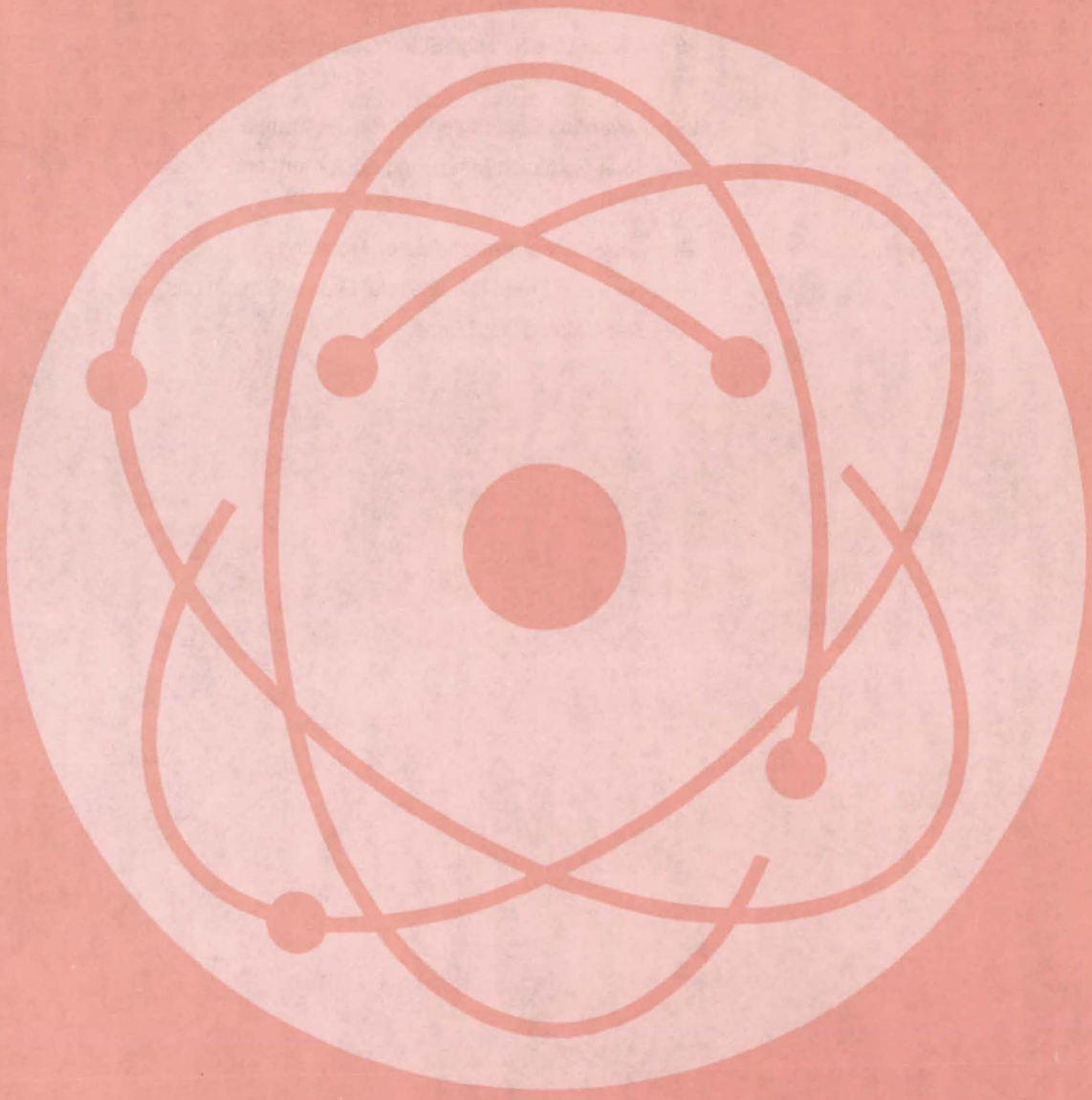

Sunlight-Pumped Laser

Organic iodide gas is stimulated by a portion of the Sun's spectrum to emit laser light.

Langley Research Center, Hampton, Virginia

A gas laser that is pumped by simulated Sunlight was tested in laboratory experiments with a solar simulator. Using a perfluoropropyliodide gas (C_3F_7I) as the lasing medium, the device produced a continuous output of 4 watts at 1.315 μm. Peak power output up to 10 watts and lasing time in excess of 60 milliseconds were obtained for a single static fill.

To verify the potential for flowing the lasant, experiments with quasi-steady gas flow produced lasing for almost 200 milliseconds at a 30-hertz pulse rate. This performance points to the feasibility of continuous lasing with a flowing medium. In previous experiments as a fusion driver, a C_3F_7I laser generated terawatt pulses, which indicates the potential for scaling the present device up to extremely high power levels.

Among possible applications of the solar-pumped laser are:

- Beaming power for the propulsion of orbiting transfer vehicles that service geosynchronous orbits from Shuttle orbits;
- Providing power for use by satellites;
- Beaming for space communications;
- Propulsion for solar-sail vehicles;
- Furnishing power for space-based scientific experiments;
- Beaming power from space to airplanes to give them virtually limitless range; and
- Beaming power from space to Earth for electricity, material processing, and fuel production.

The laser-output wavelength makes it suitable for use with well-developed optical materials for high-power infrared lasers. The internal conversion efficiency of the iodine laser is 20 percent. In the present experiment, the ratio to total power out of the laser to total power in is 0.1 percent. Enough Sunlight energy could be gathered by a modest-size solar collector, perhaps 2 meters in diameter for 4 watts output. Present research on laser power scaling indicates that relatively-simple, low-solar-concentration, troughlike collectors coupled with long laser-cavity lengths may be suitable for high-power operation in space.

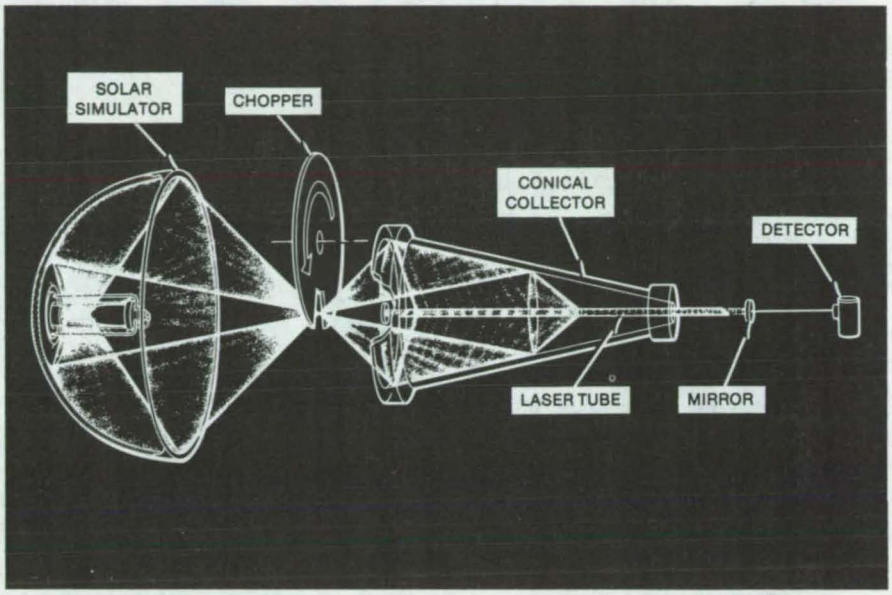

A Chopper Forms Pulses from a beam of xenon-arc light. The chopper is only necessary to avoid the buildup of laser-quenching species in the sealed tube of the present experiment. The perfluoropropyliodide lasing medium can function at temperatures of about 670 K, a fact that reduces cooling requirements in space.

In the laboratory setup, a xenon-arc lamp with an output of 4 kilowatts directs its beam into a highly-polished aluminum cone coated with magnesium fluoride (see figure). The cone reflects the beam so that it converges sideways on a quartz tube, 7 millimeters in inside diameter, containing C_3F_7I. The light, with a spectrum that closely resembles that of the Sun, optically pumps the gas — that is, stimulates it so that it emits photons that build up, after multiple reflections from the mirrors at the ends of the quartz tube, into a beam of coherent laser light at a fixed wavelength.

Only that portion of the Sunlight spectrum between 250 and 290 nanometers is effective in stimulating the gas. The laser utilizes about 1 percent of the incident solar energy. The transparency of the lasant to the solar visible and infrared results in a low waste-heat load and may require only a small thermal radiator. Other organic iodides are also promising as lasing mediums; $(CF_3)_2AsI$, for example, absorbs seven times as mush solar energy as does C_3F_7I.

The C_3F_7I dissociates as it lases, releasing free iodine that builds up and eventually prevents laser action. The experimental results indicate that only moderate flow rates are required to sweep away the free iodine to permit continuous lasing. Again, $(CF_3)_2AsI$ may be preferable, since it requires less extra-cavity processing and decomposes less readily.

This work was done by Willard R. Weaver, Jr., of **Langley Research Center** *and Ja H. Lee of Vanderbilt University. For further information, Circle 13 on the TSP Request Card.*

This invention is owned by NASA, and a patent application has been filed. Inquiries concerning nonexclusive or exclusive license for its commercial development should be addressed to the Patent Counsel, Langley Research Center [see page A5]. Refer to LAR-12870.

Improved Heat-of-Fusion Energy Storage

Alkali metal/alkali-halide mixtures are proposed for preventing solid buildup during energy recovery.

NASA's Jet Propulsion Laboratory, Pasadena, California

The heat-of-fusion method of storing energy may be made more practical by the use of some alkali metal/alkali-halide mixtures, such as Na/NaCl, for the phase-change materials. Solid material would not build up on the heat exchanger during energy recovery if such a mixture were used.

In conventional latent-heat energy storage, solidification during the energy-extraction period is likely to occur at the surface of the heat exchanger. The solid material degrades the thermal conduction and thus reduces heat transfer.

An alkali metal/alkali-halide phase-change material, at a temperature high enough to have two immiscible molten phases, would avoid this problem. For an Na/NaCl mixture at 795° C, a lighter, lower-melting-temperature, metal-rich phase exists above a salt-rich phase, which undergoes crystallization first upon cooling. Since the salt concentration in the metal-rich phase is very low, not much salt crystallizes in this phase. Immersing the heat-extraction component of the heat exchanger in the metal-rich phase, as shown in the figure, avoids the buildup of solids on the surface of the heat exchanger. Moreover, the salt crystals that form on the interface precipitate because of their greater density; hence, the interface is refreshed without agitation or forced circulation.

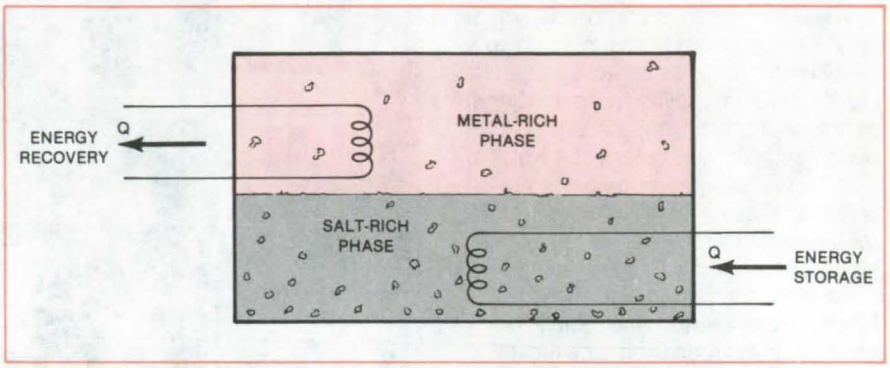

An **Alkali Metal/Alkali-Halide Latent-Heat System** for energy storage is illustrated schematically. When the mixture melts (by absorption of the heat of fusion), it forms two immiscible liquids. The salt-rich phase is heavier and has a higher melting/recrystallization temperature; so during energy recovery, salt crystallizes in this phase first. Since the heat exchanger for energy recovery is in the lighter metal-rich phase, solids do not form on it and there is no reduction of heat-recovery efficiency.

Besides avoiding buildup of solids on the heat exchanger, the alkali metal/alkali-halide mixtures have other advantages. By adding a small quantity of alkali metal, the energy-storage capacity is increased over that of the alkali-halide alone. The mixture also is more capable of releasing thermal stress so that the container and heat exchanger are less susceptible to stress damage.

This work was done by Kuo-Hung Chen and Ram Manvi of Caltech for **NASA's Jet Propulsion Laboratory.** *For further information, Circle 14 on the TSP Request Card.*
NPO-15318

Solar-Assisted Solution-Mining Concept

Brine heated in a solar pond would dissolve minerals from deposits.

NASA's Jet Propulsion Laboratory, Pasadena, California

A proposed solution-mining process would use solar energy to help dissolve minerals from layered deposits beneath the surface of a dry lake bed. Meeting the energy requirements of solution mining with fossil fuels is uneconomical; hence, no such process for mining dry-lake evaporite minerals is now in use.

The proposal envisions the mining of sodium carbonate (Na_2CO_3) from strata containing trona ($Na_2CO_3 \cdot NaHCO_3 \cdot 2H_2O$) located 35 m below the surface of Searles Lake, California. However, the same method could presumably be adapted for mining other minerals found in such sites.

In the proposed process (see figure), solar energy is collected within a brine in a thermal-gradient solar pond. Solar ponds can be excellent solar collectors, yet they are relatively inexpensive to construct. In such a pond a dense brine layer at the bottom efficiently absorbs solar energy while less-dense, cooler, brine and water layers float on top, preventing the bottom hot brine from naturally convecting to the surface. Thus, the upper layers reduce heat loss from the pond.

A brine that is sodium sulfate ($2Na_2SO_4 \cdot Na_2CO_3$) based would be heated in the pond. This hot brine would be pumped down a well to the mineral-bearing strata where Na_2CO_3 would be dissolved from the trona deposit. At the same time, sodium sulfate (Na_2SO_4) would crystallize out, physically replacing the Na_2CO_3, thereby reducing or preventing surface subsidence that would otherwise occur.

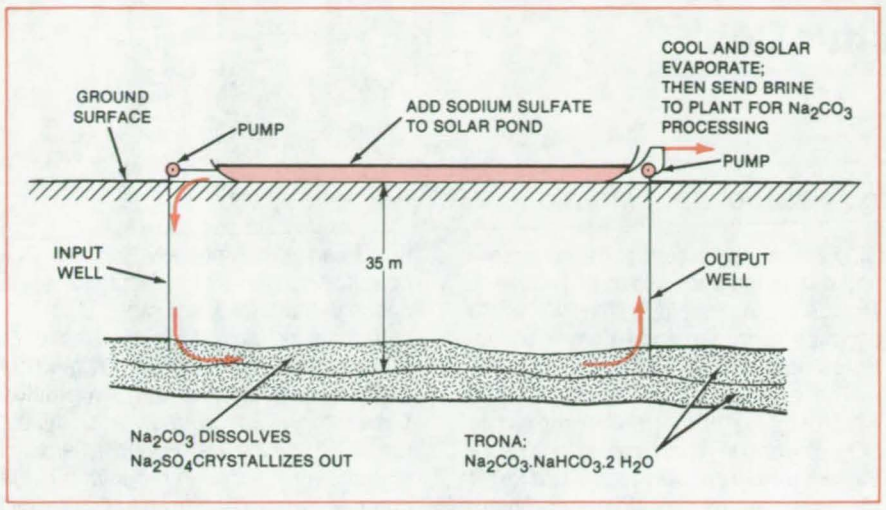

In the **Proposed Solution-Mining Process,** the hot brine could be pumped down one well and recovered at one or more other wells. The emerging brine is rich in the desired mineral (in this case, Na_2CO_3): This brine is evaporated in solar ponds to recover the mineral.

At one or more other wells the Na_2CO_3-enriched brine would be pumped back to the surface. Then solar energy would again be used, this time to concentrate the brine by evaporation in preparation for recovering the Na_2CO_3.

This work was done by Warren L. Dowler, Robert L. French, and John C. Becker, Jr., of Caltech and John Bills of Kerr McGee Corp. for **NASA's Jet Propulsion Laboratory.** *For further information, Circle 15 on the TSP Request Card.*
NPO-15343

Mapping Ocean Winds by Radar

Algorithm recovers data on windspeed, wind direction, and wind patterns from radar returns.

NASA's Jet Propulsion Laboratory, Pasadena, California

Information about ocean weather can be extracted from radar returns with the aid of a special algorithm. Originally developed for use with data obtained by microwave radar on the Seasat satellite, the algorithm can determine windspeeds and wind directions at the ocean surface and from this information can locate low- and high-pressure centers, convergence regions, and zones of strong winds and wind shear associated with ocean weather-system fronts. Although the specific method for generating weather parameters is probably limited to processing weather-satellite data, the general techniques will be of interest to those involved in radar signal analysis in other applications.

The strength of radar signals reflected by capillary waves only a few centimeters long on the ocean surface is proportional to the capillary wave amplitude, which in turn is proportional to windspeed near the surface. Signal strength also varies with the wave orientation, which is determined by the wind direction. The radar reflections from the ocean surface therefore contain information about windspeed and wind direction, and a comparison of such information over large ocean areas reveals patterns of atmospheric pressure systems.

The satellite radar illuminates with two beams that form an X-shaped "footprint" on the ocean surface. Doppler filters subdivide the footprint electronically into resolution cells measuring approximately 50 by 15 km each over swaths of 200 to 700 km from the earth track of the satellite. The two fore and aft beams allow a given point on the surface to be examined from two different angles so that wind direction can be recovered from the returns.

The algorithm used to process the returns is an empirical model function that relates radar backscatter cross section to windspeed as a function of incidence angle (the lateral location in the swath), azimuth angle of the wind direction relative to beam direction, and polarization of the antenna beam. The algorithm recovers between one and four wind-vector solutions for each cell. The solutions are nearly equal in speed and vary systematically in direction. The multiple solutions are referred to as "aliases" of the true wind vector. When the algorithm produces two solutions, they are separated by nearly 180° in a direction parallel to one of the beam directions. Four solutions consist of two pairs separated by any angle up to 90°. Further processing is necessary to obtain the correct wind-direction solution.

During the Gulf of Alaska Seasat Experiment, data on the North Pacific produced by the algorithm were compared with surface measurements. Radar windspeed measurements were within ± 2 m/s of the surface measurements and wind direction measurements differed by about 16° on the average. Further refinement of the algorithm as larger data sets are analyzed is expected to reduce statistical biases and errors.

This work was done by James E. Overland (NOAA), Morton G. Wurtele (UCLA), and Peter M. Woiceshyn of Caltech for **NASA's Jet Propulsion Laboratory.** *For further information, Circle 16 on the TSP Request Card.*
NPO-15267

A New Use for High-Sulfur Coal

High-sulfur coal could be used without environmental liability.

NASA's Jet Propulsion Laboratory, Pasadena, California

A new process would recover some of the economic value of high-sulfur coal. Although high-sulfur content is undesirable in most coal-utilization schemes (such as simple burning), the proposed process prefers high-sulfur coal to produce electrical power or hydrogen.

In the proposed process, the coal is dissolved in H_2SO_4 at the boiling point of 330° C. The reaction between the coal and the acid produces sulfur dioxide, carbon dioxide, and water vapor. Ash remains dissolved in the acid. The CO_2 appears as a concentrated stream and can be sold for use in oil recovery. The SO_2 is reacted with water to produce hydrogen and reform concentrated acid.

The process could replace one in which H_2SO_4 is thermally cracked to SO_2, O_2, and H_2O by heating to 900° C. Since the new process requires a lower temperature, the containment problem for the acid is less severe.

Any kind of coal with a high-sulfur content can be used. The thermal cracking of H_2SO_4 to CO_2 and SO_2 with coal has been experimentally verified. The potential exists for widespread application in the energy industry.

This work was done by Daniel D. Lawson and Christopher England of Caltech for **NASA's Jet Propulsion Laboratory.** *For further information, Circle 17 on the TSP Request Card.*

Inquiries concerning rights for the commercial use of this invention should be addressed to the Patent Counsel, NASA Resident Office-JPL [see page A5]. Refer to NPO-15194.

Books and Reports

These reports, studies, and handbooks are available from NASA as Technical Support Packages (TSP's) when a Request Card number is cited; otherwise they are available from the National Technical Information Service.

Advanced Coal-Based Power Generation

An evaluation of promising technologies for large-scale power generation.

Advanced power-generation systems using coal-derived fuels are evaluated in a two-volume report. The report considers fuel cells, combined gas- and steam-turbine cycles, and magneto-hydrodynamic (MHD) energy conversion. It presents the technological status of each type of system and analyzes the performance of each operating on medium-Btu fuel gas, either delivered via pipeline to the powerplant or generated by a coal-gasification process at the plantsite. The baseline technologies are those that could be commercially available in the late 1980's or the 1990's.

Combined-cycle gas- and steam-turbine systems are already commercially available. Only evolutionary improvements are needed to attain advanced-system performance. Such improvements are extensions of technology available in such systems as aircraft gas turbines.

The phosphoric acid fuel cell appears to be the next, most likely candidate for commercialization. An existing 4.5-MW demonstration plant is on a large enough scale to indicate operability in commercial power systems.

The molten-carbonate fuel cell is undergoing laboratory tests. MHD energy conversion has been demonstrated on a small laboratory scale, but technical problems remain — especially with regard to the containment of high-temperature fluids. Neither of these two systems is expected to become commercially viable before the 1990's.

The efficiencies of these advanced systems are attractive. For pipeline delivery, they range from 40.9 percent for the phosphoric acid fuel cell to 63 percent for the molten-carbonate fuel cell. In contrast, a conventional gas-fired steam station is 37 to 38 percent efficient.

For integrated powerplants, efficiencies range from 39 to 40 percent for the combined-cycle system to 46 to 47 percent for the molten-carbonate fuel cell. In contrast, the efficiency of a conventional coal-fired steam station (with flue-gas desulfurization to meet clean-air standards) is 33 to 35 percent.

This work was done by Fred L. Robson of United Technologies Research Center for **Marshall Space Flight Center.** *Further information may be found in NASA CR-161691 [N81-21538/NSP] and CR-161692 [N81-21539/NSP], "Final Study Report of an Applications Study of Advanced Power Generation Systems Utilizing Coal-Derived Fuels," Volumes I [$6] and II [$30]. Paper copies may be purchased [prepayment required] from the National Technical Information Service, Springfield, Virginia 22161. The reports are also available on microfiche at no charge. To obtain microfiche copies, Circle 18 on the TSP Request Card.*
MFS-25652.

Solar-Radiation Measuring Equipment and Glossary

Descriptions and other data for 145 instruments of 38 manufacturers.

A 1976 listing of commercially-available solar-radiation measuring equipment is presented in a 50-page report. Sensor type, response time, cost data, and comments concerning specifications and intended usage are listed for 145 instruments from 38 manufacturers. This is followed by a list of manufacturers' addresses.

An 83-term glossary defines solar-radiation and instrumentation terminology. Two short lists of reference works on radiation instrumentation, solar-energy data, and meteorology are also included. Most of the glossary entries contain a citation to one of the references.

Four types of instruments predominate in the listings: pyranometers, pyrgeometers, pyrheliometers, and radiometers. Calorimeters, photometers, Sunshine recorders, solar trackers, and calibration standards also appear.

The instrument data are given in tabular form in alphabetical order by manufacturer. A separate chart keyed to instrument type and price makes it easy to locate instruments of a given type and price range in the main listing. Price information provided by the manufacturers ranges from specific prices to price ranges to no indication of prices.

These data were collected in a mail survey of manufacturers in 1976. A copy of the survey form included in the report is recommended for adoption as a standard data sheet for describing solar-radiation measuring equipment. It could serve as a checklist when writing instrument purchase specifications.

This work was done by E. A. Carter, A. M. Patel, and S. A. Greenbaum of the University of Alabama in Huntsville for **Marshall Space Flight Center.** *To obtain a copy of the report, Circle 19 on the TSP Request Card.*
MFS-25770

Computer Programs

These programs may be obtained at very reasonable cost from COSMIC, a facility sponsored by NASA to make new programs available to the public. For information on program price, size, and availability, circle the reference letter on the COSMIC Request Card in this issue.

Cube-Corner Retroreflector Modeling

Programs compute impulse-response and interference effects of reflected pulses from optical cube corners.

A collection of computer programs analyzes arrays of optical cube corners used in laser ranging. The programs perform the computations required to construct the shape of a laser pulse (impulse response) after it has been retroreflected from a cube-corner array. The programs also calculate the interference-effects histogram and the far-field diffraction patterns. The programs model solid corner cubes with circular, unrecessed entrance faces and hollow cube corners made up of three mutually-perpendicular square mirrors.

An optical cube corner consists of three mutually-perpendicular reflecting surfaces. A laser beam entering the corner is returned toward the source regardless of the orientation of the cube corner, within the limitation of incidence angles interior to the reflecting surfaces.

The major calculations in the modeling of arrays of cube corners are the calculation of the exit-pupil area, gain, cross section for each cube corner, and strength of the return signal from the array. Impulse-response and interference-effects histograms are generated to display the characteristics of the retroreflected laser pulse.

The programs compute and display printer plots of range correction versus laser incidence beam angle, cross section versus laser incidence beam angle, cross section versus laser azimuthal angle, and return signal strength versus satellite zenith angle. They also compute and display the diffraction pattern of the cube-corner array for several laser-beam incidence angles. Separate stand-alone programs are included for computing the far-field diffraction patterns of individual solid or hollow cube corners.

Input consists of simple retroreflector descriptive parameters, incidence beam parameters, and output requests. Output may include both tabular and printer plot displays.

The programs are written in FORTRAN IV for batch execution and have been implemented on an IBM 360-series computer with a central memory requirement of approximately 550K of 8-bit bytes. The retroreflector modeling programs were developed in 1979.

This program was written by John G. Kirk, M. L. Regardie, P. N. Kumar, and J. Zimmerman of Computer Sciences Corp. for **Goddard Space Flight Center.** *For further information, Circle C on the COSMIC Request Card.*
GSC-12718

Two- and Three-Dimensional Galaxy Simulations

The dynamics of galaxies with up to 100,000 stars are simulated.

A real galaxy consists of stars and various forms of interstellar matter. Although electromagnetic and radiation effects do influence the evolution of galaxies, the large-scale structure of most systems is almost surely determined by gravitation. A set of computer programs available from COSMIC simulates the dynamics of isolated galaxies. In these computer models, a large number of simulation stars move in the combined gravitational field produced by the stars themselves (the self-consistent field) or by external matter (the fixed field).

The equations of motion for the stars are integrated by a "leap-frog"

(continued on next page)

scheme. The forces arising from the self-consistent portion of the gravitational field are derived from a gravitational potential, which is computed on a mesh by a discrete analog of Poisson's integral. This portion of the model employs a Fourier transform technique to model the galaxy as an isolated system. Programs are included for the simulation of both infinitesimally thin (two-dimensional) galaxies and fully three-dimensional galaxies. Typical simulations contain from 20,000 to 100,000 stars. The techniques employed in the galaxy simulations are very similar to those used in particle simulations in plasmas and may be adaptable to similar applications.

Input to the simulation program includes data concerning the initial conditions (such as the number of stars, initial radius, initial angular velocity, and initial velocity dispersion) and data concerning timespan of the simulation. Output consists of the positions and velocities of selected stars as well as the self-consistent forces acting on those stars at each time step in the simulation. Plots of the galaxy shapes at each time step may also be generated. A relocatable plot library is supplied with the program and can be adapted to almost any X-Y plotter.

The galaxy-simulation programs are written in FORTRAN IV and Assembler for batch execution and have been implemented on a CDC CYBER 170-series computer with the largest program having a central memory requirement of appproximately 200K (octal) of 60-bit words. The programs were developed in 1979.

This program was written by Frank Hohl of **Langley Research Center** *and Thomas A. Zang of the College of William and Mary. For further information, Circle D on the COSMIC Request Card.*
LAR-12907

Star-Catalog Data Base

System supports data on approximately 250,000 stars.

SKYMAP is a collection of computer programs and utility software for creating and maintaining a master star catalog and a hierarchical set of derivative star catalogs. It was developed to provide accurate stellar position and magnitude information for attitude-determination and analysis systems utilizing star sensor observations. The current master star catalog includes all documented stars with blue or visual magnitudes brighter than magnitude 9.0.

The principal sources for data on the approximately 250,000 stars in the SKYMAP master catalog are the Henry Draper Spectral Catalog and the Smithsonian Astrophysical Observatory Positional Catalog. The size of the master catalog precludes its use in most operations, so SKYMAP creates smaller, specialized catalogs including only those stars of interest for a particular application.

The SKYMAP system includes utility software for maintaining the master catalog and user-created catalogs. Software for integration into user programs to access the SKYMAP-generated catalogs is also included.

To provide complete and accurate star data at the user level with acceptable access time and storage requirements, SKYMAP furnishes a hierarchy of catalogs of decreasing size. As mentioned earlier, the master catalog contains data on approximately 250,000 stars. A much smaller mission catalog may be generated from the master catalog by excluding all parameters not required by a specific mission. This mission catalog may be reduced even more to generate a run catalog to meet the day-to-day needs of attitude-determination programs. The run catalog may be reduced to generate temporary core catalogs required for specialized rapid-access applications.

SKYMAP includes a collection of support and utility software for maintaining and implementing star catalogs. Programs are included for updating and modifying the master catalog and mission catalogs and for generating mission, run, and core catalogs from the master catalog or in hierarchial sequence.

The SKYMAP system also includes programs for computing statistical data describing the stars in a particular region of the sky to aid the user in developing star sensor utility criteria and selecting parameter exclusions for generating the reduced-size catalogs. SKYMAP also includes a collection of programs and routines developed since SKYMAP's inception to aid in the processing of stellar data and in the development of systems utilizing the SKYMAP-generated catalogs.

The SKYMAP distribution package consists of the SKYMAP system software and the complete, current master catalog. SKYMAP software is written in FORTRAN IV and Assembler for batch and interactive execution and has been implemented on an IBM 370-series computer. The largest program in SKYMAP has a central memory requirement of approximately 220K of 8-bit bytes. The SKYMAP system was originally developed in 1977 and was last updated in 1980.

This program was written by Dave Gotlieb and Steve McLaughlin of Computer Sciences Corp. for **Goddard Space Flight Center.** *For further information, Circle E on the COSMIC Request Card.*
GSC-12445

Materials

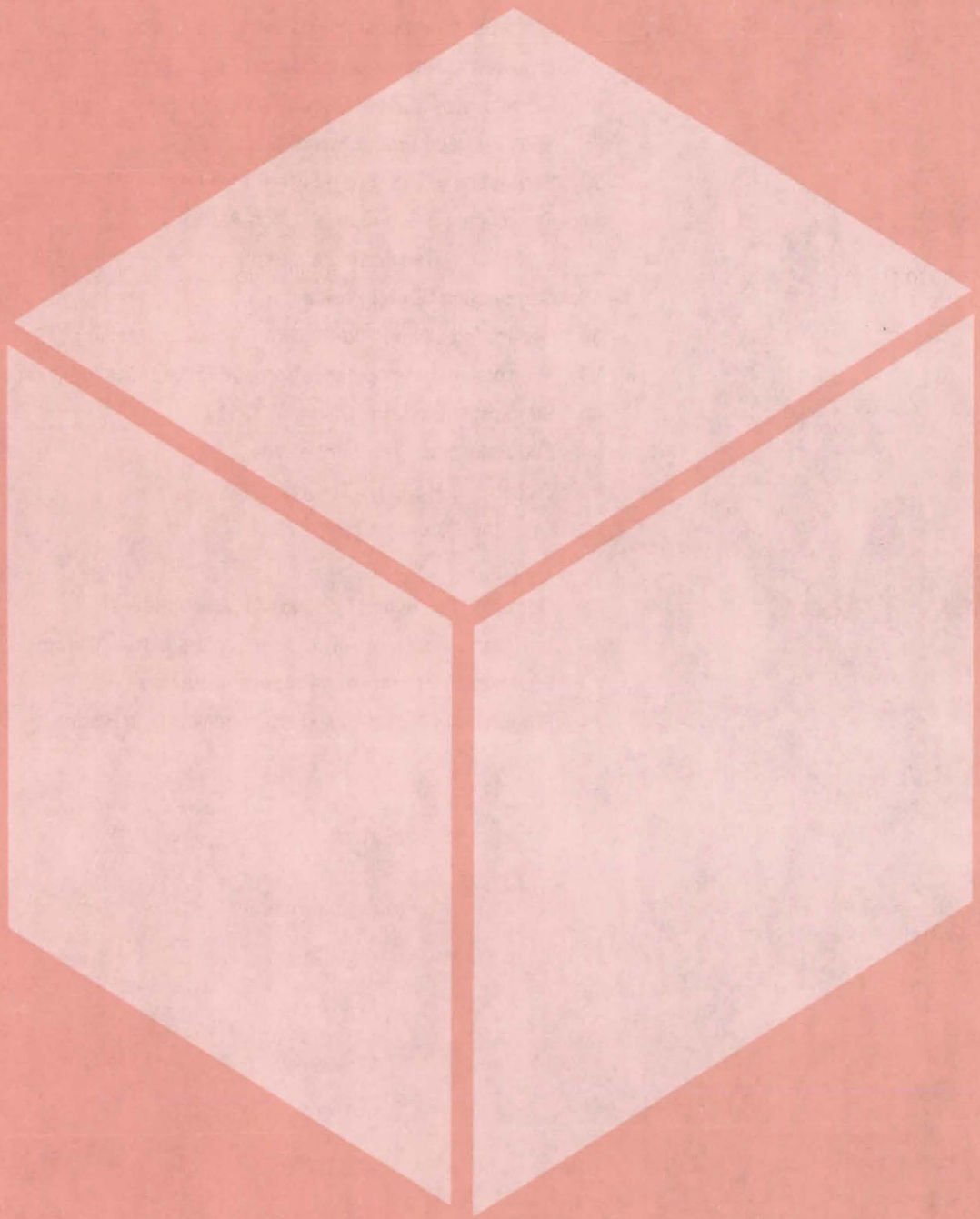

Hardware, Techniques, and Processes

Books and Reports

Clear Film Protects Against Ultraviolet Radiation

Weather-resistant material is a copolymer of a screening agent and an acrylic resin.

NASA's Jet Propulsion Laboratory, Pasadena, California

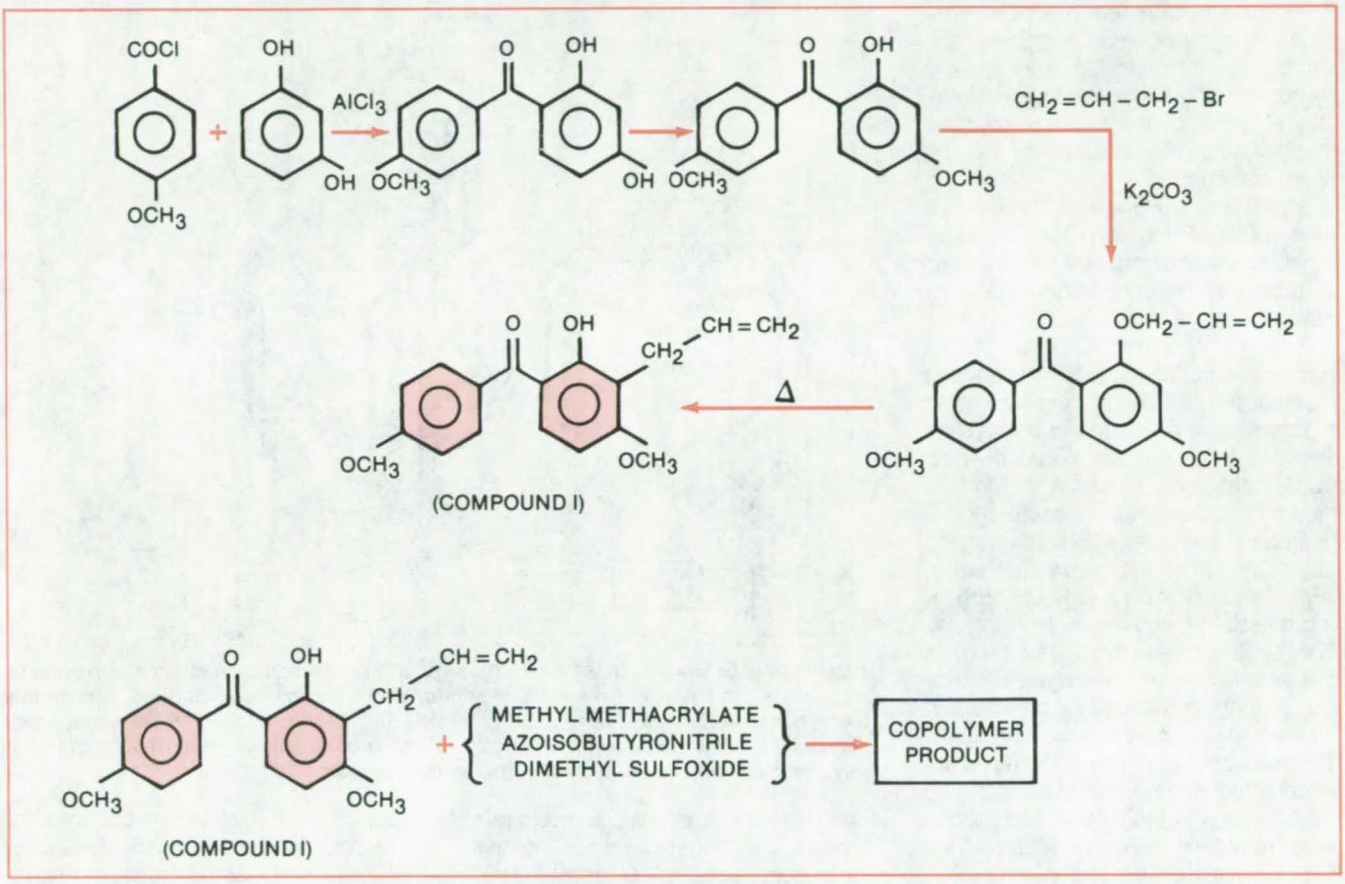

Synthesis and Copolymerization of Compound I are illustrated schematically, with ingredients.

An acrylic film contains a screening agent that filters ultraviolet radiation up to 380 nanometers in wavelength but passes other components of Sunlight. The film can be used to protect such materials as rubber and plastics that are degraded by ultraviolet light. It can be used as a protective cover on outdoor sheets or pipes made of such materials as polyethylene or polypropylene and on solar cells.

The new film, which contains about 0.5 percent by weight of 3-allyl-4,4′-dimethoxy-2-hydroxybenzophenone ("compound I") in copolymerization with the acrylic base (see figure), absorbs substantially more ultraviolet energy than typical commercial materials with similar properties. The new film is hard and dust-resistant. Its light absorption cuts off sharply as wavelength increases above 380 nm, so that it does not decrease the efficiency of solar devices.

A common problem with some ultraviolet screens is that the active agent is not chemically bonded to the base material; after a short period of outdoor exposure, the agent becomes lost. In the new film, however, the agent and the base form a copolymer; compound I does not leach out of the acrylic even after accelerated testing and long outdoor exposure. After long immersion in methanol, for example, the new film remained unchanged, but ordinary agents were extracted from the matrix. After accelerated tests in which mercury-arc light simulated Sunlight, the new film showed no signs of oxidation or of breaking or cross-linking of the polymer chains.

The molecular weight of the compound I-acrylic copolymer is approximately 60,000. The film may be applied to surfaces by solvent casting, coextrusion, or laminating. It may also be applied as a latex.

This work was done by Amitava Gupta and Andre Yavrouian of Caltech for **NASA's Jet Propulsion Laboratory.** *For further information, Circle 20 on the TSP Request Card.*

Inquiries concerning rights for the commercial use of this invention should be addressed to the Patent Counsel, NASA Resident Office-JPL [see page A5]. Refer to NPO-14971.

Closed-Loop Process Yields Ultrapure Silicon

Metallurgical-grade silicon is converted into semiconductor-grade silicon.

NASA's Jet Propulsion Laboratory, Pasadena, California

A closed-loop process produces ultrapure silicon from metallurgical-grade silicon by forming, purifying, and hydropyrolizing tribromosilane ($HSiBr_3$). The essence of the process involves manipulating the equilibrium of the chemical reaction

$$HSiBr_3 + H_2 \rightleftharpoons Si + 3HBr$$

in a product reactor. The ultrapure granular silicon produced can be used to produce semiconductors and solar cells.

The only material that needs replenishing once the process begins is metallurgical-grade silicon; all other reactants are separated and recycled. The metallurgical-grade silicon, of about 90 percent purity or better, is fed to a fluid-bed hydrogenation reactor and a hydrogen bromide (HBr) reactor, at about 300° to 750° C, to produce a mixture of silicon tetrabromide, tribromosilane, and unreacted material. The hydrogen and hydrogen bromide are separated, and hydrogen bromide and part of the hydrogen are then recirculated to the reactors as feedstock. The balance of the hydrogen is fed to the silicon-product reactor. The remaining mixture of tribromosilane and silicon tetrabromide is then separated by fractional distillation into its constituents, and a vapor stream of tribromosilane is fed to the silicon-product reactor; the separated silicon tetrabromide is vaporized and then used as feedstock for the hydrogenation synthesis reactor.

The silicon-product fluid-bed reactor receives reactants in the molar ratio of from 5-to-1 to 26-to-1 hydrogen to tribromosilane and produces ultrapure silicon and hydrogen bromide. The reaction occurs between 900° and 1,200° C. At the bottom of the product reactor, the large silicon particles, which have grown to about 0.125 inch (0.327 cm) in diameter, are withdrawn. A fraction of the silicon withdrawn is ground to fine particles 50 to 500 microns in diameter, and returned to the reactor to serve as a deposition substrate. The overhead vapor stream from the product reactor, which is composed of HBr, unreacted $HSiBr_3$ and H_2, and $SiBr_4$, is recycled into the loop.

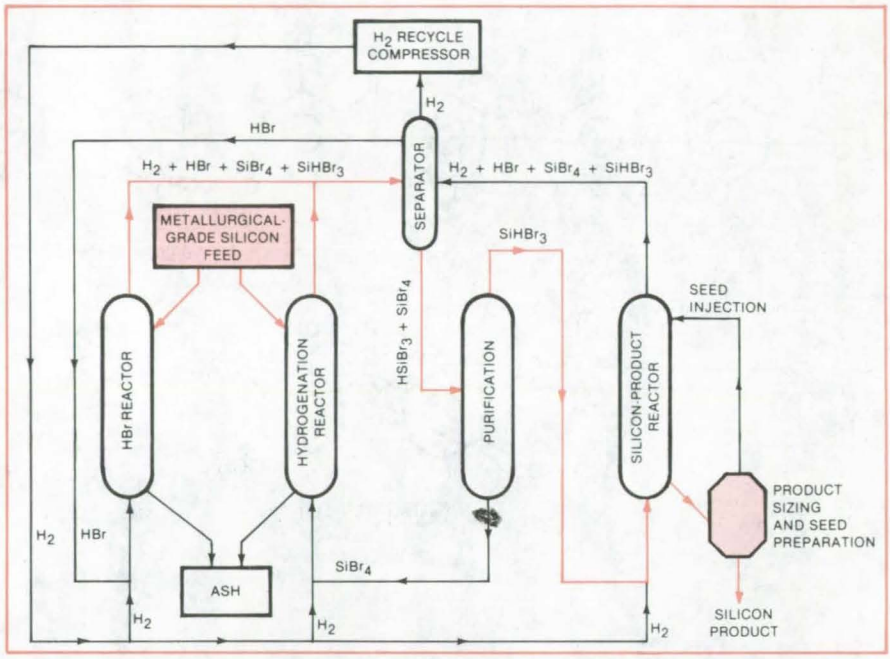

Metallurgical-Grade Silicon is transformed into tribromosilane by reacting it with process byproducts. The tribromosilane is separated from the mixture, purified, and finally decomposed in the presence of hydrogen in the silicon-product reactor. Conversion efficiencies of 30 to greater than 60 percent of tribromosilane to ultrapure granular polycrystalline silicon are typical in the product reactor.

This work was done by John C. Schumacher and Edward B. Moore of the J. C. Schumacher Co., for **NASA's Jet Propulsion Laboratory.** *For further information, Circle 21 on the TSP Request Card.*
NPO-15283

Bipulsating Technique for Silicon Production

Method controls reaction temperature and rate of reaction of sodium and silicon tetrafluoride.

NASA's Jet Propulsion Laboratory, Pasadena, California

The reduction of silicon tetrafluoride by sodium, to produce high-purity silicon, is very fast and highly exothermic. It begins at temperatures around 150° to 200° C and the temperature can reach more than 2,000° C. A new proposal suggests that the temperature and rate of reaction can be regulated by alternately adding measured amounts of the reactants. This technique could be used in a large reactor, where heat dissipation becomes a serious problem, to control reactor temperatures. It would be a highly efficient method, which would utilize almost 100 percent of the raw materials.

A flow chart of the method is shown in the figure. A small amount of liquid

sodium (Na) — for example, 1 gram — is "pulsed" into a nickel-lined reactor, which is held above the reaction temperature. A pulse of silicon tetrafluoride (SiF_4) then follows. As the reaction proceeds, the temperature rises, and the pressure of the SiF_4 drops. Additional pulses of SiF_4 follow periodically until, after a fresh SiF_4 pulse, no drop in pressure is observed. At that point SiF_4 is evacuated from the reactor, fresh sodium is pulsed in, and the process begins again.

The method has several benefits: The reaction products can be grown in columns, the only contact of which is with the base of the reactor, which simplifies removal of the reaction products and minimizes contamination. Since the process can be carried out at low temperatures, the impurities picked up from the reactor walls can be minimized. The process avoids premature reaction of the reaction products by delivering the sodium to the reactor under vacuum. It also avoids diffusion problems because the small drops of sodium splash on the bottom of the reactor to form a very thin layer.

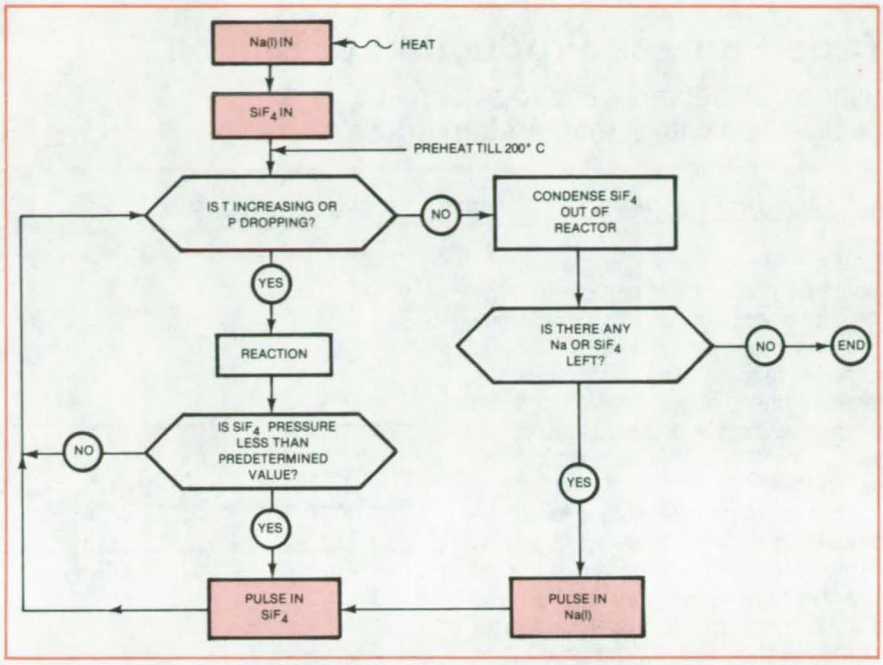

Pulses of Sodium and Silicon Tetrafluoride are added and the progress of the reaction monitored according to the flow scheme depicted. The pulses contain small amounts of the reactants.

This work was done by Angel Sanjurjo of SRI International for **NASA's Jet Propulsion Laboratory.** *For further information, Circle 22 on the TSP Request Card.*
NPO-15367

Cryolite Byproduct in Silicon Production

Process reacts alumina hydrate with HF and NaF from silicon-production process.

NASA's Jet Propulsion Laboratory, Pasadena, California

Cryolite (Na_3AlF_6), important as an electrolyte in aluminum refining, can be produced by adding a reaction step to a process that makes high-purity silicon from fluorosilicic acid (H_2SiF_6). The new extended process has been demonstrated in the laboratory and could be used in a commercial plant.

One of the silicon-production processes comprises the first three reactions listed in the figure. In addition to silicon, the H_2SiF_6 reactant contains another valuable element, fluorine, which is utilized in the cryolite-production reaction, shown as reaction (4) in the figure.

In reaction (1), H_2SiF_6 is converted to Na_2SiF_6, leaving the byproduct hydrofluoric acid (HF). The Na_2SiF_6 from reaction (1) is thermally dissociated in reaction (2), producing silicon fluoride

(1) $H_2SiF_6(aq) + 2NaF(s) \rightarrow Na_2SiF_6\downarrow + 2HF(aq)$

(2) $Na_2SiF_6 \xrightarrow{\Delta} SiF_4(g) + 2NaF(s)$

(3) $4Na(l) + SiF_4(g) \rightarrow Si(s/l) + 4NaF(l)$

(4) $\frac{1}{2}H_2SO_4(l) + 4NaF(s) + 2HF(aq) + \frac{1}{2}Al_2O_3(H_2O)_3(s) \rightarrow Na_3AlF_6\downarrow + \frac{1}{2}Na_2SO_4 + 3H_2O$

aq – Aqueous Solution
g – Gas
l – Liquid
s – Solid
↓ – Precipitate
Δ – Energy Added

High-Purity Silicon and Cryolite are produced in a four-reaction process starting from fluorosilicic acid. The form in which each reactant is used is indicated in parentheses.

(SiF_4) and sodium fluoride (NaF), which is recycled back to reaction (1). In reaction (3), the SiF_4 is reduced with sodium to produce the product silicon and the byproduct NaF.

In the final reaction, the byproducts HF and NaF from the first three reactions react with alumina hydrate [$Al_2O_3(H_2O)_3$] to precipitate cryolite. This precipitation reaction requires an acid, such as the sulfuric acid (H_2SO_4) shown. Finally, the cryolite is separated from the waste liquor by filtration, then washed and dried.

This work was done by Robert W. Bartlett of SRI International for **NASA's Jet Propulsion Laboratory.** *For further information, Circle 23 on the TSP Request Card.*
NPO-15364

Tube-Furnace Production of Silicon

Silane gas decomposes to silicon in a packed bed with a temperature gradient.

NASA's Jet Propulsion Laboratory, Pasadena, California

Silicon of semiconductor-grade purity would be produced in particle form by the decomposition of ultrapure silane gas in a proposed packed-bed tubular furnace reactor. The decomposition temperature is about 700° C, and the product size depends on the size of the silicon particles that constitute the packed bed.

The tube-furnace technique for silicon production is shown in the figure. Silicon particles to form the packed bed are fed into the furnace and are packed and pushed along by an auger. A heater located at the center of the tube raises the temperature of the adjacent particles to approximately 1,000° C and creates a temperature gradient that is essential to the operation of the process.

The silane gas, fed into the packed bed of moving particles in the temperature-gradient region, decomposes to form more particles. This heterogeneous decomposition occurs without excessive formation of submicron fines.

The silicon particles fall out of the end of the furnace tube. Some are taken away for use in semiconductor manufacture, and some are returned to the furnace to form the packed bed for the continuing process. Whatever fines are produced are screened out and also reinserted into the furnace.

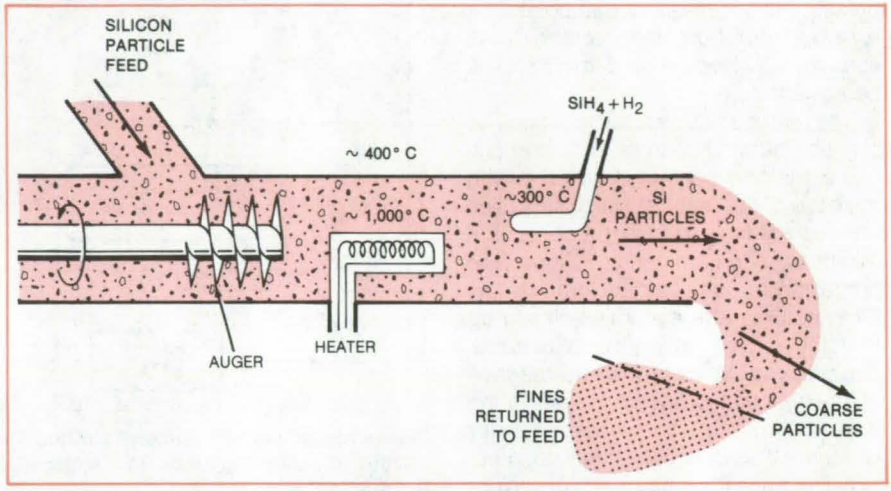

A **Packed-Bed Reactor** would produce silicon by decomposing ultrapure silane gas in a temperature gradient. On the basis of previous experiments with relatively low decomposition temperatures and with temperature gradients, it is expected that the heterogeneous decomposition will produce few fines.

This work was done by Ernest G. Farrier, Joachim Rexer, and Paul J. Timmel of Union Carbide Corp. for **NASA's Jet Propulsion Laboratory.** *For further information, Circle 24 on the TSP Request Card.*
NPO-15274

Separating Silicon From Si/NaF Mixtures

A new method takes advantage of the lower melting point of NaF.

NASA's Jet Propulsion Laboratory, Pasadena, California

Silicon can be extracted from the mixture produced when silicon tetrafluoride is reduced by sodium, by taking advantage of the lower melting point of NaF. Previously, the finely interspersed mixture of NaF and silicon was separated by heating above the melting point of silicon (1,410° C). The new method is effective at temperatures up to 400° C below the melting point of Si. This results in energy and economic savings: simpler and smaller furnaces, less volatization loss, and a high percentage of separation.

In the new method, the Si/NaF mixture is heated in a graphite crucible to around 1,100° C, which is above the melting point of NaF but well below the melting point of silicon. The bottom of the graphite crucible has openings through which the NaF is discharged. At this temperature, a silicon sponge and part of the NaF remain in the crucible after discharging most of the molten NaF. The silicon sponge and very small amounts of NaF can be melted by raising the temperature to 1,450° C and the NaF traces removed by subsequent acid leaching.

An experiment showed that the NaF extracted by the process is uncontaminated with silicon particles. A 1-inch (2.54-cm) inner diameter, 3 inches (7.62 cm) high crucible with a 7/64-inch (0.28-cm) hole at the bottom, was loaded with a 10-gram Si/NaF mixture; the mixture was in the ratio of 1 part silicon to 4 parts NaF. At 1,100° C, it took 10 minutes to separate more than 80 percent of the NaF.

This work was done by Angel Sanjurjo and Leonard Nanis of SRI International for **NASA's Jet Propulsion Laboratory.** *For further information, Circle 25 on the TSP Request Card.*
NPO-15365

Consolidating Submicron Silicon Particles

Fine silicon powder melts and solidifies atop a silicon pedestal.

NASA's Jet Propulsion Laboratory, Pasadena, California

Two proposed techniques would use a molten pool of silicon at the top of a silicon pedestal to consolidate the submicron silicon particles produced by the silane process. The techniques avoid the contamination produced by casting containers. The consolidated material could be used directly to produce high-efficiency polycrystalline solar cells.

In one process, fine silicon powder is fed into the molten pool created by partially melting the top of a cylindrical silicon pedestal (see figure). The powder melts and becomes part of the pool. The second approach combines silane pyrolysis and silicon-powder consolidation by directly decomposing silane on the silicon pool. By controlled cooling of the bottom of the silicon pedestal with gas, it should be possible to form polysilicon material with grain boundaries predominantly parallel to the axis of the pedestal.

In both processes, the shape of the molten layer together with the surface tension of molten silicon stabilize the layer and control the diameter of the consolidated material. The molten layer is formed by surface induction heating, electron-beam bombardment, or other energy-efficient methods. After a stable molten layer forms, the silicon pedestal is lowered as the molten layer is fed with either silicon powder or droplets.

This work was done by Kazuo A. Yamakawa and Ralph Lutwack of Caltech for **NASA's Jet Propulsion Laboratory.** *For further information, Circle 26 on the TSP Request Card.*
NPO-15250

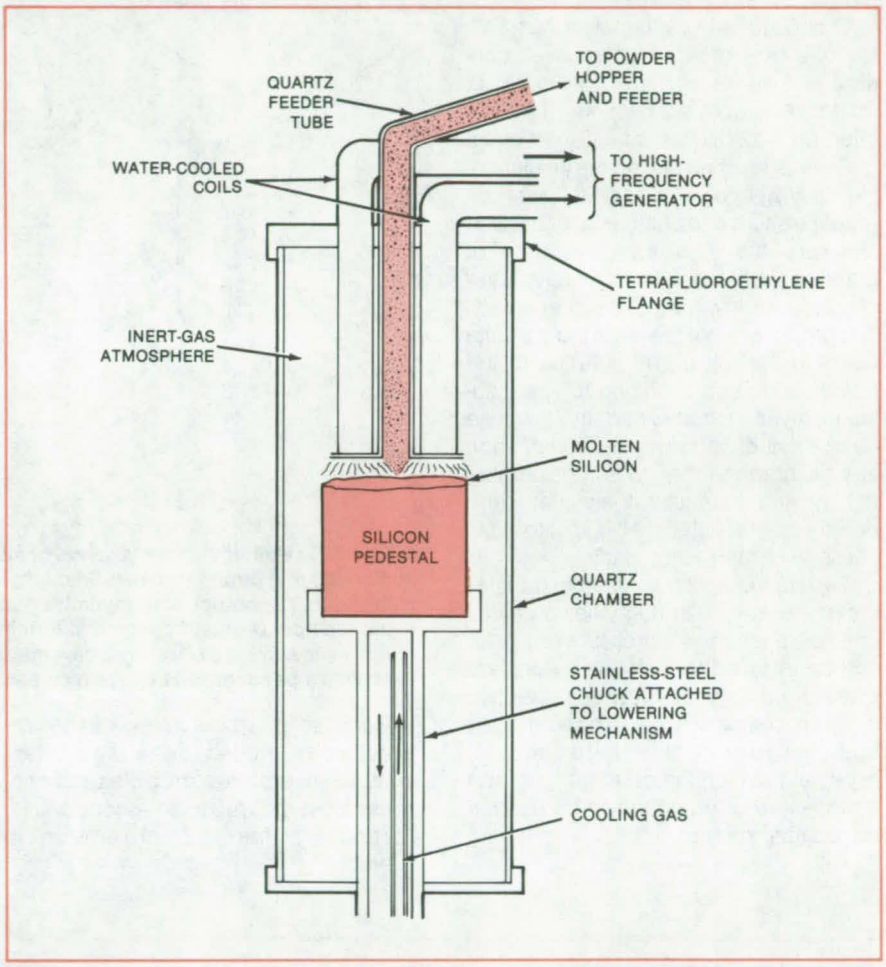

The **Molten-Silicon Pool** receives fine silicon powder and melts it. After a stable molten layer forms, the pedestal is lowered at a rate equal to the silicon-powder feed rate. If silane is directly decomposed on the silicon pool, the powder feeder is replaced by a jet of silane on the silicon surface, and the hydrogen produced in the decomposition of silane is pumped from the bottom end of the chamber.

Conduit for Transferring Molten Silicon

A proposed three-part conduit would transfer pure silicon between cruicibles.

NASA's Jet Propulsion Laboratory, Pasadena, California

Transferring molten silicon from one vessel to another without solidifying or contaminating it would be possible with a proposed conduit. Silicon oxide and other impurities would be removed by extracting molten silicon through the conduit and away from the slag that forms on the surface of the melt. The conduit could be used in a process for growing continuous crystal ribbon for solar cells, where there would be no size limitation on the finished product, because the crystallization crucible could be continuously replenished with pure silicon.

(continued on next page)

The conduit (see figure) is composed of three major parts: a transfer tube, a heater, and a multilayered thermally insulating and reinforcing structure. The molten silicon only comes in contact with the quartz transfer tube, with which it is compatible, while the outer insulating layers reinforce the quartz tube, which becomes somewhat soft at molten-silicon temperatures.

The heater is in contact with the transfer tube over most of its length. It consists of a series of four resistive strips, made of graphite sheeting, that are interconnected in pairs near their ends.

Several layers make up the insulation. Helically-wound silica tape followed by graphite sheet and another layer of silica tape are the inner core. A layer of graphite sheet followed by a heavy layer of graphite felt surround the inner layers. The graphite sheet prevents the graphite fibers in the felt from migrating to the heater and short-circuiting it. The insulation layer is completed by a dense outer shell of refractory material, such as solid graphite, that adds considerable rigidity and strength at elevated temperatures. The outer shell is split to allow passage of the heater leads.

Two methods can be used to transfer the molten silicon through the conduit: It can be siphoned, or a pressure regulator can be installed to maintain a constant pressure difference between the two crucible compartments. Since nitrogen and oxygen contaminate silicon, especially at high temperatures, an inert atmosphere of argon would be used in the compartments.

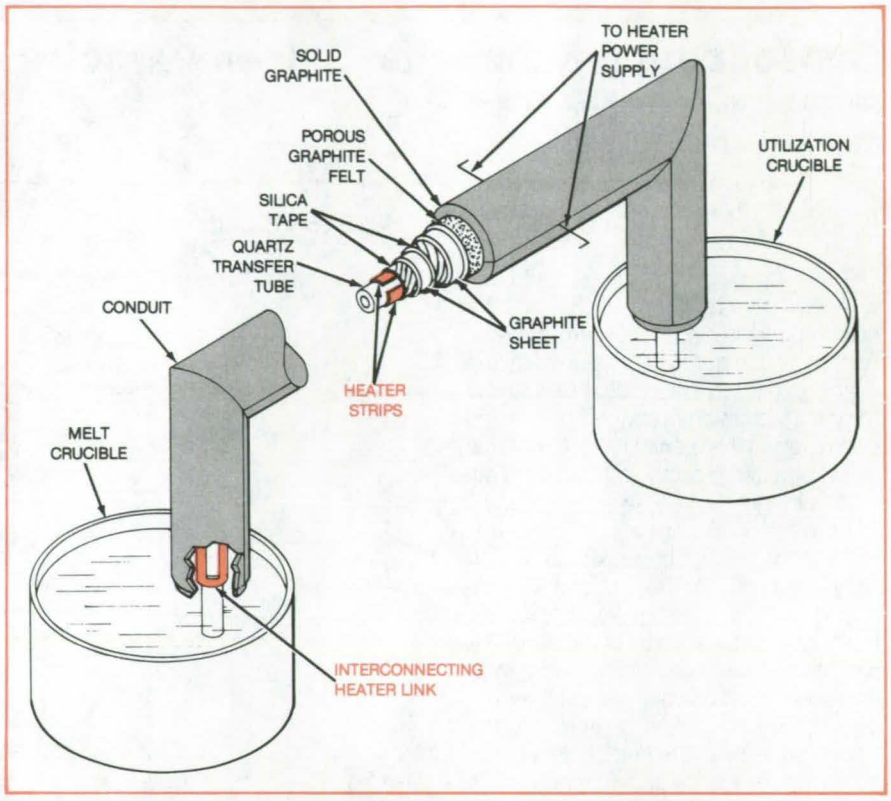

A **Four-Strip Heater** augments layers of insulation to prevent molten silicon from cooling and solidifying during transfer. Since the melt is maintained at a temperature relatively close to its fusion point, to minimize quartz erosion, even relatively-minor heat losses could precipitate solidification and terminate work in progress. Though only one pair of crucibles is shown, several crucibles may be fed through conduits from a central crucible. Each would be contained in its own compartment under an inert atmosphere.

Because quartz is fairly rapidly reduced and eroded away at molten-silicon temperatures, crucibles and conduits must be replaced occasionally. Fortunately, the rate of erosion is tolerable.

This work was done by George Fiegl and Walter Torbet of Siltec Corp. for **NASA's Jet Propulsion Laboratory.** *For further information, Circle 27 on the TSP Request Card.*
NPO-15109

Compacting Silicon Powder

Silicon powder is converted into flakes by passing it through a rolling mill.

NASA's Jet Propulsion Laboratory, Pasadena, California

When powdered silicon is produced by the free-space decomposition of silane gas, the average particle size of the silicon produced is typically low-micron to submicron, which makes the particles difficult to handle. To convert the silicon powder into flakes, making it easier to handle, the powder is passed through a rolling mill.

Silicon powder was compacted by sandwiching it between two flat sheets of metal and passing it through a horizontal rolling mill. This demonstrated the feasibility of the method. However, when the method is scaled up for production, the choice of metal making contact with the silicon will be important, if the high purity of the silicon is to be preserved.

The feasibility tests also showed that vacuum sintering the flakes at 1,350° C (60° C below the melting point of silicon) for 1 hour in a quartz crucible significantly increases their breaking strength.

This work was done by Ernest G. Farrier and Joachim Rexer of Union Carbide Corp. for **NASA's Jet Propulsion Laboratory.** *For further information, Circle 28 on the TSP Request Card.*
NPO-15271

Separating Silicon and Sodium Fluoride by Melting

Silicon is withdrawn from the bottom of a crucible after two immiscible liquids form.

NASA's Jet Propulsion Laboratory, Pasadena, California

A method for separating mixtures of silicon and salts of sodium and fluorine takes advantage of the immiscibility of the two components. The method may be used in conjunction with the reduction of SiF_4 gas by sodium to prepare large quantities of silicon for solar-cell fabrication and other uses. It could replace the method of multiple leachings to dissolve NaF and Na_2SiF_6 salts, which exposes the silicon to possible oxidation loss and contamination.

When heated in a graphite crucible to temperatures above the melting point of silicon (1,410° C) a powder mixture of NaF, Na_2SiF_6, and silicon rapidly separates into a molten-salt mixture and large drops of silicon that range in size from 1 to 10 mm in diameter. These drops combine and settle to the bottom of the crucible. Silicon can be continuously removed by tapping silicon from the crucible bottom (see figure) while feeding a fresh powder mixture through the top.

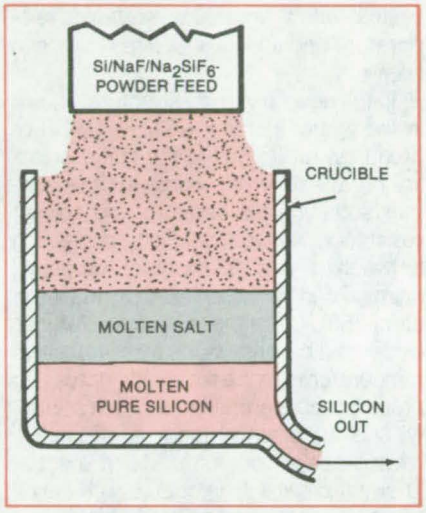

Silicon Is Withdrawn from the bottom of the crucible, once two immiscible liquid stages form, in this quasi-continuous method of separating silicon from other reaction products. The process would be periodically halted to remove the accumulated buildup of salts.

It is speculated that this separation occurs because the molten-salt phase coats the silicon and acts as a flux that aids in combining the smaller drops of silicon into larger drops that ultimately drop to the bottom of the crucible. The coating also prevents the silicon from wetting the graphite and producing a silicon carbide contaminant.

This work was done by Leonard Nanis and Vijay K. Kapur of SRI International for **NASA's Jet Propulsion Laboratory.** *For further information, Circle 29 on the TSP Request Card.*
NPO-15363

Thermoset/Thermoplastic Aromatic Polyamides for Composites

Pendent propargyl groups serve as latent cross-linking agents in a new series of polyamide resins.

Langley Research Center, Hampton, Virginia

New aromatic polyamides are processed at a relatively low temperature, then heat-treated to attain the high softening temperature required when the polyamides are used as matrix resins in structural composites. The new polyamides are compatible with the organic fibers (such as duPont Kevlar® aramid fibers, or equialent) often used as reinforcing agents in such composites.

The softening temperature of a thermoplastic matrix resin must be at least 50 K above its use temperature, so that the resin will have acceptable elastic modulus and stiffness. This problem is compounded when an organic fiber is the reinforcing agent in the composite, because the fiber has a characteristic temperature at which it begins to

(continued on next page)

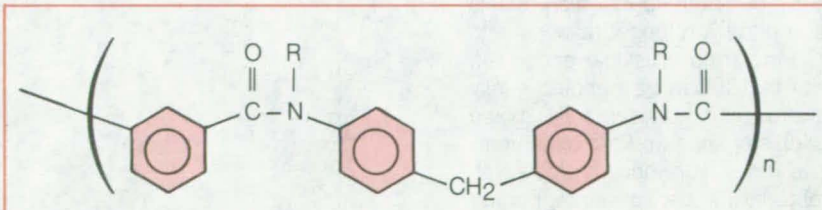

where n represents the repeating polymer unit and

R = $-CH_3$ and $-CH_2-C\equiv CH$ in varying ratios, ranging from $-CH_3$ at 99 percent and $-CH_2-C\equiv CH$ at 1 percent to $-CH_3$ at 0 percent and $-CH_2-C\equiv CH$ at 100 percent.

New Aromatic Polyamides contain pendent propargyl groups ($-CH_2-C\equiv CH$), which serve as latent cross-linking agents.

irreversibly lose its stiffness. This is generally due to a relaxation phenomenon occurring in a highly oriented fiber.

Aromatic polyamides with relaxation temperatures slightly below 573 K (300° C) are attractive as organic fibers for structural composites. In order to fabricate a structural laminate with this fiber reinforcement, a processing temperature of 553 K (280° C) should not be exceeded to ensure that the fiber stiffness is retained. This thermal restriction is in turn imposed on the resin or polymer, requiring that it be processable at a temperature below 553 K.

The new series of polyamides is processed no higher than 553 K. They are converted to a higher softening temperature due to a chemical reaction that occurs during this 553 K heat treatment. These thermoset/thermoplastic aromatic polyamides, suitable for fabricating structural composites, have the added advantage of being soluble before thermal processing but solvent-resistant after thermal processing.

The new process incorporates a propargyl cross-linking agent at various levels along the backbone of an aromatic polyamide, to produce a polymer of high molecular weight that softens at a relatively low temperature (427 K) and subsequently "sets up" when treated at a higher temperature (553 K). The sites of latent cross-linking do not enter into any chemical reactions during the fabrication of the thermoplastic component. However, on heating to the elevated temperature, the sites form cross-links that result in a polymer system with an increased softening temperature and an increased resistance to solvents.

In the new polyamide structure, shown in the figure, it is the $-CH_2-C\equiv CH$ or propargyl group that is the latent cross-linking agent, which increases the polymer softening temperature and solvent resistance. Polyamide films containing between 1 and 33 percent propargyl diamine can be cross-linked by heating in air at 553 K. The thermal cross-linking is evidenced by a rise in the glass-transition temperatures of the films with increasing propargyl concentration, a loss in solubility, and the disappearance of propargyl-related peaks from infrared film spectra. Thermal cross-linking occurs with only a slight loss in thermo-oxidative stability.

The propargyl-containing polyamides are attractive as matrices for polyamide fiber (for example, aramid fiber) composites. These materials are processable at advantageously low temperatures and thermally cross-linkable at temperatures below the relaxation temperature of the fiber. The compatibility of these resins with aromatic polyamide fibers gives them high potential for success as matrix resins for composites.

This work was done by Terry L. St. Clair, Anne K. St. Clair, and John D. Barrick of **Langley Research Center;** *James F. Wolfe of Virginia Polytechnic Institute and State University; and Thomas D. Greenwood of King College. Further information may be found in NASA TM-81918 [N81-14080/NSP], "Crosslinking of Aromatic Polyamides via Pendant Propargyl Groups" [$5]. A copy may be purchased [prepayment required] from the National Technical Information Service, Springfield, Virginia 22161.*

This invention is owned by NASA, and a patent application has been filed. Inquiries concerning nonexclusive or exclusive license for its commercial development should be addressed to the Patent Counsel, Langley Research Center *[see page A5].* *Refer to LAR-12723.*

Sterilizable Binder Is Stable at 135° C

Material with few unsaturated double bonds has the needed stability.

NASA's Jet Propulsion Laboratory, Pasadena, California

A polyurethane binder for solid propellants that can endure heat sterilization without decomposition is based on an ester diol. The binder, which resists oxidation under prolonged exposure to 135° C temperature, is low enough in viscosity that it can be handled easily during processing and readily mixed with oxidizers, such as ammonium perchlorate. The polyurethane is also a suitable material for encapsulants, potting compounds, and coatings that must be sterilized.

Conventional polyurethanes, in contrast, quickly oxidize during sterilization because of their unsaturated double bonds. Attempts to improve their stability by hydrogenating the double bonds result in a viscous liquid that cannot carry the necessary high loading of propellant oxidizer.

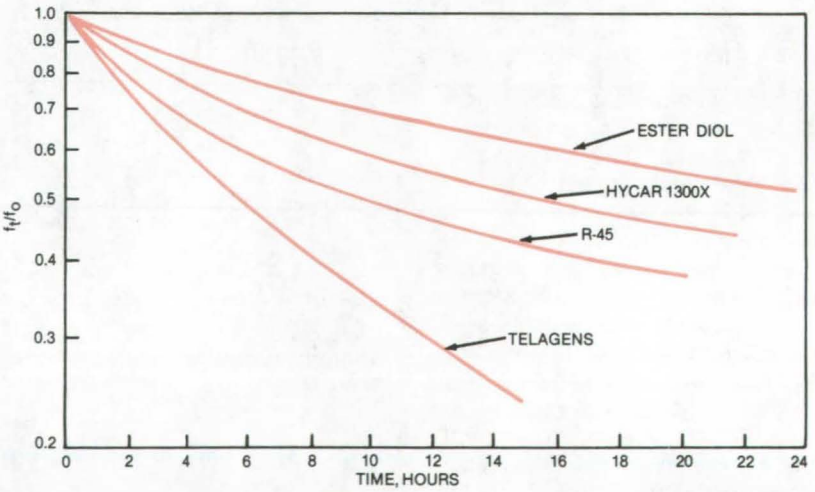

Stress Relaxation — a measure of resistance to degradation — is higher for ester-diol-based polyurethane than for other binders. In this plot, the horizontal axis represents the time of exposure to 135° C in nitrogen, and the vertical axis represents the ratio of stress after heat exposure to that before.

Polyurethanes are usually made from high-molecular-weight glycols or polyhydric alcohols and diisocyanates or triisocyanates. Such extenders or cross-linking agents as polyhydric alcohols or polyfunctional amines are added for further polymerization and cross-linking, to impart elasticity to the polymers.

The new polyurethane is based on a commercially-available dimerized fatty acid having high molecular weight (600) and low unsaturation and viscosity. Known as Empol 1010 dimer acid, the material is made from animal or vegetable fat by a proprietary dimerization process. The dimer acid is changed by esterification with a dihydric alcohol into an ester diol. Various molecular weights can be obtained by control of the ratio of dihydric alcohol to dimer acid. The product is converted to polyurethane by reaction with diisocyanates.

In stress-relaxation tests, the ester-diol-based polyurethane outperformed other major candidates for heat-sterilizable propellant binders (see figure). In other tests, cylindrical castings of the new binder, 3 inches (7.6 centimeters) in diameter, showed no change after four cycles of sterilization at 135° C, 55 hours per cycle, when they were subjected to X-ray inspection.

In an experimental procedure, the ester diol was synthesized by adding 500 grams of Empol 1010, 17.2 grams of p-toluene sulfonic acid, and 434 grams of 1.5 pentanediol to 1 liter of toluene. The solution was refluxed for a total of 13 hours to drive off water. The toluene solvent was then removed by evaporation under reduced pressure. The solution was then washed with deionized water in a separatory funnel. Finally, the product ester diol was dried for 2 hours at 100° C on a rotary evaporator under reduced pressure. A representative propellant composition is 9.93 grams ester diol with 3.03 grams isophorone diisocyanate, 3.04 grams castor oil, 67.80 grams ammonium perchlorate, and 16.00 grams aluminum.

This work was done by Sarkis H. Kalfayan and Andre H. Yavrouian of Caltech for **NASA's Jet Propulsion Laboratory.** *For further information, Circle 30 on the TSP Request Card.*
NPO-15020

Fire-Retardant Epoxy Adhesives

Phosphorus in both resin and curing-agent molecules prevents fire propagation.

Ames Research Center, Moffett Field, California

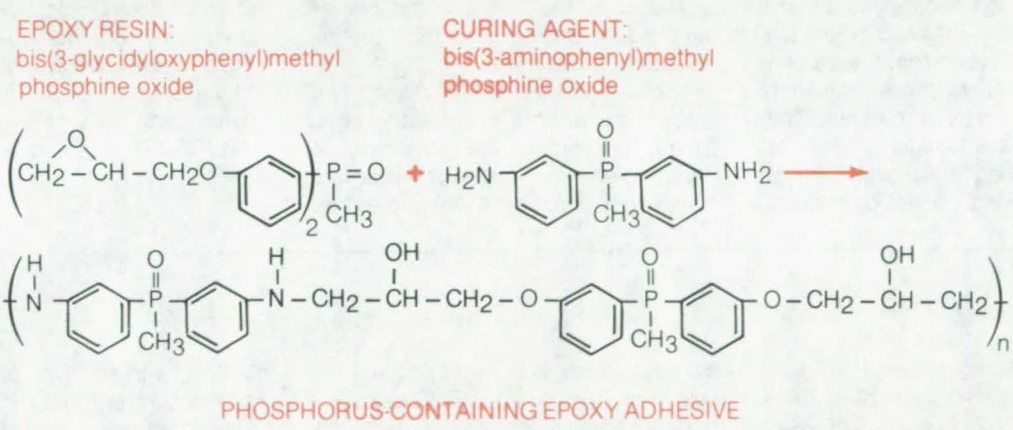

A Reaction for Representative Phosphorylated Components is shown here. The mole ratio is 1:1. When the resulting adhesive is used to bond phenolic/glass laminate to a titanium dioxide-pigmented film, the adhesive bond strength exceeded the tear strength of the film.

A new phosphorus-containing epoxy is fire-retardant and translucent. Intended as an adhesive for laminated plastic sheets, the new material bonds well to titanium dioxide-filled plastic film, which ordinarily shows little surface interaction with adhesives.

Both the epoxy resin and its diamine curing agent include covalently bonded phosphorus in their molecular structures (see figure). Since the curing agent contains phosphorus — unlike such typical curing agents as aminoethylpiperazine, it does not dilute the phosphorus in the epoxy resin. It is therefore possible to keep the phosphorus content of the adhesive above 7 percent, a condition necessary to ensure fire retardancy in air. For a phosphorus-containing epoxy mixed 1:1 on a molar basis with a phosphorus-containing diamine curing agent, for example, the net phosphorus content will be about 10 percent.

Tests have confirmed the desirable properties of the new adhesives. Of two experimental formulations, both adhered to a TiO_2-filled plastic film with a bond strength that exceeded the tear strength of the film. Fire retardancy has been demonstrated, and smoke density is low enough to avoid smoke obscuration.

This work was done by Norman Bilow and Thomas W. Giants of Hughes Aircraft Co. for **Ames Research Center.** *No further documentation is available.*
ARC-11430

Etchant for $Hg_xCd_{1-x}Te$ Crystals

A mixture of nitric and hydrochloric acids reveals crystal defects.

Marshall Space Flight Center, Alabama

A mixture of nitric and hydrochoric acids is a satisfactory etchant for $Hg_xCd_{1-x}Te$ crystals. Preferential etching by the acid solution reveals crystal-dislocation defects (type D) and impurity-dislocation defects (type S) in these crystals, which have optical and electrical applications.

The $Hg_xCd_{1-x}Te$ crystals are immersed in mixtures of nitric acid and hydrochloric acid. A crystal treated for 5 seconds with 0.25 HNO_3, 0.25 HCl, and 0.5 H_2O reveals both the S-type and D-type etch pits. The etching progresses more rapidly with added HNO_3 and progresses more slowly with more HCl and water, with more sensitivity shown to water.

This work was done by E. A. Irene of IBM Corp. for **Marshall Space Flight Center.** *No further documentation is available.*
MFS-25705

Liner for Silicon Reactor

A coating of sodium tetrafluoride minimizes contaminating high-purity silicon.

NASA's Jet Propulsion Laboratory, Pasadena, California

The production of high-purity silicon by the reaction of silicon tetrafluoride and sodium results in reaction products, sodium fluoride and silicon, that adhere to the reactor walls. The reaction, which begins at 150° C, can reach temperatures of 2,000° C. At these high temperatures, there exists the danger of the nickel reactor walls melting.

To avoid melting the nickel or contaminating the silicon, either by contact with the walls or by handtools needed to dislodge the NaF/Si, the reactor walls are coated with a layer of NaF. By using an NaF liner, the reaction products are removed by simply turning the reactor chamber upside down.

There are other benefits to the NaF liner. The liner acts as a seeding agent for the NaF formed during the reaction; thus, a clean segretation of silicon and NaF occurs, making it easy to extract the silicon. Also, the liner insulates the nickel walls from the hot reaction products.

This work was done by Angel Sanjurjo of SRI International for **NASA's Jet Propulsion Laboratory.** *For further information, Circle 89 on the TSP Request Card.*
NPO-15366

Books and Reports

These reports, studies, and handbooks are available from NASA as Technical Support Packages (TSP's) when a Request Card number is cited; otherwise they are available from the National Technical Information Service.

Corrosion-Protection Coatings for Aluminum

Study investigates 21 combinations of surface treatments, primers, and topcoats.

Test results show that outstanding protection can be afforded to 2219-T87 aluminum alloy in severe seacoast and seawater environments. The tests were part of a study of the developments that have been made on protective coatings for aluminum since early in the Space Shuttle program. The study considered several types of coatings, including primers, enamels, chlorinated rubbers, alkyds, epoxies, vinyls, polyurethanes, water-based paints, and antifouling paints; but many were eliminated from consideration because they were not expected to protect the Space Shuttle during launch and reentry. A 20-page report summarizes the study.

For the tests, sets of panels were primed and topcoated, subsequent to a surface treatment, using a conventional air-spray gun. Panels of 2219-T87 aluminum were prepared, primed, and coated with 21 different combinations, scribed with an 'X' on one side, and exposed to a 5-percent salt spray for 4,000 hours. Following the salt-spray test, a section was cut from each sample and exposed in a forced-air oven to determine resistance to high temperature [400° F (200° C)]. Application properties, adhesion, heat resistance, and corrosion protection were among the properties evaluated.

Results of these tests indicated four combinations with outstanding performance and four additional combinations with corrosion protection almost as good. These combinations are generally based on a chromated pretreatment, a chromate epoxy primer, and a polyurethane topcoat.

Of the outstanding samples, all had only very small blisters and light white corrosion products in the scribe marks

after over 4,000 hours of salt-spray exposure; there was no undercutting of the paint at the scribe marks. In these tests, there was no discernible difference between the polyamide or amine cured epoxy primers, though primer choice must be compatible with the topcoats.

Because of the increasing demands to reduce the use of toxic materials, the survey included nonchromated inhibitors for use with aluminum alloys. The combinations without chromates, either in a conversion coating or the primer, failed along the scribe marks by blistering, undercutting the paint films, and losing adhesion. In general, it was found that these inhibitors are still in the development stage and are not satisfactory for severe corrosive environments.

The combination that afforded the least protection, with the exception of two zinc primers, used a wash primer pretreatment. The deterioration of two zinc-rich systems, phenoxy and epoxy polyamide, began almost immediately.

This work was done by R. H. Higgins of **Marshall Space Flight Center.** *Further information may be found in NASA TM-82402 [N81-19274/NSP], "Evaluation of Several Corrosion Protective Coating Systems on Aluminum" [$6]. A paper copy may be purchased [prepayment required] from the National Technical Information Service, Springfield, Virginia 22161. The report is also available on microfiche at no charge. To obtain a microfiche copy, Circle 31 on the TSP Request Card.*
MFS-25640

Environmental Durability of Electroplated Black Chromium

Coated aluminum solar panels were tested in rural, industrial, and seacoast environments.

A recent report describes tests of the durability of electroplated black-chromium coatings on solar-collector panels in rural, industrial, and seacoast environments for 60, 36, and 13 months, respectively. The black-chromium coating showed exceptionally-good optical durability in all three environments. As expected, the seacoast environment proved most severe. While optical degradation was not severe, considerable corrosion occurred.

Panels for collecting solar energy as heat are usually prepared from metals coated to increase the absorption of solar radiation (wavelengths in and near the visible region) without significantly increasing emissivity at the longer infrared (IR) wavelengths at which losses due to reradiation occur. Electroplated black chromium is one of several known coatings with suitable optical properties; namely, solar absorptance higher than 0.9 and infrared emittance around 0.1. Obtaining such optical selectivity requires the use of coatings so thin that their ability to protect the metal substrate from corrosive environments tends to be limited.

Commercial flat-sheet solar-collector panels made from 1100 aluminum were first plated with bright nickel 0.0005 inch (0.0127 mm) thick to improve corrosion resistance and then plated with a thin layer of black chromium to an unspecified thickness to obtain the desired absorptance/emittance ratio. The panels were 2 by 3 feet (0.6 by 0.9 m) and contained integral flow passages fabricated by the silk-screen/hot-roll process.

The panels were exposed bare to produce a "worst-case" condition. (In normal use, covers over the panels help to protect them from the environment.) A portable solar and infrared reflectometer was used to obtain the solar absorptance and IR emittance information shown in the figure.

The rural site at Marshall Space Flight Center near Huntsville, Alabama, is low in or essentially free of various corrosive pollutants. The industrial site was a highly industrialized area in North Birmingham, Alabama. At the seacoast site, Kennedy Space Center near Titusville, Florida, panels were tested at two locations, 120 feet (37 m) from the mean high-tide line and 1 mile (1.6 km) inland.

The panels were mounted at 45°, facing south except at the seacoast sites where the panels were mounted 30° from horizontal, facing east toward the ocean. At the rural site, corrosion was slight (some minute specks surrounded by small areas of discoloration), solar absorptance was unchanged, and IR emittance increased only slightly.

At the industrial site, corrosion resistance was considered good, but small brown spots 0.02 to 0.03 inch (0.05 to 0.08 cm) in diameter (apparently caused by cinder particles from a nearby metal furnace clinging to the panels and rusting) were scattered over the panels. Solar absorptance and IR emittance both increased slightly.

At the seacoast sites, corrosion was more severe with panels at both sites showing white corrosion spots 0.13 to 0.19 inch (0.32 to 0.48 cm) in size. Spots were more numerous at the beach site. Solar absorptance was essentially unchanged, but IR emittance increased slightly inland and moderately at the beach.

This work was done by James R. Lowery of **Marshall Space Flight Center.** *To obtain a copy of the report, Circle 32 on the TSP Request Card.*
MFS-25797

Equations for Composite-Propellant Burning

Progress is made toward a predictive model.

A reported study of composite-propellant burning summarizes recent advances in understanding the behavior of propellant formulations based on ammonium perchlorate (AP), binder, and aluminum in various proportions and particle size distributions. The approach presented in this report incorporates an adapted version of an earlier model for monopropellant AP. The objective is to predict the burning-rate characteristics of composite propellants at high pressure.

The report begins with a presentation of the revised model of AP monopropellant combustion. A trial surface temperature is selected and inserted into equations for mass flux, the fraction of AP reacted in the gas phase, the fraction of AP reacted in the condensed phase, heat content of the adiabatic flame, net surface heat, net heat release, flame standoff distance, and heat balance at the surface. The heat-balance equation yields a value of surface temperature that is then compared with the trial value and iterated until the two values converge.

An important concern is the allocation of AP/binder burning rates among particles of various sizes in multimodal propellants. As a first approximation, the finer particles are considered to burn more fuel rich than the coarser particles because of their greater surface area per unit mass. There is, however, some interaction among the various particle-size fractions: This is taken into account in deriving more realistic expressions for the oxygen/fuel ratios and burning rates as a function of the concentrations of particles of different sizes.

(continued on next page)

The diffusion-flame analysis generally follows that of the earlier model but with some changes to improve the continuity of the changing flame structure and to give more importance to the binder. The concept of flame interactions is discussed but is not incorporated into the model for a lack of data.

The effect of aluminum in bimodal and trimodal propellants is considered. It is concluded that aluminum agglomerates to a lesser extent with decreasing coarse AP size, increasing AP fine size, increasing fraction of fine AP, increasing pressure, and increasing aluminum size. It is further concluded that there is a coarse-aluminum regime in which agglormeration is independent of pressure. Formulas are given for the ignition and combustion distances of aluminum particles above the surface and for an effective aluminum flame height.

Surface-area and burning-rate equations are introduced. A new equation is derived for the burning rate of multimodal propellants, reflecting more closely than do earlier models the way propellants really burn.

The energy-balance equations for AP monopropellant are recited in a more sophisticated form for composite propellants. The new equations account for the heat feedback from the diffusion flame closing over the AP flame. A modified surface-temperature equation includes additional terms for the effects of the binder and the aluminum.

It is anticipated that the completed model will be applicable to many different propellants. Although the report does not discuss industrial applications, this work should stimulate further developments in combustion science and engineering.

This work was done by Leon D. Strand and Norman S. Cohen of Caltech for **NASA's Jet Propulsion Laboratory.** *To obtain a copy of the report, Circle 33 on the TSP Request Card.*
NPO-15324

Properties of Nickel-Based Hydrogen-Turbine Blades

Tests on alloys for hydrogen-burning engines of the future are described.

A 120-page report presents data on mechanical properties of cast nickel-based alloys for turbine blades operating in hydrogen and steam at high temperatures. In particular, the document deals with three alloys: single-crystal MAR-M-246 + Hf, single-crystal PWA 1480, and directionally-solidified MAR-M-246 + Hf. Properties were measured at 760° C and 871° C (1,400° F and 1,600° F). The alloys have been proposed for use in space propulsion systems operating on high-pressure hydrogen.

Described in the report are tensile properties (yield and ultimate strengths, elongation, reduction of area, and modulus of elasticity), creep-rupture properties (creep rate, rupture life, elongation, and reduction in area), low-cycle fatigue, and crack growth. Measurements were made on solid specimens exposed to gaseous hydrogen and hydrogen-enriched steam at a pressure of 5,000 lb/in.^{2} (34.5 MPa). Specimens were tested in both transverse and longitudinal orientations.

The report is arranged in sections covering: general results and conclusions; descriptions of materials, specimens, and tests and specific results and conclusions for each of the property tests. The report includes information from monthly progress reports previously issued in the test program and pertinent test results from previous contract work. In general, single-crystal PWA 1480 performed better than the other alloys, although there were some exceptions for low-cycle fatigue.

This work was done by D. P. Deluca, J. R. Warren, B. A. Cowles, D. P. Shoemaker, J. R. Teel, Jr., D. L. Pearson, C. G. Annis, Jr., D. A. Wilson, and B. J. Schwartz of United Technologies Pratt & Whitney Aircraft for **Marshall Space Flight Center.** *Further information may be found in NASA CR-14844 [N81-31192/NSP], "Mechanical Properties of Turbine Blade Alloys in Hydrogen at Elevated Temperatures" [$13.50]. A paper copy may be purchased [prepayment required] from the National Technical Information Service, Springfield, Virginia 22161. The report is also available on microfiche at no charge. To obtain a microfiche copy, Circle 34 on the TSP Request Card.*
MFS-25733

Life Sciences

Hardware, Techniques, and Processes

Spine Immobilizer for Accident Victims

A conformal bladder would safely blanket, immobilize, and restrain spine injury victims.

Ames Research Center, Moffett Field, California

In spite of advances in methods and appliances for the protection of the cord in spinal injuries, many victims who are able to move their extremities shortly after an accident receive irreparable damage to the spinal cord during transport from the scene of the accident to a hospital.

There are a number of techniques for the transport or removal of an accident victim suspected of having a spinal injury. In general, the techniques involve providing support for the body before any lifting takes place. Examples of this technique are the use of a spine board or an articulated chair to which the victim is strapped. Makeshift pads are placed between the victim and the board or chair. Unfortunately, the victim can be further injured while he is being fastened to the back support, and the pads often create undesirable pressure points on the victim.

A proposed conformal bladder, which is filled with tiny spheres called "microballoons," would enable the spine of an accident victim to be rapidly immobilized and restrained and permit the victim to be safely removed from the accident scene in an extremely short time after help arrives. The microballoons expand to form a rigid mass when the pressure within the bladder is less than ambient.

The bladder, which is made of resilient plastic, is strapped about the head and torso of the victim, as shown in the figure. The victim is secured with a pair of straps that cross one another over the chest, above the stomach region, and another pair of straps that engage a lower portion of the torso beneath the stomach region, so that the stomach region is kept free of any restraining forces. This is important because the stomach muscles are required in breathing under these circumstances, and any restraint on these muscles could be harmful.

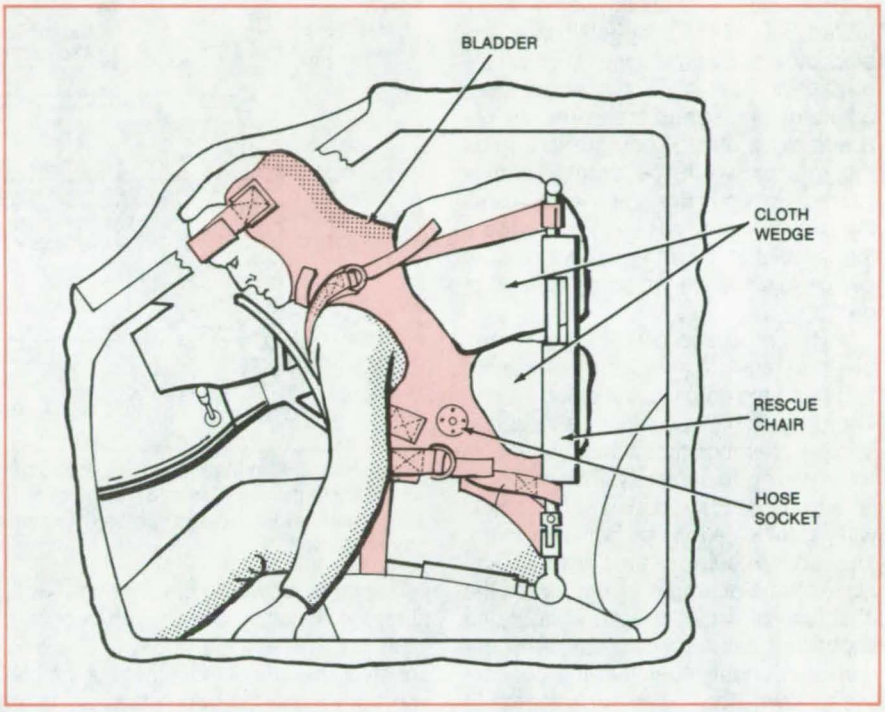

The **Spine Is Immobilized** by a bladder and support. The bladder, which is strapped to the victim (here behind the wheel of a car), is also strapped to a rescue chair. The void between bladder and chair is filled with cloth wedges.

Once the straps are adjusted, a hose is plugged into a socket on the bladder, and air is withdrawn by a pump. When the air is withdrawn, the tightly compressed microballoons that fill the bladder become as firm as concrete and rigidly support the victim's spine.

Included in the connection tubing is an adjustment valve that controls the air evacuation rate. In this way, a paramedic can reversibly soften and harden the microballoons and the conformal blanket formed by the bladder so as best to fit the victim. The rigidified bladder is then secured to a support, and the victim is transported from the accident scene by using the rigid support. When the victim has reached the hospital (or any other time that it is desired to soften the bladder) a valve is opened to admit air to the bladder.

In the flexible bladder is a filter for filtering air and for preventing the microballoons from escaping. The apparatus also includes an inlet/outlet coupling for connecting the interior of the bladder to a vacuum pump, and for securing the bladder in position on the patient and straps for assisting in securing the bladder to a rigid support for enabling the patient to be transported.

This work was done by Hubert C. Vykukal of **Ames Research Center** *and Kenneth Lampson of Kenneth Lampson & Associates. For further information, Circle 35 on the TSP Request Card.*

Inquiries concerning rights for the commercial use of this invention should be addressed to the Patent Counsel, Ames Research Center *[see page A5].* *Refer to ARC-11167.*

Implantable Drug Dispenser

Differential vapor pressure allows fine control.

NASA's Jet Propulsion Laboratory, Pasadena, California

Drugs such as insulin would be injected as needed directly into the bloodstream by a compact implantable dispensing unit. The dispenser uses counteracting vapor pressures on opposite sides of a diaphragm to control the rate at which the drug is administered. Previous designs use liquids as the pressure media, but they require a larger volume than the vapor-pressure device to dispense the same amount of drug.

In the proposed device (see figure), heaters regulate the vapor pressures that force the drug into the bloodstream. The drug, in liquid solution, is held in a central chamber that connects with a tube leading to an artery. The chamber is surrounded by concentric bellows with a saturated vapor between them. The space outside the bellows and above the diaphragm at the top of the chamber is also filled with a saturated vapor that has a lower vapor pressure than that contained within the concentric bellows. The gases are selected to provide balanced forces at body temperature on the sides of the diaphragm. This stabilizes the diaphragm position without power input. The gases can be fluorocarbons or other material for which the vapor pressure varies widely with temperature and thus responds readily to heating.

Each of the vapor cavities defined by the concentric bellows contains an electric heater. A battery supplies power to the heaters under the control of a microprocessor. If heater 1 heats the vapor in cavity 1, the pressure in that cavity will increase and drive the diaphragm toward the bottom wall, thereby expelling the drug through the exit port. If heater 2 in cavity 2 is also heated, the rate of movement of the diaphragm can be regulated or even balanced so that it is held in a fixed position with respect to the wall.

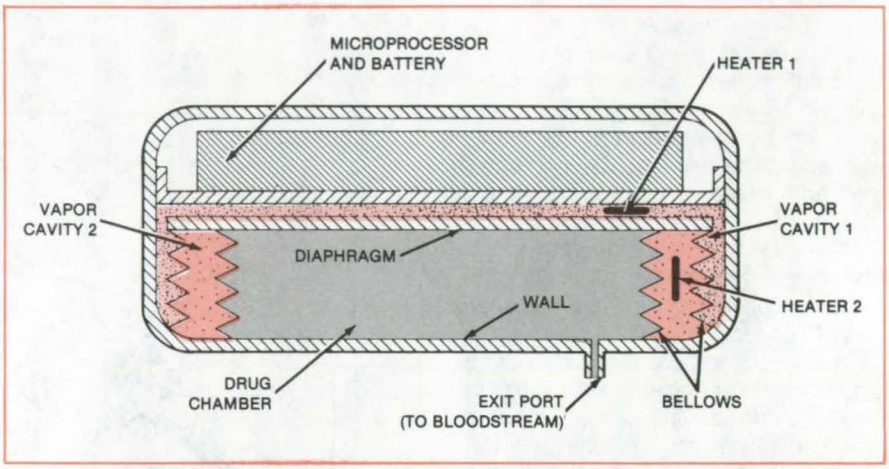

Two Vapor Cavities produce opposing forces on the drug-chamber diaphragm. Heaters in the cavities allow control of the direction and rate of motion of the bellows. The dispensing capsule can be fitted with a coil so that the batteries can be recharged by induction.

When the programed amount of drug has been dispensed at the programed rate, current may be cut off from one or both heaters to establish a stable diaphragm position. No more drug is dispensed until a command is received from the microprocessor. Feedback can be provided to the microprocessor by temperature sensors in each cavity. The sensors would allow the microprocessor to monitor temperature and, indirectly, the rate and amount of dispensation.

When it is necessary to replenish the liquid in the drug chamber, heater 2 is energized while heater 1 is not. The diaphragm moves away from the wall, creating a negative pressure in the drug chamber that draws in a new supply of the drug from an external source. A dispensing device of implantable size could hold a 30-day supply of insulin to be dispensed at a rate of 1 cm^3 per day.

This work was done by Earl R. Collins, Jr., of Caltech for **NASA's Jet Propulsion Laboratory.** *For further information, Circle 36 on the TSP Request Card.*

Inquiries concerning rights for the commercial use of this invention should be addressed to the Patent Counsel, NASA Resident Office-JPL [see page A5]. Refer to NPO-15160.

Mechanics

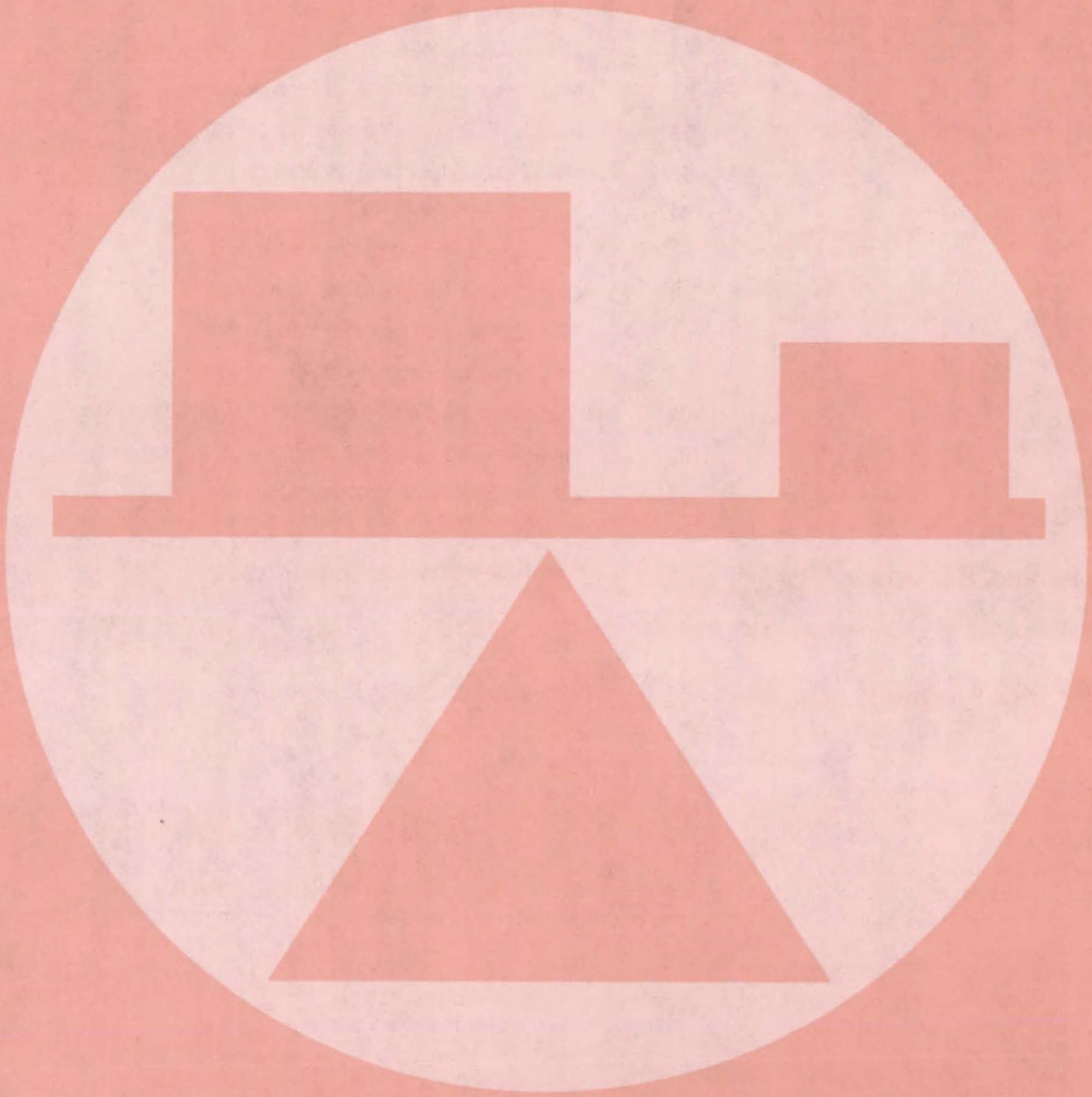

Lightweight Thermal-Protection System

Hexagonal honeycomb panels are light, durable, and easy to maintain.

Langley Research Center, Hampton, Virginia

A thermal-protection system originally proposed for the exterior of Earth-to-orbit transports employs external hexagonal honeycomb panels held in place by Y-shaped plates. The system uses lightweight materials and novel assembly methods to reduce weight and simplify maintenance. Other advantages include complete symmetry of components — there are no left- or right-hand parts and no asymmetry in thermal expansion.

Previously-proposed thermal-protection systems, including ablators, corrugated metallic panels, and sintered silica fibrous tiles have various drawbacks: Ablators are not reusable. Corrugated metallic panels are not smooth for aerodynamic flow. Reusable surface insulation (RSI), a lightweight highly-insulative sintered-fiber tile, is relatively new; and the full implications of this system are not yet known. If tiles are used over an isogrid tank, a carrier panel is needed onto which the tiles are mounted.

As shown in the figure, the thermal-protection system designed for Earth-to-orbit transports consists of an external hexagonal honeycomb panel that resists aerodynamic loads and the high temperatures associated with exit from, and entry into, the Earth's atmosphere. The hexagonal panel is clamped in place by 6 Y-plates, which in turn are held by 18 fasteners. The fasteners are threaded into the female end of standoffs, which are screwed into the isogrid ribs in the vehicle propellant tanks. The repair of individual panels is very easy, since a single panel can be removed without removing adjacent panels.

High- and low-temperature insulation materials are installed beneath the panels. The thicknesses of the insulation are chosen to handle the local temperatures and heat loads.

For installation over an isogrid tank, this system is lighter than ceramic tile bonded to a carrier panel because the honeycomb panel serves as both carrier panel and outer thermal shield. Further, the lightweight flexible fibrous materials beneath the honeycomb serve as insulation instead of the heavier tile.

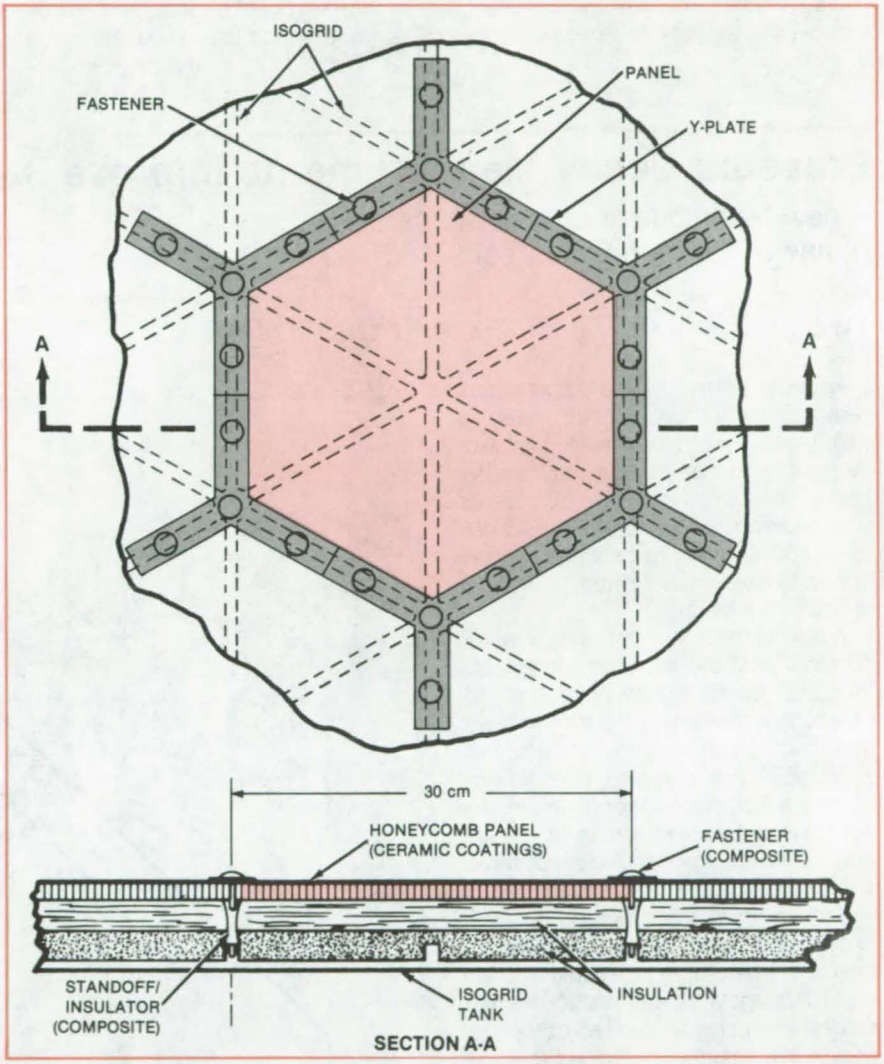

Hexagonal Honeycomb Panels secured by Y-shaped plates would form a lightweight, easily-maintained thermal-protection system.

Another feature that makes the system lightweight is component sharing. For example, the 6 fasteners shown at the corners of the hexagon are shared among 3 panels, while the 12 fasteners located on the legs of the Y-plate are shared by 2 panels. Therefore, out of 18 fasteners used for panel retention, the weight of only 8 is charged to any one panel. Also, each Y-plate is shared with three panels; therefore, the weight of only two Y-plates (6 divided by 3) is charged to any one panel.

In use, the outer facesheet of the panel becomes hot and radiates and conducts heat to the inner facesheet. As a result, there is very little difference between outer and inner facesheet temperatures and, therefore, almost no distortion of the panel. The hexagonal panel has the least perimeter for a given area of coverage, the second most attractive shape being a square panel and the third a rectangular panel. Also, it is advantageous to have the shortest continuous panel-edge length possible, to

(continued on next page)

discourage the flow of hot gases at the panel joints.

The honeycomb outer panel and fastener materials are selected to match the local heating rates. Typical materials could include composites, titanium, superalloys, and refractory metals.

An alternate configuration includes 120° flush-mounted fasteners. The Y-plates are countersunk by dimpling. In this design, the Y-plate thicknesses are increased to retain the honeycomb panels. In another configuration, an additional fastener could be placed at the center of the panel to provide additional support, since expansion due to temperature change is theoretically zero at the panel geometric center.

The system is flexible in that areas with different heating rates and flow properties could be fitted with different sandwich materials, all held in place by the Y-plates. The resulting surface would have a continuously low profile and would have improved aerodynamic surface characteristics.

This work was done by Ian O. MacConochie, Ashby G. Lawson, and Thomas C. Whiteman of **Langley Research Center** *and Evans P. Brien of Kentron International, Inc. For further information, Circle 37 on the TSP Request Card.*
LAR-12880

Pressure-Decay Measurements Improve Bubble-Point Test

A new technique improves the detection of flaws in wire-mesh screens.

Lyndon B. Johnson Space Center, Houston, Texas

Flaws in screen mesh are sometimes detected by a "bubble-point" test, in which the screen is immersed in a liquid, removed, and then pressurized from below until a steady stream of bubbles emerges from somewhere on the screen surface. The pressure at which bubbles are first observed is related to the size of flaws on the screen.

A new technique reduces by a factor of about 100 the minimum detectable flaw size in the bubble-point test. By measuring the rate of slow leakage, flaws as small as about 10^{-4} in.^{2} (0.06 mm^2) are detected (see figure). Since the technique does not require observation of the screen, tests can be run on screens already installed inside tanks and pipes.

To test an installed screen, its container is filled and then drained, leaving the screen saturated with liquid. A pressure differential is applied across the screen and increased until an abrupt decrease in pressure is noted on pressure-monitoring instruments. This pressure is the conventional bubble point.

To detect smaller flaws than those that determine the conventional bubble point, the screen is resaturated with liquid. This time, a pressure differential of about two-thirds to three-fourths of the bubble-point pressure is applied. There is no rapid drop in pressure this time. Instead, a slow leakage occurs, which is observed on the pressure gage.

Equations have been derived relating the leakage rate to the flaw size. The equations have been calibrated using screens with known flaw sizes. Tests show excellent agreement between the theoretical and measured pressure decays.

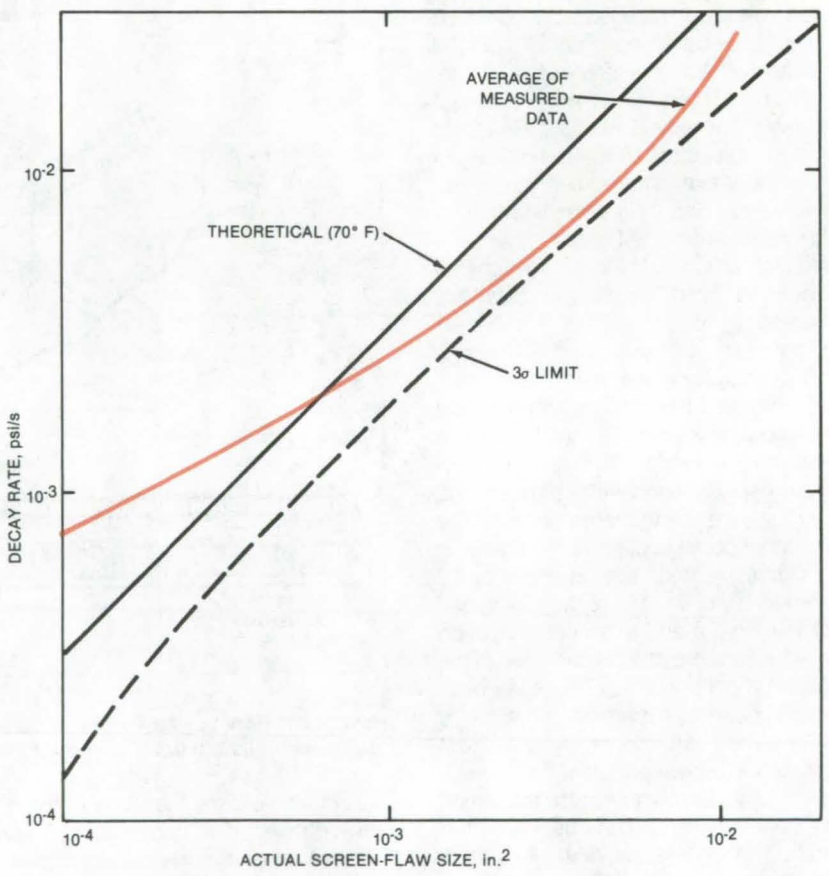

Predicted and Measured Pressure-Decay Rates for screens with known flaw sizes agree well enough to allow determinations of unknown flaw sizes from the measurement of decay rates. These data were obtained using a fluorocarbon gas and simulated screens for the Space Shuttle orbital-maneuver propellent system.

This work was done by Joseph S. Silkey and George F. Orton of McDonnell Douglas Corp. for **Johnson Space Center.** *For further information, Circle 38 on the TSP Request Card.*
MSC-18970

Connector for Composite Tubes

Elements made of composite join tubes at various angles.

Langley Research Center, Hampton, Virginia

Difficulties in joining tubular structural members made of composite materials are overcome by improved connectors. The connectors are made from the same composite as the structural shapes, eliminating the stress and weight problems experienced with metal connectors. The composites also allow the joint strength to be optimized by properly choosing the fiber orientation and the fabric. Only two basic shapes are required to make 90° and T-joints in a plane.

The shape of the basic joint element is a cylinder with a tab on each side of a longitudinal gap as shown in Figure 1. The inner surface of one tab lies in a plane through the centerline of the cylinder. The other tab is offset to leave a gap equal to the tab thickness. The inner diameter of the cylinder is 0.005 to 0.010 inch (0.0127 to 0.0254 cm) larger than the tube to be joined to allow for the adhesive thickness. To join tubes of different diameters, the cylinder diameter is changed, but the tab thickness and gap width are kept constant.

The basic element is made by placing fabric and resin over a mandrel, then vacuum bag molding and curing in an oven at the appropriate temperature. Eight connector elements are cut from a 12-inch (30.48-cm) piece, when sized for joining tubes in the diameter range of 0.75 to 1.25 inches (1.905 to 3.175 cm). The cuts are made perpendicular to the cylinder centerline. Then the tabs are trimmed to an angle required by the type of joint being made.

A right-angle joint is made by placing a connector element on each tube so that the inner surfaces of the tabs on the centerline face each other. Inserting one of these tabs into the gap of the other connector insures that the centerlines of the two tubes are in the same plane. The tabs may be trimmed along a 45° line as shown in Figure 1.

To make a T-joint, two of the basic connector elements are slid on the tube to each side of where the other tube is to join. Both basic elements are placed with their centerline tabs in the same plane. To complete the joint two different parts called web elements are used (see Figure 2). The tabs of each web element are one-half the thickness of the gap between the tabs of a basic element, so they will fit into the gap of the basic element. To keep the centerlines of the tubes in a plane, the tabs of the web elements are offset so that the outer surface of one lies on a plane through the centerline of the tube.

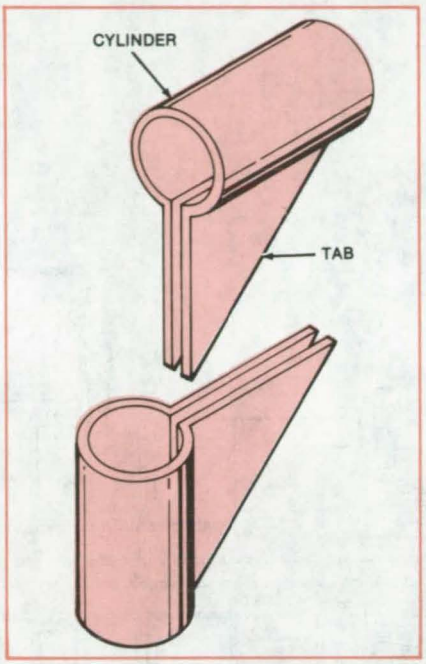

Figure 1. A **90° Joint** is made by combining two of the basic connector elements. The inner surface of one tab lies in a plane through the centerline of the cylinder.

This technique can be applied to other regular-cross-section components made from composite materials. It can be used to assemble strong, lightweight, three-dimensional structures.

This work was done by Ernest Harrison, Jr., of the Mississippi Methodist Rehabilitation Center for **Langley Research Center.** *For further information, Circle 39 on the TSP Request Card.*

This invention is owned by NASA, and a patent application has been filed. Inquiries concerning nonexclusive or exclusive license for its commercial development should be addressed to the Patent Counsel, Langley Research Center [see page A5]. Refer to LAR-12744.

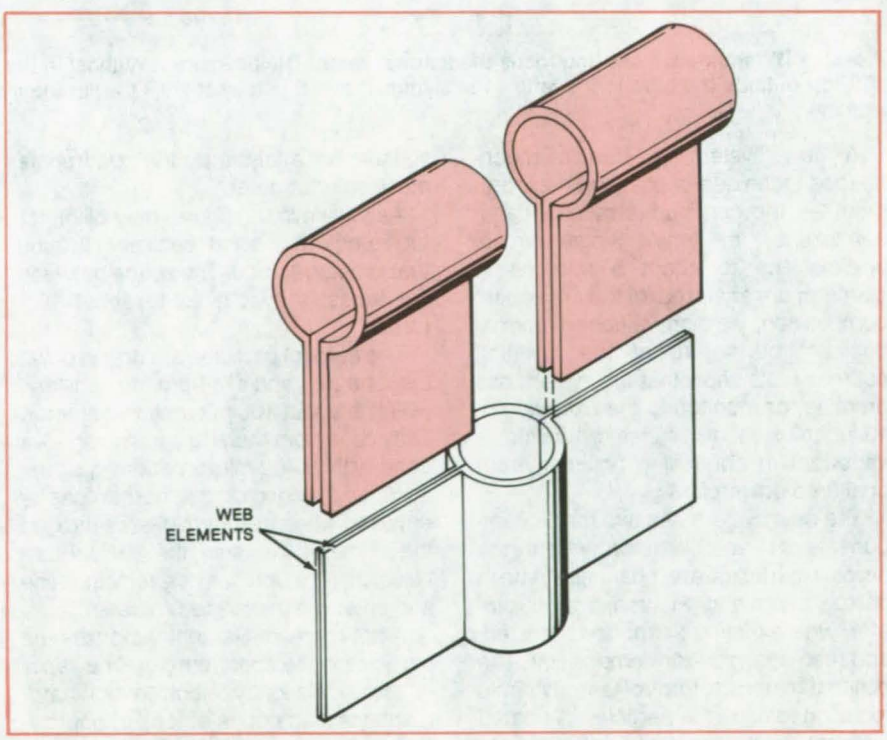

Figure 2. **Two Web Elements and Two Basic Elements** are combined in a T-joint. The elements can also be designed to handle structural elements with noncircular cross sections.

Continuous Monitoring of Aerosols

Online spectrometer monitors the composition of individual aerosol particles.

NASA's Jet Propulsion Laboratory, Pasadena, California

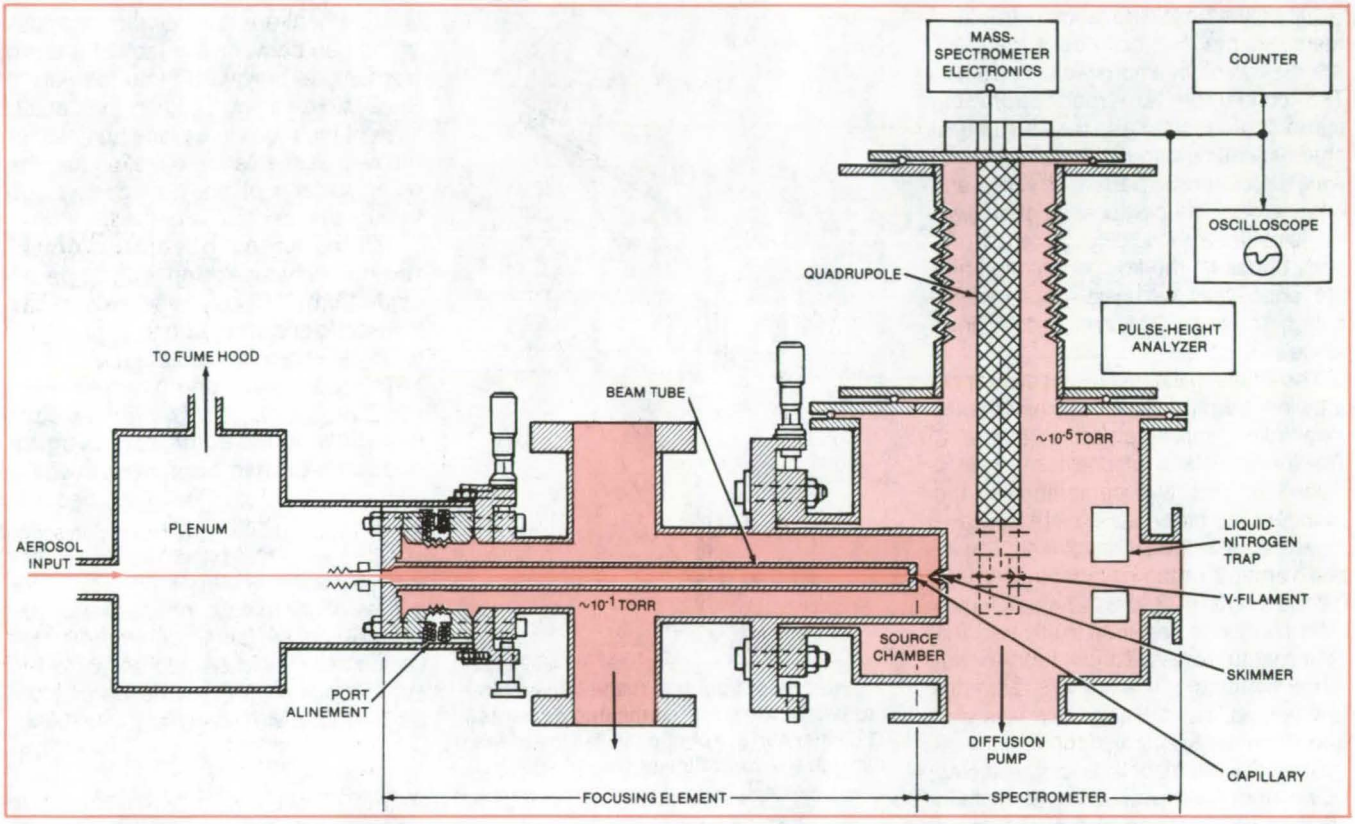

Pressure Differentials move and focus the aerosol beam. The pressure is highest in the innermost tube of the focusing element; it is 10^{-1} torr outside the tube to the left of the skimmer; and it is lowest (10^{-5} torr) in the mass-spectrometer chamber to the right of the skimmer.

A new system realizes a much-needed technique of pollution measurement — the continuous monitoring of aerosols in "real time." Single aerosol particles up to about 5 microns in diameter are analyzed for their chemical composition, yielding valuable information on the nature of the pollution source. Tests show that the system has promise for monitoring the oxidation of sulfur dioxide to sulfates, which is important in controlling pollution from coal-fired powerplants.

The new system has two major components: (1) a collimator, where the aerosol particles are channeled into a narrow beam and (2) a mass spectrometer, where they are vaporized, ionized, and then analyzed for composition. The collimator uses a form of aerodynamic focusing to aline the particles. A heated filament and electron bombardment convert the aerosol particles into ions suitable for analysis by the quadrupole mass spectrometer.

As shown in the figure, the collimator tube ends in a short capillary. Around that is a larger tube. The space between the tubes is evacuated to about 10^{-1} torr.

The aerosol particles are drawn down the tube axis and exit from the capillary, which is about 100 microns in diameter. They pass from there to a skimmer, — a cone with a 400-micron opening at the input end. Most of the carrier gas is removed when the beam passes through the skimmer; however the aerosol particles, being much heavier, remain in line and enter the mass spectrometer.

A hot rhenium filament vaporizes the particles in the spectrometer. The vapor is then ionized by electron bombardment, yielding bursts of ions of approximately 80-μs pulse width. The bursts are mass-analyzed by the quadrupole mass spectrometer.

Thus far, satisfactory analyses have been made of aerosols containing sodium sulfate and sulfite, ammonium sulfate, lithium nitrate, adipic and glutaric acids, dioctyl phthalate, and some of the amino acids. By comparing the analysis with that for a referance aerosol, it is possible to determine the sulfate-to-sulfite ratio of individual particles.

This work was done by Mahadeva P. Sinha, Charles E. Giffin, David D. Norris, and Sheldon K. Friedlander of Caltech for **NASA's Jet Propulsion Laboratory.** *For further information, Circle 40 on the TSP Request Card.*

Inquiries concerning rights for the commercial use of this invention should be addressed to the Patent Counsel, NASA Resident Office-JPL [see page A5]. Refer to NPO-15292.

Mobile Air Sampler

Vehicle-mounted sampler gathers specimens along highways and in tunnels.

NASA's Jet Propulsion Laboratory, Pasadena, California

A simple device for collecting air samples is used on a moving vehicle. It therefore provides realistic specimens for the analysis of air quality along highways and in tunnels. In contrast to fixed air-collection installations, the mobile sampler requires no official approval for its use on highways.

The device consists of an open tube 1.6 inches in diameter and 6 inches long (4.1 by 15.2 cm). However, size is not critical; the essential requirement is that the tube not restrict the flow of air through it. Sealing caps at both ends of the tube are spring-activated and are held open by a thread (see figure). When a wire loop around the thread is energized by an operator, it heats up and severs the plastic thread.

As soon as practial after a sample has been enclosed in the device, it is wired shut to prevent accidental opening of the end caps. When the collected sample is to be analyzed, a nipple on one of the end caps is uncovered, and tubing is connected to it. The tubing leads to a collection syringe or directly to a gas chromatograph or other instrument. The opposite end cap contains a mandrel-mounted seal that, when screwed to a pushrod, becomes a piston for expelling the sample.

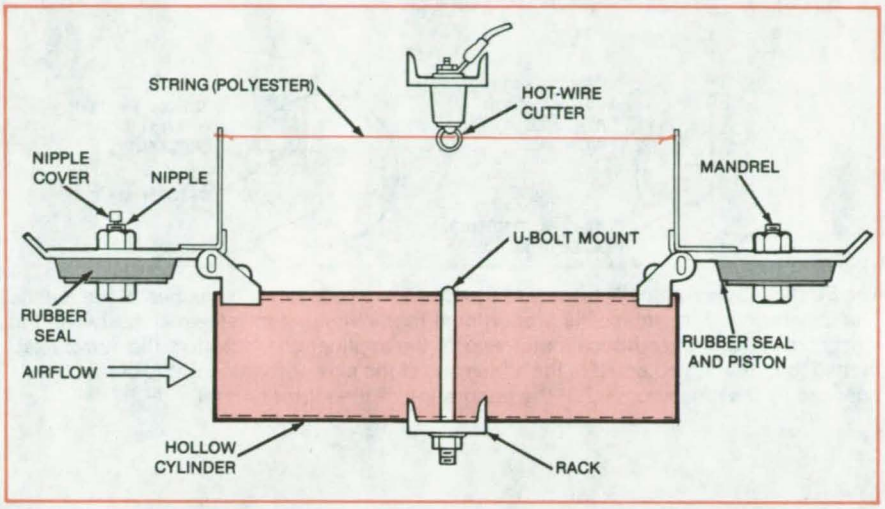

The **Mobile Air-Sampling Device** closes when the hot-wire cutter melts the plastic string.

After the sample has been removed from the container, the safety wire is removed from it, the nipple is covered, the piston seal is restored to its original position, and a new thread is installed. The sampler is then ready for reuse.

Many samplers can be installed on a vehicle. For example, 30 samplers were mounted on a frame on a pickup truck and used to sample air in one of the tunnels on the northbound Pasadena Freeway in southern California. The hot-wire cutters are operated either separately or in unison by switches in the truck cab.

This work was done by Curtis E. Tucker and Harold P. Holway of Caltech for **NASA's Jet Propulsion Laboratory.** *For further information, Circle 41 on the TSP Request Card.*
NPO-15220

Measuring Mirror Tilt With High Accuracy

Stroboscopic technique freezes mirror motion so that displacements can be measured.

Goddard Space Flight Center, Greenbelt, Maryland

An improved autocollimator accurately measures the angular tilt of plane mirrors in rotational or reciprocating motion. The device is a conventional autocollimator in which the steady light source is replaced by a stroboscope that can be synchronized with the mirror motion. It is accurate to 1 second of arc.

The stroboscopic autocollimator produces a collimated beam of light, the cross section of which is in the shape of a reticle pattern. The moving mirror reflects the light back to the autocollimator, which reimages the light on the source reticle pattern (see figure). When the autocollimator light is strobed in synchronism with the motion, it freezes the image of the mirror position for measurement.

For a translating mirror, the limits of motion must not exceed the diameter of the autocollimator objective lens. If the mirror is normal to the autocollimator beam, the reimaged pattern will match the source pattern precisely. However, if the mirror is tilted, the return image will be displaced. The displacements are measured and directly interpreted in terms of tilt.

Modification of the autocollimator for stroboscopic operation is straightforward. The original lamp is removed. An aperture plate with a typical hole diameter of 1 inch (2.54 cm) is placed

(continued on next page)

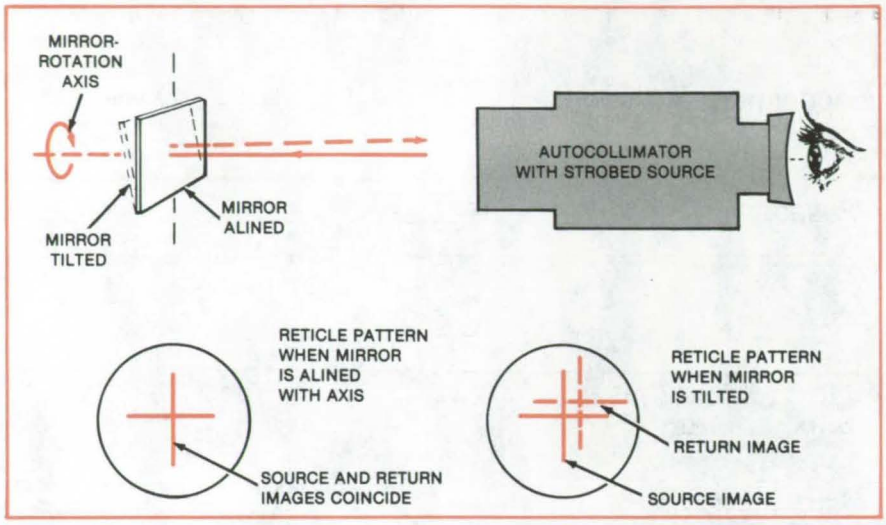

The **Stroboscopic Autocollimator** forms strobed source and return images of the reticle. The separation of the images is proportional to the angle of misalinement between the mirror normal and the autocollimator axis. In the application illustrated, the mirror is attached to a rotating object. It is the alinement of the axis of rotation of the object that is checked by the measurement of the orientation of the mirror normal.

over the stroboscopic light source. The stroboscope is provided with a mounting that mates to instrument in the place of the lamp assembly.

The stroboscopic autocollimator can also be used for vibration analysis. For example, to measure the frequencies of vibration of a component, a mirror is attached to the component, and the autocollimator is alined with the mirror. The return image is viewed through the autocollimator while the strobe frequency is adjusted. The strobe frequency at which the return image is stationary is the vibration frequency of the component. The procedure is repeated to find other vibration frequencies of the component.

This work was done by Thomas J. Magner of **Goddard Space Flight Center.** *No further documentation is available.*

This is the invention of a NASA employee, and a patent application has been filed. Inquiries concerning license for its commercial development may be addressed to the inventor, Mr. Thomas J. Magner, Goddard Space Flight Center, Code 702.1, Greenbelt, MD 20771.
GSC-12701

Exhaust-Plume Impingement Characteristics

Model estimates the effects on nearby objects.

Marshall Space Flight Center, Alabama

A new model for rocket-exhaust plumes calculates the effects of heat, pressure, and particle-impingement on nearby structures. The model compares well with experimental data. It is the result of theoretical and experimental studies of objects exposed to the plumes of rocket exhausts at low altitudes. The model has potential industrial applications in studies of the impingement of multiphase mixtures inside coal-gasification equipment and turbines.

Objects exposed to rocket exhaust are subjected to severe pressure and thermal loads. Furthermore, the exhaust from solid-fueled rockets can contain many solid and liquid particles, because aluminum or other metals is present in the propellant. A complete model must give both the gaseous and particulate contributions to the design loads.

At low altitudes, the exhaust-plume flow includes viscous effects that mix the exhaust gases with the air. The flow is further complicated by afterburning,

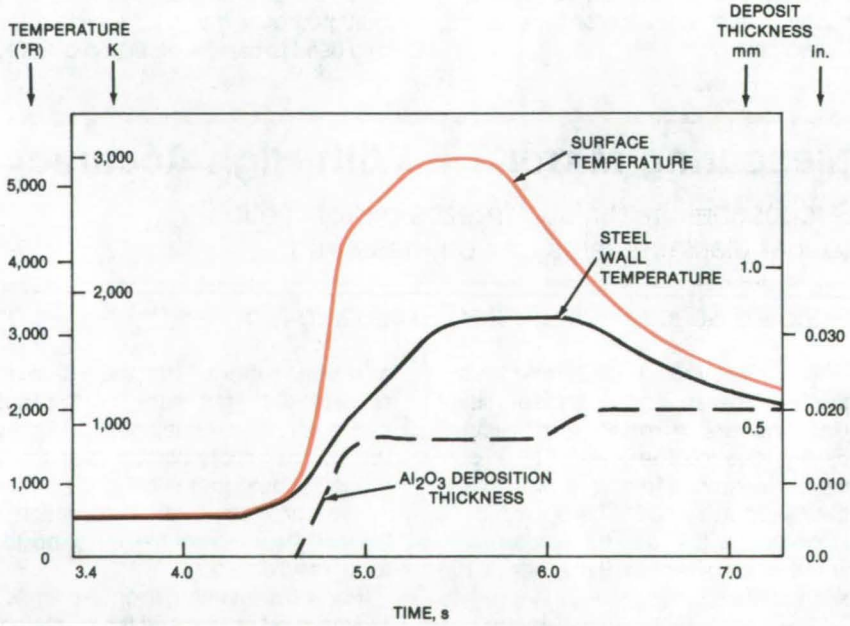

Thermal and Particle-Deposition Loads were calculated for the edge of the exhaust hole on the Space Shuttle Mobile Launch Platform. This represents the most severe condition expected to be encountered on the platform.

by shock waves developing ahead of solid objects in the plume, and by the effects of these shocks on the entrained particles. The model takes all the major contributing phenomena into account.

The nozzle/plume flow field is calculated according to an inviscid-flow computer code that considers the exchange of momentum and energy between the gas and particles. This code also handles equilibrium thermochemistry and takes into account the variations of specific-heat ratios.

Viscous and mixing effects are computed with a code that solves the boundary-layer form of the governing equations. Inputs to the code are the initial-jet and free-stream conditions (pressure, temperature, velocity, Prandtl number, Lewis number, and species distribution). A turbulent-kinetic-energy model relates the turbulent shear stress to a viscosity.

A plume-impingement flow-field calculation establishes the shock conditions ahead of the impinged body. The paths of typical particles in the flow field are traced through the shock to the wall to obtain the mass, momentum, and energy fluxes. The total pressure on the wall is calculated as the sum of the local gas pitot pressure and particle momentum flux at the surface.

The convective contribution to surface heating is relatively straightforward to calculate, but the particle contribution is somewhat more complex. Particle accumulation must be considered, along with the fraction of particle energy transferred to the wall and other effects.

Some final results of the complete model are shown in the figure. The temperature and particle-deposit thickness are plotted as a function of time for a point on a rocket-launching platform.

This work was done by Sheldon D. Smith and Carl J. Wojciehowski of Lockheed Missiles & Space Co., Inc., for **Marshall Space Flight Center.** *For further information, Circle 42 on the TSP Request Card.*
MFS-25489

Heat Pipes Cool Power Magnetics

Configurations originally developed for space use are effective in any orientation.

Lewis Research Center, Cleveland, Ohio

A high-frequency, high-power, low-weight transformer and inductor developed for space use were redesigned with heat-pipe cooling, which allows both a reduction in weight and a lower internal temperature rise. These particular magnetic devices are used in the power stage of a 3-kW ion-beam thrustor.

The use of heat pipes to cool power magnetics in a space environment is a practical solution in high-power designs, but imposes a severe problem when performing testing on Earth. The Earth's gravity field has an effect upon the heat-pipe wicking. If several heat pipes are required, as in modular designs, or if they are used in conjunction with a heat sink cooled by heat pipes, the packaging constraints of keeping all heat pipes horizontal for Earth test become so severe that their use becomes impractical. These newly-developed heat-pipe configurations overcome this limitation.

The high heat-transfer capability of these unique newly-developed, double-ended methanol/stainless-steel heat pipes (Figure 1) allows simultaneous reduction in both mass and internal temperature, which permits the 40-percent weight reduction of the transformer.

The heat pipe exploits the ability of the electrostatic shield to draw heat from the primary and secondary coils of the transformer. Figure 2 shows the electrostatic shield and heat-pipe assembly. Since the shield is physically located near the transformer hotspot and consists of a thin copper sheet, it forms a natural heat collector for the heat-pipe evaporator. There are two heat pipes per coil. The shield heat collector is formed as two separated sheets, one inside toward the primary and one outside toward the secondary. The two shields thus collect the heat generated in the coil winding wire. The shields are used to insure a smooth surface facing each

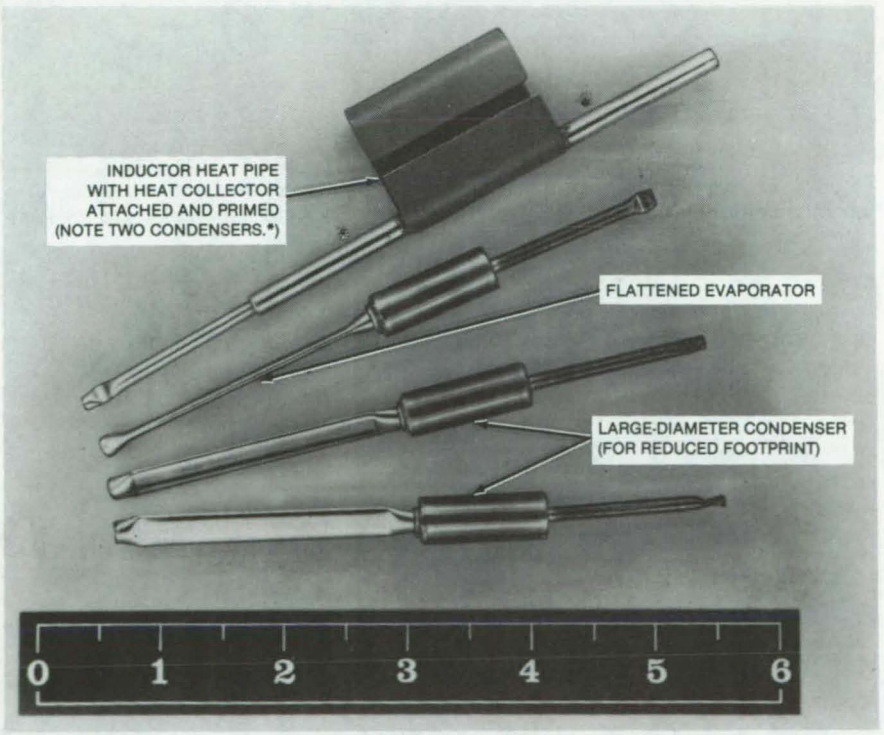

Figure 1. **Heat Pipes** integrated into high-power, high-frequency, high-voltage spaceflight magnetics reduce weight and improve reliability by lowering internal temperatures.

(continued on next page)

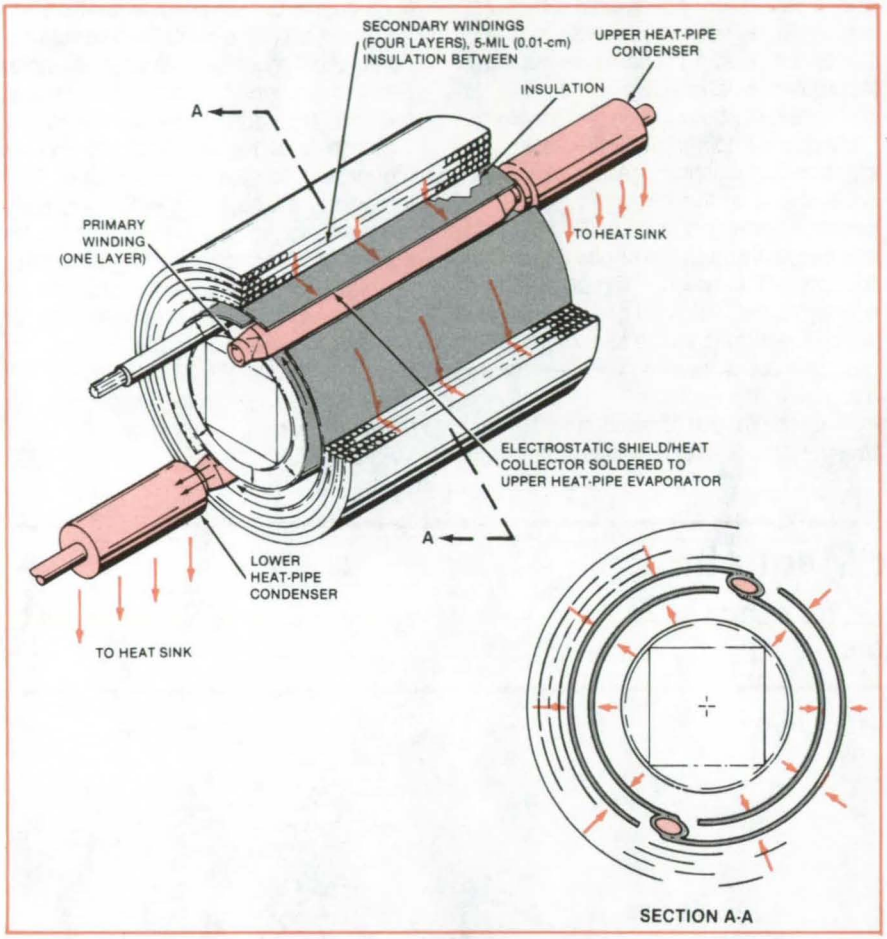

Figure 2. **Two Heat Pipes** integrated in the design of a power transformer cool the unit in any orientation. The electrostatic shield conducts heat from the windings to the heat-pipe evaporator.

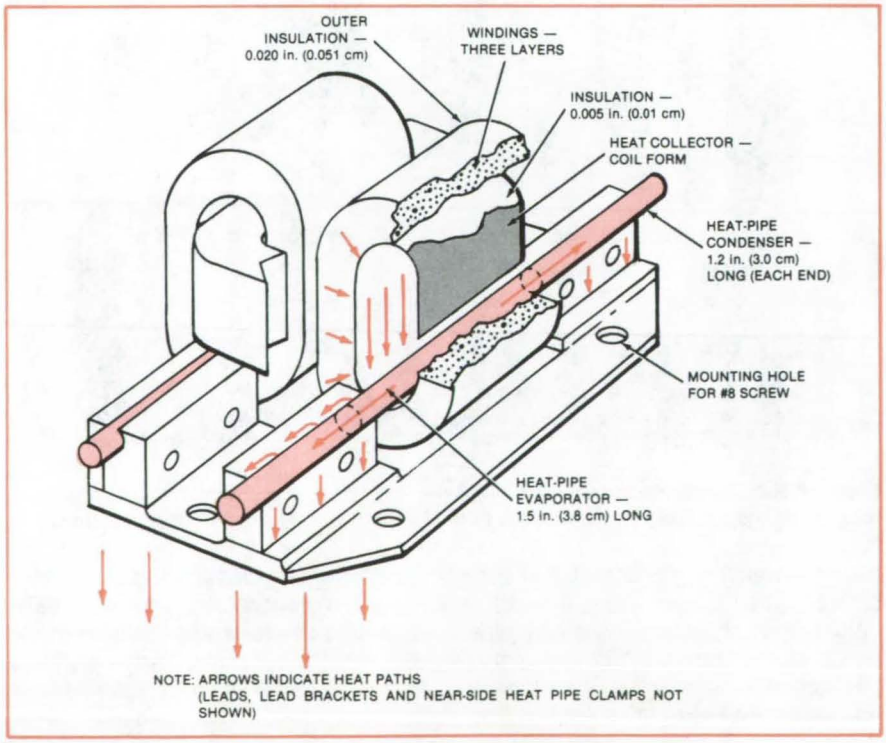

Figure 3. **Double-Condenser Heat Pipes** cool these power inductors.

winding, thus controlling the voltage gradients and meeting the high-voltage corona requirements.

Weighing 1,200 grams, this transformer is one-third lighter than the 1,750 grams of the previous design. To maintain the desired reliability, while handling over 3,000 volt-amperes, the internal thermal rise was previously limited to 45° C. With the new design the temperature reaches a maximum of 25° C. Since the life of an insulation system doubles for each 10° C reduction in temperature, the expected life of this transformer has been quadrupled.

For space applications involving vacuum operation and total absence of convective cooling, this technology allows single-unit transformers to be built with ratings in excess of 10 kilowatts. The use of two condenser sections with a single evaporator allows the heat pipe to operate at maximum capability with any gravitational orientation. The pipe performs as if there were two short pipes end-to-end with a transport capability of over 50 watts. However, if the Earth's orientation places the pipe in a vertical position, the pipe must overcome the effects of gravity. In this position, while one condenser does not operate, the opposite condenser has 15 watts of transport capability, which is more than enough for the worst-case losses generated by the filter inductor.

Figure 3 depicts the heat flow from the inductor frame and heat-sink clamp. The incorporated heat pipe enabled a 40-percent weight reduction with a low (10° C) heat rise and a 5.5-watt loss increase at 12 A nominal operation.

This technology allows dramatic reductions in size and weight, while significantly improving reliability. In addition, the all-attitude design of the heat pipes allows operation of the heat pipes independent of local gravity forces.

This work was done by I. Hansen of **Lewis Research Center** *and M. Chester and E. Luedke of TRW, Inc. Further information, may be found in NASA CR-159659 [N80-13362/NSP], "Heat Pipe Cooled Power Magnetics" [$16.50]. A copy may be purchased [prepayment required] from the National Technical Information Service, Springfield, Virginia 22161.*

LEW-13507

Tapped-Hole Vent Path

Meshing threads create a long vent path for hot, pressurized gas.

Lyndon B. Johnson Space Center, Houston, Texas

A long helical vent path safely releases hot gases from a pyrotechnically activated valve. Before it was fitted with the vent, the valve leaked pressurized pyrotechnic gases into a gas-sampler bottle, contaminating the sample and creating a potentially explosive mixture.

A schematic of the valve incorporating the vent is shown in the figure. The vent consists of a threaded hole and a mating stud. The gas vents slowly through the helical path between the threads of the hole and the stud. The outer diameter of the stud is slightly reduced to create a controlled cross-sectional area.

In the valve for which it was designed, the vent path was about 8 inches (20 cm) in length for a stud 0.62 inch (1.6 cm) long. The equivalent diameter of the threaded vent is about 0.020 inch (0.50 mm). In tests, the gases vented slowly over the long path so that they were cool enough to present no ignition hazard.

Other uses are possible for this vent. It could be used to meter the flow in refrigeration, pneumatic-control, and fluid-control systems by appropriately adjusting the size and length of the vent path.

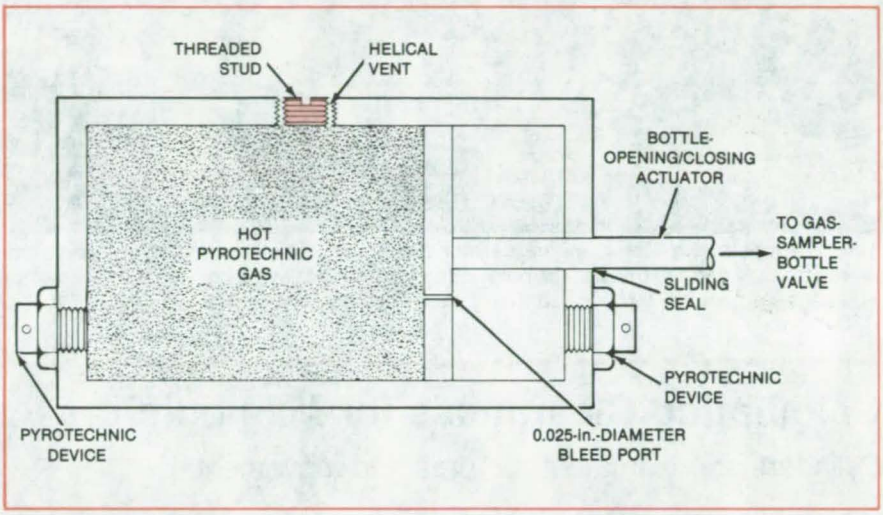

The **Long Helical Vent Path** cools and releases the hot pyrotechnic gas that exits along its spiraling threads. The current design uses 1/4-28 threads, with the outer diameter of the stud reduced by 0.025 in. (0.62 mm). To open or close the gas-sampler bottle, the pyrotechnic charges on either one side or the other of the valve cylinder are actuated.

This work was done by Joseph A. Chandler of **Johnson Space Center.** *No further documentation is available.*

Inquiries concerning rights for the commercial use of this invention should be addressed to the Patent Counsel, Johnson Space Center [see page A5]. *Refer to MSC-20146.*

Field Measurement of Thermal Inertia

Radiometric measurements determine thermal inertia for geologic materials.

NASA's Jet Propulsion Laboratory, Pasadena, California

A simple method and apparatus measure the thermal inertia of geologic materials in the field. Such measurements are correlated with data obtained by remote sensing, for discriminating varieties of rock encountered when exploring for minerals by aircraft or by satellites equipped with infrared scanners.

Thermal inertia (TI) is a derived property of a material; it incorporates the thermal conductivity (κ), density (ϱ), and specific heat (c) of the material and is expressed by

$$TI = \sqrt{\kappa \varrho c}$$

High values of thermal inertia indicate a high resistance to change in temperature.

The thermal-inertia meter measures the TI in situ by recording the surface-temperature rise of the materials. As can be seen from the photograph, a target and two standards are radiantly heated with calibrated quartz infrared heat lamps. Each lamp, three in all, pivots so that it can be quickly moved into position to heat the surface and removed to allow monitoring of the surface temperature. The lamps are mutually balanced by connecting them to voltage regulators.

The surface-temperature rise is monitored by an infrared radiometer. The detector head is mounted for rapid movement from reference standard to target. A portable digital voltmeter measures the voltage from the thermometer. The apparatus consists of three compartments, two for the standards and one for the target.

Comparison of the target-heating history with that of the two reference standards yields the target thermal inertia. The TI is calculated from a simple algebraic equation involving the measured quantities.

(continued on next page)

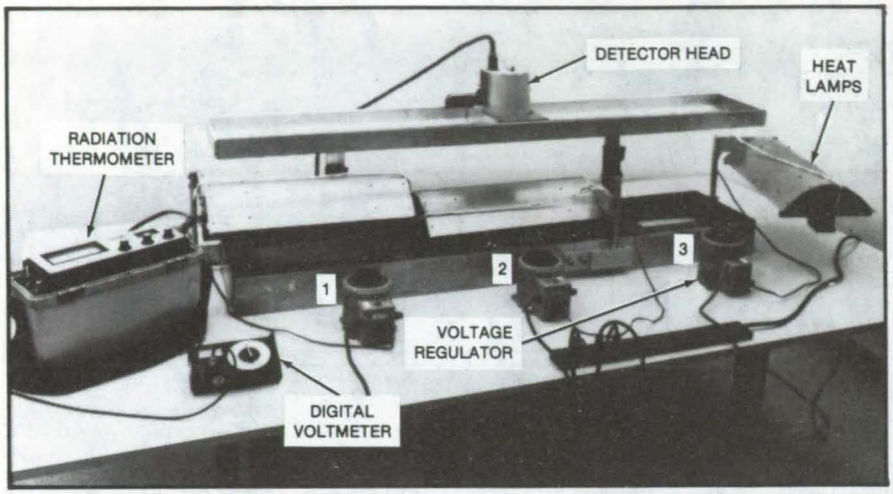

This **Thermal-Inertia Meter** apparatus includes three sample-measurement compartments that are open to the surface below. Compartments 1 and 3 contain the standards, and compartment 2 is left open to the surface to be measured.

The apparatus has been used to determine the TI of a variety of rock and soil types. The thermal-inertia reference standards chosen were geologic materials with high and low thermal-inertia values: dolomite (high) and 20/30-mesh Ottawa sand (low). The results indicate that fairly accurate values can be obtained in situ by this technique. In the field use of the TIM, such environmental conditions as wind and surface moisture must be taken into account.

This work was done by Anne B. Kahle, John P. Schieldge, and Stuart E. Marsh of Caltech for **NASA's Jet Propulsion Laboratory.** *For further information, Circle 43 on the TSP Request Card. NPO-15309*

Calculating Clearances for Manipulators

Cylinders approximate structures and movements.

Lyndon B. Johnson Space Center, Houston, Texas

A set of algorithms rapidly calculates the minimum safe clearances for remote manipulators. Such calculations are used in the design of trajectories for manipulators to ensure that they do not accidentally strike surrounding objects — particularly important when the manipulator is sometimes out of view of its operator.

Earlier attempts to calculate manipulator clearances required excessive computer time and memory. These attempts employed accurate and detailed models of the manipulator geometry and motion. The new set of algorithms describes the manipulator and adjacent structures in terms of enclosing cylinders (see figure). The problem then becomes one of calculating the minimum clearance between finite cylinders in space.

The structural parts are considered as cylindrical shells having circular plane areas for ends. The possible kinds of contacts are then:

- Shell-to-shell
- Shell-to-circle
- Circle-to-plane
- Circle-to-circle

The algorithms exhaust the possibilities for such contacts through an executive logic scheme that can also be applied to general situations.

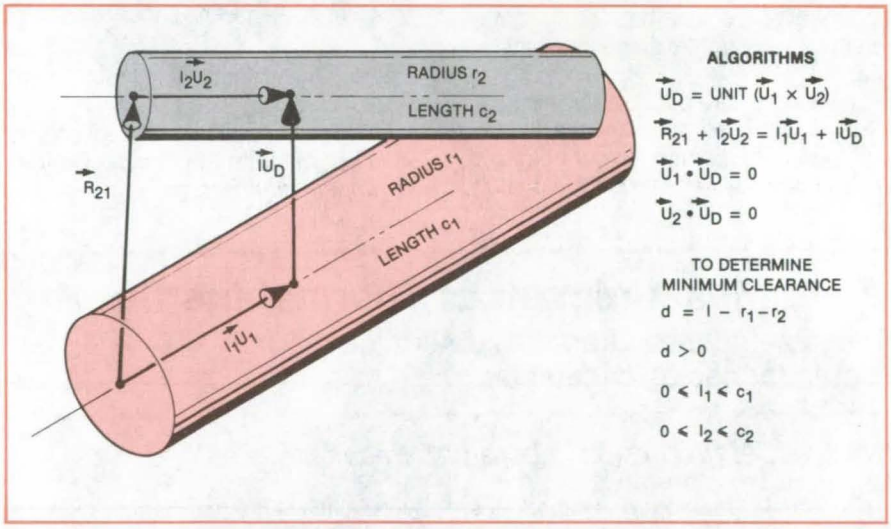

Structures Are Treated Mathematically as Cylinders for the purpose of calculating working clearances. The algorithm for the clearance between two skewed cylinders is shown here. This algorithm might be applied, for example, to find the clearance between two manipulator arms or between a crane and a tower.

Developed for the Space Shuttle remote-manipulation system, the clearance calculation method offers special benefits in industrial robotics, particularly in automated machining. Cutting tools can be described accurately as cylinders, and therefore the algorithms can predict interference efficiently. For more complex applications, surfaces of revolution may be used.

This work was done by Edward L. Copeland, John D. Peticolas, and Larry D. Ray of Lockheed Engineering and Management Services Co. for **Johnson Space Center.** *For further information, Circle 44 on the TSP Request Card. MSC-20208*

Rod-Wall Sound Shield for Wind Tunnels

Test model is shielded from turbulence radiated from wind-tunnel walls.

Langley Research Center, Hampton, Virginia

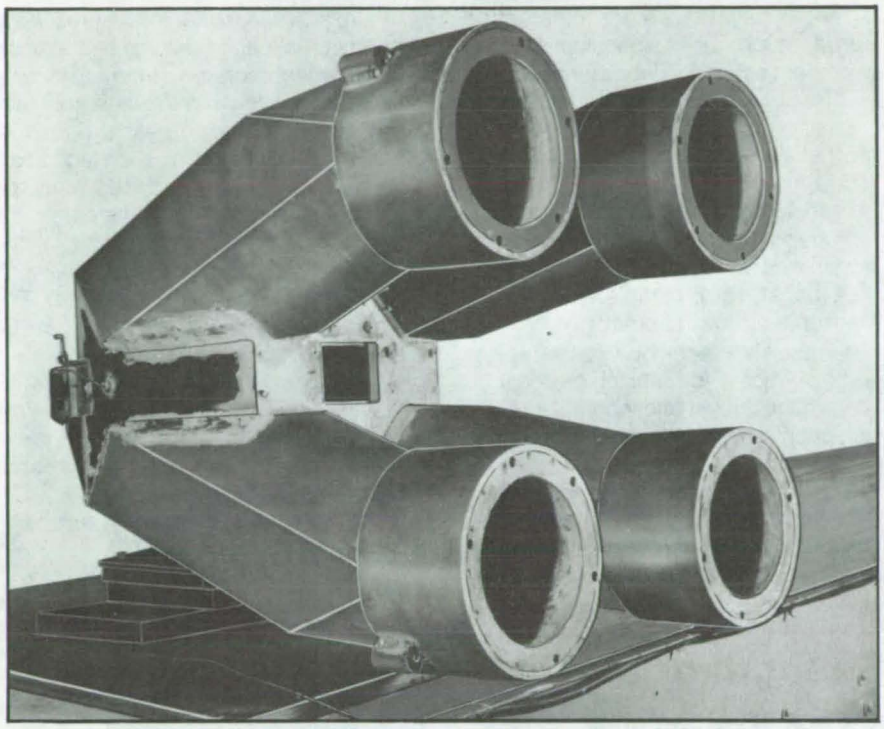

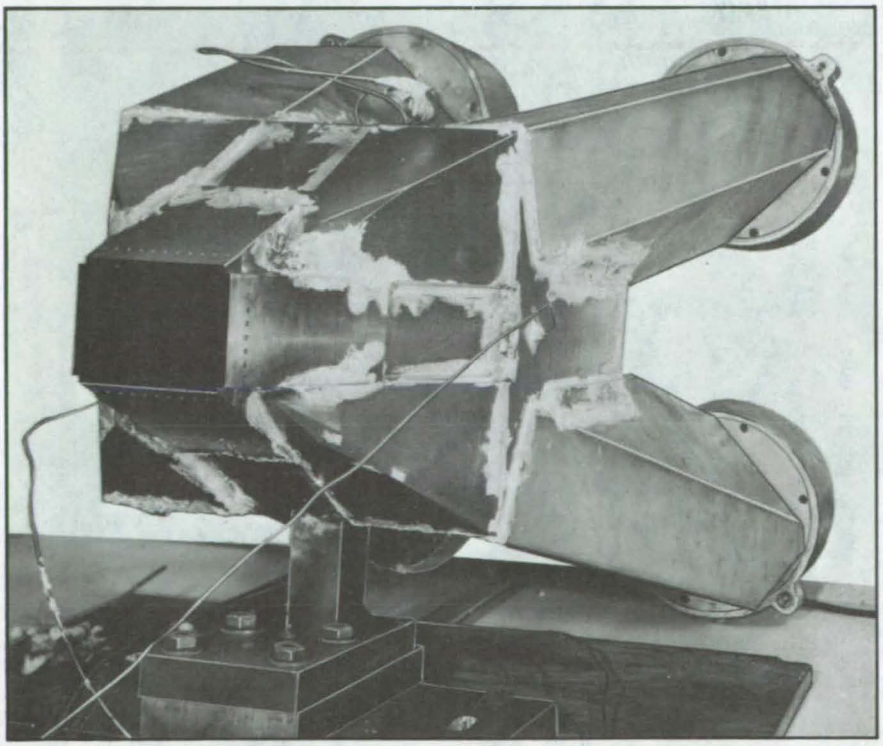

The **Rectangular Rod-Wall Sound Shield** shown in these two views protects models from noise radiated from wind-tunnel walls.

In supersonic and hypersonic wind tunnels, noise (pressure fluctuations) radiating from a turbulent boundary layer on the tunnel wall can cause premature transition of the model boundary layer. Two basic methods have previously been used to prevent or reduce the radiated noise. In the first, a laminar boundary layer is maintained on the tunnel wall by using longitudinal rods for the nozzle walls. Suction is applied between the rods to hold the boundary layer on the wall. The second method is to shield the model from the turbulent tunnel-wall boundary layer.

The rectangular structure shown in the figure shields an aircraft model from boundary-layer noise radiated from wind-tunnel walls. The shield is composed of four walls forming an open-ended box surrounded by a vacuum chamber. Each wall is composed of rods 0.25 inch (0.63 cm) in diameter spaced 0.040 inch (0.1 cm) apart. Vacuum pumping pulls the boundary layer around the rods, reducing the tendency of the layer to become turbulent.

The new shield overcomes problems caused by leading-edge configuration and leading-edge angle of inclination of previous designs. It has successfully maintained a laminar rather than turbulent boundary layer.

This work was done by Theodore R. Creel, Jr., and Ivan E. Beckwith of **Langley Research Center.** *Further information may be found in NASA TP-1672 [N80-26622/NSP], "Noise Reduction in a Mach 5 Wind Tunnel with a Rectangular Rod-Wall Sound Shield" [$9.50]. A copy may be purchased [prepayment required] from the National Technical Information Service, Springfield, Virginia 22161.*

This invention is owned by NASA, and a patent application has been filed. Inquiries concerning nonexclusive or exclusive license for its commercial development should be addressed to the Patent Counsel, Langley Research Center [see page A5]. Refer to LAR-12883.

Semiempirical Estimate of Aircraft Wing Weight

Method draws on theoretical equations and a data base to optimize estimates.

Ames Research Center, Moffett Field, California

A computational method estimates the weight of aircraft wings from theoretical relationships and empirical data. It permits the comparison of alternative materials, methods of construction, and design philosophies. The method can be used to make tradeoffs in preliminary design phases on the basis of simple input data and for more accurate calculations in later phases when more data are available. It eliminates the discontinuity inherent in comparing calculations made by different methods in different design phases.

The method is applicable to all types of fighter aircraft, commercial, general aviation, and others. Although developed expressly for aircraft wings, the principle can be adapted to weight and strength calculations for other structures, such as suspension bridges, warehouses, and indoor arenas.

The new method is a synthesis of previous methods:

- Strictly theoretical techniques based on simple beam theory,
- Techniques based on more elaborate models modified by experience, and
- Statistical techniques based on regression analysis of parameters known or assumed to be important.

The result is a technique that relies on a rational model for bending material but determines constants, coefficients, and exponents by regression analysis to include nontheoretical influences on the box-beam weight.

The model draws on a data base representing the characteristics of 50 types of airplane wings. Factors representing the materials and methods of construction are incorporated in the basic wing equations. Weight penalties for fuel, engines, and landing gear are also included. The weight of such additional items as control surfaces can be estimated from values in the data base or from detailed data available at the final design stage (for example, such data as wing area and flap area). The weights of major components can be estimated from the data base with a standard deviation of only 8.6 percent.

This work was done by Peter York and Raymond W. Labell of Grumman Aerospace Corp. for **Ames Research Center.** *For further information, Circle 45 on the TSP Request Card.*
ARC-11435

Measuring the Tensile Strength of B/Al Composites

A proposed nondestructive technique correlates damping measurements with material strength.

Lewis Research Center, Cleveland, Ohio

The fabrication and maintenance of high-strength composite materials consisting of aluminum alloys reinforced by boron fibers are complicated by the fact that the strength of the fibers is significantly degraded by a boron/aluminum (B/Al) reaction at temperatures above 750° F (400° C). Composite material processing is often not fully documented due to unknown or complicated thermal fabrication histories. Thus, there exists a strong need to develop nondestructive test techniques for quantitatively evaluating the tensile strength of B/Al composite materials throughout the various stages of their structural lives.

Fundamental studies at Lewis Research Center have established that a principal source of the high-temperature strength degradation of B/Al composites is the diffusion of boron atoms into the aluminum matrix and the subsequent formation of a weak interfacial reaction

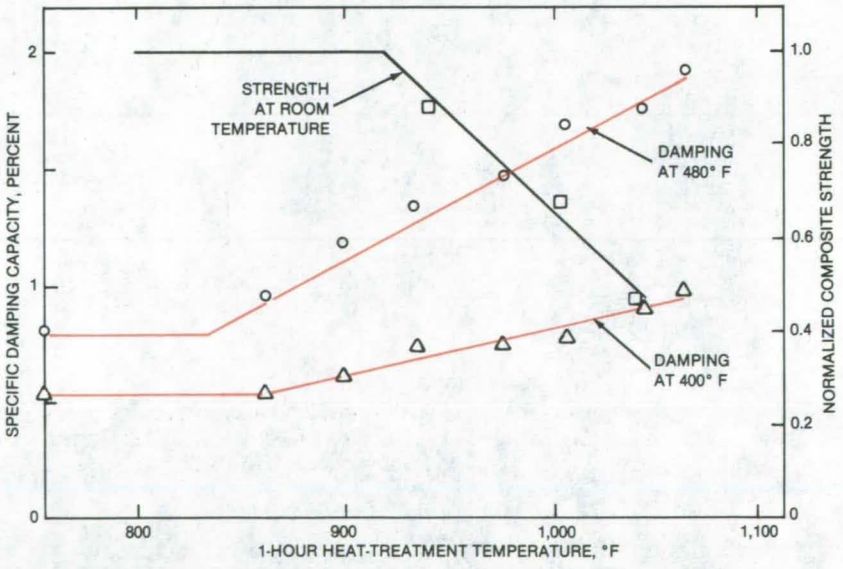

Increasing Axial Damping and Decreasing Axial Tensile Strength are observed after 1-hour heat treatment of B/Al composites that contain about 50 percent fiber. Damping was measured in a vacuum at frequencies near 2,000 Hz, and tensile strength was normalized by the maximum strength observed before thermally induced degradation.

phase on the fiber surface. Since the diffusion of small atoms such as boron is often accompanied by an increase in material damping, attempts were made to detect boron atoms within the aluminum by means of simple nondestructive damping measurements on B/Al composites that were heat-treated for 1 hour at temperatures above 750° F before testing.

For B/Al composites with a 6061-aluminum-alloy matrix, an increase in material damping was observed at test temperatures between 300° and 660° F (150° and 350° C) and stress frequencies near 2,000 Hz. As indicated in the figure by test data at 400° and 480° F (200° and 250° C), the B/6061-Al axial damping increased linearly with increasing heat-treatment temperature above 860° F (460° C). Also shown in the figure are room-temperatures results for B/6061-Al axial tensile strength after 1-hour heat treatment in the same temperature range.

Comparison of the damping and strength data shows that not only does the composite strength begin to degrade at approximately the same treatment temperature as the damping begins to increase but it also changes linearly with increasing temperature. Thus the degradation in composite tensile strength can be empirically correlated with the increase in composite damping. In terms of nondestructive evaluation, these results indicate that by developing damping-strength correlations for a B/6061-Al structure, one should be able to determine by periodic damping measurements not only the onset of thermally-induced strength degradation but also the quantitative magnitude of the structure's residual strength.

This work was done by James A. DiCarlo of **Lewis Research Center.** *Further information may be found in NASA TM-79080 [N79-16077/NSP], "High Temperature Dynamic Modulus and Damping of Aluminum and Titanium Matrix Composites" [$7.50]. A copy may be purchased [prepayment required] from the National Technical Information Service, Springfield, Virginia 22161.*
LEW-13807

Ceramic-Cord Gas Seal

High-temperature gasket material seals at temperatures above 1,100° C.

Lyndon B. Johnson Space Center, Houston, Texas

Braided cord made of ceramic fibers can form a low-pressure gas seal for temperatures up to 1,160° F (630° C). The alumina/boria/silica cord has been used as an exhaust-duct seal on the Space Shuttle orbiter. Those designing high-temperature seals may find the braided ceramic superior to asbestos in some applications.

The ceramic-cord seal between concentric pipes is shown in the figure. First, the cord is wrapped around the inner pipe. The wrapped inner pipe is then slid into the outer pipe. Following insertion, an expander tool is placed inside the inner pipe and used to expand the inner pipe, thus compressing the cord between the two pipes to form a seal.

The ceramic-fiber cord is adaptable for emergency repairs, quick replacement, or permanent installation. It requires less-stringent machining tolerances than are demanded by metal or elastomeric O-rings. Typical applications might include engine exhaust ducts or hot pipes passing through firewalls.

This work was done by Charles W. Etzel of Rockwell International Corp. for **Johnson Space Center.** *For further information, including a specification for preparing the braided ceramic cord, Circle 46 on the TSP Request Card.*
MSC-20200

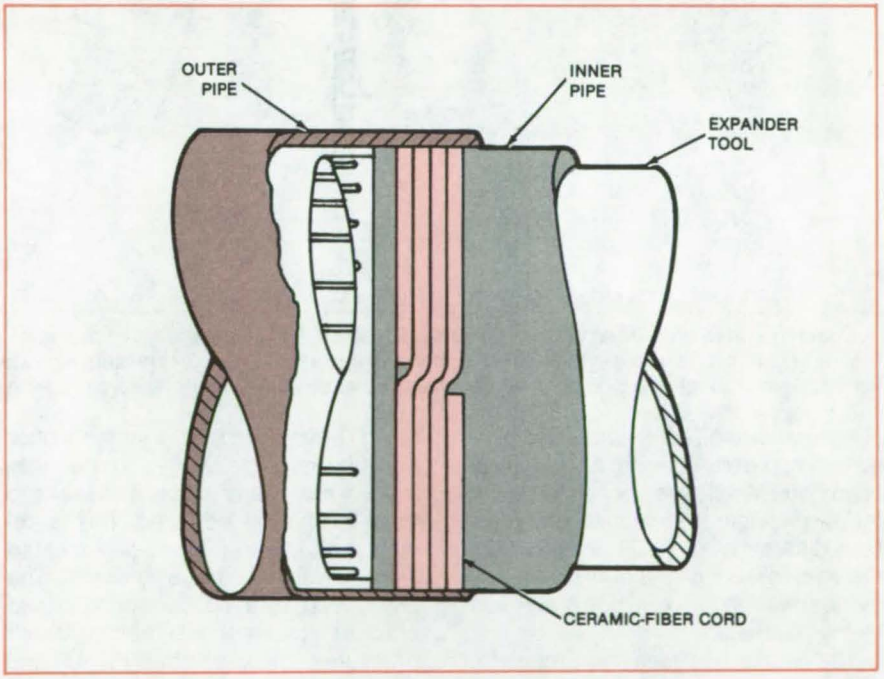

Concentric Exhaust Pipes are typical of applications in which ceramic-cord seals might be used. The cord is crushed to form a seal between the inner and outer pipes when the inner pipe is expanded into place.

Flexible Seal Accommodates Part Mismatch

Seal accommodates movement up to ½ inch as pressure is applied.

Marshall Space Flight Center, Alabama

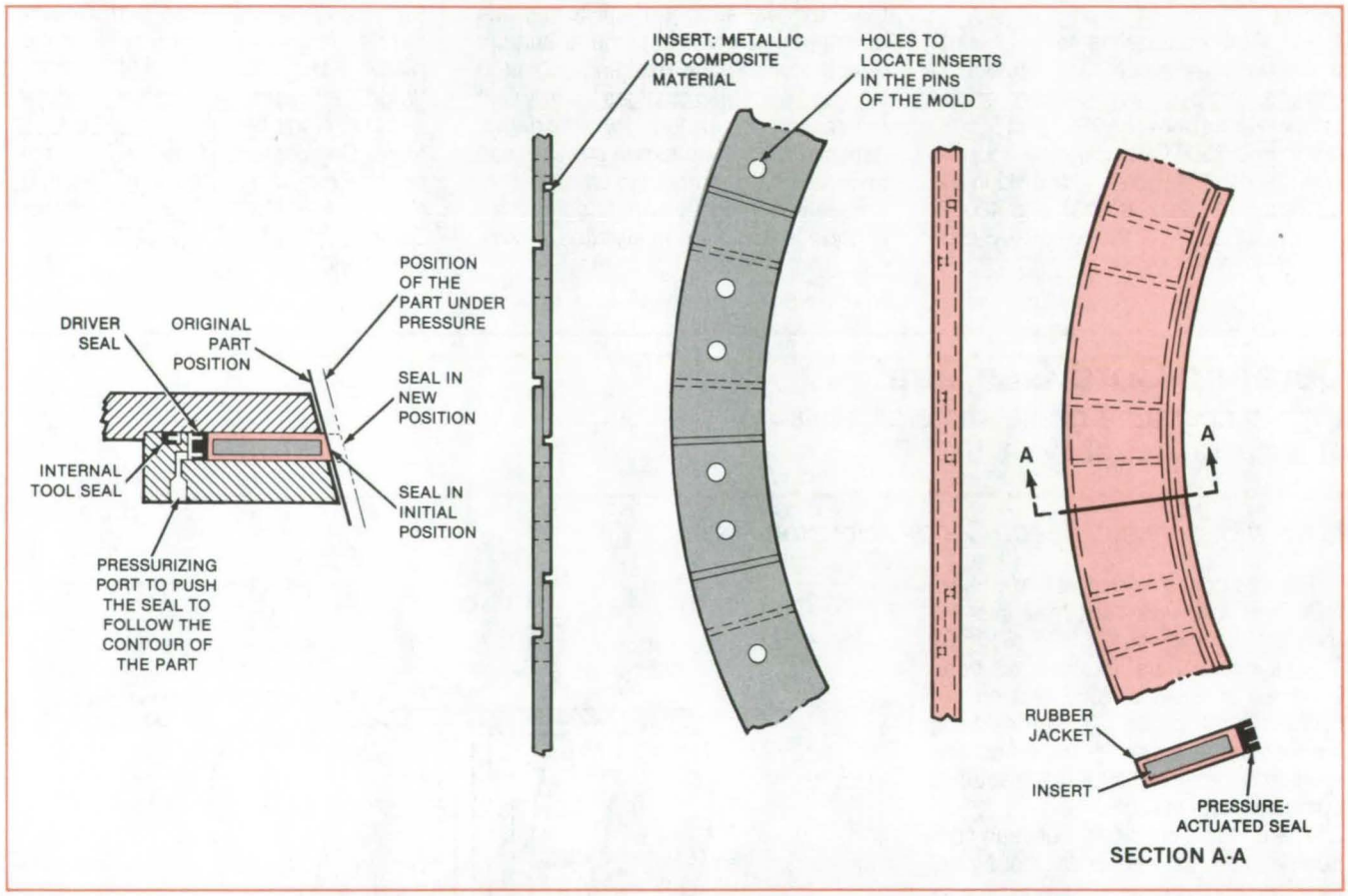

A Chain of Plates embedded in the flexible seal enables it to withstand side loading of 2,300 psi (16 MPa) while sealing a gap of up to 0.5 inch (13 mm) between a cylindrical chamber wall and a test fixture. A pressure-actuated seal along the inner edge forces the seal into contact even though the cylinder wall becomes eccentric as cylinder pressure increases.

A new flexible seal deforms as needed during pressure testing of cylindrical chambers. Metal plates encapsulated in the seal enable it to withstand a pressure differential of 2,300 psi (16 MPa). Gaps up to 0.5 inch (13 mm) between a cylinder wall and a test fixture are closed by the new seal.

The primary seal (see figure) consists of overlapping metal or composite segments molded into a rubber jacket. The segments provide the rigidity needed to withstand side loads, and the rubber provides the sealing surface and the flexibility required to conform to the variable eccentric shape.

Since the primary seal must follow the constantly changing contour of the part being pressurized, a slightly higher pressure must be applied to the inner edge of the seal to enable it to seal and to withstand the side load. This is accomplished with a driver seal located along the inner edge of the seal. The driver seal is a double spring-loaded pressure-actuated configuration. At high pressures between the driver and primary seals, two split metal backup rings may be used to prevent flow of the driver seal into the rubber jacket of the primary seal.

The new seal should have many industrial applications, particularly where heat or pressure causes distortion of the chamber being sealed. This can occur when cylinder wall thickness is nonuniform or when parts of the chamber are at different temperatures. Multiple seals could be used to divide a chamber into regions of different pressures. The seal might also be used around the outside of a chamber so that external pressure could be applied.

This work was done by Imrich Bobb of Rockwell International Corp. for **Marshall Space Flight Center.** *For further information, Circle 47 on the TSP Request Card.*

Inquiries concerning rights for the commercial use of this invention should be addressed to the Patent Counsel, Marshall Space Flight Center [see page A5]. Refer to MFS-19710.

Books and Reports

These reports, studies, and handbooks are available from NASA as Technical Support Packages (TSP's) when a Request Card number is cited; otherwise they are available from the National Technical Information Service.

Theory of Compound Liquid Drops

Dynamic behavior is analyzed for a drop within a drop within an infinite fluid.

A report delves into the theory of the dynamics of compound liquid drops. Compound drops consist of three fluids: an infinitely-extending host fluid surrounding a second fluid in the form of a shell, which in turn surrounds a third, core fluid.

The report gives a theoretical basis for understanding the behavior of compound drops. It can aid in planning and interpreting experiments in the laboratory, in spacecraft, and in research aircraft. It also can provide insight into the fabrication of target pellets for nuclear fusion.

It considers the oscillations of a system when the two fluid interfaces are spherical and concentric. In particular, it examines the frequencies and relative displacement of the interfaces. The report notes that there are two types of oscillation: the "+" class, in which the two interfaces move in phase, and the "−" class, in which they move out of phase. As a core shrinks, the + modes produce oscillations of the core boundary alone, whereas the − modes produce oscillations of the outer boundary alone. It covers the equations of motion, linear approximation of the modes, the eigenvalue problem, and qualitative results.

It also contains development of the linear approximation and obtains exact solutions and linear approximations for the system velocity potential, energy, and angular momentum. It uses the energy solution to normalize the displacements and angular momentum.

The report presents numerical results for mode frequencies and interface displacements.

This work was done by Melvin M. Saffren, Daniel D. Elleman, and Won Kyu Rhim of Caltech for **NASA's Jet Propulsion Laboratory.** *To obtain a copy of the report, Circle 48 on the TSP Request Card.*
NPO-15389

Large, Easily Deployable Structures

Compactly folded structures are assembled quickly with relatively little effort.

A reported study of concepts for large space structures will interest those designing scaffolding, radio towers, rescue equipment, and prefabricated shelters.

A double-fold, double-cell module was selected for further design and for zero-gravity testing. The double-fold, double-cell concept is viable for deployment by humans outside a space vehicle as well as by a remotely operated manipulator. It was also found that rigid stops and supports should be built into the folded structure and that the members should have smooth faces so that they do not snag equipment or clothing.

The tests were carried out in a neutral-buoyancy simulator — a large, deep pool in which a weightless environment is simulated. Test operators wearing diving gear performed 15 separate tests. Test activities included unstowing (that is, releasing latches, holddowns, and other fasteners), deploying, transporting, and attaching the structural elements. In some tests, the objective was to restow the structural components from an already-assembled structure. A typical eight-step procedure for two divers was as follows:

1. Unstow first module.
2. Transport first module to aft mounting base.
3. Attach module to base at four corners.
4. Unfold first module.
5. Unstow second module.
6. Transport second module to end of previously installed module.
7. Attach second module to first module at four corners.
8. Unfold second module.

As an outgrowth of the work on manually deployable structures, there emerged a concept for self-deploying structures involving a double-fold, double-cell module system. Accessory arms are actuated to release all restraint cables around the folded structure. Cables driven by springs then open the structure and drive its elements into unfolded, locked positions. If the structure is to be self-refolding, a small 28-volt dc motor can be added to each deployment-cable reel.

This work was done by W. E. Agan of Vought Corp. for **Marshall Space Flight Center.** *To obtain a copy of the report, Circle 49 on the TSP Request Card.*
MFS-25647

Computer Programs

These programs may be obtained at very reasonable cost from COSMIC, a facility sponsored by NASA to make new programs available to the public. For information on program price, size, and availability, circle the reference letter on the COSMIC Request Card in this issue.

Trajectory-Estimation Error Analysis

Program computes errors caused by assumed values of unadjusted parameters.

The Orbital and Geodetic Parameter Estimation Error Analysis Program (ORAN) is a Bayesian least-squares simulation program for orbital trajectories. ORAN does not process data; rather, it computes the accuracy of the results of a data reduction if measurements are processed by a minimum-variance data-reduction program. Actual data may be used to provide the time when a given measurement was available and the estimated noise on

(continued on next page)

that measurement. ORAN considers a data-reduction process in which a number of satellite data periods are reduced simultaneously. If there is more than one satellite in a data period, satellite-to-satellite tracking may be analyzed.

The least-squares estimator in most orbital-determination programs assumes that measurements can be modeled by a nonlinear regression equation containing a function of assumed constant parameters and parameters to be estimated. The partitioning of parameters into those to be estimated (adjusted) and those assumed to be known (unadjusted) is somewhat arbitrary.

For any particular problem, the data will be insufficient to adjust all parameters subject to uncertainty, and some reasonable subset of these parameters is selected for estimation.

The final errors in the adjusted parameters may be decomposed into a component due to measurement noise and a component due to errors in the assumed values of the unadjusted parameters. Error statistics associated with the first component are generally evaluated in an orbital-determination program. ORAN simulates the orbital-determination processing and computes error statistics associated with the second component.

Satellite observations may be simulated with desired noise levels given in many forms, including range and range rate, altimeter height, right ascension and declination, direction cosines, X and Y angles, azimuth and elevation, and satellite-to-satellite range and range rate. The observation errors considered are bias, timing, transit time, tracking-station location, polar motion, solid-earth tidal displacement, ocean-loading displacement, tropospheric and ionospheric refraction, and space plasma. The force-model elements considered are Earth's potential, the gravitational constant, solid-earth tides, polar radiation pressure, Earth-reflected radiation, atmospheric drag, and thrust errors. The errors are propagated along the satellite orbital path.

ORAN is written in FORTRAN IV and Assembler for batch execution and has been implemented on an IBM 360-series computer with a central memory requirement of approximately 570K of 8-bit bytes. ORAN was developed in 1973 and was last updated in 1980.

This program was written by Barbara Putney of **Goddard Space Flight Center.** *For further information, Circle F on the COSMIC Request Card.*
GSC-12766

Machinery

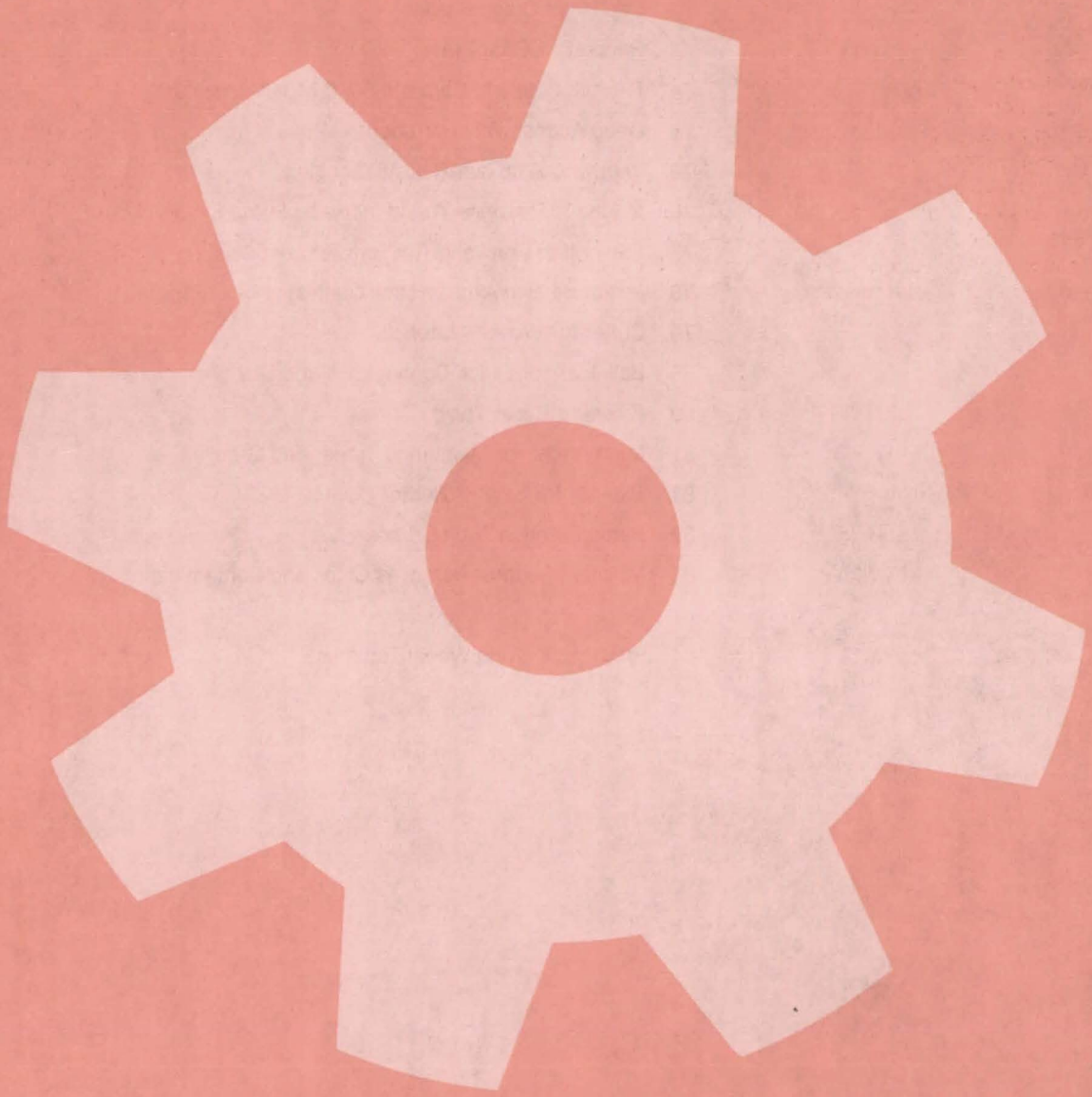

Hardware, Techniques, and Processes

Books and Reports

Device Makes Handtools "Dropproof"

Wrench handle and socket cannot be separated unless both are tethered.

Lyndon B. Johnson Space Center, Houston, Texas

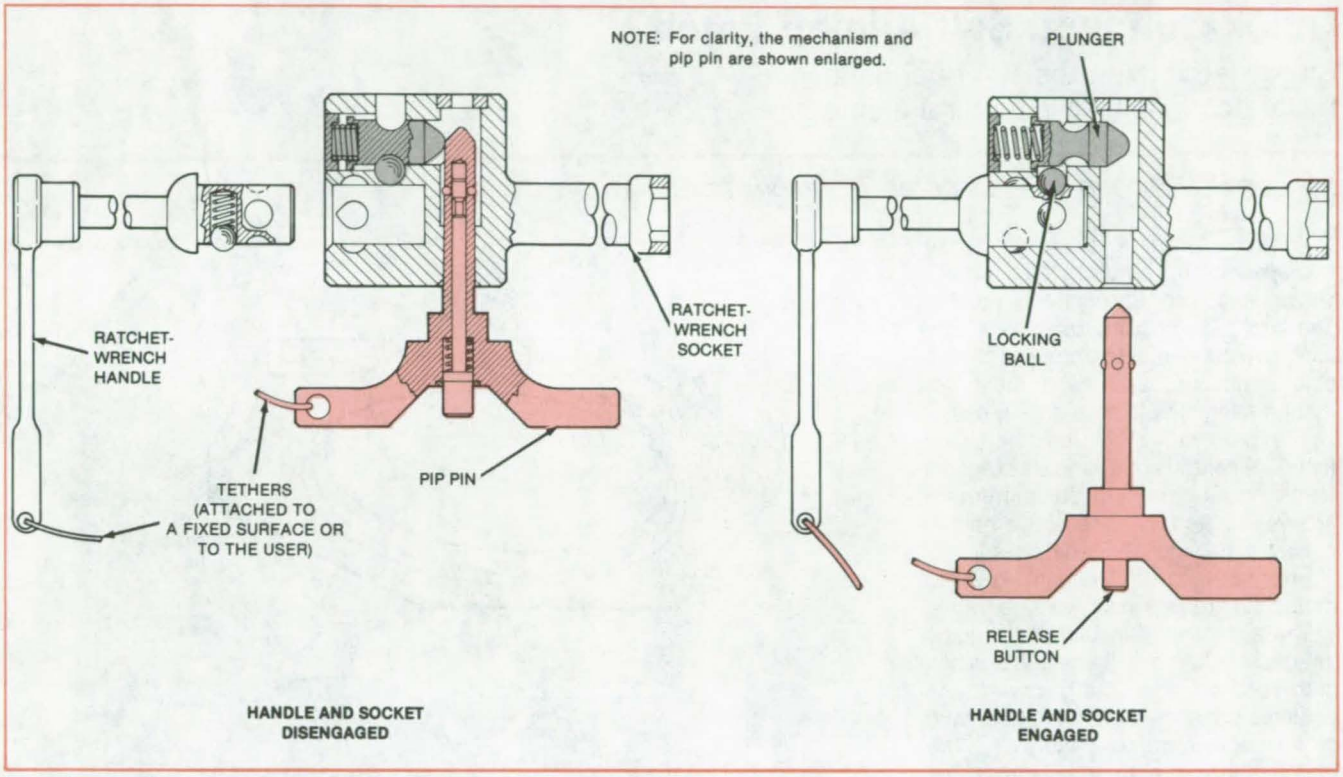

Interchangeable-Socket Dropproof Wrench comprises three essential parts: handle assembly, socket assembly, and pip-pin assembly. The socket assembly can be disengaged from the handle assembly only when it is engaged to the pip-pin assembly. The socket assembly therefore remains tethered and cannot be dropped or lost except by deliberate removal of the pip pin.

Two-part handtools are made "dropproof" by a mechanism originally developed for tools used by astronauts. The mechanism can be added to ratchet wrenches and other composite tools for which there is relative motion between the parts.

An advantage of the new mechanism is that it secures both parts of the tool — for example, a ratchet wrench handle and a wrench socket — yet only one tether is attached to the tool while it is being used. In previous systems, a tether was needed for each part, but the tethers interfered with the movement of the parts.

The key element of the new mechanism, shown in the figure, is a retaining pin called a "pip pin." The two components of the tool can only be joined together if the pip pin is in place. When the pip pin is removed, the components become locked together. To separate the components, the pip pin must be reinserted.

In the application shown in the figure, a ratchet-wrench handle is to be attached to a wrench socket. The pip pin is shown inserted in a drilled passageway wrench socket. Tethers are attached to the handle and to the pip pin but not to the socket.

When the two parts of the wrench are disengaged, as shown at the left of the figure, the tether on the handle keeps the handle from being lost if it is dropped; and the tether on the pip pin prevents loss of the pip pin and socket if they are dropped.

After both parts of the wrench are engaged, the pip pin is extracted as far as possible without releasing the pip-pin ball locks. This lowers a plunger and forces a locking ball to lock the wrench handle in the socket. It is then impossible to disengage the parts.

The integrity of the wrench-socket lock mechanism may be tested prior to complete removal of the tethering pip-pin from the socket. After verification, the pip-pin ball locks are released by depressing its actuator button and the pip-pin is removed, as shown at the right of the figure. The tool assembly is now ready for use. The tether on the wrench handle prevents the wrench from being lost if it is dropped. The wrench is secure, operational, and not encumbered by two tethers.

The pip pin and socket are disengaged if the release button on the pin is depressed while the pin and socket are pulled apart. Although the required combination of pushes and pulls is unlikely to be encountered accidentally, a pawl could be added to the socket to prevent the pip pin from being removed unless the wrench handle is inserted in the wrench socket.

(continued on next page)

The dropproof tool is useful wherever the loss of a component would be inconvenient or hazardous. It can be used by divers, for example, and by people working on scaffolds. The mechanism is easily operated by technicians wearing thick gloves, space suits, diving suits, or other protective attire.

This work was done by Bruce McCandless II of **Johnson Space Center.** *For further information, Circle 50 on the TSP Request Card.*

This invention is owned by NASA, and a patent application has been filed. Inquiries concerning nonexclusive or exclusive license for its commercial development should be addressed to the Patent Counsel, Johnson Space Center [see page A5]. Refer to MSC-20319.

Quick-Connect, Self-Alining Latch

Sturdy latch tolerates 10° of angular mismatch in joining structural elements.

Lyndon B. Johnson Space Center, Houston, Texas

A latch originally developed for joining two spacecraft in orbit holds securely, yet connects and disconnects quickly. The latch has possible uses as a pipe joint, as a connector for the parts of portable structures, and as a fitting for marine risers on offshore drilling rigs.

The passive half of the latch (see Figure 1) consists of a simple hexagonal frame containing three alinement grooves on its face. The active half includes a hexagonal frame on support struts that bears alinement keys to match the grooves in the passive frame.

Three slanting triangular plates guide the passive frame to its nested position in the active frame. The passive frame actuates proximity switches in the face of the active frame (Figure 2). The switches in turn actuate solenoids that release latches in the guide plates so that they capture the passive plate.

Once released, the latches are driven by springs to the "capture" position. Then the latch drive actuators pull the latch drive links down to engage the alinement keys and clamp the two frames together. Small motors retract the latches when it is necessary to release the passive frame. Dual solenoids, springs, and motors for each latch mechanism ensure that the latch operates even if one of a pair of components is defective.

Lateral and forward closing velocities between passive and active plates can be as much as 0.1 ft/s (3 cm/s). Pitch, roll, and yaw of 1° per second are acceptable. A lateral mismatch of 4 inches (10 cm) between passive and active plates can be accommodated, as can an angular mismatch of 10° in pitch, roll, and yaw. After mating, the angular mis-

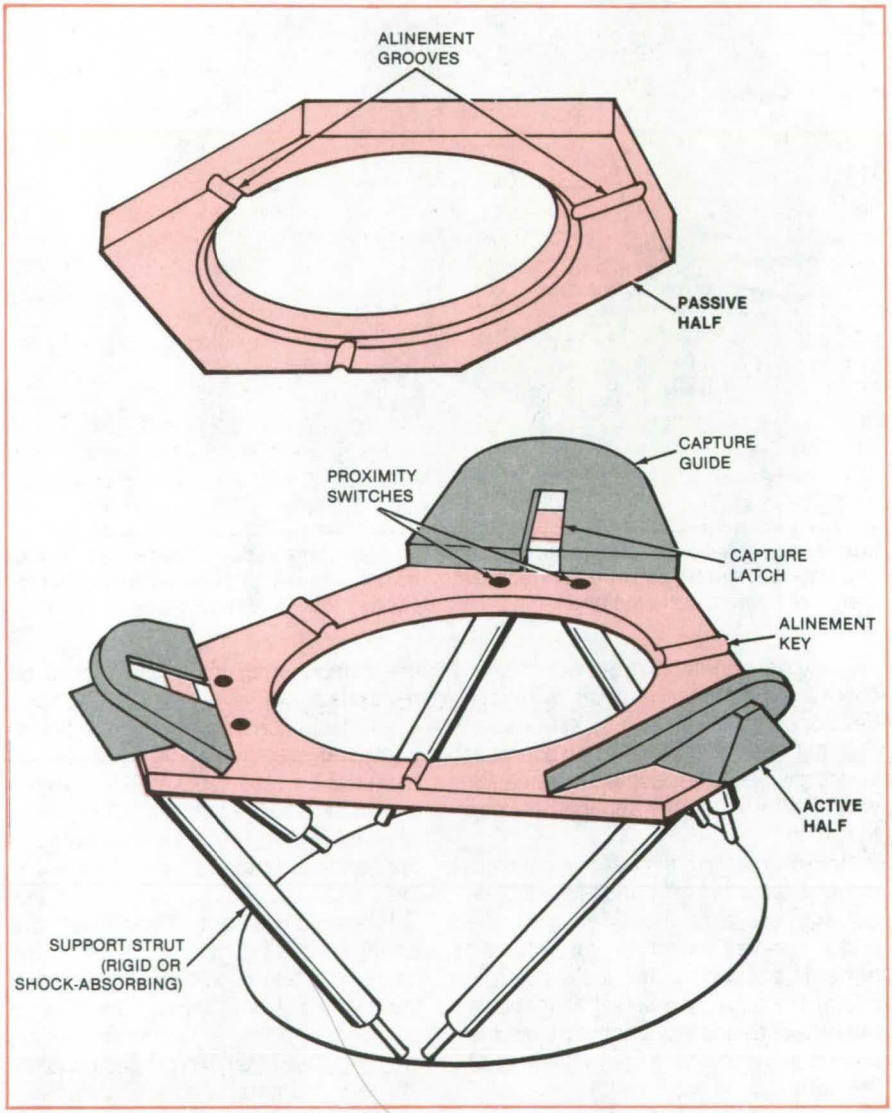

Figure 1. **Hexagonal Passive Plate Nests** in active plate, guided by capture plates and alinement keys and grooves. The center hole in both active and passive plates is 1 meter in diameter.

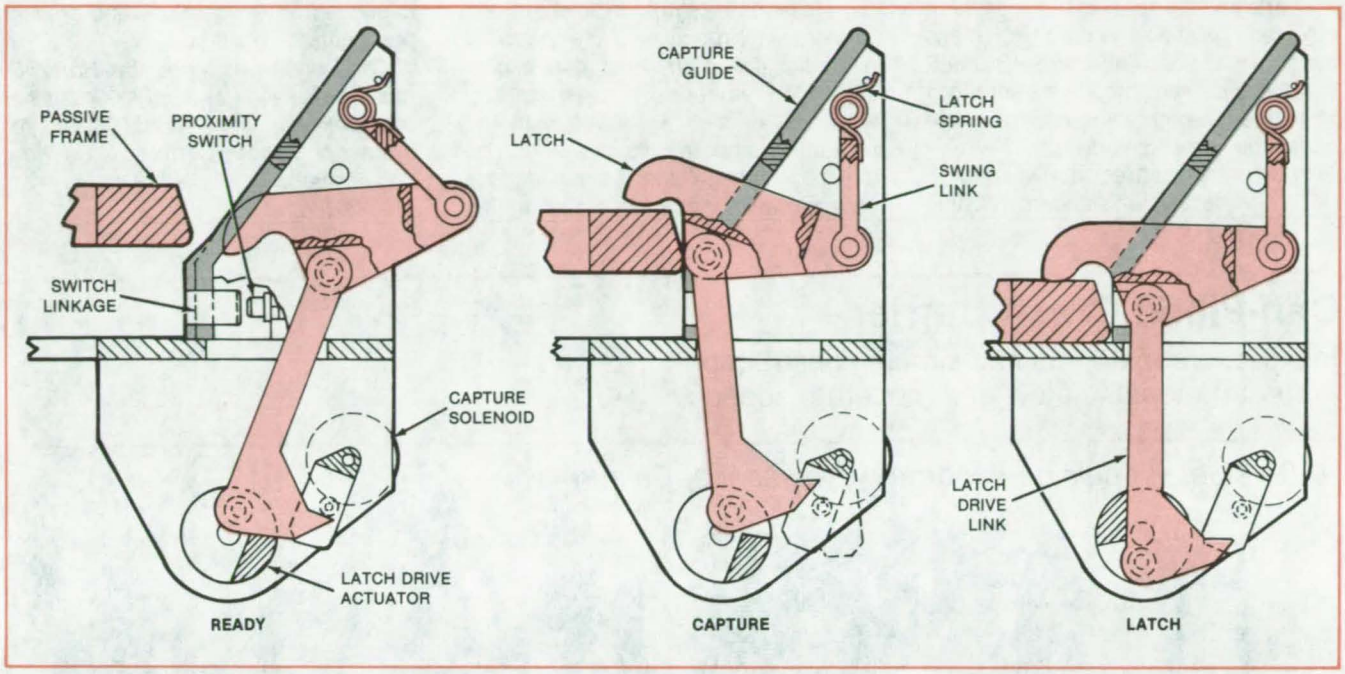

Figure 2. **In the Ready Position,** a latch is retracted below the surface of the capture guide. When the passive frame is within capture range, it actuates three or more of the six proximity switches on the active frame, causing the latches to move to the capture position. Latch drive actuators pull the latch drive link down, clamping the two frames together.

alinement in pitch, roll, and yaw is within ±1.32 minutes of arc. After mating, the latch can withstand a thrust load of 20,000 lb (90,000 N) and moments in pitch, roll, and yaw of 16,000 lb-ft (22,000 m-N).

The active half of the latch operates on 28 to 33 volts dc. The peak power consumption during latching is 1,000 watts; no power is drawn before and after latching. In case of a power failure, the latch can be operated manually by means of a crank.

The weight of the active half, including controls, is less than 200 lb (91 kg). The weight of the passive half is less than 50 lb (23 kg). Switches on the active half control indicator lamps that show progressively that the latch is ready to berth, the capture is complete, and the latch mechanisms are secure.

The support struts on the active half are rigid. However, they can be replaced by shock mounts if energy absorption is required.

This work was done by Gene C. Burns and Edward J. Williams of McDonnell Douglas Corp. for **Johnson Space Center.** *No further documentation is available.*

MSC-20205

Screen Secures Detonator to Explosive Charge

The distance between cap and charge is easily controlled with a brass-screen sleeve.

Lyndon B. Johnson Space Center, Houston, Texas

A brass-screen sleeve (see figure) attaches a blasting cap to a fuse, shaped charge, detonating cord, or other formed explosive. The screen makes it easy to control the distance between the cap and the charge, because the user can see both parts, and to cool the cap by convection, making the use of low-cost blasting caps possible for some hot environments. Previously, a wooden spool was used to connect the parts.

To attach the cap to the charge, the brass-screen sleeve is positioned over

(continued on next page)

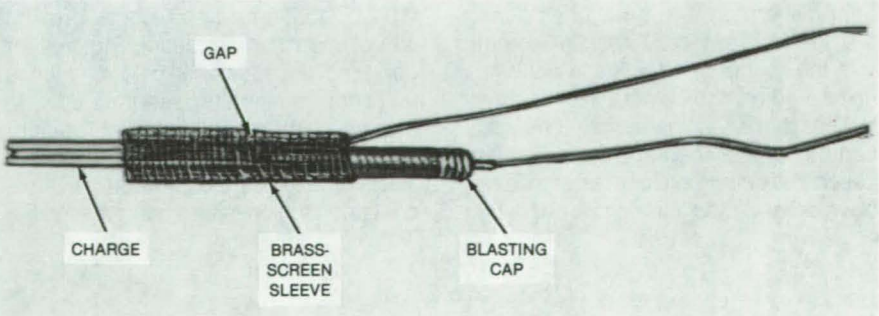

The **Brass-Screen Sleeve** allows the user to adjust visually the gap between the charge and the blasting cap.

the parts and the spacing between them adjusted. Twisting the screen tightens the grip on the cap and charge. By pouring glue or cement through the screen to fill the gap, a permanent cap-to-charge connection can be made.

With temperatures above 300° F (150° C), the use of standard blasting caps to detonate pyrotechnic charges is very unreliable because of the possibility of autoignition; normally, a more-expensive high-temperature blasting cap would be needed. However, with the new attachment, a cold gas jet can be directed through the screen at the charge/cap interface to maintain an acceptable cap temperature and prevent premature detonation.

This work was done by Harry D. Moshenrose and Raymond A. Kindsfather of Rockwell International Corp. for **Johnson Space Center.** *No further documentation is available.*
MSC-20138

Can-Filled Crash Barrier

Inexpensive materials and simple construction protect motorists at low and moderate speeds.

NASA's Jet Propulsion Laboratory, Pasadena, California

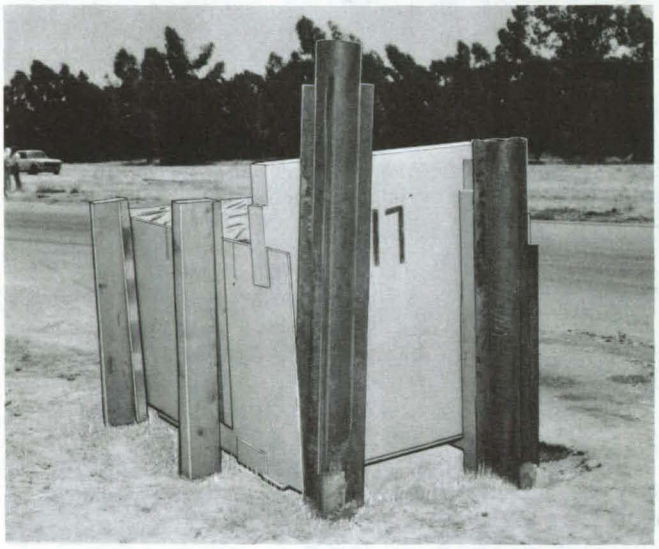

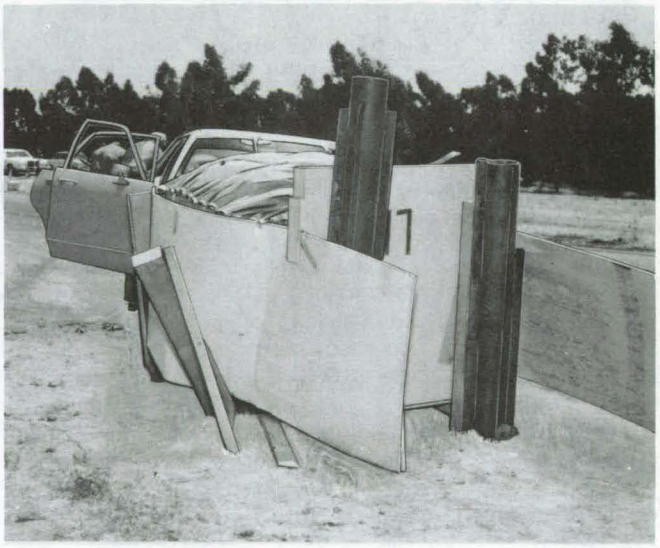

This **Collapsing Crash Barrier** is filled with empty beverage cans that collapse and thereby absorb the vehicle kinetic energy.

A crash barrier composed largely of used aluminum beverage cans protects the occupants of cars in collisions with poles or trees. Tested at NASA's Jet Propulsion Laboratory, the lightrweight, can-filled barrier was very effective in softening the impact of an automobile in head-on and off-angle collisions. A professional test driver experienced only brief discomfort and no injuries during the tests. Preliminary results indicate that the barrier is effective in collisions up to a 40 mi/h (64 km/h).

The barrier holds empty beverage cans in a tear-resistant cloth bag encased in a collapsible container made of plywood and steel (see figure). The bag is flame-retardant and weather-resistant. Cans in the front part of the barrier bag are randomly oriented, and cans in the rear are oriented parallel to the direction of a head-on collision.

The barrier used in the tests is 6 ft (1.8 m) long, 3 ft (0.9 m) high, and 3½ ft (1.1 m) wide. Its side panels slide past its backstop as a car hits. Two 4-by-6-inch (10.2-by-15.2-cm) wood posts prevent lateral motion or rotation. The tree or pole and an additional pole 11 inches (27.9 cm) in diameter serve as a backstop support and further resist rotation.

When a car strikes the barrier, it starts to collapse the plywood-and-steel container, which in turn compresses the cans. The energy of the car is absorbed by the buckling metal of the cans and by air within the cans as it is compressed.

Accelerometers on the car frame and the driver's helmet measured acceleration during impact, and high-speed motion-picture cameras photographed the crashes. Impact against barriers of 55-gal (208-l) cans was harder than against the new collapsing barrier, according to both measured data and the driver's subjective experience.

This work was done by Abraham H. Wilson of Caltech for **NASA's Jet Propulsion Laboratory.** *For further information, Circle 51 on the TSP Request Card.*
NPO-15188

Redundant Gear Train

Tandem harmonic drives are immune to single-point failure.

NASA's Jet Propulsion Laboratory, Pasadena, California

Simply duplicating the motor and gears does not significantly improve the reliability of a mechanical drive train. There is always the possibility of a single-point failure, in which a failure in one drive path jams the other drive path as well.

Now, however, an arrangement of two harmonic drive mechanisms offers true redundancy. One mechanism continues transmitting power regardless of how the other fails. Besides being highly reliable, the dual harmonic drive is compact, occupying a smaller volume than a conventional gear train for the same power and speed reduction.

The harmonic drive is a simple compact gear system for achieving large speed reductions and large output torques. The "pancake" harmonic drive, used here, includes four main elements as shown in Figure 1. The wave generator is the input member, and either circular spline can serve as the output member. Speed reduction is achieved by engagement of a differential number of teeth on the flexible spline and stationary circular spline.

The redundant gear trains are shown schematically in Figure 2. Motor 1 drives spur gear No. 1 and an inner shaft. The inner shaft (to harmonic drive 1) passes through the center of a hollow outer shaft and continues through harmonic drive 2 without physical contact. The inner shaft is connected to the input of harmonic drive 1 through a cone clutch. The clutch is nonfunctional during normal operation. The clutch provides a redundant point of relative motion within the system 1 drive train and is required only when nonbackdrivable input gears are used.

When operation of system 2 is desired, the motor 2 drives spur gear 2, which rotates the input shaft to harmonic drive 2. That input shaft is located concentrically around the system 1 drive shaft. The input drive elements of system 1 and system 2 are totally separate and noncontacting. However, the operation of system 2 causes the entire

(continued on next page)

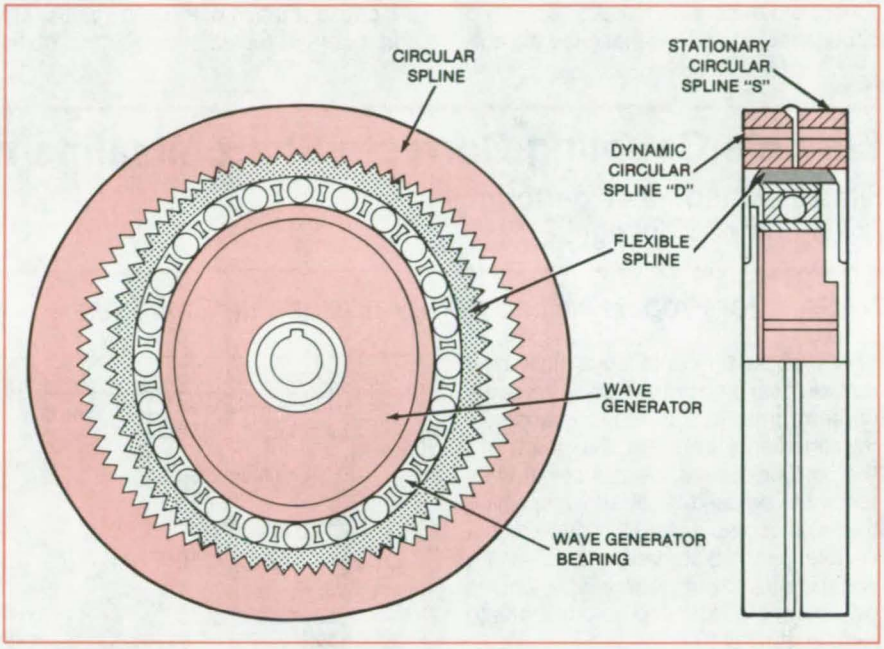

Figure 1. In a **Harmonic Drive Mechanism,** the combination of an elliptical wave generator and a tooth differential between the flexible spline and the circular spline produces a rotational speed reduction in a compact volume.

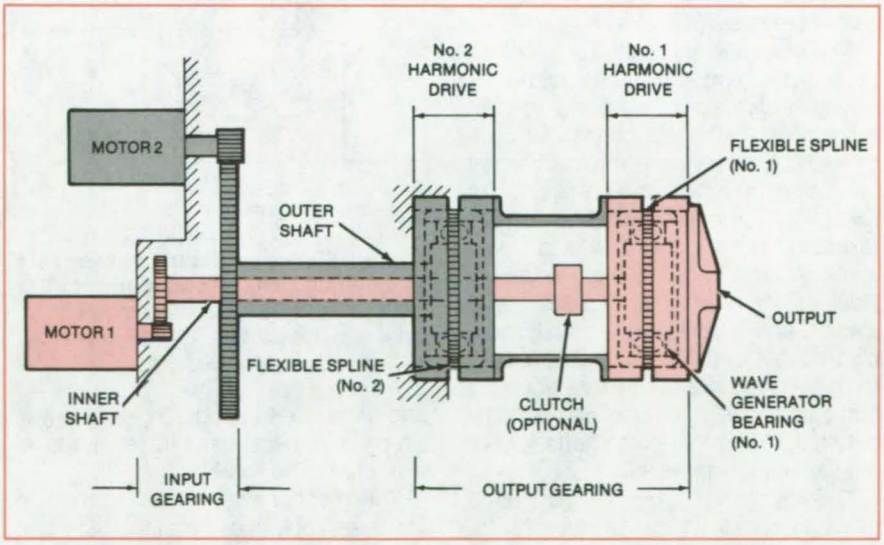

Figure 2. A **Fully Redundant Drive** is normally operated by motor 1. In the event of a failure in drive train 1, however, motor 2 operates harmonic drive 2 via shaft 2, which is concentric with drive train 1.

system 1 harmonic drive to rotate as a single mass. The torque produced by system 2 is transmitted across harmonic drive 1 by the tooth mesh of flexible spline 1.

If motor 1 or any of the elements it drives should fail to rotate, motor 2 may be turned on, and the output shaft can still be rotated via the system 2 gear train. Both motors can also be operated simultaneously, and in that case the output rotational speed will be about twice that for single-motor operation. The output torque will be the same as for single-motor operation.

This drive train can also be designed to be "backdrivable." The term "backdriving" refers to the condition in which a torque applied at the output shaft of a nonoperating electromechanical drive will cause rotation of the unit input shaft and motor. The backdriving action does not damage either system, and in applications where torque limiting or manual override is required, a backdrivable configuration can satisfy those requirements.

This work was done by Douglas T. Packard of Caltech for NASA's **Jet Propulsion Laboratory.** *For further information, Circle 52 on the TSP Request Card.*
NPO-15317

Flexible Coupling Corrects Shaft Misalinements

Simple slotted tubes perform like a complex linkage.

NASA's Jet Propulsion Laboratory, Pasadena, California

A proposed flexible coupling would provide nearly error-free measurements of shaft rotation in the presence of misalinements between the shaft and the position-sensing transducer. It is intended to be used in situations in which the input or output shaft is mounted on a flexible joint. Its function is to insure equal input and output angular velocities by forcing the input and output shafts to remain parallel.

The coupling consists essentially of a concentric pair of cylinders that act as a flexible link between two shafts (Figure 1). The cylinders are machined and fastened together so that they function as a pair of universal joints.

The mechanism is based on Hooke's joint — the simple universal joint consisting of two yokes attached to their respective shafts and connected by a crossbar. Kinematically, the mechanism can be represented as a parallelogram linkage with Hooke's joints at its vertexes. In Figure 2, links 2, 4, and 5 with joints A and B constitute a double Hooke's joint. Links 2, 3, and 5 with joints C and D constitute a parallel double Hooke's joint. The linkage A, B, C, D forms a parallelogram, thereby ensuring that output shaft 5 remains parallel to input shaft 2 and that both shafts turn at the same angular velocity.

The linkage in Figure 1 uses slotted tubes to construct the Hooke's joints. Flexure at the slots corresponds to joint motion in the kinematic representation. The rods that join the inner and outer tubes keep the tube ends parallel, thus implementing the "rigid single links" seen in Figure 2. The concentric-tube construction is accurately concentric and parallel and is rigid in torsion. It is simple and, because of its few parts, is expected to be reliable.

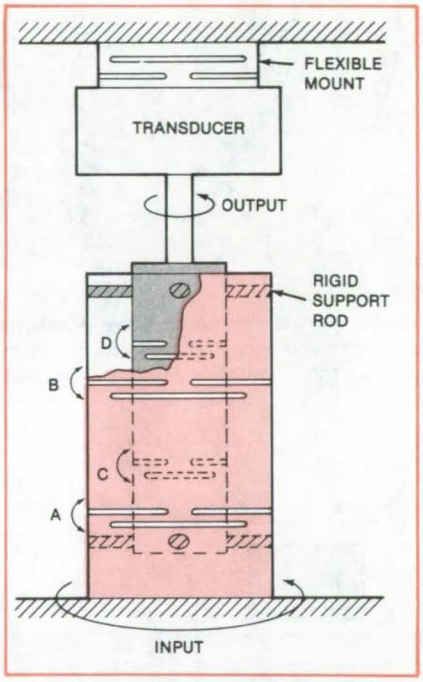

Figure 1. **Slots in Concentric Cylinders** act as universal joints, allowing them to flex and compensate for misalinements of input and output shafts. Walls A-B and C-D always remain parallel.

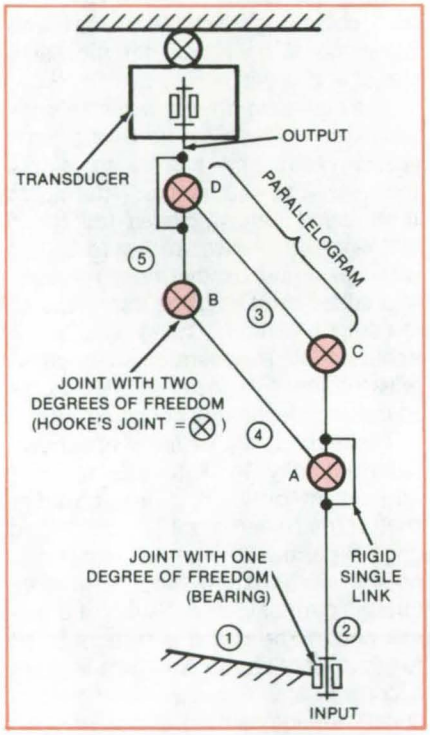

Figure 2. **Linkage Composed of Universal Joints** (Hooke's joints) ensures that opposite sides of the parallelogram ABDC remain parallel. The height of the parallelogram is exaggerated here; actually, the sides would be almost collinear.

The mechanism can accommodate all three possible (small) input- and output-shaft misalinements — lateral, angular, and axial — in any combination. Moreover, any or all of these misalinements can vary in magnitude and direction.

The coupling concept was originally developed for antenna-position control systems. It may also find application in machinery having higher rates of rotation than the antenna.

This work was done by Robert A. Mayo of Caltech for **NASA's Jet Propulsion Laboratory.** *For further information, Circle 53 on the TSP Request Card.*
NPO-15393

Deep-Access Valve Wrench

A rod attached to an extension pipe holds the wrench jaw against the valve stem.

John F. Kennedy Space Center, Florida

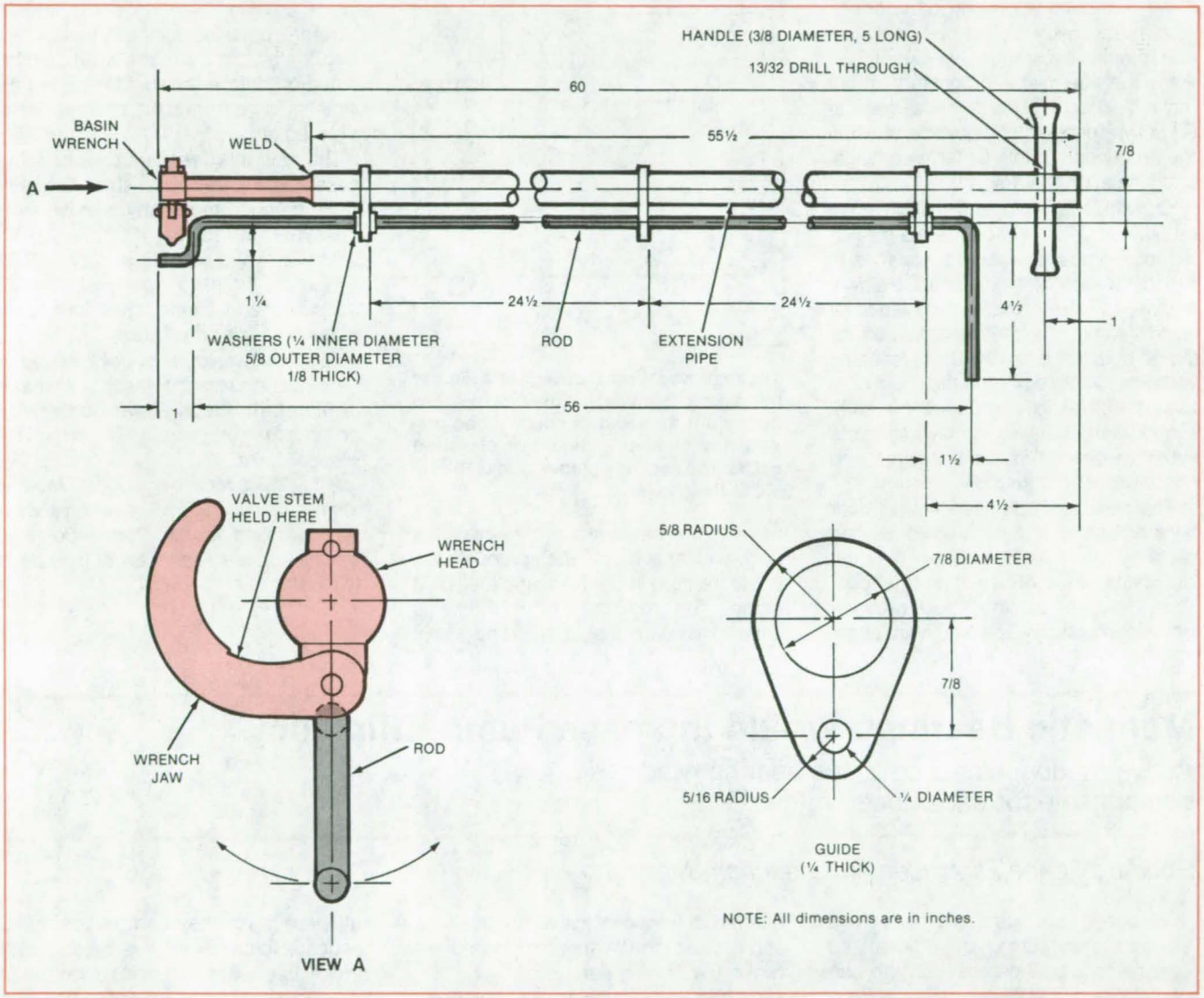

The **Bent Rod on the Modified Basin Wrench** holds the wrench jaw against the valve stem. The rod swivels to accommodate the 180° rotation of the wrench jaw. Valves 5 feet (1.5 meters) underground can be operated with the tool.

A modified basin wrench makes it easier to open and close valves in deep valve boxes. Underground water valves, with broken or corroded handles can be operated with the tool.

The basin wrench is modified by a long handle and a rod for holding the wrench jaw against the valve stem (see figure). To extend the reach of the wrench, a 55-1/2 inch (1.4 m) length of 1/2-inch (1.3-cm) galvanized pipe is welded to its shaft. Welded to the pipe are three stainless-steel guides that hold the stainless-steel rod, 1/4 inch (0.64 cm) in diameter. Three stainless-steel washers are tack-welded to the rod, near the guides, to keep it from sliding away from the wrench jaw.

The rod swivels to hold the jaw of the wrench against the valve stem for both opening and closing the valve. At its bottom, the rod bends outward 1-1/4 inches (3.2 cm) and then turns down for 1 inch (2.5 cm) to form a surface that can butt against the wrench jaw; at its top, the rod bends outward 4-1/2 inches (11.4 cm) to provide a handle for maneuvering the bottom portion. A steel handle near the top of the pipe extension helps to turn the wrench.

This work was done by Harold E. Fleck of Boeing Services International, Inc., for **Kennedy Space Center.** *No further documentation is available.*
KSC-11229

Improved Atomizer Resists Clogging

A simple new design eliminates clogging.

Marshall Space Flight Center, Alabama

An improved atomizer produces a uniform mist with droplet concentration that remains substantially constant over time. The fine mist and constant-output make it especially useful for the generation of aerosols, cloud-physics studies, the production of thin uniform coatings, and inhalation therapy.

Conventional atomizers are subject to output fluctuations because the gas/liquid mixing passages contain spaces in which the gas or mixture flows slowly enough to permit the accumulation of liquid. At intervals, the accumulated liquid is caught up in the flow, causing variations in the output. If the liquid contains dissolved solids (for example, salt), evaporation of the liquid may cause the solids to deposit in the passages and possibly obstruct the flow.

The new atomizer (see figure) contains no spaces in which liquid or solid could accumulate. Because of the conical shape of the orifice, the air jet continually sweeps out any liquid, preventing accumulation. The liquid is channeled to the jet in a steady stream by the capillary action of the groove, the pressure drop in the flow, and the liquid pump. The regularity of the flow is limited mainly by that of the liquid pump, and a precise metering pump should therefore be used for best results. To keep the nozzle clear, the air should be turned on before the liquid is turned on and should be turned off after the liquid is turned off.

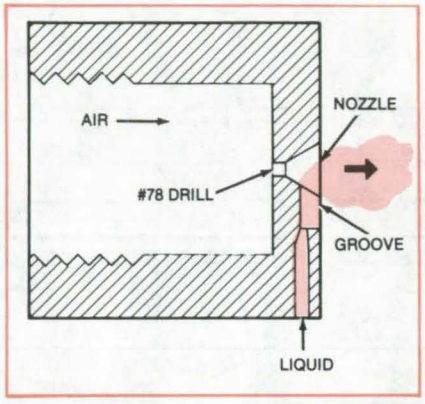

The **Improved Constant-Output Atomizer** has a conical orifice that permits the air to sweep out all liquid thoroughly and prevent any buildup of liquid or dissolved solids. The capillary groove guides the liquid to the gas jet.

The new atomizer has been used to make mists with micron-sized droplets. It can be operated in any position, with pressures of 10 to 100 psi (69 to 690 kN/m^2) and liquid-flow rates of 0.05 to 2.0 cm^3/min. In general, higher pressures and lower liquid-flow rates produce smaller drop sizes.

This work was done by Jack Y. Dea of the Nevada Desert Research Institute for **Marshall Space Flight Center.** *For further informatin, Circle 54 on the TSP Request Card.*

Inquiries concerning rights for the commercial use of this invention should be addressed to the Patent Counsel, Marshall Space Flight Center [see page A5]. *Refer to MFS-25631.*

Magnetic Bearings Would Increase Pump Efficiency

Active feedback applied to the bearing windings compensate for unbalanced forces.

Goddard Space Flight Center, Greenbelt, Maryland

Magnetic bearings would make a two-element rotary pump more efficient, according to a new proposal. In the concept developed at Goddard Space Flight Center, active feedback applied to the bearing windings would compensate for rotor displacements. The result would be lower friction and less backflow.

In the proposed compressor (see figure), counterrotating tapered screws force the gas through a tapered chamber, decreasing the gas volume until it discharges at higher pressure from the exit port. Ideally, the screws rotate without touching each other or the walls of the chamber and the motors are synchronized. Frictional losses are minimal, and a clearance seal is maintained between the moving parts.

In practice, however, the compression and transport of the gas create unbalanced radial and axial forces that displace the screws from their equilibrium positions. These forces tend to throw the drive motors out of synchronization. The result is higher frictional losses, gas leakage back toward the inlet port, and an overall lowering of efficiency.

Although conventional bearings cannot compensate for these effects, magnetic bearings are ideal for this configuration because they can be used with feedback to balance the radial and axial forces. Each screw shaft is supported at one end by a magnetic bearing and by a drive motor with radial control at the other end. Capacitive elements sense the axial and radial displacements of the shafts and develop error signals that are converted to changes in magnetic flux in the bearing and motor windings. The phases of these error signals are such that the flux changes tend to restore the shafts to their equilibrium positions.

Electro-optic devices keep the motors in synchronism. A slotted disk is mounted on each drive shaft, and an

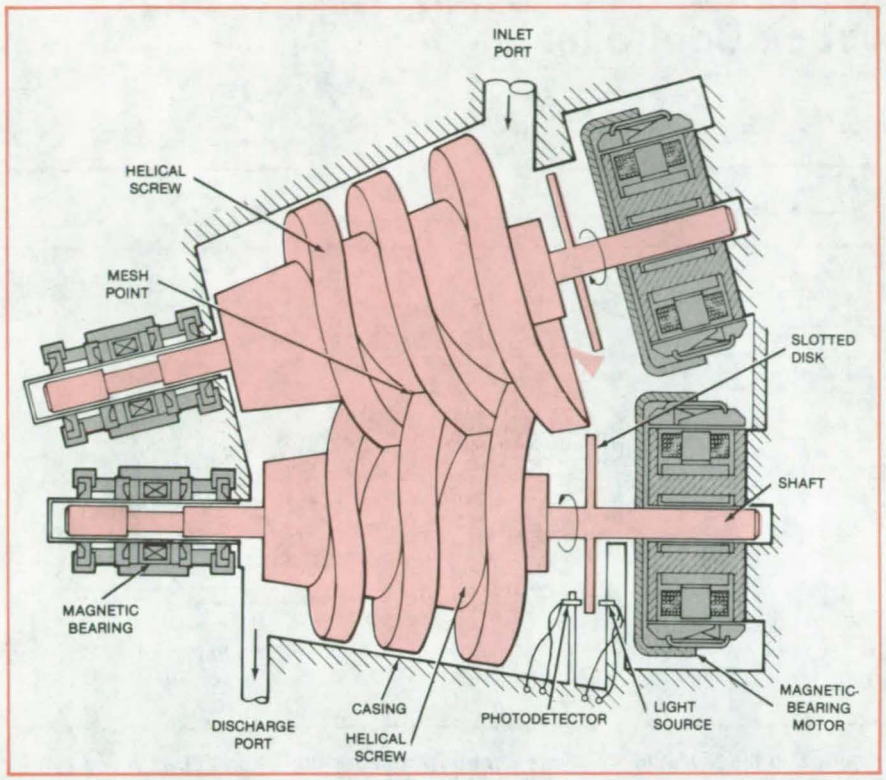

Helical-Screw Rotation compresses and transports gas charges, which subject the shafts to forces that tend to displace them from their equilibrium positions. Magnetic bearings would restore the shafts to equilibrium, lowering friction and increasing efficiency.

LED and a photodetector are mounted adjacent to the disk. Each time a slot moves into the space between the light source and the detector, an electric pulse is generated. If the rotations are synchronized, the relative phase of the two pulse trains is constant. Phase changes are sensed by a phase-locked loop, which develops an error signal. The error signal is amplified and applied to the motor armatures to synchronize the rotations.

This pump could be used to compress fluids or gases in a mechanical refrigerator. Other types of counterrotating machinery may also use magnetic bearings and motors to maintain close clearance between rotating parts.

This work was done by Philip A. Studer of **Goddard Space Flight Center.** *For further information, Circle 55 on the TSP Request Card.*

This invention is owned by NASA, and a patent application has been filed. Inquiries concerning nonexclusive or exclusive license for its commercial development should be addressed to the Patent Counsel, Goddard Space Flight Center [see page A5]. Refer to GSC-12668.

Preventing Cracks in Titanium Rotary Seals

A plastic insert maintains a seal while it prevents rubbing of metal parts.

Marshall Space Flight Center, Alabama

An improved rotating cryogenic joint employs a seal composed of polytrichlorofluorethylene (PTCFE) between titanium moving parts and other metal parts. In a cryogenic pump, a PTCFE labyrinth seal separates the housing from the titanium impeller (see figure).

Rotating seals that must operate at cryogenic temperatures present a particularly-difficult design problem. Often, titanium is selected as the material for at least one of the rubbing surfaces of a rotating seal for liquid hydrogen. However, titanium surfaces that rub against other metal surfaces are prone to cracking that eventually destroys the seal. Apparently, friction between the surfaces generates enough localized heat to initiate cracks in the titanium.

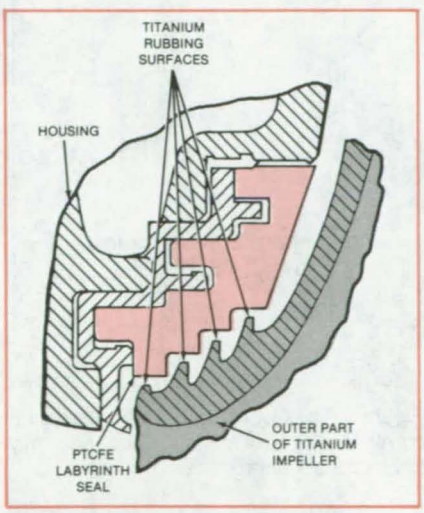

Titanium Rubs Against Plastic instead of metal in a new rotary seal for a cryogenic pump. Friction-induced cracks in titanium parts are thereby avoided.

In the improved joint, the titanium impeller rubs against plastic, not metal. As a result, localized heating of the titanium — and its subsequent cracking — is eliminated.

This work was done by James J. Ciana of Rockwell International Corp. for **Marshall Space Flight Center.** *No further documentation is available.*
MFS-19686

Miniature Two-Axis Joystick Controller

Pilots like the feel of a new device.

Ames Research Center, Moffett Field, California

A novel movable-button-actuated self-centering controller uses optoelectronics to produce X and Y signals for aircraft control. In addition to being extremely compact [1.0 in. (2.5 cm) in diameter by 1.3 in. (3.3 cm) tall, excluding the button], the device puts out voltages having a high signal -to- noise ratio, especially at the critical center position where in many controllers this ratio is poorest. The combination of a new saddle-shaped button and positive centering gives a "feel" and "breakout" (the pressure necessary to overcome the self-centering action) that have met with pilot approval.

As shown in Figure 1, a rocker, housing a lensed light-emitting diode (LED), is positioned over the truncated cone of a rocker plate and held there by pressure from a coil spring. The knife-edged rocker fits closely around the base of the cone, enabling the rocker to be tilted but not moved laterally. The spring exerts a downward force for self-centering and, additionally, when the rocker is tilted, a side force that prevents slippage away from the base of the cone.

Collimated light from the LED passes through a small aperture in the cone and forms a spot on the square photosensitive area of a commercially-available two-axis photodetector in a reduced-diameter case. When the spot is centered, the four output photocurrents are equal. When the rocker is tilted (see lower part of Figure 1), the spot is moved, and the ratio between the currents is varied. Operational amplifiers, within the controller, convert these currents to voltages as shown in Figure 2. Normalization, which is necessary for this type of device, and scaling are performed externally.

The new controller was developed for use in piloting flight-simulator vertical-takeoff-and-landing aircraft. It has not yet been flown. Other suitable applications would include radar trackers/cursors, aircraft moving-map display controls, weapon pointing, and others where size, weight, and ability to function in an electrically noisy environment are critical.

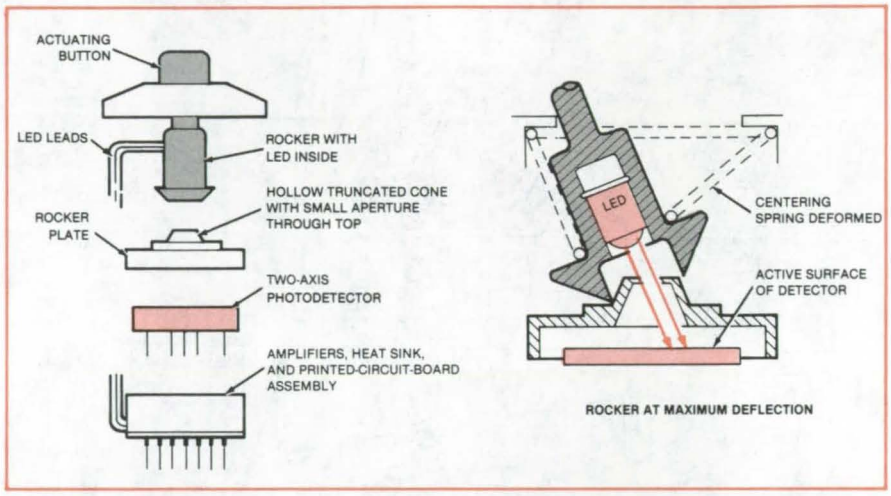

Figure 1. In the **Miniature Two-Axis Controller,** the position of an LED is varied by the motion of a spring-centered rocker. The position is detected by a dual-axis photodetector.

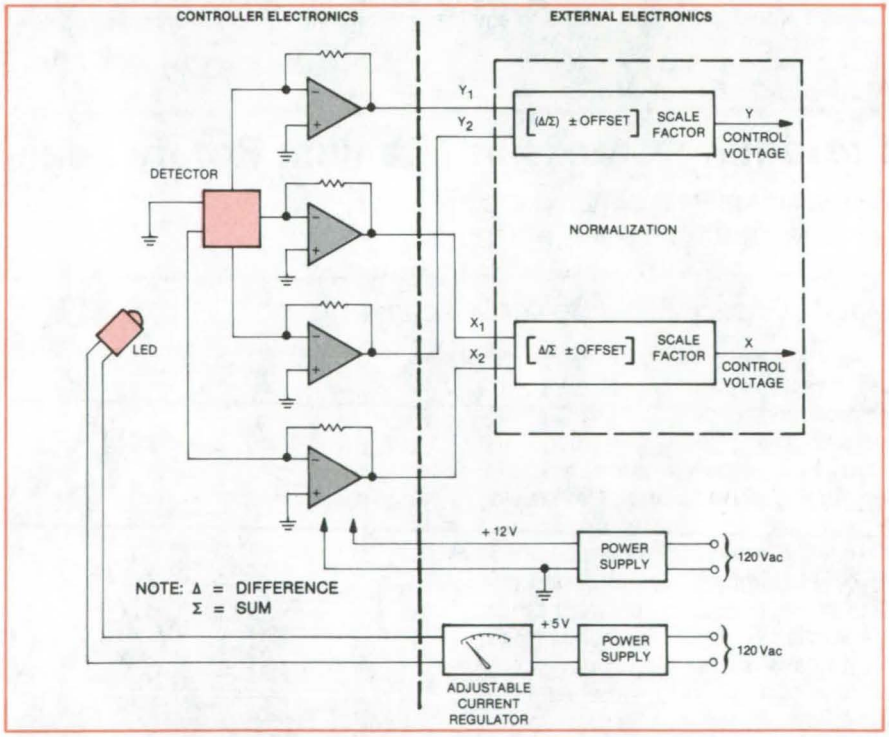

Figure 2. The **Controller Electronics and External Electronics** convert the photodetector currents to control signals. Because of high signal levels, the system is relatively immune to electrical noise.

This work was done by Richard Hollow of Computer Sciences Corp. for **Ames Research Center.** *For further information, Circle 56 on the TSP Request Card.*

Inquiries concerning rights for the commercial use of this invention should be addressed to the Patent Counsel, Ames Research Center [see page A5]. Refer to ARC-11372

Cutter for Woven Materials

"Guillotine" cutting tool makes clean cuts in fabric strips.

Lyndon B. Johnson Space Center, Houston, Texas

A simple tool makes accurate square cuts through strips of woven or felted materials, such as high-temperature aramid fabric. Scissors, papercutters, and a knife with a roller were slower than the new "guillotine" cutter in preparing aramid fabric strips for the Space Shuttle thermal-protection system. The new cutter gave the operator better control over the cut and resulted in sharper, well-defined edges.

The cutter (see figure) has a slotted base for accepting the material to be cut. A razor blade is clamped in a holder that moves vertically in a bushed support bracket. A pivoted handle with a mechanical advantage of about 4 applies a downward force on the razor-blade holder.

The blade works against a slotted anvil of tough plastic. This reduces wear on the cutting edge and provides a clean cut. Two plastic blocks mounted on the base prevent rotation of the blade assembly, assuring a square cut.

This work was done by John M. Hammons and Andrew R. Keir of Rockwell International Corp. for **Johnson Space Center.** *For further information, Circle 57 on the TSP Request Card.*
MSC-20178

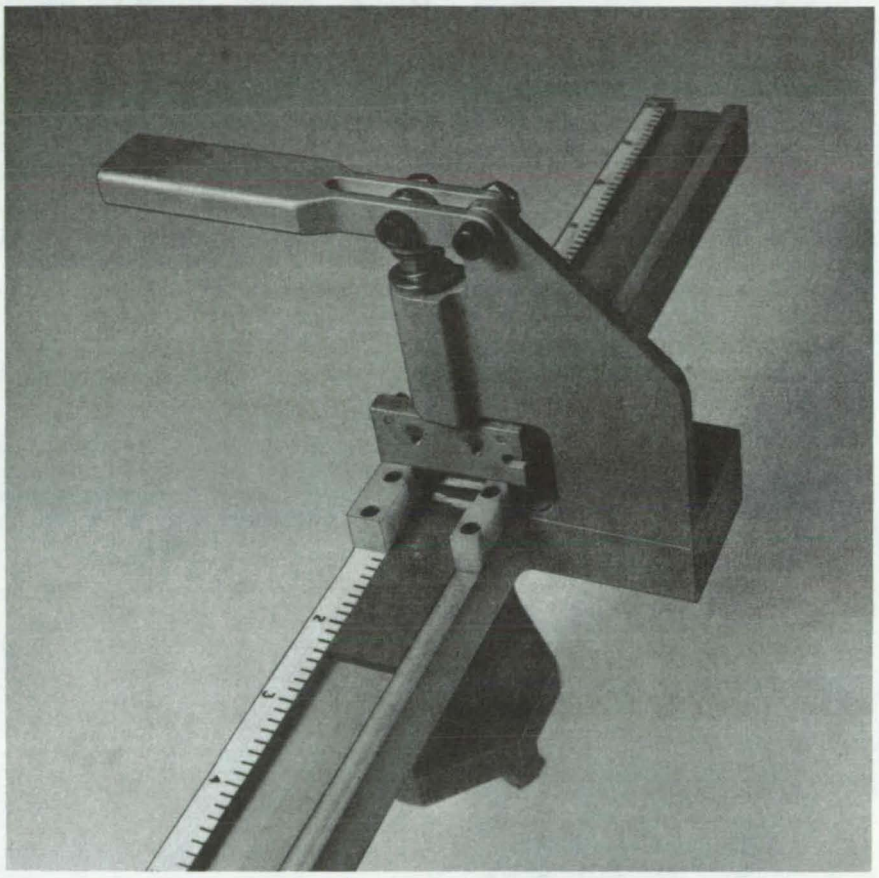

Pressing the handle on this **Guillotine Cutter** forces a razor blade through the strip of material in the slot, cutting the strip off squarely. The scale is for measuring the length of material to be cut. The cutter accepts strips 0.09 to 0.16 inch (2.3 to 4.1 mm) thick and 0.75 inch (19 mm) wide.

Ball Joint for Quick Connections and Disconnections

Joint is strong in shear and tension.

Langley Research Center, Hampton, Virginia

A proposed quick-connect/disconnect joint could be operated remotely, offers high strength in shear and tension, and allows rotational freedom. The joint consists essentially of an expandable collet that can be locked over a ball to form a ball-and-socket joint.

To attach the joint, the user depresses a button protruding from the center of a release tool handle and inserts the tool into a sleeve on the collet (see figure). Releasing the button allows locking balls in the tool shank to grip the sleeve when the user applies a lifting force. The lifting action allows fingers on the collet to expand.

With the collet fingers in the open position, the user can place the collet over a ball, which forms the fixed side of the joint, and then release the sleeve so that the collet fingers close over the ball. The quick-connect/disconnect joint is then secure. To disconnect the joint, the user inserts the release tool and raises the collet. The fingers open and free the ball.

(continued on next page)

The joint was proposed for possible use on the Space Shuttle for the attachment of heat-protection panels where deflection or thermally-induced moment loads are undesirable. It has a variety of other potential applications, for example:

- Quick attachment and detachment in hazardous, inaccessible, or blind locations;
- Linking parts of mechanisms (as a replacement for a spherical bearing, the joint would simplify assembly and design and allow easy replacement of bearing surfaces);
- Grasping spherical objects in robotic machines; and
- Coupling pneumatic tubes (besides quick connections and disconnections, the joint would allow flexure).

This work was done by Louis W. Palmer of Rockwell International Corp. for **Langley Research Center.** *For further information, Circle 58 on the TSP Request Card.*
LAR-12896

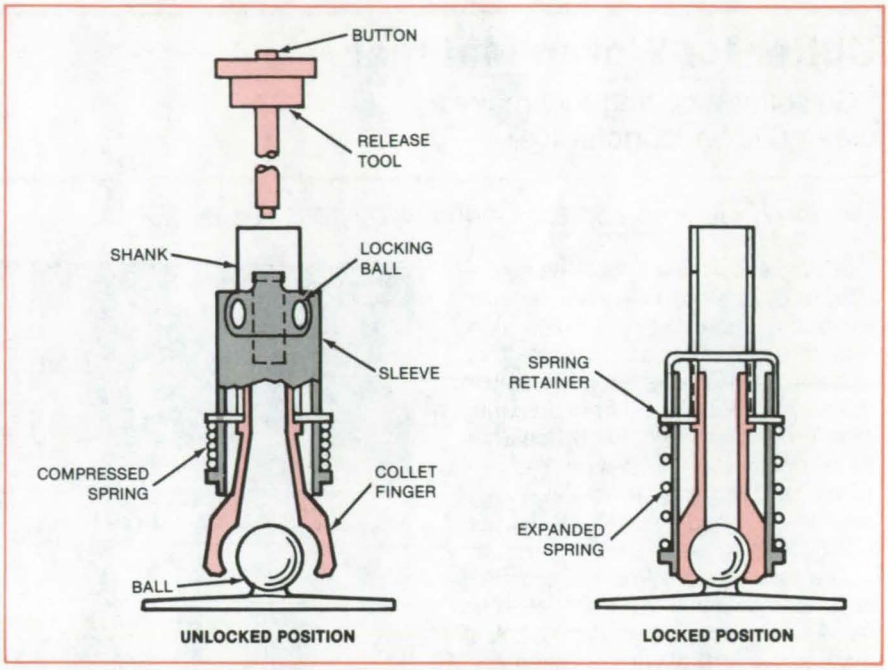

When a **Release Tool** is inserted into the sleeve of the joint, locking balls engage the sleeve and allow it to be pulled upward, compressing the spring and releasing the collet fingers. When the sleeve is released, the spring forces the sleeve and collet fingers over the ball on the fixed part of the joint.

Pressure Relief Valve

A cap with O-ring protects subatmospheric systems.

Lewis Research Center, Cleveland, Ohio

Many ordinary pressure relief valves used to protect subatmospheric instruments are very prone to leak, especially over extended periods of time. Some occasionaly fail to function after long periods of use.

A very simple design has been found to solve these problems. No failures have been seen after several years of test use. As shown in the figure, a body or housing is attached by a standard screw fitting to the piping circuit. The top surface of the housing has a machined groove in which is placed an O-ring. A simple cap with a pin made to fit very loosely in the housing simply rests on the O-ring. The undersurface of the cap is a machined surface. Thus, the weight of the cap presses the O-ring between two machined surfaces, effecting an adequate seal. The vacuum is fully maintained.

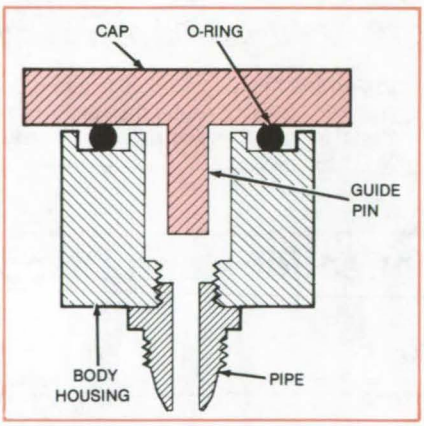

The **Valve Cap,** which is seated on an O-ring, lifts to relieve positive pressure. It is attached to the vacuum system by a screw-on housing.

If a system failure puts a positive pressure to the valve, the cap lifts to relieve the pressure. If there is a sudden severe change in pressure, the cap will pop off; but the stem prevents damage to the machined surface of the cap, making the cap reusable. Caps may be loosely tied to the pipe with twine or thin wire to make recovery simple. The weight of the cap and O-ring diameter can be sized to fit the desired overpressure limits.

This work was done by Theodore A. Brabbs of **Lewis Research Center.** *No further documentation is available.*
LEW-13800

Micrometer for Measuring Trepanned Grooves

Tool accurately measures groove diameter where standard calipers are not feasible.

Marshall Space Flight Center, Alabama

A special micrometer measures the diameter of a circular groove on the face of a large part, while the part is mounted in a lathe chuck. The tool has a curved frame (like that on an ordinary micrometer, but larger), so it can reach around an obstruction on the centerline of the part. At one end of the frame there is a blade/micrometer spindle for reaching into the groove to be measured; this type of spindle does not rotate when the micrometer thimble is turned in taking a measurement. The other end of the frame has a sliding foot with a blade.

The special tool was developed to permit measurements during the machining of a 26-inch (66 cm) groove on the flat face of an engine nozzle, which has a tolerance of 2 mils (0.005 cm). The groove and the obstacle to its measurement are seen at the top of the figure. The tool can also be used in other face-groove measurements where standard methods, such as vernier calipers, are not feasible.

As seen at the bottom of the figure, the large frame and blade/micrometer barrel that slides in and out without turning makes this tool very practical. The adjustable sliding foot at the anvil end of the frame allows the tool to measure a wide range of face-groove diameters, with accurate calibration in the 1-inch (2.54-cm) range of the blade/micrometer spindle.

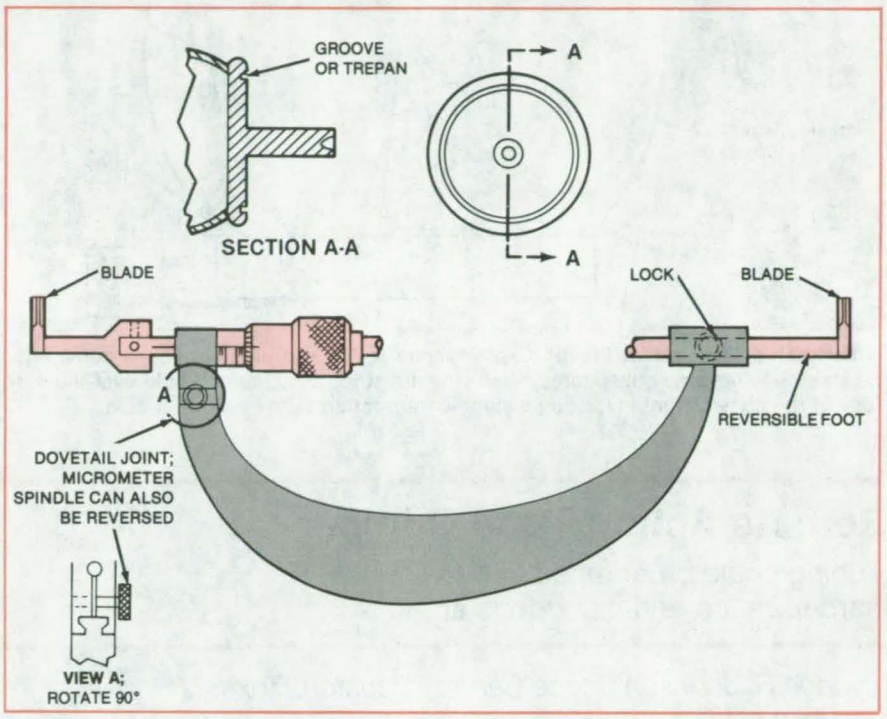

A Circular Face Groove (trepan groove), such as the one on the part shown at the top, can be measured accurately during the machining process with the special micrometer shown at the bottom. The large curved frame is not obstructed by the shaft projecting from the center of the part.

This work was done by Samuel K. Bird of Rockwell International Corp. for **Marshall Space Flight Center.** *No further documentation is available.*
MFS-19704

Cleaner for Solar-Collector Covers

A cleaning solution would be pumped over the collector cover.

NASA's Jet Propulsion Laboratory, Pasadena, California

A simple self-contained cleaning system has been proposed for solar collectors or solar-collector protective domes. Current cleaning methods are uneconomical because they are labor-intensive or because they require expensive machinery.

A thin transparent perforated polymeric film cap would be attached to the top of the dome (see figure). A small, low-pressure pump would pump a cleaning solution up under the cap. It would flow out through the perforated cap and then down over the surface of the dome, washing off any dirt. The cleaning fluid would be collected in a gutter around the bottom of the dome, filtered to remove particulate dirt, and then returned to a sump for reuse.

The pump could be controlled remotely or by a timer. The addition of fluid to

(continued on next page)

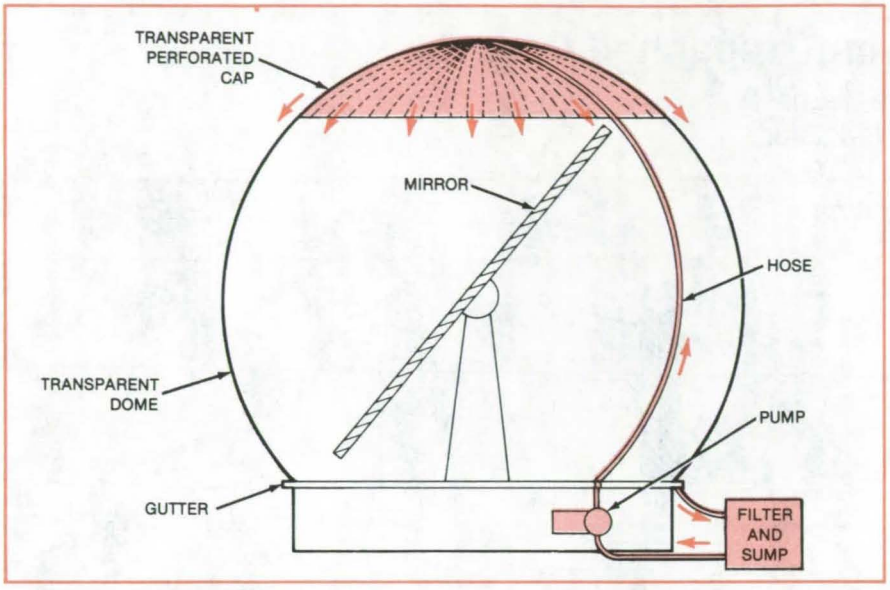

A **Perforated Transparent Plastic Cap** attached to the top of a protective dome in a heliostat solar-energy collection system would distribute a cleaning fluid over the surface of the dome without blocking a significant fraction of the solar radiation.

replace evaporation losses would be controlled by a float switch. In a large multidome installation such as a heliostat field, a single centrally-located filtering and pumping system could be used.

The hardware required for the proposed cleaning system (including filters, sump, pump, timers, and float switch) is commercially available. The perforated-film technology required is similar to that used in permeable bleeder membranes developed in the aerospace reinforced-plastics industry. The system should be tested to verify that satisfactory cleaning is achieved with the relatively-gentle fluid flow proposed.

This work was done by Peter O. Frickland and Edward L. Cleland of Caltech for **NASA's Jet Propulsion Laboratory.** *For further information, Circle 59 on the TSP Request Card.*
NPO-15414

Remote-Action Tube Crimper

Tubing could be crimped in hard-to-reach and hazardous areas.

Lyndon B. Johnson Space Center, Houston, Texas

A proposed long-handled tube crimper could stop leaks or reduce fluid flow in hard-to-reach and hazardous areas. It is similar to tools for pinching off vacuum equipment and sealing it from its pumping source.

As shown in the figure, the tool includes a steel plunger, which is contained within a pipe, and long cam-action handles that open and close the crimping jaw. The movable jaw is wedge shaped and the stationary jaw is cylindrical. The length of the plunger and surrounding pipe can be varied from tool to tool to accommodate the reach required.

An adjustable stop in the handle avoids severing the tubing by stopping the handle closure at the proper distance for tube crimping. The stop is marked for various tube sizes so that the correct crimping pressure is applied.

This work was done by Richard L. Robbins and Shawn T. Harrison of Rockwell International Corp. for **Johnson Space Center.** *No further documentation is available.*
MSC-20197

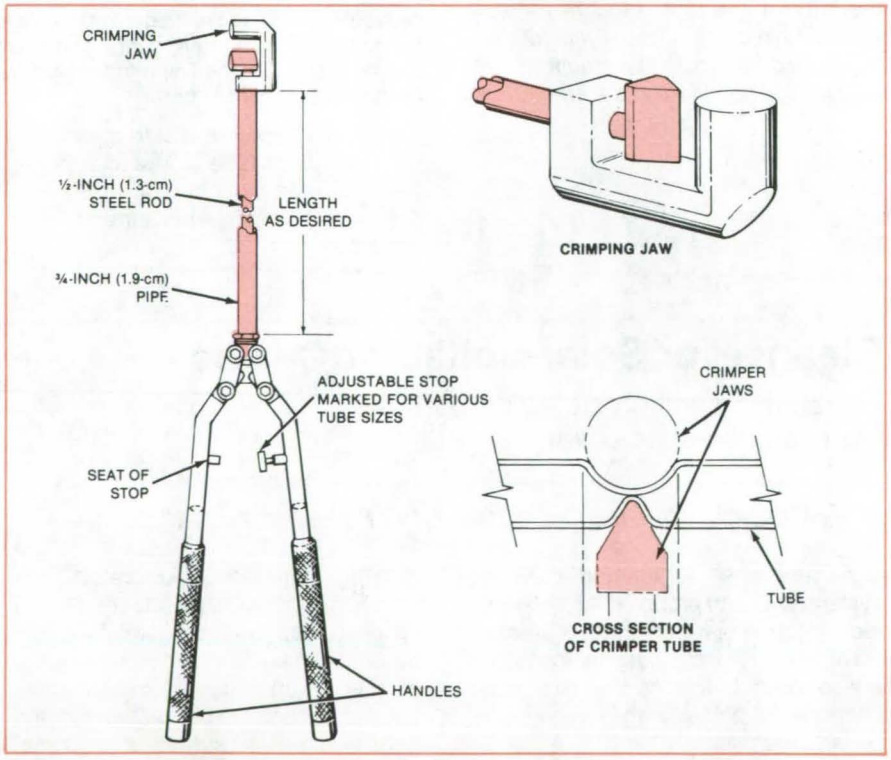

The **Length of the Steel Rod and Surrounding Pipe** determines the reach of the long-handled crimper. An enlarged view of the crimping jaw and a cross section of a crimped tube are also shown.

Modified Reamer Removes Chips and Contaminants

A proposed tool would prevent chips and lubricant from contaminating the cutting area.

Marshall Space Flight Center, Alabama

A proposed modification to a reamer would draw cutting chips and lubricant away from the cutting area. The tool would be especially useful when the surroundings must be kept free from contamination.

The modified reamer (see figure) has an internal passage connected to a vacuum source. Cuttings are drawn into the passage through holes in the reamer grooves. They exit the shaft through outlet holes that lead into a vacuum manifold, located near the machine chuck. The manifold collects the debris and passes it to a trap that protects the vacuum source. A positive pressure of 1 to 2 psi (7×10^3 to 14×10^3 N/m^2) inside the orifice helps to extract the chips.

Among the factors that need to be accounted for when modifying a reamer are the type of material being reamed and the size of the hole to be made. These factors will determine the size of the passage and the sizes of the inlet and outlet openings in the reamer shaft. Furthermore, the O-rings that maintain the vacuum seal on the manifold must be made of an elastomer that resists wear from the rotating reamer shaft.

This work was done by Larry L. Larson of Rockwell International Corp. for **Marshall Space Flight Center.** *No further documentation is available.*
MFS-19711

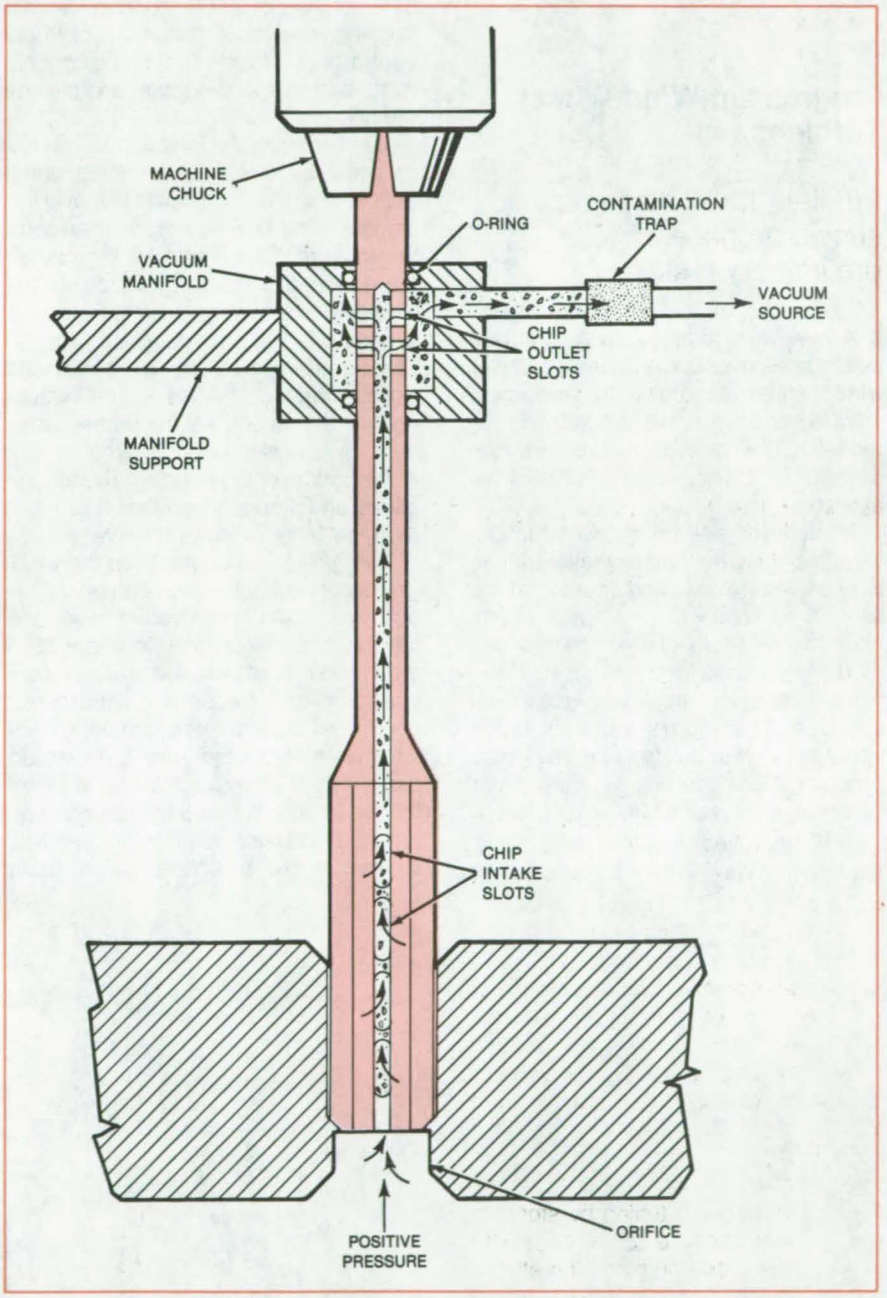

The **Reamer Shaft** is modified by a central passage and intake and outlet slots. To help draw away chips and lubricant and augment the vacuum, a positive pressure is applied inside the orifice of the part being reamed.

Books and Reports

These reports, studies, and handbooks are available from NASA as Technical Support Packages (TSP's) when a Request Card number is cited; otherwise they are available from the National Technical Information Service.

Progress in Wind-Wheel Turbines

Efficient turbine concept shows promise in preliminary tests.

A new wind turbine offers important advantages over conventional propeller wind tubines according to theoretical studies and tests of small working models. The project results are described in a final report that is now available.

Because of their simple construction, it seems likely that wind-wheel turbines will cost less to build and operate; at the same time, wind wheels are just as efficient as conventional wind machines in extracting energy from moving air. Wind wheels operate at lower rotational speeds and therefore are less subject to vibratory stress and fatigue. They also produce higher torque — useful for powering pumps and similar machines.

The improved wind wheel is described in "Wind-Wheel Electric Power Generator" (MFS-23515) on page 276 of *NASA Tech Briefs*, Vol. 3, No. 2. A streamlined version is described in "Aerodynamics Improve Wind Wheel" (MFS-25506) on page 78 of *NASA Tech Briefs*, Vol. 6, No. 1. The wind-wheel turbine consists of a bladed wheel, a main housing, two forward ducts (front concentrators), two side ducts (side concentrator and a base to support and elevate the housing.

Wind entering the forward ducts is accelerated by venturi tubes, which funnel the flowing air upward toward the blades. Wind flowing across the top of the forward ducts impinges directly on the exposed blades at the top of the wheel. Wind flowing over the sides is scooped by the side ducts into venturi tubes that reverse the airstream and direct it against blades at the bottom rear of the wheel. As the wheel turns, used air leaves through an exhaust vent at the bottom of the housing. The turbine pivots on its support so that it turns to face the wind like a weather vane.

Two sets of experiments on the wind-wheel concept have been carried out — one on a model composed of paper and cardboard and the other on a stainless-steel model. A simplified analytical model based on four blades has been developed, and performance characteristics have been computed from it. A detailed performance analysis of the wind-wheel turbine is difficult since the device does not fit a classical pattern. It behaves somewhat like a simple water-paddle wheel and somewhat like an impulse gas turbine. A complete performance analysis should include the interaction between the inlet flow, the wheel-blade flow, and the outlet flow.

A practical version of the wind wheel will probably require more than four blades. The final wheel design will be a result of blade size, shape, and quantity. Variable-pitch stator blades may be added to control wheel speed, maintaining constant rotational frequency so that constant-frequency electric power is produced.

The wind-wheel turbine bearings present a much-simpler design problem than the bearings for a propeller-type wind turbine. The forces on the blades exert only a torque on the wheel, which in itself produces no load on the bearings. There is little side or thrust load on the bearings since the transverse airflow forces are balanced.

Sufficient information is available for a final design of a functional turbine using off-the-shelf parts and components. This design can now avoid special engineering-design and development tasks, which are unnecessary and costly. However, final performance of the system can only be determined by field testing a prototype unit.

This work was done by Walter Frost and Philip A. Kessel of FWG Associates, Inc., for **Marshall Space Flight Center.** *To obtain a copy of the report, Circle 60 on the TSP Request Card.*
MFS-25796

Fabrication Technology

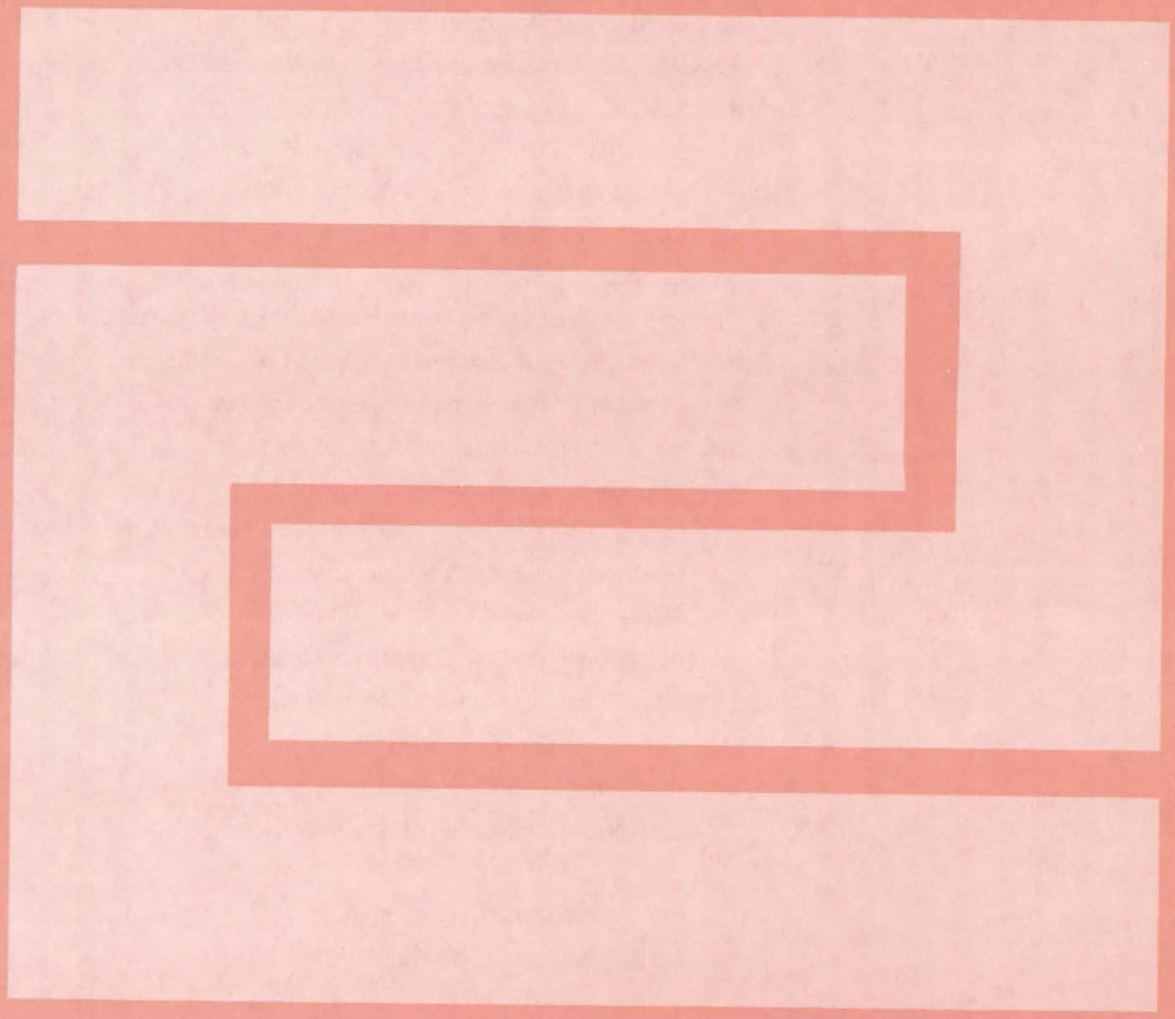

Hardware, Techniques, and Processes

Books and Reports

Assembly of Photovoltaic Arrays

Heat lamps on a trolley
melt preapplied solder.

NASA's Jet Propulsion Laboratory, Pasadena, California

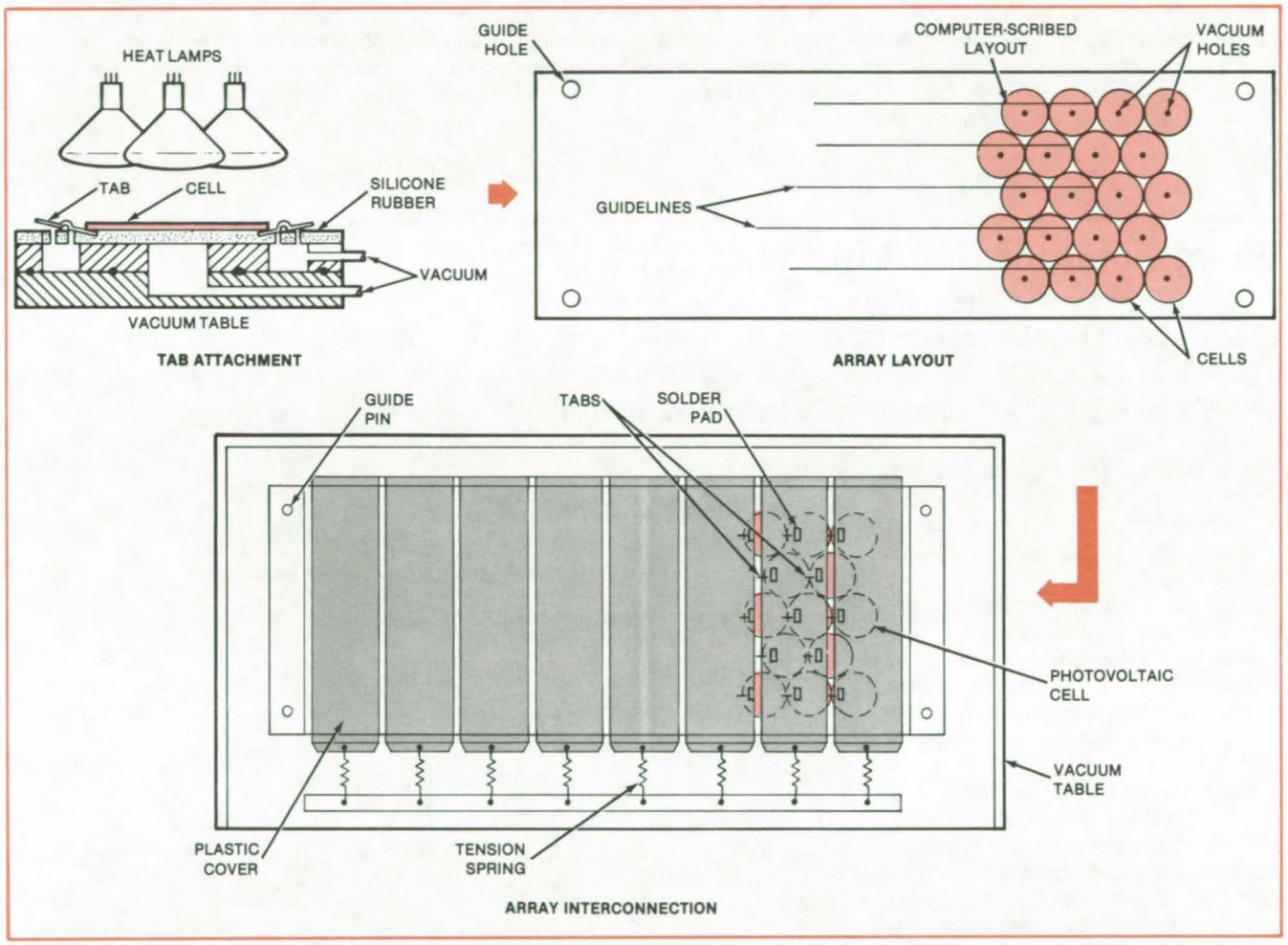

Vacuum Holddown Fixtures hold photovoltaic solar cells during assembly into an array. The tab-attachment fixture holds a single cell and interconnecting tabs during heat-lamp soldering. The array-layout fixture has a computer-scribed layout template and holds the cells (with attached tabs) while they are being placed in position and while they are being transferred to the array-interconnection fixture, which holds the cells during the final soldering step. A group of heat lamps on a trolley passes slowly over the interconnection fixture to heat the cells to soldering temperature.

In a new system for assembling photovoltaic arrays, solder and flux are applied to pads on the individual cells by a screen process and then heated to soldering temperature by heat lamps during final assembly. Fixtures with vacuum holddowns keep the cells and interconnecting tabs in proper alinement. [A description of the interconnection geometry is given in "Parallel Connections Would Improve Array Reliability" (NPO-15310) in *NASA Tech Briefs*, Vol. 6, No. 4, Spring/Summer 1982, page 375. The radiant-heat soldering technique is described in "Heat Lamps Solder Solar Array Quickly" (NPO-14866) in *NASA Tech Briefs*, Vol. 6, No. 1, Spring 1981, page 101.]

The steps of the new assembly process (see figure) are as follows:

- Flux and solder are applied at solder pads on the front and back of the individual solar cells.
- Two types of interconnecting tabs (contact strips) with crimps for strain relief are prepared. Tabs for connecting from the front of one cell to the back of another have a Z-shaped crimp; those for connecting between solder pads on the same surface of two cells have a U-shaped hump in the middle.
- The first vacuum holddown fixture holds a single solar cell and tabs while infrared lamps heat the cell to solder the tabs to the cell.
- The cells (with attached tabs) are then arranged by hand on the second vacuum holddown fixture. This layout fixture has a computer-scribed template to guide the operator in placing the cells. The vacuum holddown holds the cells

(continued on next page)

securely (see next step), yet loosely enough that they can be adjusted in position.

- With vacuum still applied, the second fixture is turned over and placed face down on a third fixture. Locating pins ensure proper registration. Vacuum is then applied to the third fixture and released from the second, transferring the cells to the third fixture while maintaining cell alinement. The second fixture is then removed.
- A series of narrow transparent-plastic cover sheets is placed across the fixture, over the cells, and held tautly in place by springs. The covers hold the exposed interconnecting tabs against the cells during soldering. (A one-piece cover sheet proved unsatisfactory because creeping of the sheet as the heat lamps passed over the array caused the tabs to shift.)
- The heat-lamp carriage passes over the array at 1 ft/min (0.3 m/min), raising the cells to soldering temperature and completing the interconnection of the cells into an array.

During the final soldering step all the soldering points are under compression by essentially flat surfaces (between cover and cells or between cells and fixture). Thus the solder joints tend to come out flat without solder lumps. In methods used previously, such lumps caused the cells to be unduly vulnerable to breakage in later handling.

This work was done by Peter J. Coyle, Angelo G. Lazzery, and Marvin S. Crouthamel of RCA Corp. for **NASA's Jet Propulsion Laboratory.** *For further information, Circle 61 on the TSP Request Card.*
NPO-15311

Pellet Feed for Dendritic-Web Growth

Silicon pellets automatically added to the crucible would sustain crystal growth for days.

NASA's Jet Propulsion Laboratory, Pasadena, California

A technique for replenishing the silicon melt during the growth of a continuous dendritic web would permit uninterrupted crystal growth for several days or longer.

In dendritic-web growth, a crystal ribbon is formed by freezing a liquid supported on each edge by a needlelike dendritic crystal. The growth is thus shaped by crystallographic forces and surface tension rather than by dies (see figure).

The technique for melt replenishment uses a compartmented crucible. It has a large compartment from which web is grown, and a smaller compartment into which silicon pellets are fed as needed to maintain the desired melt level. The barrier that separates the two compartments prevents unmelted pellets from floating to the growing web and interfering with growth. It also prevents ripples, caused by pellets falling into the melt, from moving across the melt surface and disturbing the growth. The barrier has an opening below the surface of the melt, which permits continuous equalization of the melt levels in the two compartments. Pellets as large as 4 millimeters in diameter have been used successfully.

The remainder of the system consists of a pellet reservoir, a mechanism for feeding pellets one at a time, a feed tube, and suitable penetrations through the susceptor lid and shields into the crucible.

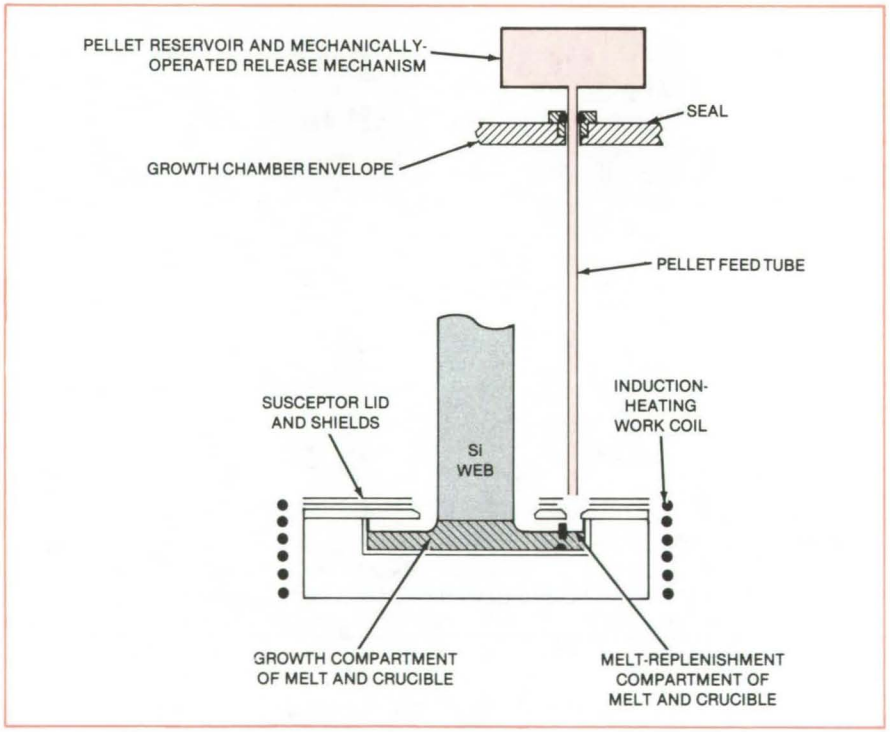

This **Melt Replenishment** system would sustain the continuous growth of silicon dendritic web for several days. It thus substantially increases the size of a batch, which would then be limited mainly by the level of impurities and the life of the crucible.

This work was done by Charles S. Duncan, Marie E. Skutch, and James P. McHugh of Westinghouse Electric Corp. for **NASA's Jet Propulsion Laboratory.** *For further information, Circle 62 on the TSP Request Card.*
NPO-15198

Barrier for Continuous-Crystal-Growth Crucible

Properly designed openings permit free flow of melt while restraining pellets.

NASA's Jet Propulsion Laboratory, Pasadena, California

A redesigned partition between the growth region and the melt-replenishment region of a crystal-growth crucible makes it less likely that the crucible will run out of feed material in the middle of a cycle. Melt replenishement makes possible the continuous growth of silicon web and thus is an important factor in low-cost production of quality solar cells. The supply of molten silicon is maintained by the addition of silicon pellets to a compartment at one end of the heated crucible, and a partition or barrier is required to hold the pellets while allowing the melted silicon to flow from the compartment.

The original barrier design is shown at the left of the figure. To allow more-flexible thermal conditions and prevent emptying of the replenishment compartment, the barrier shown at the right of the figure was developed. This new design includes a low wall along the bottom of the crucible, preventing liquid flow between compartments until a substantial fraction of the silicon has melted.

Above the low bottom barrier is a gap that allows the flow of melted silicon from the feed compartment into the growth compartment. Above the gap is the rest of the barrier, which keeps the silicon pellets from floating into the growth compartment and also keeps gas from carrying stray particles of silicon over from the space above the feed compartment to the crystal-growth compartment.

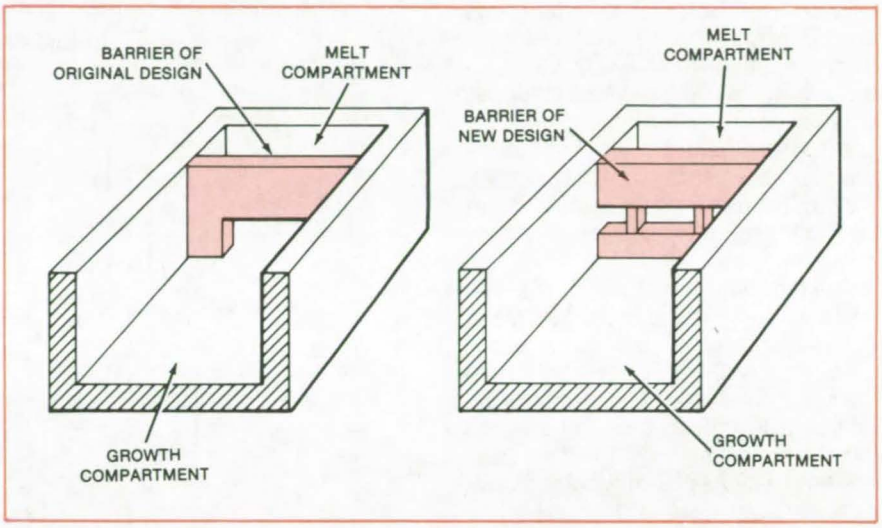

The Old and New Designs for the barrier between the feed compartment and the crystal-growth compartment in a heated crucible for continuous growth of silicon web are shown here. The old design (left) had a gap at the bottom to let melted silicon flow between compartments. The new design (right) has a low wall along the bottom and a gap above the low wall.

This work was done by Marie E. Skutch and Paul A. Piotrowski of Westinghouse Electric Corp. for **NASA's Jet Propulsion Laboratory.** *For further information, Circle 63 on the TSP Request Card.*
NPO-15338

Closed-Loop Process Yields Ultrapure Silicon

A closed-loop process produces ultrapure silicon from metallurgical-grade silicon by forming, purifying, and hydropyrolizing tribromosilane ($HSiBr_3$). The ultrapure granular silicon obtained can be used to produce semiconductors and solar cells. The only material that needs replenishing once the process begins is metallurgical-grade silicon; all other reactants are separated and recycled. The metallugrical-grade silicon is transformed into tribromosilane by reacting it with process byproducts. The tribromosilane is separated from the mixture, purified, and finally decomposed in the presence of hydrogen in a silicon-product reactor.
(See page 34.)

Bipulsating Technique for Silicon Production

The reduction of silicon tetrafluoride by sodium, to produce high-purity silicon, is very fast and highly exothermic. A method is proposed that controls the temperature and rate of reaction by alternately adding measured amounts of reactants. This technique could be used in a large reactor, where heat dissipation becomes a serious problem, to control reactor temperatures. It would be a highly efficient method that would utilize almost 100 percent of the raw materials. One of the benefits of the method is that the reaction products can be grown in columns, the only contact being with the base of the reactor.
(See page 34.)

Cutter for Woven Materials

A simple tool makes accurate square cuts through strips of woven or felted materials, such as high-temperature aramid fabric. Scissors, papercutters, and a knife with a roller were slower than the new "guillotine" cutter in preparing aramid fabric strips for the Space Shuttle thermal-protection system. The new cutter gave the operator better control over the cut and resulted in sharper, well-defined edges. The cutter has a slotted base for accepting strips 0.09 to 0.16 inch thick and 0.75 inch wide. A razor blade is clamped in a holder that moves vertically in a support bracket.
(See page 79.)

Modified Silicon Furnace Lowers Crystal Cost

Functional changes reduce cycle time and prolong crucible life.

NASA's Jet Propulsion Laboratory, Pasadena, California

A modified Czochralski setup grows several large crystals in succession from one crucible. Previously, the crucible would be destroyed by thermal-contraction differences during the cool-down phase and would have to be replaced after each crystal was completed. The modified apparatus is expected to reduce the cost per crystal by about 50 percent.

The redesign allows the crucible to be kept hot, the hot zone of the furnace to be always under vacuum or low argon pressure, crystals to be removed from the furnace without the admission of air, and polysilicon feedstock to be added safely and reliably to the hot crucible. The key features are: an isolation valve between the growth and pulling chambers, an enlarged pulling chamber, and a recharging mechanism. These features are seen in the figure.

The water-cooled vacuum-tight isolation valve is closed when a completed crystal is being removed from the pull chamber or new feedstock is being introduced. While a crystal is growing, the feedstock is suspended on a cable at the side of the pull chamber. After the crystal has been grown and removed, the recharge material is moved forward and lowered into the crucible. The material is lowered slowly as it melts and continually weighed so that the correct amount is added to the crucible. When the recharge material is retracted, reseeding proceeds immediately without opening of the furnace chamber.

Operation of the modified furnace has demonstrated that high-quality crystals can be grown from at least three successive melts in the same crucible and that the crucible can be filled to a capacity, in excess of cold filling techniques.

This work was done by Richard L. Lane of Kayex Corp. for **NASA's Jet Propulsion Laboratory.** *For further information, Circle 64 on the TSP Request Card.*
NPO-15041

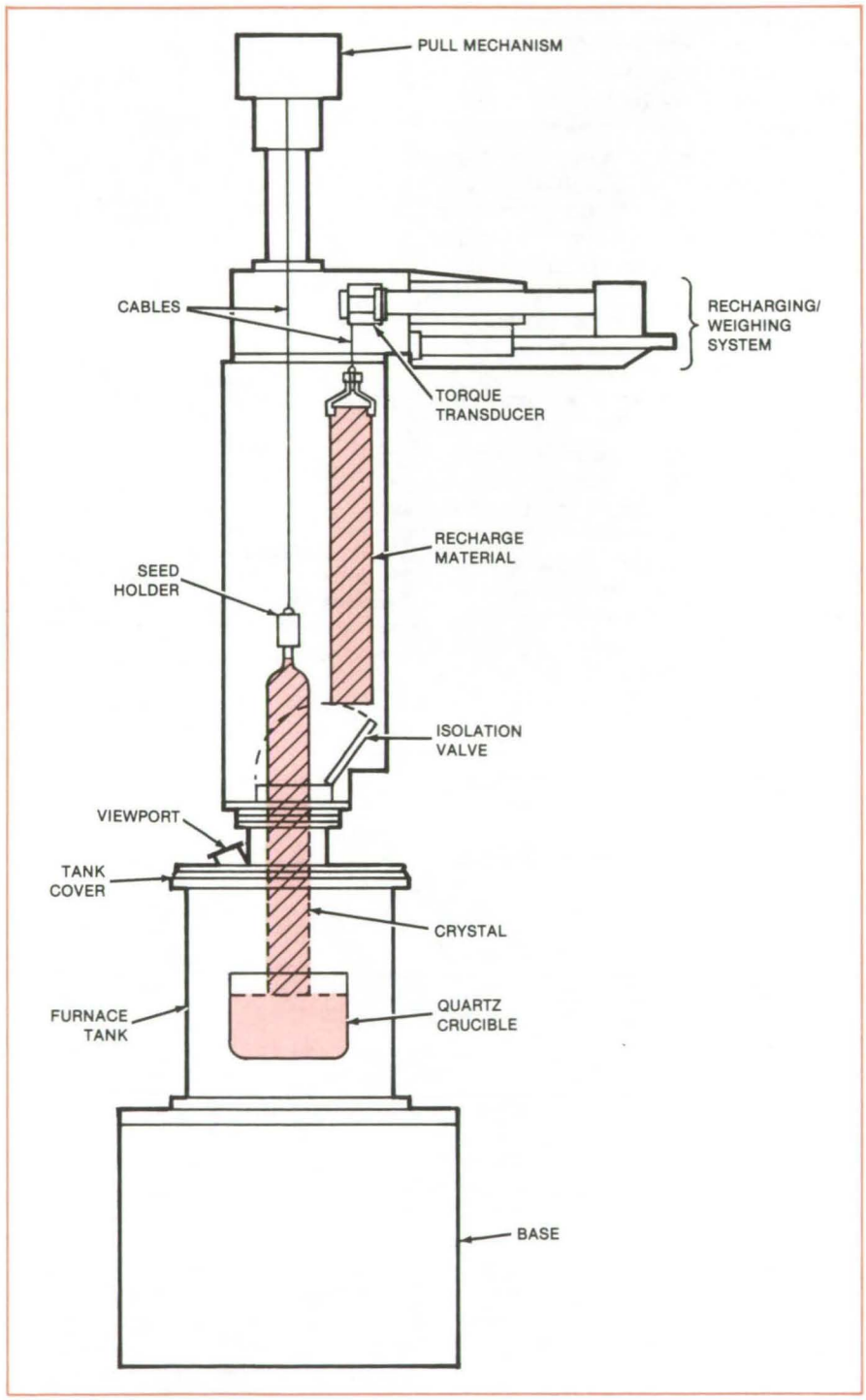

Czochralski Growth Facility, modified for continuous operation, is shown in the crystal-growth mode. The recharge material at the right will be moved in position over the crucible after the crystal has been grown and removed. An isolation valve keeps the air from contacting the hot crucible when the crystal is removed.

Controlling Thermal Gradients During Silicon Web Growth

A slotted susceptor helps keep the melt-replenishment region hot.

NASA's Jet Propulsion Laboratory, Pasadena, California

A strategically placed slot helps to control critical thermal gradients in a crucible for silicon web growth. The slot thermally isolates the feed region of the crucible from the growth region, so that the region where pellets are added stays hot.

Silicon ribbons for solar cells are grown continuously from a crucible inside an inductively heated susceptor [see "Crucible Grows Wide Silicon Ribbon" (NPO-14859) and "Improved Facility for Producing Silicon Web" (NPO-14860) in *NASA Tech Briefs*, Vol. 6, No. 1, Spring 1981, pages 91 and 93, respectively]. To maintain the supply of melted silicon in the crucible, pellets of silicon are fed in at one end. Unfortunately, the heat absorbed by the pellets during melting causes a thermal unbalance that can upset the growth conditions.

The slot is machined in the susceptor underneath the crucible, between the melt-replenishment and the growth compartments of the crucible. It does not extend all the way to the walls of the susceptor (see figure), so the inductive-heating currents are not interrupted; only the thermal conduction mode of heat transfer is interrupted. The slot size depends on the amount of temperature difference desired. Increased shielding at the melt-replenishment compartment requires a larger (i.e., wider or deeper) slot to keep the gradients essentially flat and symmetrical in the growth region.

Use of the slotted susceptor in several crystal-growth runs has confirmed the improved thermal geometry. This method of temperature-gradient control should be applicable to other types of crystal growth from the melt; for example, the Czochralski method.

This work was done by Charles S. Duncan, James P. McHugh, Marie E. Skutch, and Paul A. Piotrowski of Westinghouse Electric Corp. for **NASA's Jet Propulsion Laboratory.** *For further information, Circle 65 on the TSP Request Card.*
NPO-15337

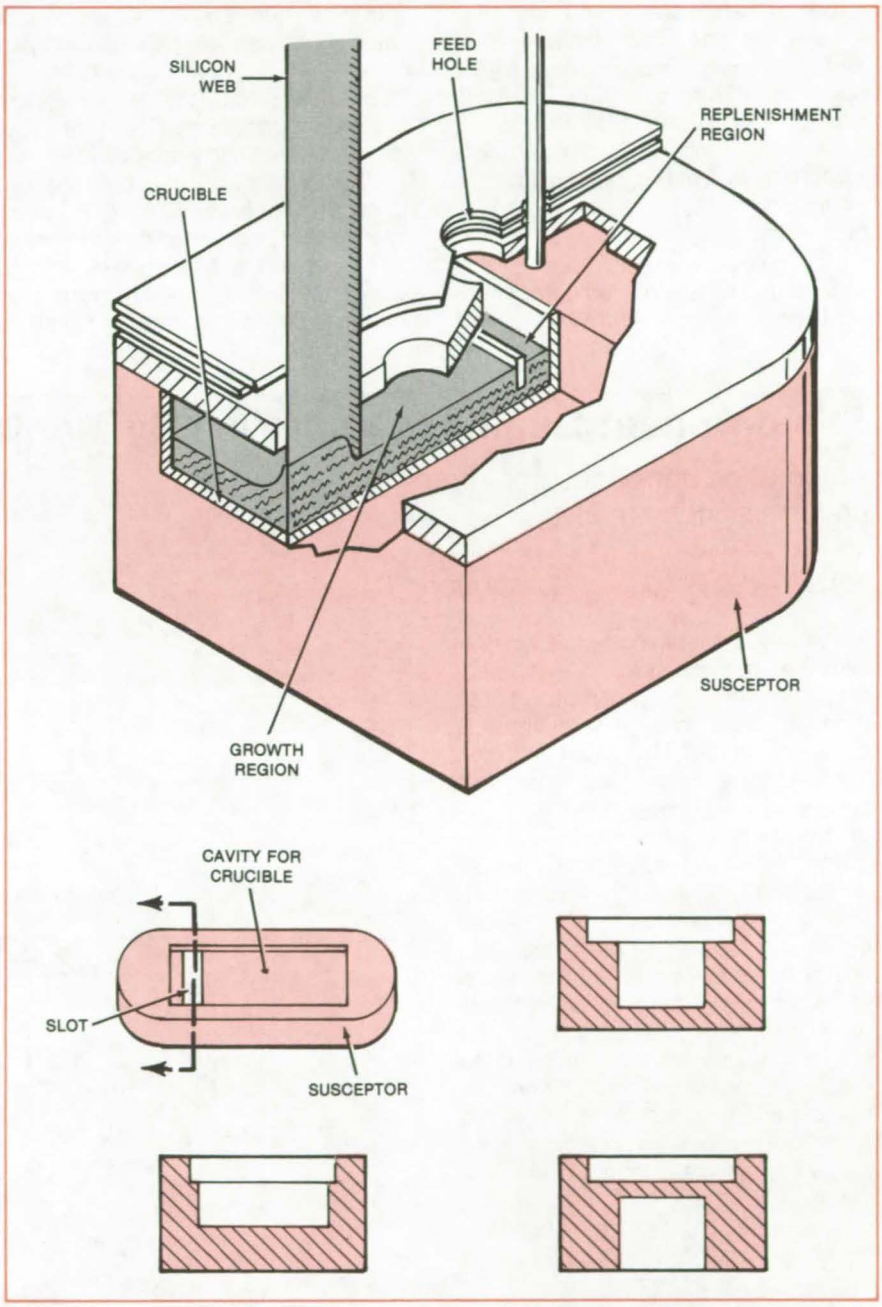

Cutaway Views show various shapes that the thermal-isolation slot may have in the susceptor. The slot permits inductive heating of both regions of the susceptor, but prevents thermal conduction between them.

Gettering Silicon Wafers with Phosphorus

Phosphorus absorbs impurities to improve the efficiency of solar cells.

NASA's Jet Propulsion Laboratory, Pasadena, California

Silicon wafers subjected to gettering in a phosphorus atmosphere have longer diffusion lengths and higher solar-cell efficiencies than untreated wafers. The gettering treatment improves the properties of solar cells manufactured from impure silicon and is compatible with standard solar-cell processing.

To remove impurities, the silicon wafers are immersed in an atmosphere containing phosphorus at 900° C for a half hour. After immersion, the surface layer containing the phosphorus dopant is removed from the wafers in the normal etching step that follows saw cutting the wafers from ingots. The wafers then are processed into solar cells.

The phosphorus treatment, when applied to solar-grade wafers, increases the minority-carrier diffusion length. Before gettering, typical values of diffusion length are 70 to 100 microns; after gettering, these values increase to about 120 to 150 microns. The corresponding solar-cell efficiencies for the two cases are 11.5 percent without the phosphorus treatment and 13.2 percent with the treatment.

This work was done by Robert V. D'Aiello of RCA Corp. for **NASA's Jet Propulsion Laboratory.** *For further information, Circle 66 on the TSP Request Card.*
NPO-15357

Silicon Sheet Quality is Improved By Meniscus Control

Automatic control ensures more uniform silicon sheets.

NASA's Jet Propulsion Laboratory, Pasadena, California

Better-quality silicon crystals for solar cells are possible with an instrument that monitors the position of the meniscus as a sheet of solid silicon is drawn from a melt. Using information on the meniscus height, the instrument generates a feedback signal to control the melt temperature.

The instrument is intended for use with the edge-defined film-fed growth technique in which molten silicon rises inside a graphite capillary die (see figure). When the silicon reaches the top of the capillary, it cools, solidifies, and is pulled away as a continuous sheet. The instrument observes the position of the meniscus between the silicon liquid/solid interface and the die edge. The height of the meniscus is determined by the pulling speed and the temperature of the melt at the growth interface. A change in height indicates a change in operating conditions that could affect the sheet cross section.

The position of the liquid/solid interface is sensed through the contrast in radiation reflected from the liquid and solid phases, the solid phase being more strongly reflective. A lens forms an image of the liquid/solid interface with a magnification of about 2. Located at the

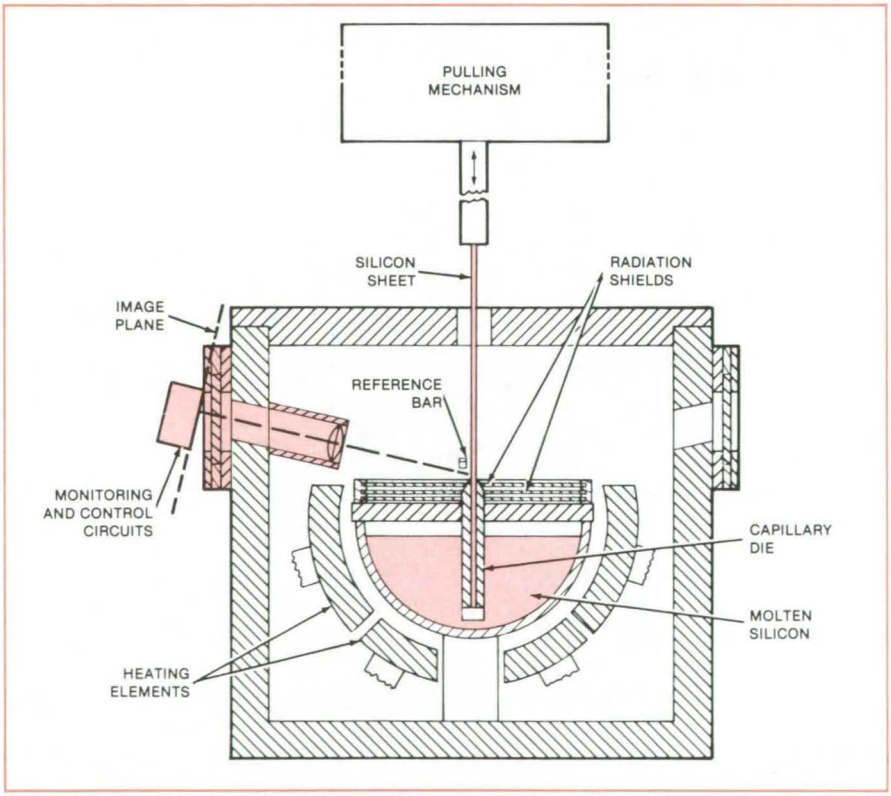

A Sheet of Solid Silicon is pulled at a constant rate from a capillary die as the melt temperature is adjusted by the monitoring and control unit. The adjustment maintains a nearly constant position of the liquid/solid interface at the top of the capillary.

image plane of the lens is a vertical linear array of light detectors sensitive to radiation at 0.5 micrometer, a wavelength at which silicon reflects strongly. The electrical output of each detector in the array is proportional to the intensity of the light impinging on it. The position of the detector having the greatest output therefore indicates the position of the solid side of the liquid/solid interface.

The monitoring and control unit adjacent to the detector array contains an analog shift register for storing the output values of the individual detectors. The register periodically releases its stored values to a comparator, which compares them with reference values that define the ideal position of the liquid/solid interface. If the interface is above or below its ideal position, the control unit increases or decreases the voltage to the heating elements, thereby raising or lowering the melt temperature and restoring the interface to its proper position.

The reference bar shown in the figure eliminates convection-current jitter — shifts in the image on the sensors caused by variations in the index of refraction of the hot vapor surrounding the liquid/solid interface. Any shift of the image of the interface caused by convection currents will produce an equal shift in the image of the edge of the reference bar. The control unit recognizes such simultaneous shifts as spurious and discounts them.

This work was done by Douglas A. Yates, Arthur E. Hatch, and Jeff M. Goldsmith of Mobil Tyco Solar Energy Corp. for **NASA's Jet Propulsion Laboratory.** *For further information, Circle 67 on the TSP Request Card.*
NPO-15384

Technique for Crystal-Ribbon Growth

Ribbon is formed by pulling nearly horizontally from a shallow melt.

NASA's Jet Propulsion Laboratory, Pasadena, California

In a proposal originated at NASA's Jet Propulsion Laboratory, a single-crystal ribbon of silicon or other material would be grown by pulling it at a low angle from a shallow melt. The thin monocrystalline ribbon would then be scored and broken into shapes required for the manufacture of such devices as solar cells. By pulling the crystal at a small angle, the technique prevents the overflow problem experienced with horizontal growth. It also creates a meniscus that minimizes growth defects in the main portion of the ribbon. The use of a shallow pool, prevents convection problems.

As the figure shows, there is a thermal stabilizer beneath the surface of the silicon melt to shape the temperature gradients in the melt, and there is a quartz wall with its top just flush with the surface of the melt. The temperature is adjusted so that a seed crystal placed on the surface of the liquid causes the surface liquid to solidify. The seed is then pulled at a slight angle over the edge of the wall, producing a raised meniscus behind the wall and between the ribbon and the surface of the molten silicon.

The shape of the ribbon is determined by the temperature gradients introduced by the stabilizer. The leading edge, where the crystal forms, is arc shaped; this shape directs imperfections toward the side edges. The thickness of the ribbon, like the width, is determined by the temperature gradients; but the thickness can also be varied slightly by varying the pulling speed.

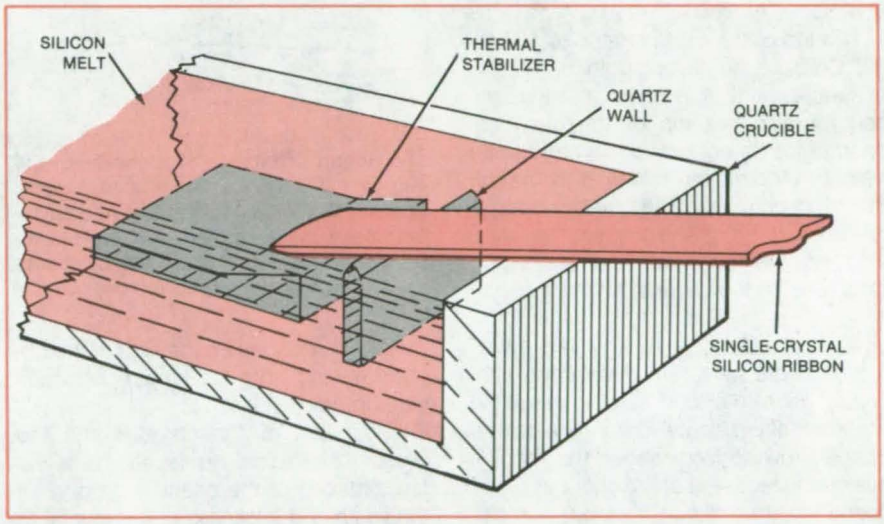

Single-Crystal Ribbon of silicon or other material can be grown from the melt by placing a seed crystal on the surface and then pulling it away at a slight angle from the horizontal. The bottom configuration in the crucible establishes temperature gradients that determine the shape of the ribbon.

This growth technique can be used to form ribbons of materials other than semiconductors. For example, sapphire ribbon for windows may be formed with this procedure and so can such bubble-memory materials as gallium, gadolinium, and garnet.

This work was done by David N. Jewett and Herbert E. Bates of Energy Materials Corp. for **NASA's Jet Propulsion Laboratory.** *For further information, Circle 68 on the TSP Request Card.*

Inquiries concerning rights for the commercial use of this invention should be addressed to the Patent Counsel, NASA Resident Office-JPL *[see page A5].* *Refer to NPO-15177.*

Asymmetric Die Grows Purer Silicon Ribbon

Graphite die distributes silicon carbide impurities asymmetrically.

NASA's Jet Propulsion Laboratory, Pasadena, California

The concentration of carbide impurities in silicon ribbon is reduced by growing the crystalline ribbon with a die that has one wall higher than the other. The height difference controls the shape of the meniscus at the liquid/crystal interface and concentrates the silicon carbide impurity near one of the broad faces. The opposite face is left with above-average purity. This significantly improves the efficiency of solar cells made from the ribbon.

The new die has several vertical capillaries that feed the molten silicon into a top channel. The top of the channel is beveled and cut back on one side (see figure), so that its two sides are of unequal heights.

The top of the die is heated to 10° to 30° C above the melting point of silicon. A seed crystal is lowered and kept in contact with the top of the die long enough for its bottom to melt and connect with the molten silicon at the top of the die channel. The metal has a relatively short meniscus on the high side of the channel and a longer meniscus on the lower side of the channel.

As the seed crystal is pulled away from the die at a rate consistent with crystal growth, silicon carbide particles preferentially migrate to the side of the ribbon growing from above the meniscus on the high side of the channel. Consequently, the silicon carbide particle density is reduced on the side of the ribbon growing from the longer meniscus side of the melt film.

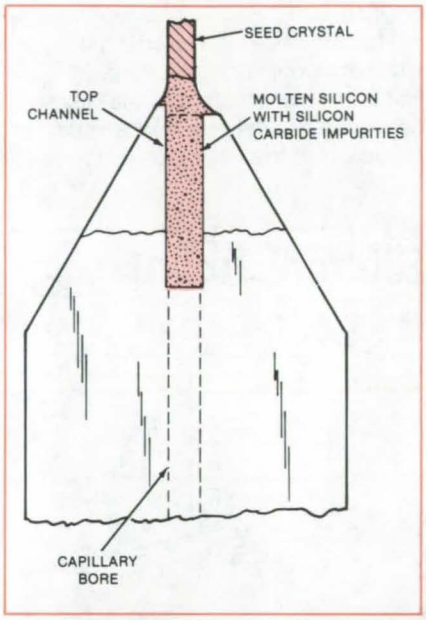

The **Height Difference** of the walls of the capillary die causes the silicon carbide impurity in the silicon to distribute asymmetrically in the grown ribbon. The impurities form when pure silicon reacts with the walls of the graphite capillary.

The width of the channel and the amount of vertical displacement of the top surfaces of the channel depend on the width and thickness of the crystal to be grown. To sustain the growth of silicon ribbons with widths up to 7.5 cm and thicknesses between 0.01 and 0.05 cm, the top surfaces of the die are displaced preferably by no more than 0.012 cm.

Ribbons made from the new capillary die have a substantial concentration of silicon carbide (1 to 10 particles per cm^2) on one side, while the opposite ribbon surface is virtually free of such particles and smooth in appearance. Solar cells made with the purer side as the junction side have efficiencies of between 9 and 10.6 percent. In contrast, solar cells made from the opposite side of the ribbon have efficiencies of less than 5 percent.

The same principle of displaced die-channel tops can be used in growing other crystalline materials where dissolved die materials precipitate in the grown crystal; for example, sapphire ribbons using molybdenum dies. Dies with displaced top surfaces also can be used for growing undoped silicon ribbon of other cross sections. Still another possible application of the die is for intentionally distributing impurities asymmetrically in the crystal.

This work was done by Juris P. Kalejs, Bruce Chalmers, and Thomas Surek of Mobil Tyco Solar Energy Corp. for **NASA's Jet Propulsion Laboratory.** *For further information, Circle 69 on the TSP Request Card.*
NPO-15385

Striped Electrodes for Solid-Electrolyte Cells

Gas flows freely between contact stripes.

NASA's Jet Propulsion Laboratory, Pasadena, California

Striped electrodes have been tested as a way of improving solid-electrolyte cell performance. The spaces between the contact stripes facilitate the flow of gases into and out of the electrolyte. [A wire-mesh electrode based on the same principle is described in "Integrated Solid-Electrolyte Construction" (NPO-15471), page 227, *NASA Tech Briefs*, Vol. 6, No. 2, Summer 1981.]

A striped electrode pattern is shown in the figure. The electrodes are made of platinum that is deposited as a thick film of ink or paste on the electrolyte surface and then fired. Typical solid electrolytes include sintered stabilized zirconia, doped alumina, or other ion conductors.

In previous designs, the platinum was deposited in a thin layer over the entire contact surface. The layer had to be sufficiently porous to allow gases to pass through. In practice, it has been difficult to achieve the required porosity, and the obstruction to gas flow by the platinum layer is responsible for most of the electrical resistance of the cell.

In cells with striped electrodes, the platinum is too thick to be porous. However, the spaces between the contact stripes remove the barrier to gas

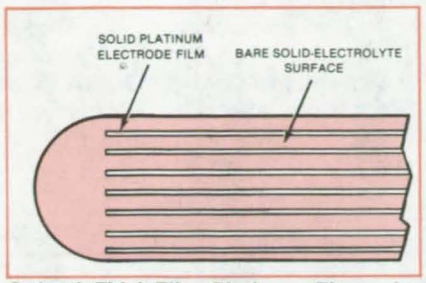

Striped Thick-Film Platinum Electrodes help to insure lower overall cell resistance by permitting the free flow of gases in the gaps between the stripes. The thick-film stripes are also easier to fabricate than porous thin-film electrodes that cover the entire surface.

flow across the electrolyte/atmosphere interface. The failure to cover the entire surface with electrode material does not significantly degrade cell performance as long as the electrode gaps do not exceed the ion conduction thickness of about 1 mm.

The additional electrode thickness also lowers the electrical resistance of the electrodes themselves, which contribute a large part of the total cell resistance. Possible applications for the improved cells include oxygen production from carbon dioxide, the extraction of oxygen from air, small fluidic pumping, sewage treatment, and fuel cells.

This work was done by Robert Richter of Caltech for **NASA's Jet Propulsion Laboratory.** *For further information, Circle 70 on the TSP Request Card.*

This invention has been patented by NASA [U.S. Patent No. 4,331,742]. Inquiries concerning nonexclusive or exclusive license for its commercial development should be addressed to the Patent Counsel, NASA Resident Office-JPL [see page A5]. Refer to NPO-15269.

Carbon Cloth Supports Catalytic Electrodes

New design requires less catalyst.

NASA's Jet Propulsion Laboratory, Pasadena, California

Carbon cloth is the starting material for promising new catalytic electrodes. Originally developed for a sulfur-cycle hydrogen process, the carbon-cloth electrodes are more efficient than the sintered-carbon configuration previously used. They are also chemically stable and require less catalyst — an important economic advantage when the catalyst is a noble metal such as platinum.

In the sulfur-cycle process, the carbon-cloth-supported electrode is the anode, or "electrolyzer." Sulfur dioxide is oxidized electrochemically in water, producing sulfuric acid at the anode. Hydrogen gas is removed at the cathode. The sulfuric acid is continuously drawn off and concentrated, then catalytically reduced at 870° C to produce water, sulfur dioxide, and oxygen. The sulfur dioxide is recycled into the hydrogen-generating reaction.

A comparison of a cell containing a carbon-cloth-supported anode with a conventional one (that is, one composed of pressed carbon powder, catalyst, and binder) demonstrated the better stability and efficiency of the new electrode. The voltage of the conventional cell rose steadily, while that of the carbon-cloth-supported cell remained nearly constant (see figure).

Other tests showed that the catalyst content is not critical. For example, an electrode containing about 7 mg/cm^2 of platinum performs just as well as one containing 12 mg/cm^2.

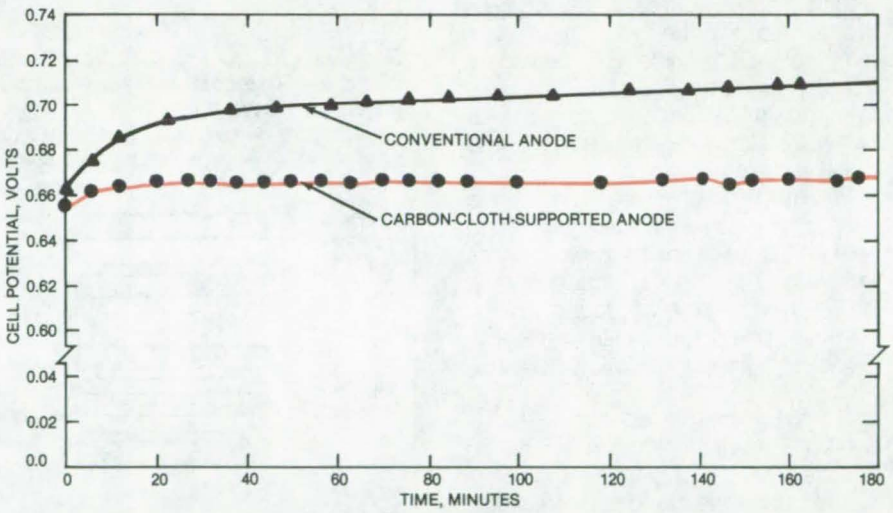

These **Two Curves** are for elecrolyzers operated at a constant current density of 100 mA/cm^2 in 50 weight percent sulfuric acid. After 2½ hours, the cell voltage of the more-efficient carbon-cloth-electrode cell is 40 mV less than that of the conventional cell.

The first step in the fabrication of an electrode is degreasing in acetone a piece of commercial carbon cloth measuring 5 by 5 cm and cleaning it ultrasonically in distilled water. The cloth is 0.08 cm thick and has a flexural strength of 330 MPa.

Next, 0.55 g of platinum-catalyzed carbon powder is mixed with 20 ml of distilled water. The catalyzed carbon contains 10 percent by weight of platinum particles, 80 percent of which are smaller than 80 μm. To the carbon suspension is added a binder solution composed of 60 weight percent of polytetrafluoroethylene (PTFE) in distilled water.

The carbon cloth, while it is still wet, is placed on a perforated stainless-steel plate. Supported in a special fixture, the underside of the perforated plate is exposed to a cavity connected to a vacuum pump. The carbon/PTFE suspension is spread over the cloth and allowed to filter through it as the vacuum pump provides a pressure differential of about 1 mm of mercury. Meanwhile the cloth and its newly-applied carbon layer are heated by an infrared lamp for about an hour.

(continued on next page)

Compression and sintering are the final fabrication steps. The carbon-impregnated carbon cloth is transferred to a die where it is pressed between Teflon (or equivalent) sheets at a pressure of 15 to 30 MPa. The cloth is sintered at 320° C for 2 hours in a hydrogen atmosphere. (Oxides such as platinum oxide can also be used as the catalyst, but must be sintered in a nitrogen atmosphere.)

The product is a flexible electrode having a 0.03- to 0.05-cm layer of catalyzed carbon on the cloth substrate. It contains 20 to 23 weight percent of PTFE binder and about 2 mg/cm^2 of platinum.

This work was done by Wen-Tong P. Lu and Robert L. Ammon of Westinghouse Electric Corp. for **NASA's Jet Propulsion Laboratory.** *For further information, Circle 71 on the TSP Request Card.*
NPO-15268

Laminating Polyimide Films

New processes yield void-free flexible laminates.

Langley Research Center, Hampton, Virginia

A new process for laminating large areas of high-temperature polyimide film has applications in vehicle construction and in preparing flexible printed circuits. Linear polyimides are excellent candidates for such applications because of their high thermal stability at temperatures between 477 K (400° F) and 589 K (600° F), their flexibility, and their light weight. The objectives of the process are to improve the bonding of high-temperature polyimide film, to prepare flexible, large-area, void-free laminates from polyimide film, and to laminate polyimide film not only to itself but to metal surfaces.

Polyimide adhesive (see Figure 1) was used to bond Kapton® H polyimide film to itself and to metal sheets in two process variations. The first variation (Figure 2, left) involves the following four steps:

1. Priming one polyimide film with a thin coat of a linear polyamic acid adhesive solution,
2. B-staging the primed film to 493 K (428° F) in air for 1 hour to remove excess solvent and to convert the polyamic acid adhesive to the more stable polyimide,
3. Thermoplastically bonding the B-staged film to another sheet of primed or unprimed film in a steel mold at 616 K (650° F) for 5 minutes under 50 to 300 psi (3 to 20 MPa) pressure, and
4. Cooling the polyimide film laminate under pressure before removing from the mold.

The resulting laminate is clear yellow, extremely flexible, and 100 percent void-free. Attempts at peeling the laminate cause the film itself to fail.

The second variation (Figure 2, right) involves the following five steps:

1. Fabricating a thin film of the polyamic acid adhesive by casting the solution on a flat surface,

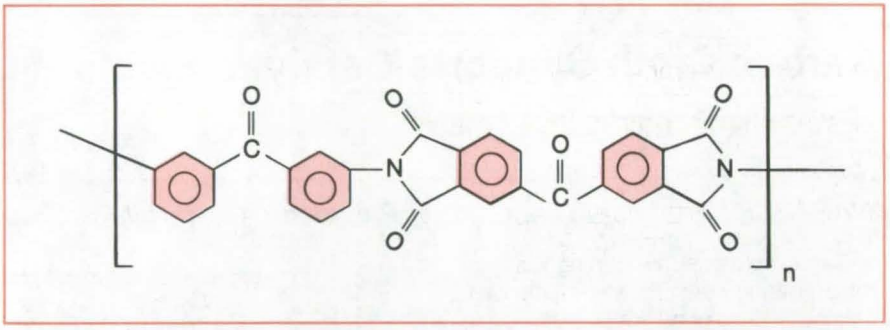

Figure 1. A **Thermoplastic Polyimide Adhesive** is used to bond polyimide sheets into flexible laminates.

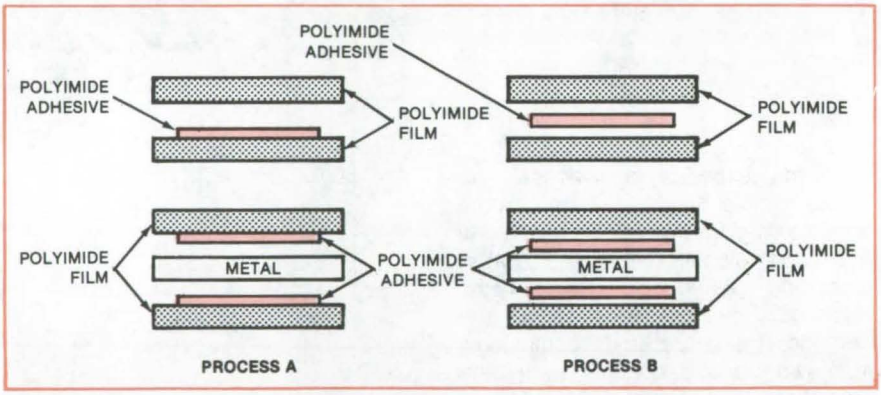

Figure 2. **Processes for Laminating Polyimide Films** with each other or with metal are shown here. In process A, the films are first primed with polyimide adhesive, then bonded together under heat and pressure. The adhesive is cast on a separate surface in process B, then sandwiched between the polyimide and/or metal films for final assembly.

2. Thermally imidizing the polyamic acid adhesive film to the polyimide by heating in air to 493 K (428° F) for an hour,
3. Stripping the adhesive film from the casting surface and placing it between two sheets of polyimide film,
4. Placing the sandwich in a steel mold and thermoplastically laminating as before, and
5. Cooling under pressure.

Ultimate success in obtaining a void-free laminate depends on the complete removal of excess solvent and the thermal conversion of the polyamic acid adhesive to the polyimide prior to laminating. Bumping (the release of pressure followed by a reapplication of the same pressure), often used to allow the escape of excess volatiles in lamination, proved to be unnecessary in this process for the preparation of void-free laminates. Preheated platens were used for successful laminations at pressures of 50 psi, 150 psi, and 300 psi.

Success in obtaining a well-consolidated laminate depends on attaining an even distribution of pressure. The use of several layers of release cloth or woven glass fabric between the laminate and the steel mold did much to distribute the pressure evenly on the laminate.

The two variations for laminating polyimide film may also be used to prepare metal-containing laminates, as shown in Figure 2. Aluminum, brass, copper, and stainless steel have been successfully laminated to polyimide film using this process. Other metals or metal-coated film may also be used; the metals need only to be degreased with a solvent, such as ethanol or methylethylketone, prior to laminating, although a more-strenuous surface preparation may be used if desired.

(Kapton ® is a registered trademark of E. I. du Pont de Nemours & Co., Inc.)

This work was done by Anne K. St. Clair, Terry L. St. Clair, and Philip D. Robinson of **Langley Research Center.** *For further information, Circle 72 on the TSP Request Card.*

Inquiries concerning rights for the commercial use of this invention should be addressed to the Patent Counsel, Langley Research Center [see page A5]. Refer to LAR-12742.

Repairing Voids and Delaminations in Composite Materials

Proposed tool forces adhesive into cracks.

Lyndon B. Johnson Space Center, Houston, Texas

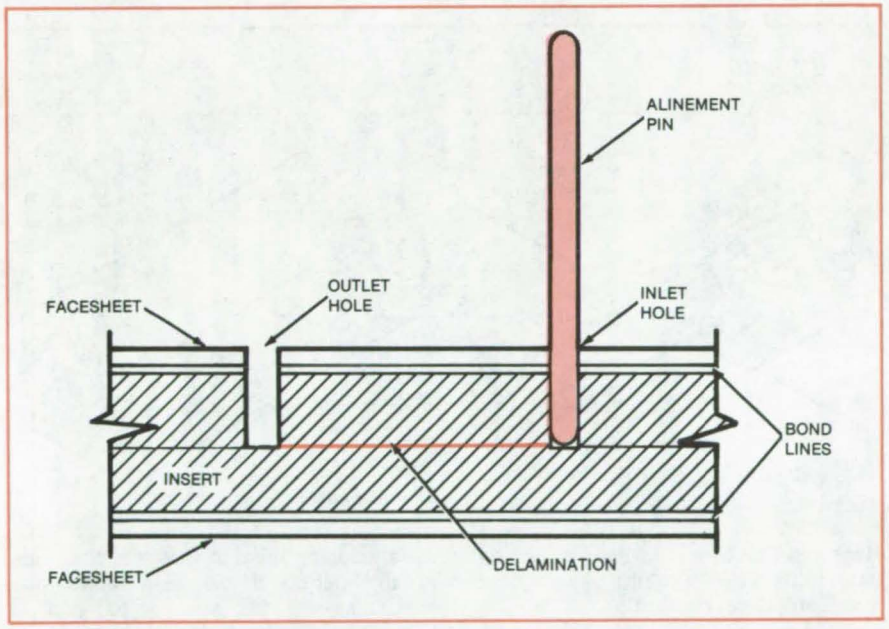

Figure 1. After **Inlet and Outlet Holes Have Been Drilled** to the proper depth, an alinement pin is inserted in the inlet hole.

A proposed method for repairing voids and delaminations in graphite/epoxy composite materials is based on the injection of an adhesive under pressure. A hole is drilled in the material to the depth of the void or delamination, and adhesive is forced through the hole into the material. The adhesive fills a void (a gap resulting from the absence of bonding material) or is forced into a delamination (a crack between unbonded layers of laminate), expanding the delamination slightly to ensure full penetration.

Previously, a syringe was used to inject adhesive. However, the poor seal between the syringe needle and the laminate prevented pressure from building up enough to ensure full penetration. A vacuum line has been attached to the outlet hole to aid adhesive penetration: This procedure has been moderately successful in filling voids but self-defeating with delaminations since the vacuum tends to force unbonded surfaces together and thus impedes penetration.

In the new method, the location of the void or delamination is first determined from X-ray photographs. Two No. 50 holes are drilled into the discontinuity at its extremities. When air can be passed from one hole to the other, the holes have been drilled to the proper depth. An alinement pin is inserted in one of the

(continued on next page)

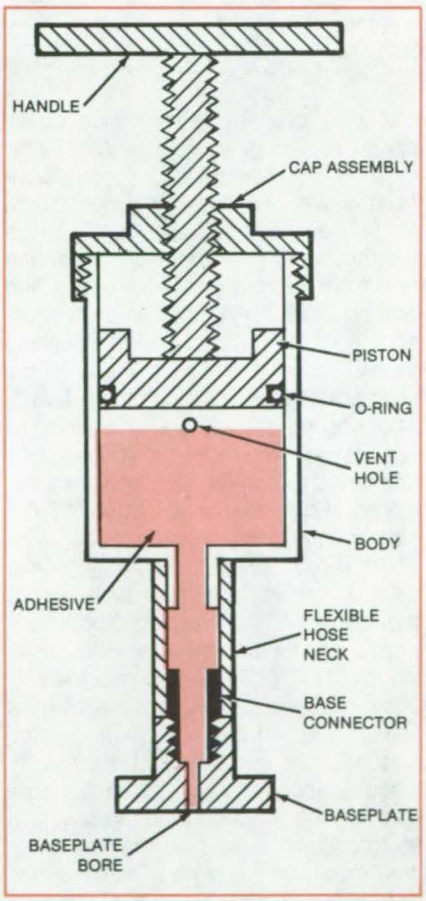

Figure 2. The **Injection Repair Tool** consists of three main sections: baseplate, body, and piston/handle/cap assembly. The sections are separable.

holes (Figure 1). Contact cement is applied to the facesheet of the laminate around the alinement pin and to the bottom surface of an injection repair tool (Figure 2). The baseplate is slipped over the pin and pressed against the facesheet so that the plate and sheet adhere, and then the pin is removed. (The alinement pin prevents contact cement from entering the injection hole and ensures that the baseplate bore and injection hole are alined.)

The body of the injection tool, less the piston, handle, and cap assembly, is threaded onto the baseplate; and the body is filled with adhesive up to its venthole. The piston, handle, and cap assembly are then attached to the body. The handle is turned so that it forces the piston downward and displaces air from the body through the vent. As the handle is rotated farther, it forces adhesive through the baseplate, into the delamination or void, and out the outlet hole. The repair is then complete.

The tool is removed and cleaned with solvent so that it is ready for reuse. The baseplate is pried away from the facesheet with a putty knife.

The proposed repair method is not limited to graphite/epoxy composites. It has potential applications in the repair of fiber-reinforced plastic structures, such as aircraft components, boats, storage tanks, and some automobile bodies.

This work was done by David D. Ott of McDonnell Douglas Corp. for **Johnson Space Center.** *For further information, Circle 73 on the TSP Request Card.*

Inquiries concerning rights for the commercial use of this invention should be addressed to the Patent Counsel, Johnson Space Center [see page A5]. *Refer to MSC-20131.*

Solventless Fabrication of Reinforced Composites

Heat and pressure convert a fiber bundle into a fiber-reinforced composite.

Langley Research Center, Hampton, Virginia

A new processing technique developed at Langley Research Center creates fiber-reinforced composites from solvent-resistant thermoplastics. In the new method, solid fibers of the thermoplastic and fibers of reinforcing agent are intimately mixed, heated, and compressed. The combination of pressure and temperature melts the thermoplastic, causing it to flow and fill the spaces between the reinforcing fibers. After cooling, the composite has properties similar to those of composites fabricated by conventional solvent processing. It can be machined, wound into filaments, and woven into fabric.

Fiber-reinforced composites are usually formed by first dissolving the thermoplastic. Reinforcing fibers are added, and the solvent is removed, leaving behind a finished composite. In some cases, however, small residues of solvent are left behind, creating voids and possible delaminations in the finished composite. For some thermoplastics, the required ratio of solvent to thermoplastic is so high that the process must be repeated many times before a sufficient amount of thermoplastic accumulates around the fiber reinforcement. Other thermoplastics are very solvent-resistant and cannot be processed at all.

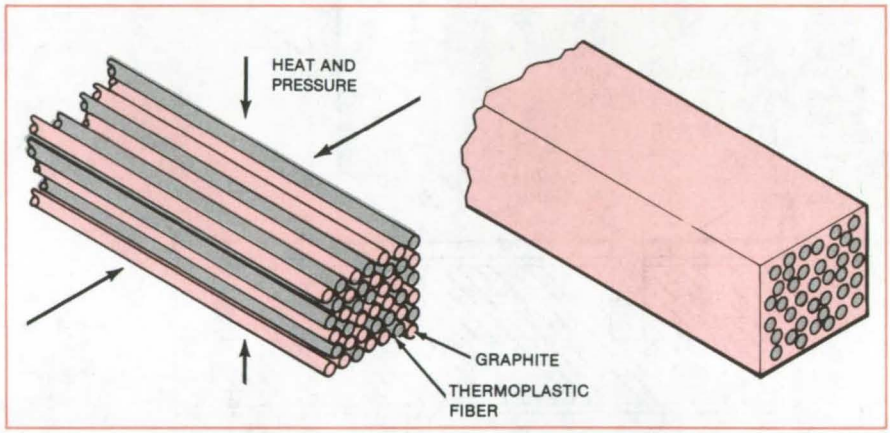

Heat and Pressure melt the thermoplastic fibers, causing them to flow into the voids around the graphite reinforcement. On cooling, the fiber bundle has been transformed into a structural composite.

The figure shows the new process schematically. Fibers of thermoplastic are mixed with fibers of reinforcing fiber (typically graphite). The two fibers have approximately the same diameter. Heat and pressure are applied simultaneously, causing the thermoplastic fiber to melt. Upon cooling, the fibers fuse into a continuous matrix. The required temperature and pressure depend on the properties of the particular thermoplastic used.

This work was done by Robert M. Baucom of **Langley Research Center.** *No further documentation is available. LAR-12856*

Solar-Cell Encapsulation by One-Step Lamination

Prefabricated covers are brought together with interconnected solar cells and cured in a single step.

NASA's Jet Propulsion Laboratory, Pasadena, California

A simple method of potting solar cells reduces encapsulating the cells to a one-step lamination process. The simplified process should save time and expense.

Two arrangements for solar-cell encapsulation are shown in the figure. In either arrangement, the interconnected solar cells are attached to one of the covers, either top or bottom, by an adhesive. In the one-step lamination process, potting material is applied over the solar cells and over the opposite cover. The two prefabricated components then are brought together, and the laminated assembly is cured in a single step.

Several different materials can be used for the assembly components depending on which cover receives the adhesive that initially holds the solar cells. Among the choices for potting material are polyvinyl butyral, ethylene vinyl acetate copolymers, and ethylene propylene rubbers. If the bottom cover receives the adhesive, then the top cover can be Korad (or equivalent) stabilized acrylic films or Tedlar (or equivalent) stabilized fluorocarbon polymers, and the bottom cover would be wood, metal, or reinforced-cement panels. If the top cover receives the adhesive (transparent), examples of materials for the bottom cover include stabilized acrylic/steel foil/stabilized acrylic, polyester/steel foil/stabilized acrylic, and polyvinyl chloride/aluminum foil/polyvinyl chloride; and the top cover would be glass.

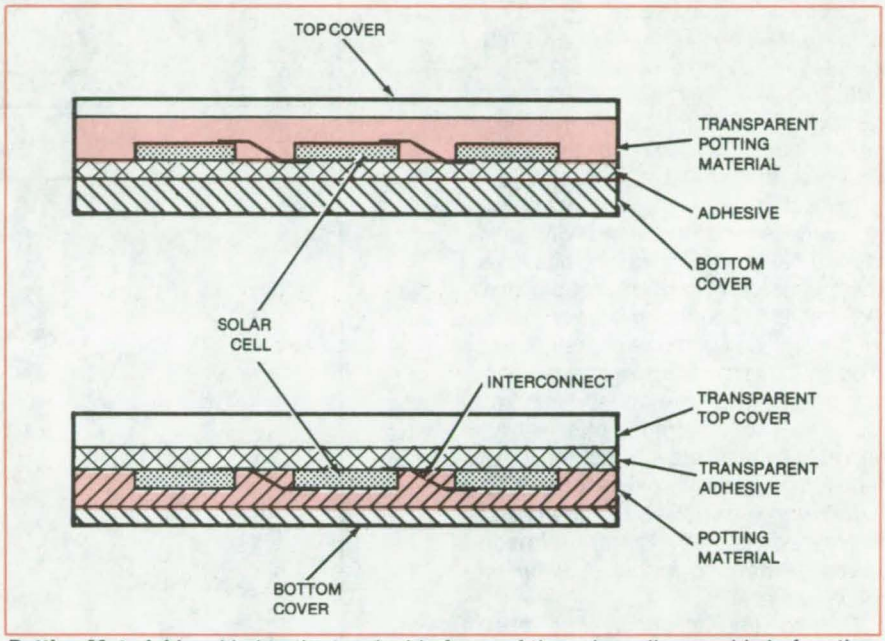

Potting Material is added to the two inside faces of the solar-cell assembly before they are sandwiched and cured. Two different assembly configurations are shown.

This work was done by Mohammad N. Sarbolouki of Caltech for **NASA's Jet Propulsion Laboratory.** *For further information, Circle 74 on the TSP Request Card.*
NPO-15222

Improved Photosensor for Light Valves

Innovations in processing optimize the CdS layer for good sensitivity and low negative memory.

Lyndon B. Johnson Space Center, Houston, Texas

Processing changes have improved the performance of a liquid-crystal light valve for displaying projection TV images. Before the changes were made, the display had an undershoot when it changed from high intensity to low (see figure). The effect occurred because a negative form of the previous image was superimposed on the new image for awhile; this negative memory phenomenon is associated with the cadmium sulfide (CdS) photosensor layer in the light valve. (The recombination rate of trapped holes exceeded the detrapping rate of electrons from shallow energy levels.)

It was discovered empirically that the negative memory in the light valve could be reduced to an acceptable level by

(continued on next page)

nitrogen doping of the CdS during sputter deposition, controlling the substrate temperature carefully during deposition, and annealing the deposited film in an argon atmosphere.

The approach taken was to monitor the performance of the finished light valves for given changes in the CdS process and experimentally to optimize the process for good sensitivity and low negative memory. The measure of sensitivity was the ratio of current amplitudes for various light inputs, relative to the dark signal. For 100 $\mu W/cm^2$ imaging light input, this ratio is typically somewhat greater than 2.0.

To hold the negative memory below 10 seconds and the sensitivity ratio above 2.5, the nitrogen doping had to be about 40 percent and the substrate level held at 140° C during deposition. Without the N_2 doping, the temperature had to be 150° C or higher to achieve a sensitivity ratio of 2. The doped films had such a dramatic increase of sensitivity with annealing, however, that the lower deposition temperature was feasible.

This work was done by N. John Koda of Hughes Aircraft Co. for **Johnson Space Center.** *No further documentation is available.*

Title to this invention has been waived under the provisions of the National Aeronautics and Space Act [42 U.S.C. 2457(f)], to the Hughes Aircraft Company, P.O. Box 90515, Los Angeles, CA 90009.
MSC-20036

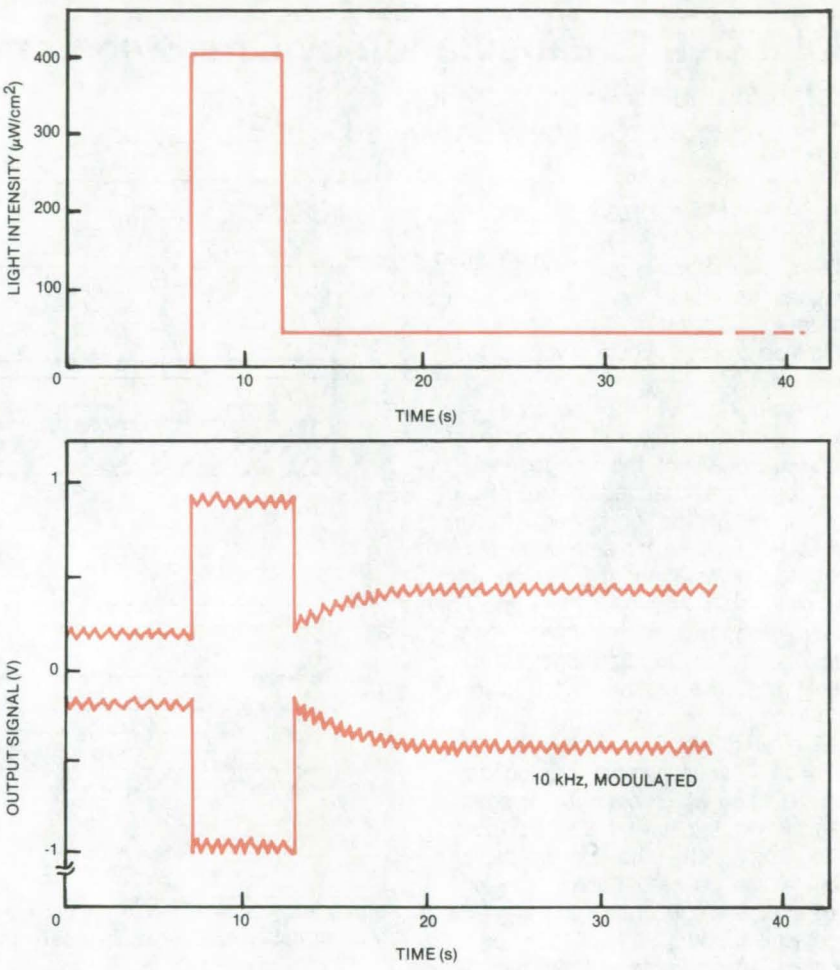

Negative Memory in a light valve is an undershoot of the output-signal envelope when the light level decreases abruptly.

Ampoule With Integral Feedthroughs

A vacuum-tight ampoule is used for crystal growth by the Bridgman method.

Langley Research Center, Hampton, Virginia

The key feature of a new crystal-growth ampoule is a molybdenum-to-quartz vacuum feedthrough that can be assembled in the laboratory. One feedthrough is attached to each end of the cylindrical ampoule, used for crystal growth by the Bridgman method, allowing interface demarcation by passing periodic current pulses through the sample during growth. The new ampoule is also vacuum-tight, so that it protects exposed areas of the furnace from corrosive vapors emanating from the sample and at the same time prevents changes in composition of the melt due to preferential vaporization of one of its components.

To form the molybdenum/quartz feedthrough (see figure), a quartz tube is sealed to a quartz capillary. As gas flows through the capillary, the walls of the quartz tube are thickened, making sure that there is still room in the thickened region for a molybdenum foil to be inserted and that the diameter of the rest of the tube is large enough for another piece of capillary to be placed inside.

A piece of molybdenum foil with a wire spot-welded to each end is inserted into the tube such that the wire feeds through each capillary up to the spot weld and the foil is surrounded by the thickened quartz wall. A seal is made at the open end of the quartz tube. This assembly is then mounted on a lathe and is attached to a vacuum system, which pumps through the capillary.

The quartz tube is collapsed onto the foil from the center out to the spot weld on each end. Another seal is made along the length of the capillary, and the excess tubing is cut off and discarded.

One feedthrough is sealed under vacuum in the end of the quartz ampoule. A press fit is made between the

wire and either a piece of oriented semiconductor (for seeded growth) or a piece of graphite with a cone cut in the end toward the semiconductor melt.

Another feedthrough with a conical piece of graphite attached to the wire is mounted in the vacuum system so that it can be lowered and positioned in the ampoule. The ampoule is then mounted on the vacuum system and evacuated. The feedthrough is lowered until it makes contact with the semiconductor material, and the final vacuum seal is made.

The ampoule is mounted in the furnace, and connections are made to the wires to apply current pulses. The system is then ready for the Bridgman growth to proceed.

Crystals have been grown in the ampoule with the hot zone temperature as high as 1,150° C, the temperature gradient along the sample as high as 240° C/cm, and current pulses up to 40 A/cm^2. The configuration has been temperature-cycled from 25° to 1,000° C up to three times without the loss of vacuum or of electrical continuity.

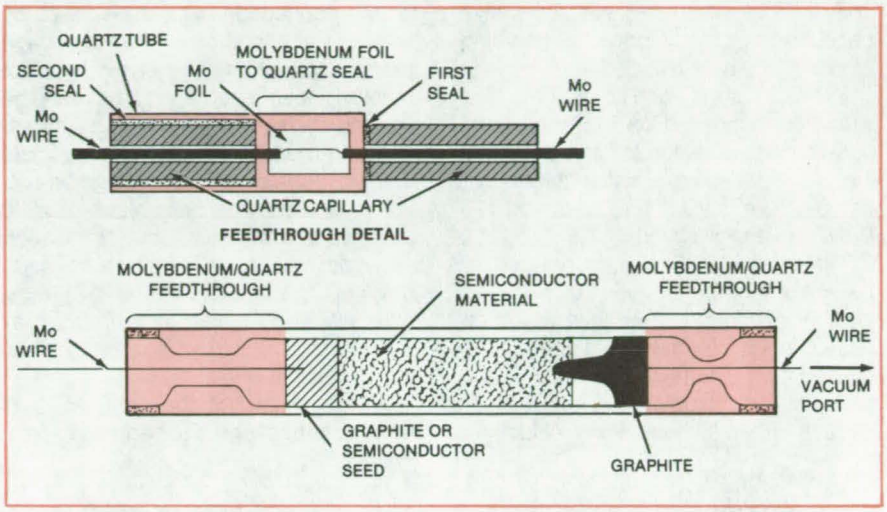

Bridgman-Growth Ampoule has molybdenum-to-quartz feedthroughs at both ends. The detail shows the feedthrough structure before the quartz tube has been collapsed onto the foil.

This work was done by Roger K. Crouch and W. J. Debnam of **Langley Research Center** *and R. Ryan of BOMCO, Inc. For further information, Circle 75 on the TSP Request Card.*
LAR-12899

Fabricating a Microcomputer on a Single Silicon Wafer

Proposed fabrication would reduce microcomputer packaging costs.

NASA's Jet Propulsion Laboratory, Pasadena, California

A concept for a "microcomputer on a slice" would reduce microcomputer costs by eliminating the scribing, wiring, and packaging of individual circuit chips. All components for a microcomputer — central processing unit, input/output circuitry, read-only memory, and random-access memory (CPU, I/O, ROM, and RAM) — would be placed on a single silicon wafer. The components would be interconnected by metal paths according to instructions from a computer. The slice would then be encapsulated as a single package of modest size.

Current practice, in contrast, is to build microcomputer circuits out of separately-packaged integrated circuits, or chips. One package contains the CPU, one the I/O, another the ROM, and others the RAM. The packages are interconnected externally on a printed-circuit board. Some commercial CPU chips do include a small amount of "scratch-pad" RAM and some ROM, however, these devices require additional memory to assemble a complete microcomputer.

Element	Unit Space	Number Required	Yield	Number Deposited	Total Spaces
CPU	2	1	20%	5	10
I/O	1	1	40%	3	3
ROM	1	2	40%	5	5
RAM	1	190	40%	475	475
					493

A **Low-Cost Microcomputer on a Silicon Slice** would contain redundant components. If the area of a RAM (of which about 510 can be placed on a 100-mm-diameter wafer) is regarded as a unit, the quantities shown in the table could be deposited. Each RAM has a storage capacity of 16,384 bits; thus at expected yield, the microcomputer would have a data capacity of 3,112,960 bits.

In manufacture of conventional integrated circuits, an entire slice of silicon is usually devoted to multiple replicas of a single component — all CPU's or all RAM's, for example. After the circuits have been deposited on a slice, they are scribed and broken into individual chips, which are wired to external leads and packaged.

In the new concept, microcomputers would be smaller because external wiring on circuit boards is unnecessary.

(continued on next page)

They would also be less expensive because the cost of individual handling of chips would be avoided.

Extra circuits of each component type would be deposited on the microcomputer slice to allow for possible defective circuits. For example, a slice might contain 5 CPU's, 3 I/O's, 5 ROM's, and 475 RAM's, even though only 1 CPU and I/O, 2 ROM's, and 190 RAM's are needed for the microcomputer (see table). The number of redundant circuits would be based on the expected yield of good circuits, which is largely a function of the area a circuit occupies on a chip. Larger circuits generally have lower yields.

Interconnections would be made by the usual method of exposure through masks. So that an excessive number of masks is not needed, elements would be located in regular geometric patterns. The interconnection computer would call up appropriate submasks from a library and automatically place them in position, and the entire interconnection network would be built up by a series of masking and deposition steps. The circuits would be tested and circuits that fail their tests would be isolated by blowing out fusible links.

Although the number of RAM's is large, connections to them and interconnections among them do not present a particularly difficult problem. A common data bus could be used, since the RAM's are addressable memories. As each RAM is tested, it is either disconnected or left connected, according to the test results. Once an adequate number of good RAM's has been found, the remainder may be disconnected whether they are good or bad to reduce power consumption.

This work was done by Vincent L. Evanchuk of Caltech for **NASA's Jet Propulsion Laboratory.** *For further information, Circle 76 on the TSP Request Card.*
NPO-15053

Electrolyte Reservoir Would Lengthen Cell Life

A proposed controlled-capillary sump would extend the life of sealed cells that depend on gas recombination.

Lewis Research Center, Cleveland, Ohio

Certain electrochemical cell types depend on the recombination of gases within them in order to insure long operating lives in the sealed condition without undue pressure buildup. Nickel/cadmium cells, in particular, depend on the recombination of oxygen that is generated on the nickel electrode during charge with cadmium metal in the presence of the potassium hydroxide electrolyte. This is generally accomplished by using separator materials (typically nonwoven nylon felts) that permit gases to cross from one electrode to the other and yet remain wetted with electrolyte so as to maintain good ionic conductivity between the electrodes. This property results from having the proper binodal pore size distribution within the wettable felt; that is, it contains some fine pores and some large pores. Due to the effects of cell aging or just the random aspects associated with the electrodes and separator materials going into any one cell, some electrodes can be kept with more than the desired amount of electrolyte while others can have too little.

It is suggested here that an electrolyte sump be placed within these cells below the assembly of anodes and cathodes to supply the proper amount of electrolyte during the course of operation. This sump cannot be simply free

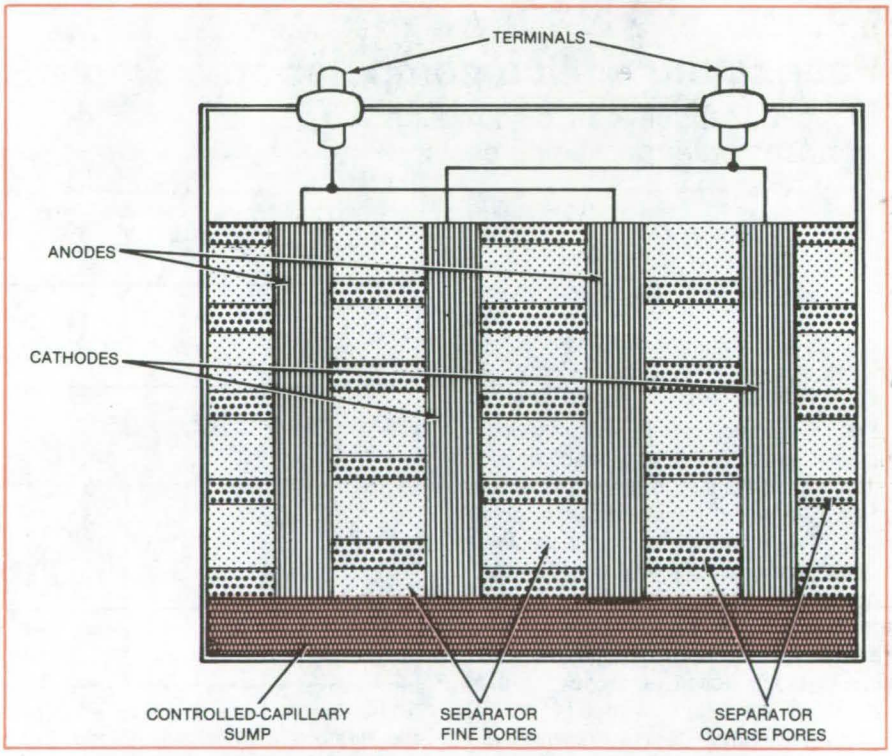

The **Controlled-Capillary Sump,** below the anode and cathode assembly, supplies the proper amount of electrolyte during cell operation. It releases the electrolyte to compensate for the electrolyte that empties from the electrodes and separators.

volume but must be of a capillarity intermediate between that of the fine pore portion of the separator and the coarse pore portion of the separator (see figure). In that way, as the fine pore portion of the separator or the pores of the electrodes begin to empty, the electrolyte within the controlled capillary sump would supply this amount and yet would not flood the large pore portion of the separator.

In cells where gaseous recombination is employed, fully flooded conditions are not desired since this would prohibit the free passage of oxygen gas from the nickel to the cadmium electrode. The term "starved" usually implies that there is a deficiency of electrolyte within the cell when the sums of all the porosities of all the cell components are considered. A certain free volume, devoid of electrolyte solution, is desired between the closely spaced electrodes. The fact that this portion of the cell that is devoid of electrolyte is in the separator results from a careful consideration of the pore size, capillarity, range of pore-size, etc. of each of the cell components.

The term "capillarity" is used to describe a component's tendency to retain electrolyte. When the capillarity of component A (C_A) is greater than that of component B (C_B), then the pores of component A will fill in preference to those of component B. Only when the pores of component A are filled will the pores of B begin to fill.

In a typical starved cell, the capillarity of the electrodes and of the separator need to be considered. Four capillarities can be considered. The separator has two separate capillarities: one for the small pores of the wettable filaments of the material used to make the felt and one for the large pores located between the bundles of filaments. In general, the capillarity for the fine pores of the separator should be greater than that of the two electrodes, and the capillarity of the two electrodes in turn should be greater than that of the large pore portion of the separator felt.

In this way, a cell can be loaded with electrolyte such that the pores of both electrodes, as well as the fine pore portion of the separator, are filled with electrolyte whereas the coarse pores of the separator are devoid of electrolyte and thus are permeable to gas. The ionic conduction between the electrodes thus permits electrochemical processes to proceed whereas the empty spaces within the large pores of the separator permit chemical recombination processes to take place.

A certain degree of electrolyte volume tolerance is displayed with this construction since the capillarity of the separator (highest) assures that there will be an electrolyte connection across the separator. Likewise, slight excesses are taken up in some of the large pores of the separator. The changes that occur within the electrodes during cycle life are such that there is a gradual tendency to require more electrolyte as the active material is repeatedly cycled. This process can slowly remove the electrolyte from the fine pores of the separator if the capillarity values are close to one another or the electrodes slowly become devoid of solution if this extra volume cannot be supplied by the separator. The life of certain cells of this type can be shortened if there is no way to provide for the increased demand for electrolyte volume.

This work was done by L. H. Thaller of **Lewis Research Center.** *No further documentation is available.*

Inquiries concerning rights for the commercial use of this invention should be addressed to the Patent Counsel, Lewis Research Center [see page A5]. *Refer to LEW-13788.*

Stable Polyurethane Coatings for Electronic Circuits

Alkane-based polyurethanes resist deterioration while maintaining good dielectric properties.

Marshall Space Flight Center, Alabama

Polyurethane coatings and encapsulation compounds based on alkanes instead of ethers have superior chemical, electrical, and mechanical properties. High temperature and humidity have little effect on the alkane-based polyurethanes. Water-vapor transmission rates through polyurethane film prepared from alkanes are low in comparison with those for ether-based material.

The alkane-based materials absorb little or no water when immersed in water at 160° F (71.1° C) and lose little weight when dried after immersion, whereas ether-based polyurethanes absorb water and swell in hot water and weigh significantly less than their original weight after drying (see figure).

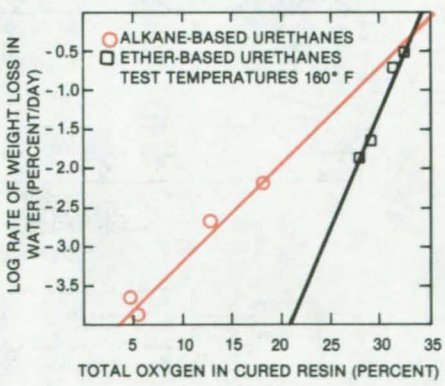

Weight Loss After Prolonged Immersion in hot water is far less for alkane-based polyurethanes than for the more-common ether-based polyurethanes, at any given oxygen content.

The alkane-based polyurethanes are prepared from polybutadiene polyols (which are sometimes used in place of ethers as a starting material in commercial resins). These types of polyurethanes were previously known to have excellent dielectric properties and to be hydrolytically stable. However, when polybutadiene-based polyurethanes are exposed to ozone under stress, they deteriorate because ozone attacks the double bond in the butadiene structure and severes the polymer chain. In alkane-based polyurethanes the double bond is removed from the polymer chain by hydrogenation of the polyol, and there is therefore no point of

(continued on next page)

attack for ozone. These urethanes are thus oxidatively stable as well as hydrolytically stable.

Major uses of polyurethanes are as connector potting materials and as conformal coatings for printed-circuit boards. An important requirement for such applications is good dielectric properties — in particular, low dielectric constant and dissipation factor. MSFC-SPEC-515, a specification for urethane molding and potting material, requires a dielectric constant of 5.0 or less and a maximum dissipation factor of 0.09. The dielectric properties of alkane-based polyurethanes are well within the specification and remain so after temperature, humidity, ozone, and immersion tests.

This work was done by Donald E. Morris of **Marshall Space Flight Center.** *For further information, Circle 77 on the TSP Request Card.*
MFS-25663

RF Sputtering of Gold Contacts on Niobium

Low-resistance contacts are stable down to 4.2 K.

NASA's Jet Propulsion Laboratory, Pasadena, California

Reliable gold contacts are deposited on niobium by a combination of RF sputtering and photolithography. The process results in structures that have gold only where desired for electrical contact. The contacts are stable under repeated cycling from room temperature to 4.2 K. They show a room-temperature contact resistance as much as 40 percent below that of indium contacts made by thermal-compression bonding.

The process consists of photolithography, gold sputtering, and metal lift-off. In the first step of the process (see figure), photoresist is applied to the niobium on the insulating substrate. Photolithography then opens windows in the photoresist, exposing the niobium to which contact is to be made. Next, the metal is RF sputtered to etch about 200 Å of the niobium surface. After this, the RF is applied to the gold target to sputter a 1,000-Å layer of gold over the niobium substrate.

Finally, the gold-coated structure is removed from the sputtering chamber and placed in a solvent for the photoresist. This removes the photoresist and lifts off the gold situated above it, leaving behind gold sputtered onto the niobium only in the regions where windows were originally opened in the photoresist.

This work was done by Daniel W. Barr of the University of Virginia for **NASA's Jet Propulsion Laboratory.** *For further information, Circle 78 on the TSP Request Card.*
NPO-15624

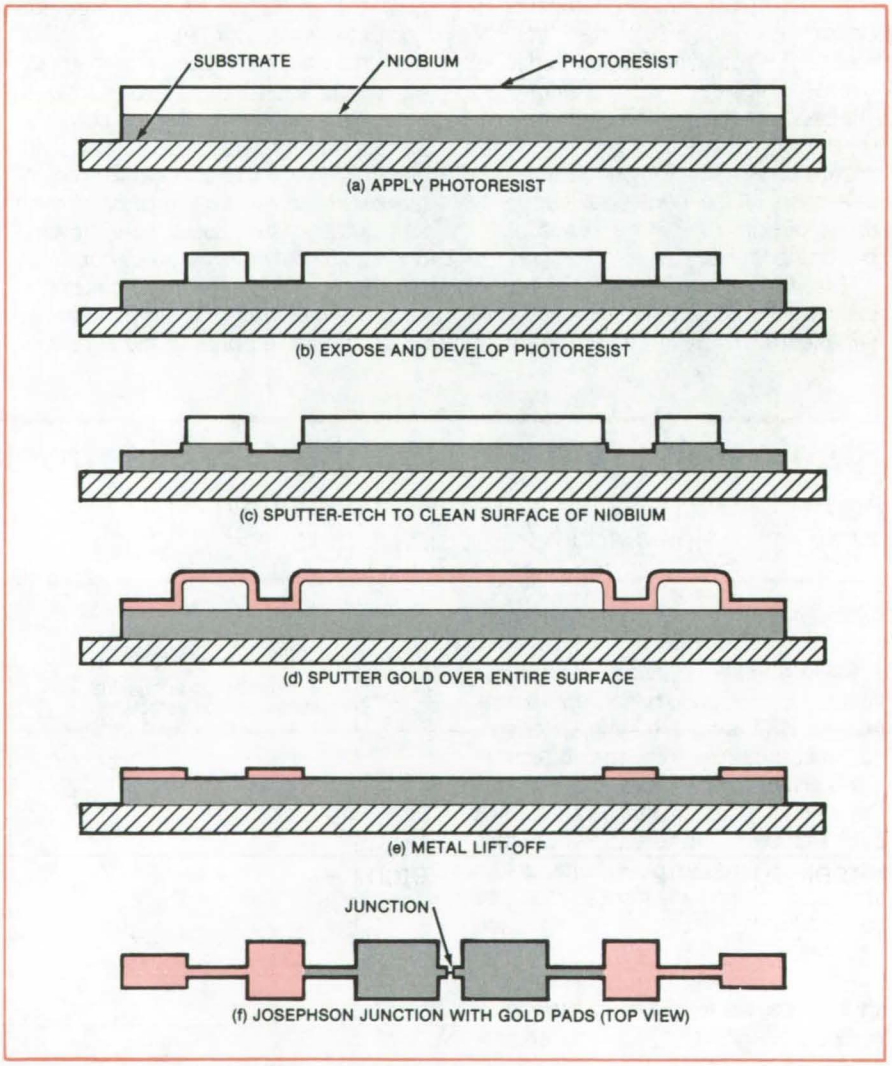

Gold Is Sputtered (d) over the entire surface after etching the unmasked niobium surface (c). The process was used to make contacts to a Josephson junction (f).

Mass Producing Targets for Nuclear Fusion

A metal-encapsulation technique would advance the prospects of controlling nuclear fusion.

NASA's Jet Propulsion Laboratory, Pasadena, California

A process tested in the laboratory could mass-produce targets for controlled nuclear fusion. Spherical capsules — the targets — are formed from molten metal and simultaneously filled with heavy isotopes of hydrogen that would serve as the nuclear fuel. Rapid solidification of the molten metal takes place while the targets are in free fall, promoting a spherical form.

Inertial-confinement fusion is one of the promising technologies for power generation in the future. A target, placed within a reactor, is imploded by an intense, focused burst of laser energy. The fuel is compressed to the high temperature and pressure needed for fusion to occur, releasing a large amount of energy. For power generation the process would be conducted with a high-repetition rate. Targets now undergoing testing are formed of glass, but newer designs employ metal shells. These are currently produced individually by the very costly method of micromachining.

In the new process, molten metal — tin, gold, or lead, for example — is forced through an axisymmetric nozzle that contains a center tube providing a flow of fill gas, which could be the fuel. The resultant hollow liquid jet spontaneously pinches off uniform lengths of the gas jet, encapsulating the fill gas. These quickly separate under free fall and become spherical before they completely freeze.

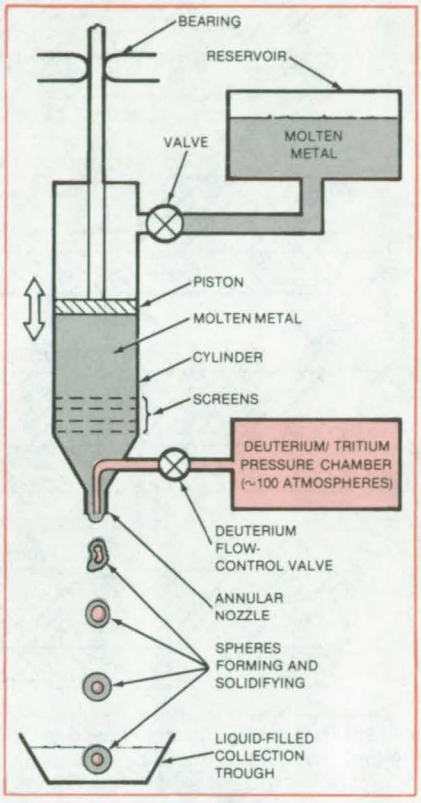

Prefilled Fusion Targets are formed at a nozzle as molten metal such as tin flows through its outer channel and pressurized deuterium/tritium gas flows through its inner channel. The molten metal completely encloses a gas charge as it drops off the nozzle.

The process is shown schematically in the figure. A piston forces the liquid metal through the annular orifice in a batch mode. The flow of fill gas is initiated simultaneously with the piston motion and proceeds at a rate commensurate with that of the liquid. The process of forming hollow shells is then continuous during the batch, with shells being formed at a rate of a few tens to a few thousands per second, depending upon the size being produced. In tests at atmospheric pressure, shells ranging between 0.7 and 7.0 mm in diameter have been produced. By placing the apparatus within a pressure vessel, it would be possible to produce targets filled to an internal pressure exceeding 2,000 lb/in.^{2} (1.4×10^7 N/m^2).

This work was done by Taylor G. Wang, Daniel D. Elleman, and James M. Kendall, Jr., of Caltech for **NASA's Jet Propulsion Laboratory.** *For further information, Circle 79 on the TSP Request Card.*

This invention has been patented by NASA [U.S. Patent No. 4,279,632]. Inquiries concerning nonexclusive or exclusive license for its commercial development should be addressed to the Patent Counsel, NASA Resident Office-JPL [see page A5]. Refer to NPO-15455.

Etching and Growth of GaAs

Precise temperature control adjusts melt composition before each etch.

NASA's Jet Propulsion Laboratory, Pasadena, California

A simple arrangement for etching away a surface layer of a gallium arsenide crystal before an epitaxial layer is deposited on it prevents an unwanted high-resistivity interface from forming. The etching and deposition setup is expected to simplify processing and improve the characteristics of gallium arsenide lasers, high-frequency amplifiers, and advanced integrated circuits.

Etching and deposition are carried out in a standard gallium arsenide liquid-phase epitaxial reactor. The arsenic source crystal and the gallium arsenide substrate crystal are held in separate slots in a graphite slider, under a graphite boat holding the etch melt and the growth melt (see figure).

The first step is to saturate the etch melt with arsenic at a temperature below the growth-melt saturation temperature. The slider is moved so that the source crystal is positioned under the etch melt at a temperature of 745° C for 1 hour — long enough to saturate the bottom of the gallium etch melt with arsenic.

Next, the slider is moved so that both the substrate and the source crystal are removed from the melts. The tem-

(continued on next page)

perature is raised 5° C, to 750° C, the growth-melt saturation temperature.

The substrate and source crystal are moved quickly under the etch melt so that only the source crystal is positioned under the growth melt. The source crystal saturates the growth melt with arsenic.

The furnace temperature is reduced to 748° C, but the etch melt is still 3° C above the temperature at which it was exposed to the arsenic source crystal and is therefore undersaturated by a precisely known amount. The substrate is moved under the undersaturated etch melt, which removes material from the substrate surface. The length of time the substrate is under the melt determines the depth of etch.

At the end of the etching period, the substrate is quickly moved under the growth melt. This melt, which was saturated by the source crystal at 750° C, is now supersaturated by 2° C and therefore deposits gallium arsenide on the substrate.

This work was done by Alan C. Seabaugh and Robert J. Mattauch of the University of Virginia for **NASA's Jet Propulsion Laboratory.** *For further information, Circle 80 on the TSP Request Card.*
NPO-15625

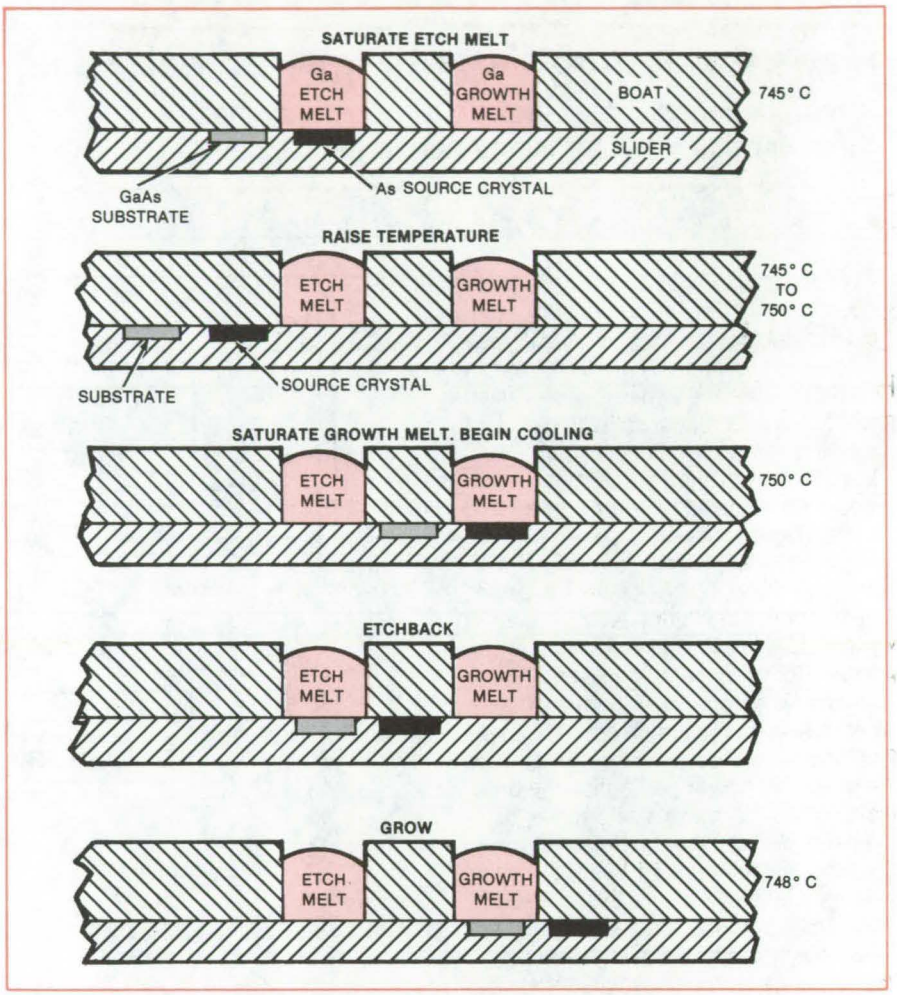

In-Place Process for the etching and growth of gallium arsenide calls for presaturation of the etch and growth melts by an arsenic source crystal. The procedure allows precise control of the thickness of the etch and of the newly grown layer on the substrate.

Recharging "Hot-Melt" Adhesive Film

Hot-melt adhesive charge is held in place by a one-sided tape.

Langley Research Center, Hampton, Virginia

A technique for recharging a surface with a "hot-melt" adhesive film makes use of a one-sided, high-temperature, pressure-sensitive adhesive tape. The technique was originally developed for use in space, where the absence of gravity can cause the adhesive charge to "float" away, due to the lack of tack.

The primary purpose of the one-sided tape is to hold the hot-melt charge in place until it is fused to the surface. After the adhesive has fused to the surface and has been cooled, the tape is removed, leaving the adhesive on the surface.

The technique will be used to recharge the surface-attachment assembly (SAA) pads of the work-restraint unit (WRU) of the Shuttle orbiter. The SAA pads utilize a high-temperature hot-melt adhesive for attachment to the surface-insulation tiles of the orbiter.

Since the adhesive is depleted from the surface of the pads after successive attachments and detachments, a way of recharging the adhesive is needed. The one-sided-tape technique satisfies this need, allowing an astronaut to recharge the adhesive on the pads and increasing the number of possible pad attachments and detachments.

The hot-melt film is sandwiched between the pressure-sensitive tape and a thin release film. Tabs are provided for removing the tape and the film.

The release film is first stripped from the hot-melt charge and the tape. While still on the tape, the charge is precisely positioned over the designated area on the pad. The adhesive tape is then pressed down on the rim and glass cloth of the pad.

To transfer the adhesive, the pad is heated to the melt temperature of the charge, in this case approximately 163° C (325° F), and is held at that temperature for a short time. The pad is then

cooled to a lower temperature, in this case approximately 66° C (150° F). The adhesive tape is then stripped from the pad, leaving the pad recharged with the hot melt adhesive and ready for use.

This technique could be used on Earth where certain constraints, such as fixed inverted position of the surface to be recharged, would limit the use of other methods for applying a hot-melt adhesive film.

This work was done by Donald J. Progar of **Langley Research Center.** *For further information, Circle 81 on the TSP Request Card.*

This invention is owned by NASA, and a patent application has been filed. Inquiries concerning nonexclusive or exclusive license for its commercial development should be addressed to the Patent Counsel, Langley Research Center [see page A5]. Refer to LAR-12881.

Simplified Heat-Source/Thermionic Converter

Heat is transferred by radiation across a vacuum gap.

NASA's Jet Propulsion Laboratory, Pasadena, California

A new design for a nuclear-powered electric generator simplifies its assembly and reduces its size and weight. Intended to supply 120 kW for propulsion of a spacecraft, the generator uses a nuclear reactor to produce heat, which is then transformed into electricity by an array of thermionic converters. The new design concept would be also applicable to terrestrial and nonnuclear thermionic power supplies.

As can be seen in the figure, heat is extracted from the reactor by heat pipes, which form a heat-radiating cylindrical wall outside of the reactor. A vacuum gap separates this inner (heat-source) cylindrical wall from an outer (converter) cylindrical wall formed by an array of heat-receiving surfaces fastened to the thermionic converters. The outside of the converter cylinder radiates any excess heat.

In this design, heat crosses the vacuum gap as thermal radiation. An earlier design had a ceramic instead of the vacuum between the reactor heat pipes and the thermionic converters and had additional heat pipes for cooling the collectors of the thermionic converters. Ceramic was used because the wall had to be electrically nonconducting to permit a series connection of thermionic converters on a common heat pipe. Elimination of the ceramic makes the entire structure shorter, narrower, and lighter and also avoids the difficult problem of generator assembly and of finding a material that is electrically insulating at the high temperature (about 1,650 K) of operation.

This work was done by Katsunori Shimada of Caltech for **NASA's Jet Propulsion Laboratory.** *For further information, Circle 82 on the TSP Request Card.*

NPO-15278

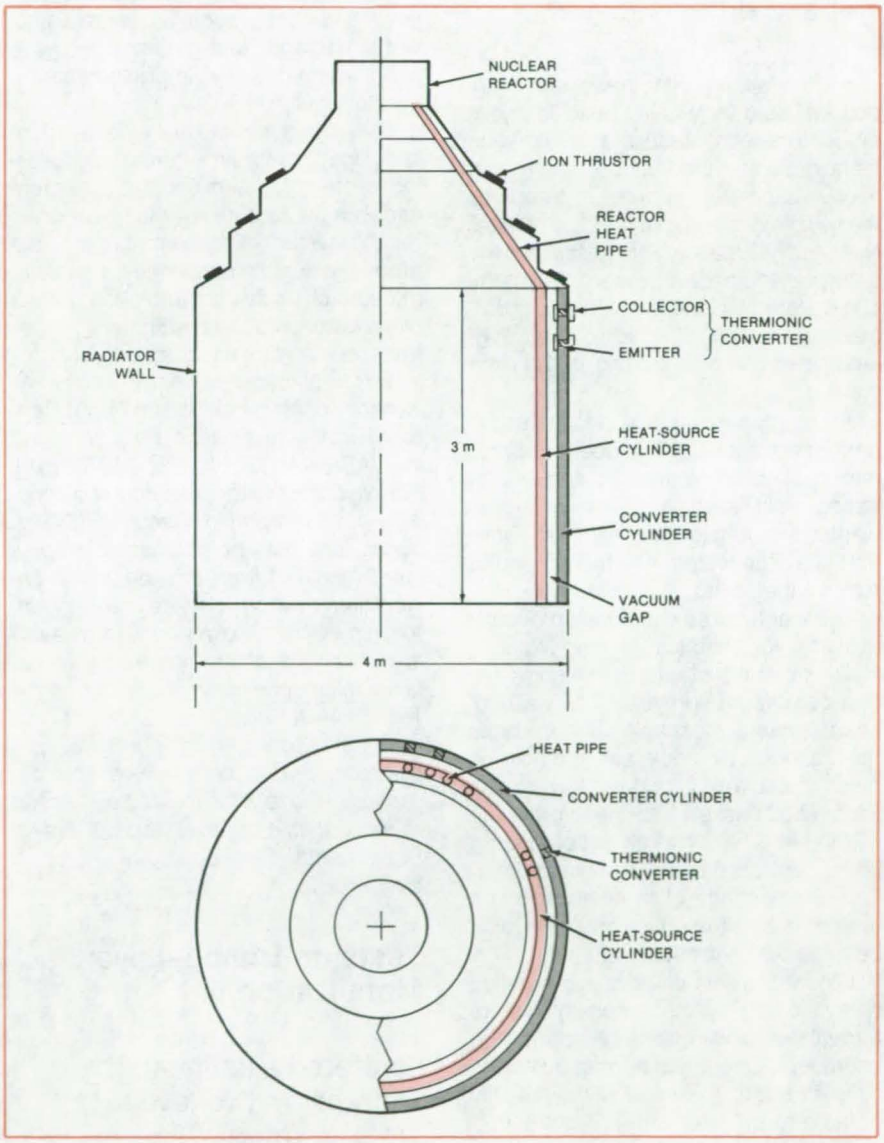

Radiation Coupling of the heat from the heat-source cylinder to the converter cylinder through the vacuum gap eliminates the need for high-temperature electrical insulators between the reactor heat pipes and the thermionic converters. In addition, no radiator heat pipe is necessary because the collectors of the thermionic converters from which excess heat must be removed radiate directly to space.

Books and Reports

These reports, studies, and handbooks are available from NASA as Technical Support Packages (TSP's) when a Request Card number is cited; otherwise they are available from the National Technical Information Service.

Etching Integrated Circuits

Report reviews manual and automatic methods, both wet and dry.

A 20-page report reviews the methods available for etching specific layers on wafers and discusses automation techniques and the features of one particular automated system. It compares the two major etching methods, chemical (wet) and plasma (dry), and discusses the areas in need of development. The methods covered include the "dip-and-dunk" manual method of chemical etching, automated chemical etching, and plasma etching.

About 85 percent of wafer etching is performed manually. The operator transfers baskets of wafers in and out of strong acid solutions to remove unwanted materials left exposed after masking. The wafers are then rinsed to remove the acids.

The mechanized equipment presently available for chemical etching includes walking-beam systems, in-line sprayers, and centrifugal sprayers. The walking-beam system mechanically duplicates the manual dip-and-dunk method: A mechanical arm lifts and lowers the wafer-filled baskets into the appropriate etching tank, with movement of the arm being controlled by an automatic timer. The disadvantage of the walking-beam system is that the entire machine must be protected against acid fumes.

Eliminating this disadvantage, in-line spray/etching systems convey wafers through etching, cleaning, and drying chambers. One machine can automatically etch and rinse and will eventually be able to process wafers from a cassette to a tray.

The batch and in-line chemical processes offer high production rates. The chemicals can etch deeply into any material, and etch rates are generally faster than with plasma etching. However, the procurement, storage, handling, and disposal of chemicals are expensive, troublesome, and hazardous; and chemical purity is a constant concern.

In the dry technique of plasma etching, highly-energized plasma particles react with the substrate to be etched, and the volatile products of the reaction are removed from the chamber by the vacuum pump. Plasma etching is commonly used to pattern such materials as silicon dioxide, silicon nitride, silicon, tantalum, tantalum nitride, tantalum oxide, molybdenum, and tungsten. Many of the previous problems associated with plasma etching, such as overheating, wafer damage, and overetching, have been alleviated by improvements in reactor design.

The report concludes with a list of specifications for an automatic processing system for semiconductor wafers and with the features of the rinser/dryer for the system. The illustrations in the report include the sequence for an automated etching system and photographs of the automatic wafer etcher, its carrier transport, and its rinser and dryer.

This work was done by Bobby W. Kennedy of **Marshall Space Flight Center.** *Further information may be found in NASA TM-82411 [N81-74978/NSP], "Chemical Etching for Automatic Processing of Integrated Circuits" [$6]. A paper copy may be purchased [prepayment required] from the National Technical Information Service, Springfield, Virginia 22161. The report is also available on microfiche at no charge. To obtain a microfiche copy, Circle 83 on the TSP Request Card.*

Inquiries concerning rights for the commercial use of the invention described in the report should be addressed to the Patent Counsel, Marshall Space Flight Center [see page A5]. Refer to MFS-25661.

Tests on Double-Layer Metalization

Sputtered aluminum patterns on two levels are separated by an insulating oxide.

A 28-page report describes experiments in the fabrication of integrated circuits with double-layer metalization. The double-layer metalization requires much less silicon "real estate" and allows more flexibility in the placement of circuit elements than does single-layer metalization.

The integrated circuit chosen for the demonstration is a complementary metal-oxide-semiconductor/silicon-on-sapphire (CMOS/SOS) solar-cell controller. Up to the metalization stage, the circuit is fabricated in the standard way: Silicon is deposited on a sapphire substrate; transistors, diodes, capacitors, and resistors are formed in the silicon by ion implantation; an oxide layer is formed over the circuit surface; and contact holes are opened in the oxide.

Then the metalization is applied. The first layer is a 0.8-μm-thick pattern of aluminum containing 2 percent silicon, deposited by sputtering. On the first layer is grown a 0.6-μm-thick insulating layer of silane oxide. Through holes 7.6 μm square are etched in the insulating layer so that the second metalization layer can make contact where needed with the first layer and with the circuit elements. Next, the second layer, a 1.2-μm-thick pattern of pure aluminum, is evaporated from a filament or sputtered on the insulating layer. Finally, a 0.6-μm-thick protective oxide film is grown over the surface.

Optical and scanning electron microscope measurements show that the first-layer metal is very smooth — an essential condition for reducing the incidence of short circuits between the two metal layers. The second-layer metal is continuous over steps in the first layer.

The probe yield of good IC chips on two wafers, each containing about 850 chips, was about 12 percent. Of the 132 chips that were encapsulated in dual-in-line packages, 95 passed final tests. Of these, 25 chips with leakage current less than 100 μA were selected for burn-in life tests consisting of three bias cycles: 168 hours at 125° C, 72 hours at 150° C, and 168 hours at 150° C. Only three chips failed the burn-in tests, probably because of a short between the metal layers through the insulating layer. The remaining 22 chips functioned well, and 18 of them maintained leakage current below 100 μA.

This work was done by D. S. Woo of RCA Corp. for **Marshall Space Flight Center.** *To obtain a copy of the report, Circle 84 on the TSP Request Card.*
MFS-25688

Mathematics and Information Sciences

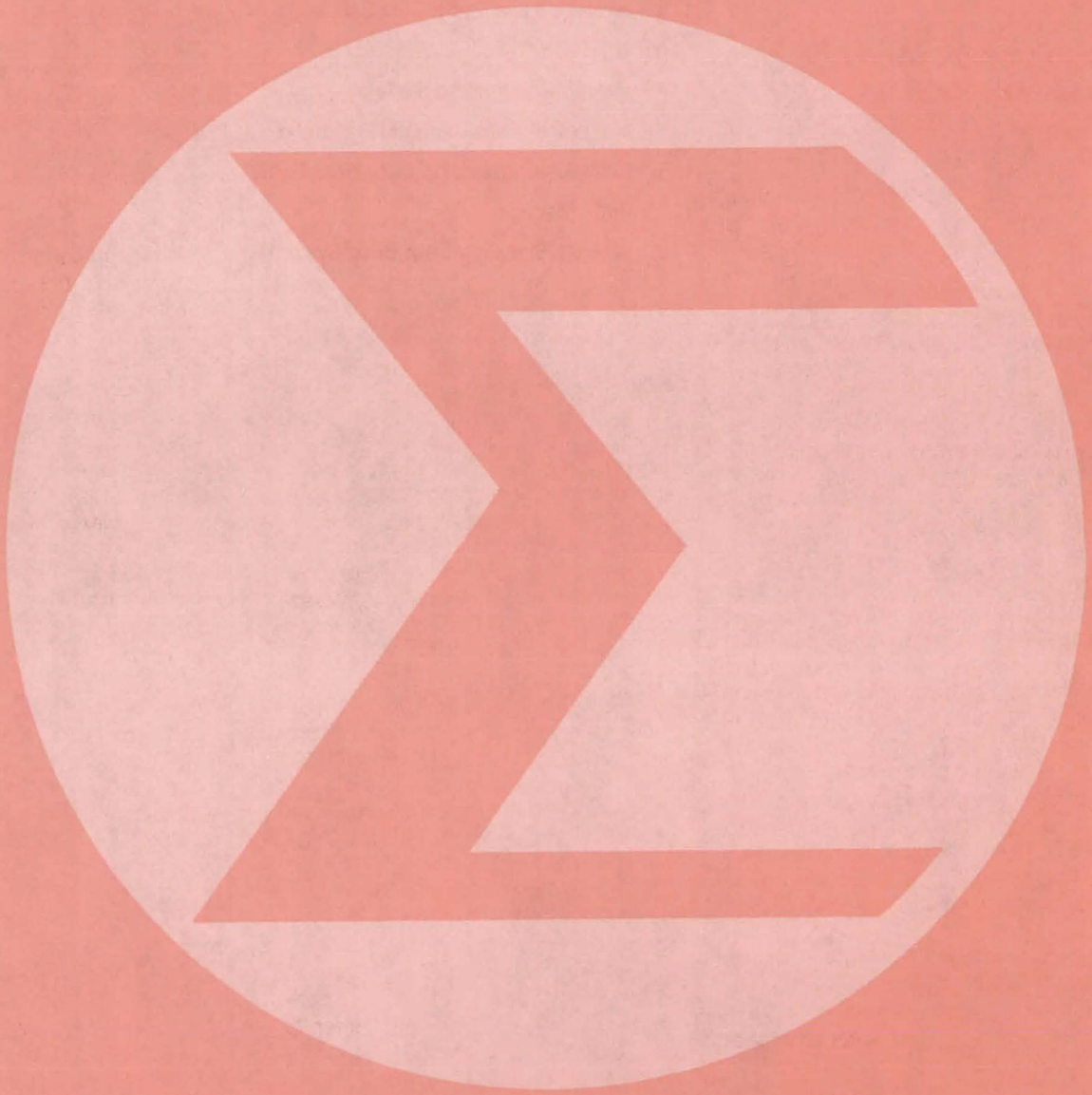

Hardware, Techniques, and Processes

Computer Programs

Consistent Tolerance Bounds for Statistical Distributions

False hypotheses are screened by using consistent tolerance bounds.

Lyndon B. Johnson Space Center, Houston, Texas

The assumption that a sample comes from a population with a particular distribution can be made with confidence C if the data all lie between certain bounds. These "confidence bounds" depend on C and on an assumption about the distribution of sampling errors around the regression line.

The analysis of Space Shuttle surface-tile strength has led to the conclusion that when the distribution of errors is assumed to be the same as the population distribution, the resulting confidence bounds lie closer to the regression line than when other common confidence bounds are used (see figure). Thus, the consistent bounds are least likely to result in the adoption of a false hypothesis.

The figure shows data plotted on normal (Gaussian) probability paper. Five sets of confidence bounds are also shown: normal-tolerance, binomial, Kilmogorov-Smirnov-Lilliefors (K.S.L.), Kilmogorov-Smirnov (K.S.), and regression. The normal-tolerance bounds (the consistent bounds) are closer to the "best-fit" line than the others, so the rejection of the normal distribution occurs more frequently with the normal-tolerance bounds. Of course, there will also be more frequent rejection of the normal distribution even when it is valid; however, in many applications, this type of error is tolerated, while the acceptance of an incorrect distribution is not.

Graphical test criteria using tolerance bounds can be applied in industry where statistical analysis can influence product development and use. They can be applied, for example, to evaluate equipment life.

This work was done by Michael A. Mezzacappa of Rockwell International Corp. for **Johnson Space Center.** *For further information, Circle 85 on the TSP Request Card.*
MSC-20090

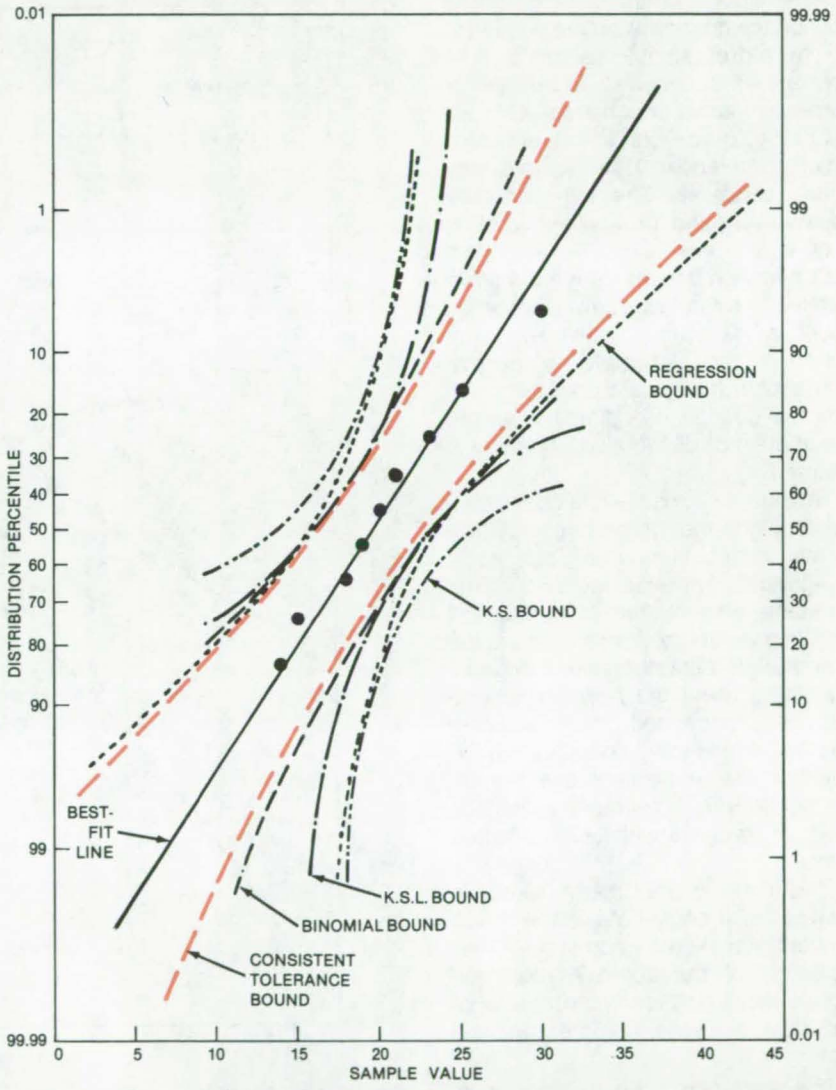

Confidence Bounds for data assumed to be from a population with normal distribution (and hence plotted on normal probability paper) are compared here. The consistent tolerance bounds shown in color are based on the assumption that errors in the data also have a normal distribution.

Computing Graphical Confidence Bounds

An approximation formula is easily computed on a programable calculator.

Lyndon B. Johnson Space Center, Houston, Texas

A new approximation for graphical confidence bounds is simple enough to run on a programable calculator. The approximation can be used in lieu of numerical tables, which are not always available, and exact calculations, which often require rather sizable computer resources. The approximation has been verified for a collection of up to 50 data points.

Confidence bounds define the limits within which a data set can be assumed to fit a particular statistical distribution — for example, a normal distribution. If any data point falls outside the confidence bounds, then the assumption of distribution normality is rejected.

The figure shows 10 data points plotted on lognormal graph paper. A true normal distribution would plot as a straight line; however, the data points are scattered about the line because of sampling variability. Also shown are the 5- and 95-percent confidence bounds, calculated using the new approximation. For comparison, the exact confidence bounds are also indicated. Excellent agreement is seen over the entire scale. The agreement is just as good for samples with up to 50 data points.

This method has been used to analyze tile-strength data on the Space Shuttle thermal-protection system. The efficiency of the approximation can reduce labor and computer costs of statistical analyses in other applications.

This work was done by Michael A. Mezzacappa of Rockwell International Corp. for **Johnson Space Center.** *For further information, Circle 86 on the TSP Request Card.*
MSC-18908

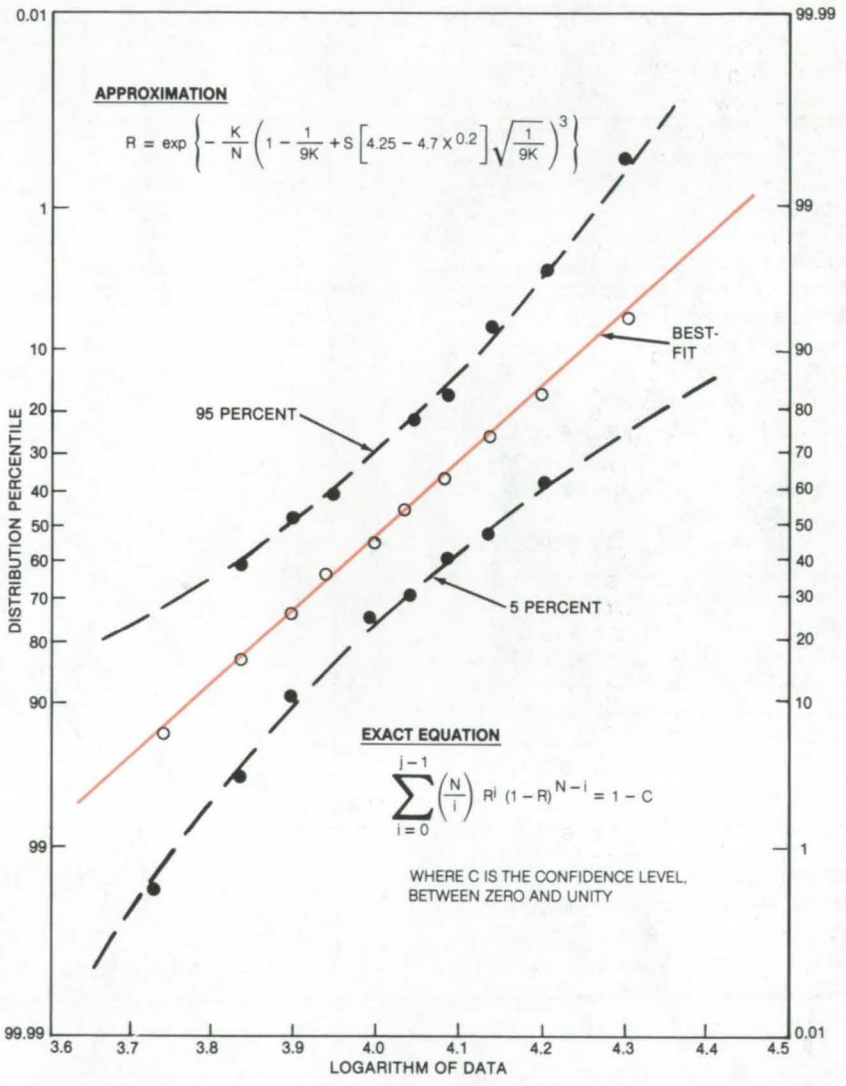

Confidence Bounds, calculated approximately, are shown as plotted points and, calculated exactly, as dashed lines. The sample data are shown in color. In the confidence-ranking approximation formula, the parameters X, S, and K are determined exactly before starting the calculation. The exact formula is solved by iteration on a computer.

Implementing Exclusive-OR Logic

A BCD-to-decimal decoder and one four-input NAND gate can be wired as a four-input exclusive-OR (XOR) gate. Combining several of the basic two-IC arrangements allows XOR of any number of inputs.
(See page 5.)

Calculating Safe Clearances for Manipulators

A method rapidly calculates the minimum safe clearances for remote manipulators. The method offers special benefits in industrial robotics, particularly in industrial machining.
(See page 60.)

Mapping Ocean Winds by Radar

Data on windspeed, wind direction, and wind patterns at the ocean surface are extracted from radar signals, using a special algorithm. From this information other weather parameters can be derived.
(See page 27.)

Formulas for Precise Transverse Mercator Projection

A new method yields
precise geodetic maps.

NASA's Jet Propulsion Laboratory, Pasadena, California

A new method for producing geodetic maps is not only easier to use than older methods but is also more precise.

The new technique is a simplified method for computing the transverse Mercator projection. In this projection, points on the surface of Earth are projected conformally onto a cylinder (see figure) that is tangent at a principal meridian (including both poles). The cylinder is then cut and flattened to form a planar map.

The new method makes use of a set of formulas that connect coordinates of points on an oblate-spheroid-shaped Earth to rectangular map coordinates. The formulas are a new generalization of the previously known formulas for a spherical Earth.

The formulas are in the form of conjugate harmonic series in odd powers of the spheroidal latitudinal eigenfunction and odd harmonics of the sine and cosine of the longitude. The coefficients of the series are rational-coefficient polynomials in the spheroidal eccentricity of Earth or other body to be mapped. These coefficients may be precomputed. The leading terms of the harmonic series are actually those of the conventional polar stereographic projection.

Tables of the calculus of the spheroidal latitudinal eigenfunction and related functions, and power series for these functions have been developed. The argument of the eigenfunction may be expressed either in distance from the pole along the meridional arc or in geodetic latitude. Besides their use in mapmaking, the functions can be applied to the design of streamlined structures — for example, when distance along an ellipsoidal surface requires a simple analytic expression.

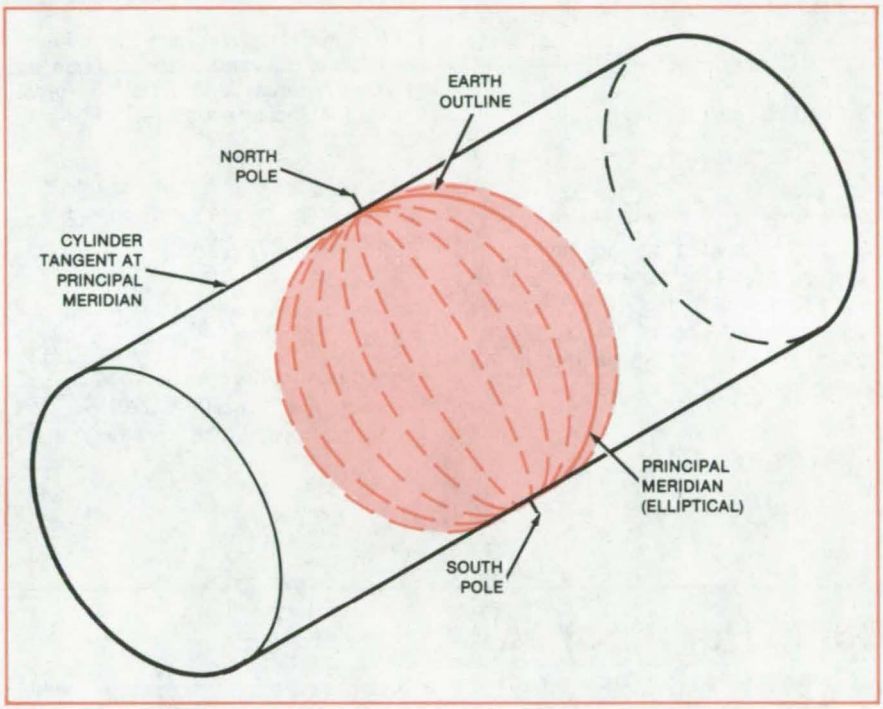

In the **Transverse Mercator Projection,** the surface of Earth or other spheroid is mapped onto a cylinder that is tangent at a meridian of longitude. The new method performs the mapping by means of a mathematical series in which the higher order terms correct for the deviation from exact sphericity.

This work was done by David E. Wallis of Caltech for **NASA's Jet Propulsion Laboratory.** *For further information, Circle 87 on the TSP Request Card.*
NPO-15409

Simplified Life-Cycle Cost Estimation

A formula using a single parameter
gives accurate results.

NASA's Jet Propulsion Laboratory, Pasadena, California

A simple method for life-cycle cost (LCC) estimation avoids the pitfalls inherent in formulations requiring separate estimates of inflation and interest rates. The method depends for its validity on the observation that interest and inflation rates closely track each other.

The LCC of a project is the lump sum of money that would have to be set aside at one time (usually at the beginning of the project) to cover all expenditures during the entire life cycle of the project. In estimating LCC the "time value of money" is taken into account. The amount of money that must be set aside to cover a future expenditure is affected by both interest and inflation rates. Interest may be earned on the money set aside, but inflation will increase the amount of the final expenditure. Thus the effects of interest and inflation rates

(continued on next page)

tend to offset each other and the net effect on LCC is essentially due to the difference in these rates.

With an annual inflation rate j, an expenditure that costs C at time t_0 will at a later time t cost

$$C(1 + j)^{t-t_0}$$

With annual interest rate i, the discounted value of this cost at time t_0 is:

$$C(1 + j)^{t-t_0}(1 + i)^{-(t-t_0)}$$

This can be reexpressed as

$$CV^{t-t_0}$$

where $V = (1 + j)/(1 + i)$. Thus LCC can be calculated by specifying an assumed value for V rather than for both i and j. Specifically, if $C_1, \ldots, C_n$ are the assumed yearly costs in present (t_0) dollars, then the LCC (evaluated at the present) is given by

$$LCC = \sum_{k=1}^{n} C_k V^k$$

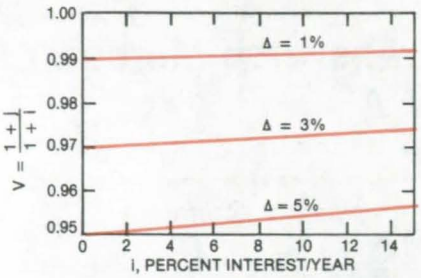

The Parameter V is shown as a function of interest rate i for various fixed differences between interest and inflation rates, $\Delta = i - j$. At low interest rates, V is nearly equal to $1 - \Delta$.

As the figure shows, V is essentially a function of the difference of rates, $i - j$. In fact, the approximation

$$V = 1 - \frac{i - j}{1 + i} \approx 1 - (i - j)$$

is good enough for most purposes.

Historically, the difference $i - j$ has fluctuated considerably less than i and j themselves, with the difference usually being about 2 to 3 percent. A modeling study has been done using actual interest and inflation rates for the period 1950 to 1976 in LCC calculations for projects of 5- to 20-year duration and starting dates from 1950 to 1972. A choice of V = 0.983 gave good results over the entire period.

The study shows that inflation and discounting largely cancel each other and that it is essentially only the difference between them that affects LCC. Furthermore, fluctuations in the rates tend to cancel out over project lifetimes. As a consequence, a single parameter V can be chosen to estimate the net effect of future discount and inflation rates with a reasonable degree of confidence.

This work was done by Donald S. Remer, Gary Lorden, and Isidore Eisenberger of Caltech for **NASA's Jet Propulsion Laboratory.** *For further information, Circle 88 on the TSP Request Card.*
NPO-15228

Computer Programs

These programs may be obtained at very reasonable cost from COSMIC, a facility sponsored by NASA to make new programs available to the public. For information on program price, size, and availability, circle the reference letter on the COSMIC Request Card in this issue.

Interactive Planning System

System helps managers plan projects within time, budget, and manpower constraints.

The NASA Interactive Planning System (NIPS) supports resources analysis and tracking and long-range resources planning. NIPS is based on a hierarchical-tree data-base structure and remote graphics terminal input and output. It assists the program-planning groups at NASA Headquarters in developing long-range plans for the total space effort. These functions involve meeting goals and objectives within time, budget, and manpower constraints. Although NIPS is oriented toward NASA planning, it is a general tool that could be adapted to any resource-management and allocation problem.

NIPS aids financial planners in monitoring resource expenditures (i.e., dollars and manpower) for ongoing projects as well as in preparing long-range plans. The NIPS data base centralizes resources data and maintains a history of data evolution. NIPS is fully interactive, enabling the analyst to enter, modify, or delete data rapidly.

Large amounts of graphical and textual data can be generated rapidly by NIPS for analysis or manager review. Upon analysis, changes can be made in minutes to respond to "what if" questions, with complete new graphical and tabular displays generated showing the impact of any changes. NIPS should find applications in any situation where resources monitoring is important and rapid evaluation of alternative resource-allocation plans is desirable.

NIPS consists of four subsystems:

- NIPS-RTOP (Research and Technology Operating Plan),
- NIPS-PCS (Project Control System),
- NIPS-PMR (Program Management Report), and
- NIPS-LRP/POP (Long Range Planning/Program Operating Plan).

NIPS-RTOP tracks the resources status of individual RTOP efforts. It is primarily an inquiry system that allows the user to obtain the status of any RTOP or groups of RTOP's quickly.

NIPS-PCS is a tool for project resource analysts. It tracks actual performance, both technical milestones and resources, against a project plan.

NIPS-PMR is oriented to the needs for resources management of programs and projects. The basic function of the system is to assist in the tracking of actual cost against planned cost over a 12-month (fiscal-year) operating period. The data base for NIPS-PMR consists of planned and actual figures for both obligations and costs and actual figures for commitments.

NIPS-LRP/POP is oriented to the needs for building, modifying, and analyzing plans composed of activities for a long period of time. The data base consists of planning data (costs, manpower, and schedules) as they are forecast for a

lifetime of an activity. This subsystem can be used for Program Operating Plan (POP) planning exercises.

NIPS is written in FORTRAN and COMPASS for the RUN compiler and has been implemented on a CDC 6000-series computer using the SCOPE operating system. The largest NIPS subsystem has a central memory requirement of 52K (octal) 60-bit words. NIPS can be accessed interactively or executed from batch. For interactive processing, a Tektronix 4014-1 terminal and supporting vendor software are required.

This program was written by David A. Nippert, T. H. Beerman, and Jerry L. Pittenger of Battelle Memorial Institute for **NASA Headquarters.** *For further information, Circle G on the COSMIC Request Card.*
HQN-10920

Manpower Allocation and Reporting

Interactive program handles data for up to 75 projects and allocations for up to 60 months.

The interactive Manpower Allocation and Reporting System (MARS) helps planners make manpower allocation decisions. MARS includes provisions to enter overall constraints for projects and persons, to assign individuals to projects, to compute automatically the overhead category, to report on deviations from constraints, and to generate manpower resource allocation reports.

The MARS data base may contain data for up to 75 projects, 75 people, and manpower allocations for 60 months. For each project, data stored include a unique project number, project name, manpower constraints, manpower totals, and manpower data pointers. For each person, data stored include their name, section number, skill code, employee code, manpower available, manpower totals, and manpower data pointers. Manpower allocation data are stored in terms of the portion of a man-month allocated for each person for each project by month.

MARS is an interactive menu-driven program consisting of an executive routine and three major components. The input/modify component allows the user to enter new data or to modify existing data in the data base. The report-generator component allows the user to look at data that are in the data base.

Three basic types of reports may be generated: A manpower report consists of either a display of persons versus time for a specific project, of projects versus time for a specific person, or of projects versus time for a specific organization. A person or project list report consists of a list of all the persons or projects in the data base. Constraint reports consist of displays of projects over constraint, projects under constraint, persons over constraint, and persons under constraint. The user has the option to see detailed constraint reports for particular persons or projects.

The interactive-scheduling component of MARS allows the user to employ a trial-and-error method of rescheduling manpower for both projects and people. The user requests the display of manpower reports and then interactively changes any of the manpower values. If a change causes manpower constraints to be exceeded, informative messages are displayed to aid the user in the formulation of further rescheduling trials.

MARS is written in FORTRAN IV Plus and Assembler for interactive execution and has been implemented on a DEC PDP-11/70 computer under RSX-11M with a central memory requirement of approximately 33K of 16-bit words. MARS was developed in 1977 and updated in 1978.

This program was written by Phillip D. Merwarth of **Goddard Space Flight Center.** *For further information, Circle H on the COSMIC Request Card.*
GSC-12708

Software-Engineering Data-Base System

System collects and maintains data for software-development efforts.

The Software Engineering Laboratory Data Base Maintenance System (SEL/DBAM) collects and maintains a data base for evaluating software-development methodologies. SEL/DBAM provides interactive facilities for the management of data collected by the Software Engineering Laboratory at Goddard Space Flight Center.

SEL/DBAM is organized into four component functions: create, archive, restore, and update. The interactive update programs may be classed into four groups based on the type of files processed and the program organization. These four classes consist of data-base summary and header files, complex data files, simple data files, and special data files. The update activities are divided into three modes: add new records, change existing records, and delete existing records. These modes allow the user to add to or modify files interactively in the data base as part of the regular data-collection procedure or in response to requests for changes by reviewers.

The create component of SEL/DBAM initializes required header records and creates new data-base files. It operates in an interactive mode and prompts the user for all information needed to add new data-base files. A tape copy of the entire data base or of a list of user-specified files is made by the archive component. This utility is useful in backing up files to tape for security and historical purposes. The restore component of SEL/DBAM recovers files from tapes generated with the archive utility.

SEL/DBAM is written in FORTRAN IV and Assembler for interactive execution. It has been implemented on a DEC PDP-11/70 computer with RSX-11M V3.1 and has a central memory requirement of approximately 64K of 8-bit bytes. SEL/DBAM was developed in 1980.

This program was written by David N. Card of Computer Sciences Corp. for **Goddard Space Flight Center.** *For further information, Circle J on the COSMIC Request Card.*
GSC-12669

Path Pascal

Pascal is extended to treat real-time concurrent systems.

Path Pascal is a high-level experimental programing language based on Pascal, which incorporates extensions for systems and real-time programing. Developed to investigate the benefits and problems that arise when path expressions are combined with a high-level language to provide a system programing tool, Path Pascal includes objects for information encapsulation,

(continued on next page)

path expressions for synchronization of processes that execute independently, and provisions for coding interrupt processes to deal with I/O devices. The language also includes abstract data and protection features. Instead of altering Pascal extensively, a few features were added such that standard P4 Pascal programs would still compile and execute, as long as the programs did not use Path Pascal reserved words as identifiers. Path Pascal can aid in investigating the problems of programing real-time concurrent systems.

The general Path Pascal system consists of a Path Pascal Compiler, a Path Pascal Interpreter, and a Path Pascal Linker. The Path Pascal Compiler accepts programs written in Path Pascal as input and generates P-code output. The Path Pascal Interpreter accepts P-code as input, which it interprets and executes based upon an extended version of the P4 interpreter virtual computer. The Path Pascal Linker combines two or more P-code files without having to recompile all of the source code.

Path Pascal is based on the P4 subset of Pascal. This subset was augmented with an encapsulation mechanism, open path expressions, and a process mechanism. Open paths are integrated with the encapsulation mechanism to enforce a strict discipline upon the programer to describe shared-information objects. All access to the encapsulated object is performed by operations synchronized by open paths. A routine invoking such operations may execute the operation only if permitted by the open path expressions associated with the shared-data object.

The Path Pascal Compiler, Interpreter, and Linker are written in the P4 subset of Pascal. The Path Pascal system has been implemented on a number of systems with the current base system for the version distributed by COSMIC being a CDC CYBER 170-series computer. The knowledgeable user should be able to implement Path Pascal on any system supporting the P4 subset of Pascal. The Path Pascal system was developed in 1979.

This program was written by Roy H. Campbell, Robert B. Kolstad, Daniel F. Holle, Thomas J. Miller, Philip Krause, Kurt Horton, and Tom Macke of the University of Illinois at Urbana-Champaign for **Langley Research Center.** *For further information, Circle K on the COSMIC Request Card.*
LAR-12854

Stability Statistics Data Base System

Four FORTRAN modules implement edit, sort, report-generation, and other functions.

The Stability Statistics Data Base System is written entirely in FORTRAN and does not require the use of outside data-management routines. It is used with a directly-accessible data base containing simple card images.

Although currently used with a data base containing data for the computation of computer hardware/software stability statistics, the Stability Statistics Data Base System could be adapted to numerous other data-base applications. With smaller data bases (approximately 15,000 records or less), the fast-response time of the report generator module makes it suitable for running in the demand mode. For larger amounts of data, the module may be run in the batch mode.

The Stability Statistics Data Base System consists of four functional modules. These are the stability data-base preprocessor (DRNEW), the data-base sort program (SORTNEW), the data-base transformation program (TRANSF10), and the data-base report generator (NEWNSTATS).

DRNEW edits raw input data, merges update records with the data-base records, and generates daily and summary time line reports. SORTNEW sorts the card image records via UNIVAC system sort package, CLINK$.

TRANSF10 transforms the sequential data base into a direct-access data base via the DEFINE FILE method. The direct-access data base generated by TRANSF10 is used by the report generator program NEWNSTATS. NEWNSTATS allows the user to perform ad hoc inquiries and report generation.

A "skip-sequential" search algorithm is implemented in NEWNSTATS to provide fast response. This module currently responds to inquiries and generates reports concerning the computer hardware/software stability statistics as mean time to failure, mean time to repair, mean time between failures, and numerous other statistics on computer system stability.

The Stability Statistics Data Base System is written in FORTRAN V for execution in the batch and demand modes and has been implemented on a UNIVAC 1108 computer with a central memory requirement of approximately 20K of 36-bit words for the largest functional module. The system was developed in 1980.

This program was written by Gee-Yin Kwok and Adrian Domingues of Computer Sciences Corp. for **Johnson Space Center.** *For further information, Circle L on the COSMIC Request Card.*
MSC-20014

SUBJECT INDEX

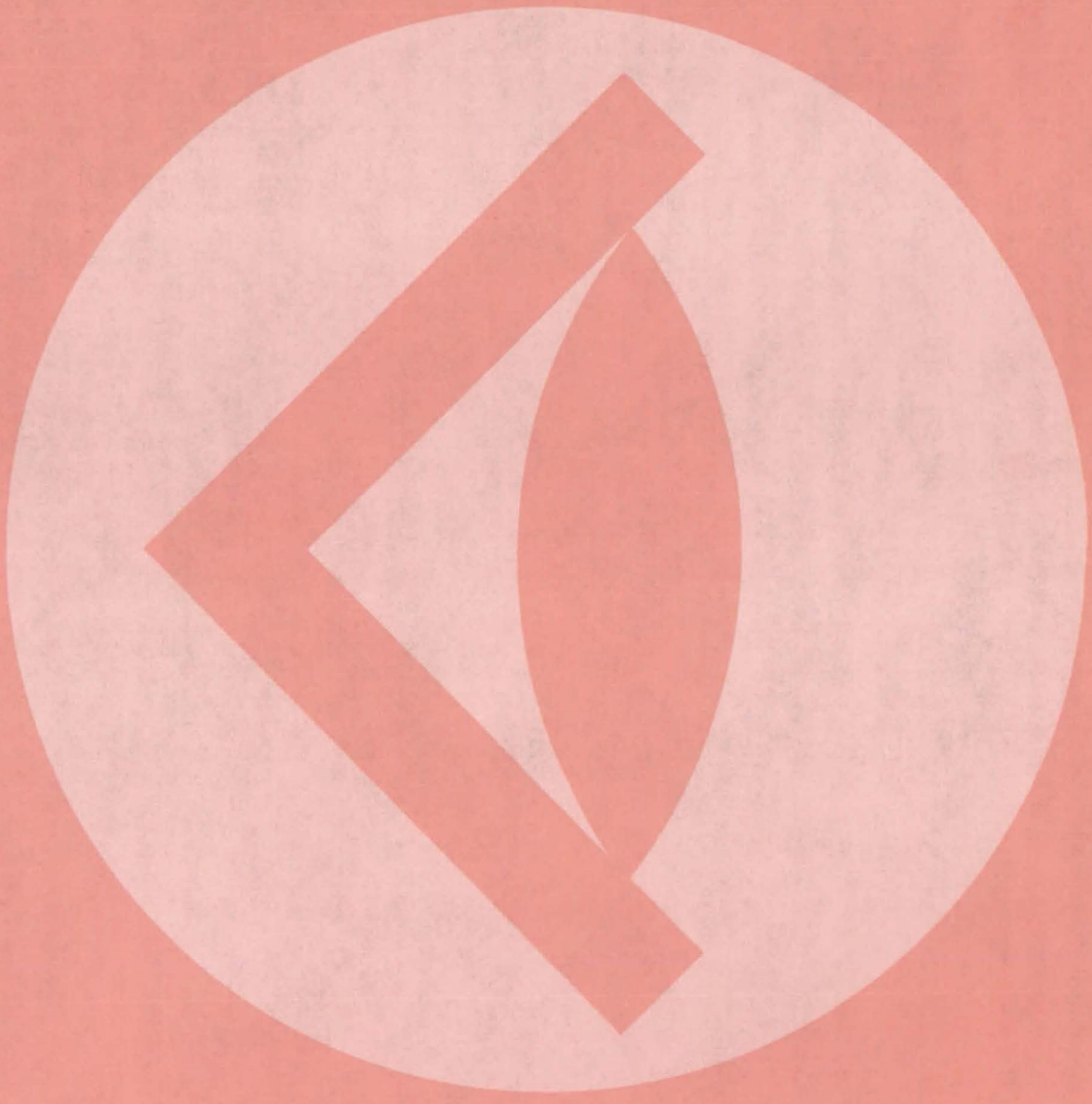

National Aeronautics and
Space Administration

Washington, D.C.
20546

THIRD-CLASS BULK

NASA

Workers prepare to install an ultrasonic sewer monitor, one of several distributed in the Washington, D.C., system to check water depths and flow rates. NASA sensor technology and circuit design techniques are combined in the monitor, which helps city engineers in sewer planning and management. [*See the bottom of page A1.*]